AN EVALUATION OF PROCEDURES FOR CALCULATING AERODYNAMIC LOADS

LEON H. SCHINDEL

MASSACHUSETTS INSTITUTE OF TECHNOLOGY

FOREWORD

This report was prepared by the Massachusetts Institute of Technology under USAF Contract No. AF 33(615)-1199. The contract was initiated under Project No. 1367, Task No. 136715. The work was administered under the direction of the Air Force Flight Dynamics Laboratory, Research and Technology Division, Mr. Charles E. Jobe, project engineer. The faculty supervisor at Massachusetts Institute of Technology was Professor Morton Finston.

This report covers work conducted from February 1964 to December 1964.

The manuscript of this report was released by the author December 1964 for publication as a RTD Technical Report.

The helpful cooperation of the following people also materially contributed to the project: W. Lansing, P.R. Dickman, H. Mead, and R. Mohrman of Grumman Aircraft Engineering Corp., A.T. Judson and C. Dragowitz of Republic Aviation Corp., J.L. Decker and W.B. Yates of the Martin Co. (Baltimore); C.T. Newby of the Bureau of Naval Weapons, W.H. Statler, W.A. Stauffer, and J. Leibolt of Lockheed Aircraft Corp. (Burbank); W.T. Shuler of Lockheed Georgia Co., C.C. Durand and H.A. Swift of General Dynamics (Pomona); M.M. Alexander of General Dynamics (Ft. Worth); J. Jackson, G.G. Gren, and G.F. Foelsch of General Dynamics (San Diego); J.E. Fischler, O.R. Dunn, R.D. Schaufele, and M. Stone of Douglas Aircraft Co., (Long Beach); R.C. Morenus and C.O. White of Aeronutronic Division; W.L. Philips, D.P. Forsmo, C.F. Talbott, Jr., and A. Rogers of Hughes Aircraft Co., L.G. Johnson, G.H. Johnson, C.L. Davis, P.F. Wildermuth and J.L. Berkey of North American Aircraft, Inc., (Los Angeles); L.J. Yancey, D.T. Wilson, Jr., C.M. Wong, S. Powers, J.R. Stevens, and J.E. Gibson, Jr. of Northrop Corp. (Norair Division); A.F. Robertson, N.N. Au and R.E. Finch of Aerospace Corp., J.S. Mason and H. James of Ryan Aeronautical Co., J.L. Jones, J. Dougherty, A.E. Anderson, and R. Carmichael of NASA (Ames); E.J. Hahn, R.E. Watson, and W. Binze of the Boeing Co., E. Utter of Beech Aircraft Corp., W.R. Shackelford of Cessna Aircraft Co., G.T. Upton of Vought Aeronautics Division; W.H. Dukes and C.L. Forrest of Bell Aerosystem Co., E.T. Ackeroyd and L.A. Carlton of McDonnell Aircraft Corp., J. Kloos, Saab Aircraft Co., and W. Knackstedt of Air Force Flight Dynamics Laboratory.

In addition, F.H. Durgin and C.J. Borland, (who is responsible for the numerical calculations), and others at MIT have worked on this project.

This report has been reviewed and is approved.

RICHARD F. HOENER
Acting Chief
Structures Division

ABSTRACT

Existing theories are examined with the object of selecting the best methods for computing aerodynamic lift distributions for use in structural design. Subsonic, transonic and supersonic Mach numbers are included. Configurations consist of wing-body combinations such as might be employed for airplane-type vehicles. The present investigation is limited to the linear range of angle of attack.

The simplest theories which give accuracy consistent with structural design practice are reduced to computational procedure; the accuracy of a theory having been established by comparison with existing experimental data. In cases where no adequate theory is available or experimental data is lacking, further research is recommended. Future extensions to nonlinear regimes, more general configurations, and higher Mach numbers are also described.

TABLE OF CONTENTS

TABLE OF CONTENTS (Continued)

TABLE OF CONTENTS (Continued)

TABLE OF CONTENTS (Continued)

TABLE OF CONTENTS (Continued)

TABLE OF CONTENTS (Concluded)

ILLUSTRATIONS

ILLUSTRATIONS (Continued)

ILLUSTRATIONS (Continued)

ILLUSTRATIONS (Continued)

ILLUSTRATIONS (Continued)

ILLUSTRATIONS (Concluded)

TABLES

SYMBOLS

A = distance from point on wing to image vortex through point a

A_{ij} = element of aerodynamic matrix

AR = aspect ratio

a = body radius

a = speed of sound

a_μ = Fourier coefficient

B = distance from point on wing to image vortex through point b

B_n = Fourier coefficient

b = wing span

C = structural influence function

C_{ij} = element of structural matrix

C_L = lift coefficient (treated here as equivalent to normal force)

C_ℓ = section lift coefficient

C_N = normal force coefficient

C_p = pressure coefficient

c = wing chord

c_r = root chord

d = body diameter

d = transformed body width $= 2\left(s + \frac{a^2}{s}\right)$

f = distance from point on wing to line joining vortices through a and b

f_a = afterbody fineness ratio

f_n = nose fineness ratio

$G = \frac{\Gamma}{bU_\infty}$ = nondimensional vortex strength

SYMBOLS (Continued)

$g(x)$ = chordwise loading parameter, defined by Eq. (IV-92)

H = one half of distance between image vortices through a and b

h = maximum height of wing camber

i = wing incidence angle

K = diagonal matrix

K_{ij} = element of diagonal matrix

K_D = strength of doublet

K_S = strength of source

$k(x)$ = chordwise loading parameter for slender wing, defined by Eq. (IV-97)

L = lift

$L(t,\tau)$ = distribution function defined by Eq. (IV-96)

ℓ = lift per unit span

ℓ = body length

M = number of steps in trapezoidal integration

M = local Mach number

M_∞ = free stream Mach number

m = number of spanwise subdivisions of wing

m' = virtual mass

n = exponent parameter varying with aspect ratio defined on page 54

P = local load

p = local pressure

p_c = cone surface pressure

SYMBOLS (Continued)

p_i = pressure on body just past station x_i

p_{i-} = pressure on body just ahead of station x_i

p_j = pressure on j^{th} element

p_∞ = free stream pressure

q_∞ = free stream dynamic pressure = $\frac{\rho_\infty}{2} U_\infty^2$

R = distance from point on wing to center of body

R = distance from point x, y, z to vortex filament

r = radial coordinate

r_e = distance from body axis to vortex

r_i = distance from body axis to image vortex

S = area of integration

S_1 = area of integration on diaphragm

S_2 = area of integration omitted on wing

s = distance along body contour

s = distance from body axis to wing tip

TR = taper ratio

t = nondimensional spanwise coordinate = $\frac{y}{b/2}$

t = wing thickness

U_∞ = free stream velocity

u = x –component of velocity perturbation

V = local velocity

V_z = vertical component of velocity

v = y –component of velocity

SYMBOLS (Continued)

w = z-component of velocity

w = local upwash velocity, proportional to local wing slope

X = streamwise plane

x = streamwise coordinate

$x_{c.p.}$ = streamwise center of pressure location

y = spanwise coordinate

$y_{c.p.}$ = spanwise center of pressure location

z = vertical coordinate

α = local angle of attack

α_i = angle of attack of i^{th} element

α_0 = local angle of attack of undeflected surface

β = $\sqrt{|M_\infty^2 - 1|}$

Γ = vortex strength

γ = local strength of vortex sheet

γ = angle between y-axis and line between image vortices through a and b

γ = ratio of specific heats

δ = cone semi-vertex angle

η = spanwise coordinate

η = interpolation parameter defined by Eq. (V-27)

θ = azimuthal coordinate measured from y-axis

θ = angle from y-axis to point on wing

θ = spanwise distance parameter

SYMBOLS (Concluded)

θ_n = spanwise distance parameter = $\frac{n\pi}{m+1}$

Λ = sweep-back of wing quarter chord line

Λ = body loading parameter defined by Eq. (V-25)

$\Lambda_{L.E.}$ = sweep-back of wing leading edge

$\Lambda_{T.E.}$ = sweep-back of wing trailing edge

ξ = streamwise coordinate

ξ = transformed streamwise plane

ρ_∞ = free stream density

τ = nondimensional spanwise coordinate = $\frac{\eta}{b/2}$

ϕ = spanwise coordinate parameter = $\cos^{-1}\tau$

ϕ = perturbation velocity potential

ϕ = azimuthal angle from bottom of body

ϕ_D = velocity potential of doublet

ϕ_S = velocity potential of source

$\mathcal{L}_A$ = linear aerodynamic operator

$\mathcal{L}_S$ = linear structural operator

SECTION I

INTRODUCTION

Increases in the speed of aircraft in recent years have resulted in the widespread use of low aspect ratio swept wings. Procedures for specifying aerodynamic load distributions for structural design that were adequate for high aspect ratio wings in low-speed flight may therefore require revision. On high-speed aircraft, also, a larger fraction of the total load is likely to be carried by the body than would be the case for the larger-winged aircraft more typical of low-speed flight. Wing-body interference effects can also become more pronounced in modern slender configurations where much of the wing area is nearly adjacent to the body. In addition, modern structural design procedures include consideration of aeroelastic loads. For these reasons, the available procedures for calculating aerodynamic load distributions have been examined with the object of selecting those which are simplest and most accurate for current use in structural design.

The present study is limited to symmetric wing-body combinations traveling at subsonic or moderate supersonic speeds (invalid in the hypersonic flow regime). Effects of external stores, nacelles, engines, propellers, wing-tail interference, etc., are not examined. Within these limitations, complete analytical procedures are specified by which wing and body normal force distributions may be obtained. Since no theory is entirely satisfactory for all of the configurations to which it might be applied, experimentally determined loads should be used whenever they are available. A theoretical method, however, provides an independent estimate of what to expect from experimental results. Empirical methods are avoided in the present investigation.

For many years, Ref. 1 provided the standard procedure for computing wing air load distribution. This method is still used in some cases where the span loading is desired on a rigid high-aspect ratio subsonic wing. However, in modern application, the wing (or body)

is a flexible structure which deforms under load changing its angle of attack distribution and hence being subjected to new aerodynamic forces. Gray and Schenk, in Ref. 2, present a matrix solution of this aeroelastic problem. A similar approach is assumed in the present investigation in which the primary objective is the selection of appropriate methods of determining the required aerodynamic matrix. A brief description of the static aeroelastic problem is presented in the following section. Solution of the problem is greatly simplified if the deflection is linearly related to the load which, in turn, varies linearly with angle-of-attack. The presentation is therefore restricted to the linear case.

Before a choice can be made from among available theories for calculating load distribution, it is necessary to select rules by which competing procedures are to be judged. In Section III, limits of acceptable error are established (10% in lift; 3% in center of pressure) as being consistent with the requirements of preliminary structural design. Then, of those methods of determining aerodynamic load distribution which satisfy these criteria, the simplest available procedure is recommended.

The aerodynamic force which is of primary interest to the structural designer is the component normal to the wing-body plane. This report, therefore, deals with the distribution of normal force. The term "lift" will often be used, no distinction being made between the two components except at very high angles of attack, since the calculations are carried out by similar procedures.

The investigation covers airplane-type configurations in steady symmetric flight (no yaw) at subsonic, transonic, and supersonic speeds. Although the shape of the aircraft may be quite general, special vehicles, such as helicopters and ground-effects machines, are not studied. The load distribution on wings is treated in Section IV; bodies are discussed in Section V. Each part is further subdivided into subsonic, transonic, and supersonic flow regimes. In each regime, the simplest theory of adequate accuracy is selected and reduced to a numerical procedure. Comparisons with experimental data illustrate the accuracy and limitations of the preferred methods.

Further investigation is indicated in Section VI for flow regimes or configuration geometries in which no available procedure meets the prescribed accuracy requirement. In addition, experimental programs are recommended where available data is inadequate to determine the accuracy or limitations of the theoretical calculation of load.

SECTION II

STATIC AEROELASTICITY

A. AEROELASTIC OPERATIONS

When a flexible wing (or body), is subjected to a net aerodynamic load, in general it will be warped to some new shape. The changes in slopes of the distorted lifting surface will then induce a modification of the load distribution and a further deformation of the surface. This process can be represented by the following simple, but general mathematical relations

$$\alpha - \alpha_0 = \mathcal{L}_S \; [P] \qquad (II-1)$$

$$P \quad = \mathcal{L}_A \; [\alpha] \qquad (II-2)$$

where $\alpha(x,y) - \alpha_0(x,y)$ represents the change in angle of attack distribution, in an x-y plane due to the deflections caused by the load $P(x,y)$. $\mathcal{L}_S[P]$ is a structural operator by means of which an angle of attack distribution can be obtained from a given load distribution. Similarly, $\mathcal{L}_A[\alpha]$, is an operator which converts angles into forces. The symbols imply, for example, that by some operation on the angle of attack distribution at all points ξ, η, a distribution of loads at points x, y is obtained. An integration of $\alpha(\xi,\eta)$ multiplied by a kernel function is usually required.

If the structural operation is applied to both sides of Eq. (II-2), then it becomes

$$\mathcal{L}_S \; [P] = \mathcal{L}_S \left[\mathcal{L}_A \; [\alpha] \right]$$

which, combined with Eq. (II-1) yields

$$\alpha - \alpha_o = \mathcal{L}_S \left[\mathcal{L}_A [\alpha] \right] \qquad (II-3)$$

The angle of attack distribution may, in principle, be determined from this implicit relation. If the operators are linear, however, a much simpler expression results.

A linear operator is one for which

$$\mathcal{L}_A [\alpha_1 + \alpha_2] = \mathcal{L}_A [\alpha_1] + \mathcal{L}_A [\alpha_2] \qquad (II-4)$$

Linear operations applied to Eq. (II-1) would yield

$$\mathcal{L}_A [\alpha - \alpha_o] = \mathcal{L}_A [\alpha] - \mathcal{L}_A [\alpha_o] = \mathcal{L}_A \left[\mathcal{L}_S [P] \right] \qquad (II-5)$$

and from Eq. (II-2).

$$P = \mathcal{L}_A \left[\mathcal{L}_S [P] \right] + \mathcal{L}_A [\alpha_o] \qquad (II-6)$$

or

$$\mathcal{L} [P] = \mathcal{L}_A [\alpha_o] \qquad (II-7)$$

where $\mathcal{L}[P]$ represents a new linear operation consisting of the combination:

$$\mathcal{L} [P] = P - \mathcal{L}_A \left[\mathcal{L}_S [P] \right]$$

If this operator has a unique inverse, $\mathcal{L}^{-1}[P]$, then

$$P = \mathcal{L}^{-1} \left[\mathcal{L}_A [\alpha_o] \right] \qquad (II-8)$$

B. EXAMPLE - SUPERSONIC WING

A specific example will illustrate the analysis. Linearized supersonic wing theory will be applied to the thin triangular wing illustrated below.

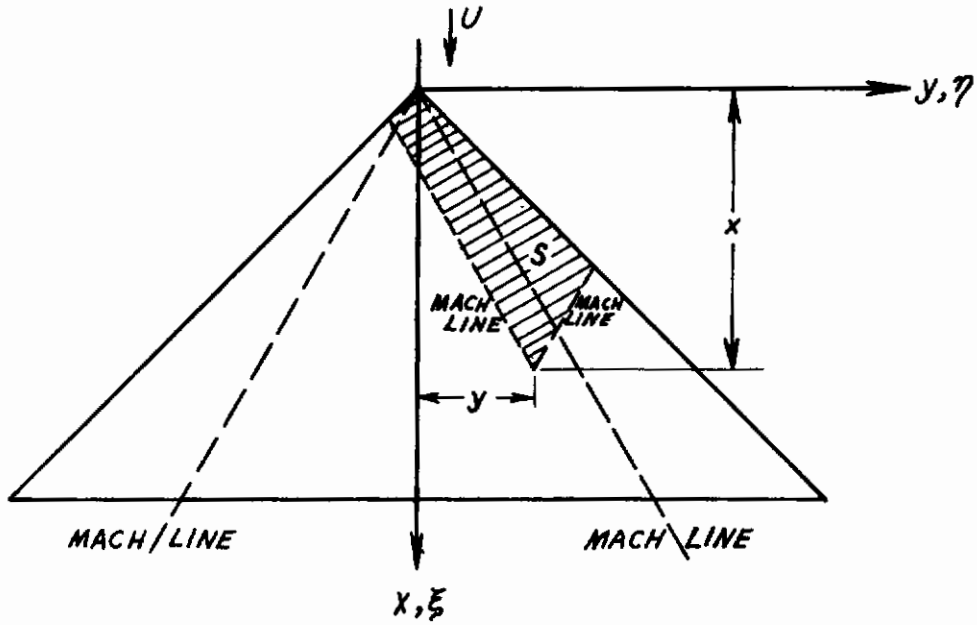

By linear theory (Section 13 of Ref. 3, for example), the pressure difference between bottom and top surfaces of the wing at the point x, y is

$$\Delta p = 4 q_\infty \frac{\partial}{\partial x} \left\{ \iint_S \frac{a(\xi, \eta)\, d\xi\, d\eta}{\sqrt{(x-\xi)^2 - \beta^2 (y-\eta)^2}} \right\} \qquad (II-9)$$

where q_∞ = free stream dynamic pressure, $\beta = \sqrt{M_\infty^2 - 1}$ (M_∞ = free stream Mach number), and S is the cross-hatched area. The operator $\mathcal{L}_A[\alpha]$ thus multiplies α by the kernel function $\frac{1}{\sqrt{(x-\xi)^2 - \beta^2(y-\eta)^2}}$, integrates over the indicated area, and differentiates the result with respect to x. The operator is linear, however, since the angle of attack distribution appears only as the object of linear operations. Consequently the total pressure can be computed by a superposition of any arrangement of distributions $\alpha_i(\xi, \eta)$ such that

$$\alpha(\xi, \eta) = \alpha_1(\xi, \eta) + \alpha_2(\xi, \eta) + \cdots \alpha_i(\xi, \eta) + \cdots$$

In particular, suppose that the wing is subdivided into a number of ordered boxes as shown below

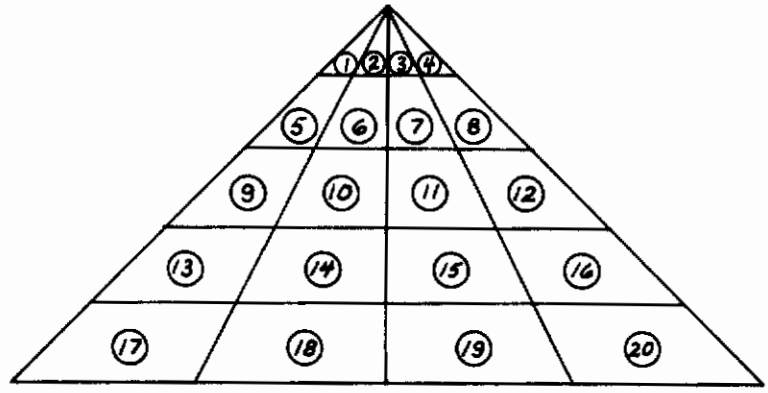

and in box ①, $\alpha_1(\xi, \eta) = \alpha$ = constant, while $\alpha_1(\xi, \eta) = 0$ outside of this region. Similarly, in the other regions, α_i = constant in box ⓘ but zero elsewhere. Formal substitution results in the equation

$$\Delta p(x, y) = \alpha_1 \mathcal{L}_{A_1}[1] + \alpha_2 \mathcal{L}_{A_2}[1] + \cdots + \alpha_{20} \mathcal{L}_{A_{20}}[1]$$

where

$$\mathcal{L}_{A_i} = 4 q_\infty \frac{\partial}{\partial x} \left\{ \iint_{S_i} \frac{d\xi\, d\eta}{\sqrt{(x-\xi)^2 - \beta^2(y-\eta)^2}} \right\} \qquad (II-10)$$

and s_j is the area of the j^{th} box. If the box lies outside of the mach lines from (x,y) then $\mathcal{L}_{A_j} = 0$. If s_j lies partially within the cross-hatched area, then its influence is to be weighted by some predetermined rule.

Thus $\mathcal{L}_{A_j}$ is a function only of the point x,y at which the pressure is to be determined, and the location ξ,η of the j^{th} box. If the pressures are assumed to be uniform in each box at the value at its centroid, then at the j^{th} position

$$\Delta p_j = \mathcal{L}_{A_{1j}} \alpha_1 + \mathcal{L}_{A_{2j}} \alpha_2 + \mathcal{L}_{A_{3j}} \alpha_3 + \cdots + \mathcal{L}_{A_{ij}} \alpha_i + \mathcal{L}_{A_{20_j}} \alpha_{20} \quad (II-11)$$

where

$\mathcal{L}_{A_{ij}} = \mathcal{L}_{A_i}$ evaluated at box j
designated by the point (x_j, y_j)

Hence the entire pressure distribution in matrix form becomes

$$\begin{bmatrix} \Delta p_1 \\ \vdots \\ \Delta p_j \\ \vdots \\ \Delta p_n \end{bmatrix} = \begin{bmatrix} \\ A_{ij} \\ \\ \end{bmatrix} \begin{bmatrix} \alpha_1 \\ \vdots \\ \alpha_i \\ \vdots \\ \alpha_n \end{bmatrix} \quad (II-12)$$

A_{ij} is just the matrix of values of $\mathcal{L}_{A_{ij}}$ and is called the aerodynamic matrix.

In a similar manner the deflection at some point x, y on the wing may be expressed in the form (see Eq. 2-55 of Ref. 4, for example)

$$w(x,y) = \iint_{\substack{wing \\ area}} c(x,y,\xi,\eta)\,\Delta p(\xi,\eta)\,d\xi\,d\eta \qquad (II-13)$$

where $c(x,y,\xi,\eta)$ is a structural influence function depending on the wing shape and boundary conditions. The change in angle of attack corresponding to this deflection would then be

$$\alpha - \alpha_o = \frac{\partial}{\partial x}\left\{ \iint_{\substack{wing \\ area}} c(x,y,\xi,\eta)\,\Delta p(\xi,\eta)\,d\xi\,d\eta \right\} \qquad (II-14)$$

This too is a linear operation, and by a procedure analogous to that for the load calculation, Eq. (II-14) may be approximated by the matrix form

$$\begin{bmatrix} \alpha_1 \\ \vdots \\ \alpha_i \\ \vdots \\ \alpha_n \end{bmatrix} - \begin{bmatrix} \alpha_{o_1} \\ \vdots \\ \alpha_{o_i} \\ \vdots \\ \alpha_{o_n} \end{bmatrix} = \begin{bmatrix} \\ \\ c_{ij} \\ \\ \\ \end{bmatrix} \begin{bmatrix} \Delta p_1 \\ \vdots \\ \Delta p_j \\ \vdots \\ \Delta p_n \end{bmatrix} \qquad (II-15)$$

$[c_{ij}]$ is the resulting matrix of structural influence coefficients

The operation corresponding to Eq. (II-6) would require left multiplication of both sides of Eq. (II-15) by $[A_{ij}]$. Then

$$\left[\ A_{ij}\ \right]\left[\alpha_j\right] = \left[\Delta p_j\right] = \left[\ A_{ij}\ \right]\left[\ c_{ij}\ \right]\left[\Delta p_j\right] + \left[\ A_{ij}\ \right]\left[\alpha_{0_i}\right] \qquad (II-16)$$

and the inverse operation implied by Eq. (II-8) becomes

$$\left[\Delta p_j\right] = \left[\left[\ I\ \right] - \left[\ A_{ij}\ \right]\left[\ c_{ij}\ \right]\right]^{-1}\left[\ A_{ij}\ \right]\left[\alpha_{0_i}\right] \qquad (II-17)$$

Here $[I]$ is the identity matrix; $[I]-[A_{ij}][c_{ij}]$ is the matrix formed by subtracting $[A_{ij}][c_{ij}]$ from $[I]$ and $\left[\,[I]-[A_{ij}]\ [c_{ij}]\,\right]^{-1}$ is its inverse.

C. AERODYNAMIC MATRIX AND OPERATOR

The structural influence coefficients, c_{ij}, are assumed to be known from a suitable structural analysis; this report presents a selection and evaluation of methods of computing the aerodynamic matrix $[A_{ij}]$. In order to accommodate an arbitrary choice of number and arrangement of elements into which the wing may be subdivided, only the aerodynamic operator $\mathcal{L}_A[\alpha]$ will be given. However, since it is eventually to be used in aeroelastic computations as just described, linear operations will be presented which convert arbitrary angle of attack distributions into local lifting pressures.

Although the example of a flexible wing was chosen to illustrate the aeroelastic problem, the result would be the same for a body. In that case, the body planform is subdivided into strips perpendicular to its long axis. The desired operator must give a linear relation between the force on a strip and the axial distribution of angle of attack. In some cases, also, the wing may be treated by a strip method. For example, a high-aspect ratio wing is sometimes analyzed as a beam rather than a plate; then only the spanwise loading need be calculated.

D. THE USE OF EXPERIMENTAL DATA

The methods prescribed in this report for determining the aerodynamic operator will be entirely theoretical. Possible empirical improvements are avoided since they may introduce large and unexpected errors when applied to new or unusual configurations. On the other hand, the designer can increase the accuracy of his load prediction by using data applicable to his configuration. Such data may be incorporated into the aeroelastic analysis by effectively substituting the experimental result for the theoretical one. Assuming that experimental pressure distributions have been obtained for some known distributions of angle of attack, then an aerodynamic matrix can be found which fits the data.

$$\left[\Delta p_j\right]_{exp.} = \left[A_{ij}\right]_{exp.}\left[\alpha_i\right]_{exp.} \qquad (II-18)$$

The unique experimental determination of the matrix $\left[A_{ij}\right]_{exp.}$ is generally impractical since it would require a number of measurements of pressure distribution equal to the number of columns of the matrix. A new linearly independent angle of attack distribution would be required for each run.

An approximate solution can be obtained from one measurement of pressure distribution (at uniform angle of attack, for example) by assuming that the pressure at a given point is most sensitive to the local angle of attack. Then let

$$\left[A_{ij} \right]_{exp.} = \left[K_{ii} \right] \left[A_{ij} \right]_{theor.} \qquad (II-19)$$

where $[K]$ is a diagonal matrix. A single measurement of pressure distribution will then suffice to determine the elements of K_{ii}. The explicit relation is

$$K_{ij} = \frac{\Delta p_{i\,exp.}}{\sum_{j=1}^{n} A_{ij\,theor.}\, \alpha_{j\,exp.}} \qquad (II-20)$$

Other approximations, based on applicable physical considerations, may be more accurate than in Eq. II-19, in some cases, and will be mentioned where appropriate. Once an experimental aerodynamic matrix has been obtained, it should supersede the purely theoretical one in making aeroelastic calculations. It should be noted, however, that the assumption of linearity is still implied.

Contrails

SECTION III

ACCURACY CRITERIA

A. STRUCTURAL DESIGN PROCEDURES

Even with the aid of high-speed computing machines, an aeroelastic analysis can be a complex and tedious process. In order to avoid losing sight of the relationship between the physical properties of a configuration and its structural performance, it is desirable to use the simplest possible method of calculating aerodynamic load without an undue sacrifice in accuracy. Aerodynamic load distributions should, therefore, be specified to an accuracy consistent with that maintained in structural design practice. Current procedures for designing aircraft structures will therefore be reviewed here to provide a basis for the formulation of a criterion for the accuracy required in calculating the distribution of aerodynamic loads.

The final structure must meet both of the following minimum requirements.

1. The structure must not yield at a specified "limit load".
2. The structure must not fail at the design "ultimate load".

The limit load is the maximum which the structure is ever expected to encounter (sometimes with a 15% margin of safety). The ultimate load is the limit load times a factor of safety usually taken as 1.5. Older types of aluminum would fail at about 1.5 times their yield, hence a structure could be designed to just meet both requirements. More modern aluminum and steel alloys fail somewhat closer to the yield point; consequently a structure using these materials which meets the ultimate strength requirement will automatically fulfill the yield specification also (Ref. 5).

A carefully designed structure is expected to just meet these requirements. If, under test, it proves either too strong or too weak it must be redesigned to save weight or to meet specifications. Sometimes

structures are deliberately designed with a negative margin. Those elements which fail during test are then strengthened until the entire structure just meets specifications.

B. EFFECT OF AERODYNAMIC LOAD DISTRIBUTION ON STRUCTURAL DESIGN

The designer of an aircraft structure knows that in a maximum load maneuver, the total lift on his configuration will equal its weight times the allowable number of "g's" acceleration. Thus, in this condition, the total force is given, and only its distribution must be determined by aerodynamic analysis or measurement. In the case of a gust, the loading depends on both the distribution of lift and its rate of change with local angles of attack.

However, although the lift distribution must therefore be accurately determined, the design of any particular element of the structure will depend on a weighted integration of all of the forces acting on the element. Hence local errors in the estimated load distribution will generally be smoothed out in the integration process. For example, integrable mathematical singularities in the theoretical lift distribution will not result in spectacular loads on structural members.

Usually, the structural designer must know the distribution of aerodynamic lift at large angles of attack as well as at moderate values. A high-speed maneuver will apply the design load at a relatively small angle of attack, but at lower speeds the aircraft may reach the design load at nearly maximum lift coefficient. The distributions of lift in these two situations may be quite different from each other. An acceptable design procedure should be based on sufficient information about the change of lift distribution at high angles of attack to be sure to design for the more critical case. Since aeroelastic analysis is at present limited to linear treatment, the effects of nonlinear phenomena, such as stall, can be only approximately estimated.

The structural design process for a given load distribution usually begins with a preliminary analysis, followed by a load test of this first design, and then by a modification as dictated by the test results.

During this process the aerodynamic load specification may also be improved as a result of wind tunnel tests. A logical procedure would thus make use of purely theoretical load distributions only for the preliminary design. Revisions of this design could then incorporate the results of wind tunnel tests to improve the specification of load distribution.

C. CRITERIA FOR ACCURACY REQUIRED IN THE SPECIFICATION OF AERODYNAMIC LOADS

If the structural designer achieves his goal, and the structure fails (or yields) exactly at the design load, then the structure incorporates any errors introduced in the specification of load distribution. Moreover, since a new design is usually similar to previous structures for which data is already available, the designer stands a good chance of attaining this result. In particular, this will be true when the structure is designed by "beefing up" the weakest members until the minimum requirements are just achieved.

However, due to variations in assembly, material properties and dimensions of members, different samples of similar built-up structures will not fail at identical loads. Some idea of the expected variation in material properties may be deduced from the specification given in Ref. 5. About a 3% difference is allowed between the minimum tensile strength acceptable to the user and the minimum guaranteed by the manufacturer. This handbook (Ref. 5) is not concerned with samples which exceed their minimum specifications; but a design based on tests of a structure which happens to be put together from overly strong components will, of course, result in generally weaker production specimens. Little data has been found on the statistical variation of strength of complex built-up structures. Some general information on the subject is described in Ref. 6.

The foregoing discussions lead to the following conclusions concerning a quantitative specification of the accuracy required in the calculation of aerodynamic load distributions.

1. The structural design process will generally involve a preliminary analysis, test, and revision during which experimental aerodynamic load data may also be acquired; hence, the initial calculation of aerodynamic load distribution, which should be applied only to the preliminary structural design, may incorporate a margin of error which will later be reduced by wind tunnel tests.

2. Even though the entire distribution of lift is computed, when actually applied in structural design the loads will be integrated over appropriate areas. Consequently, in formulating a criterion for acceptability of a proposed procedure for computing load distribution, accuracy requirements will be imposed only on the prediction of total load and centers of pressure. In keeping with the expected variations of strength among similar structures, the error in spanwise location of center of pressure of a wing panel should not exceed 3% of the maximum span of the panel. Similarly, the chordwise center of pressure should be predicted to within 3% of the maximum chord. The streamwise location of center of pressure on a body should be calculated to within 3% of the length of the body.

3. Since, in the maneuver condition, the total load is known and only its distribution remains to be determined by aerodynamic calculations, a substantial error in total lift can be tolerated. However, to avoid introducing larger errors by incorrectly distributing the load between the wing and the body, the error in total lift calculated on each component should not exceed 10% . This requirement is consistent with the 3% allowance on center of pressure error if it is assumed that one of the two components (wing or body) carries over two-thirds of the total load. Similarly, the error in gust loading corresponding to a 10% error in lift will be approximately 3% when the angle of attack induced by the gust is about one-third of the steady angle of attack. To be conservative, a 10% margin of safety should be provided for a high gust-loading condition, at least in preliminary design stages.

4. Although a 3% error in estimation of load distribution appears to be consistent with structural design requirements, the criterion must be applied with caution in certain cases. While a 3% error in net load

may be acceptable, the aerodynamic forces constitute only a portion of the total. Thus, for example, on a heavily loaded fuel-carrying wing, the aerodynamic lift may be nearly balanced by the wing's own weight. If the wing weight is 50% of its lift, a 3% error in wing lift calculation could amount to 6% or more of the net load. In such cases, experimental data and extra safety margins would probably be required.

On the other hand, a slender body with a very small camber will have some pitching moment at zero lift; hence its center of pressure will lie at infinity. In such cases a 3% error in center of pressure becomes meaningless, and an equivalent criterion must be expressed in terms of the structural load rather than the center of pressure position.

Contents

SECTION IV

WING LOAD DISTRIBUTIONS

A. GENERAL CONSIDERATIONS

1. Coordinate System

The wing is assumed to lie in the x,y plane, as shown in Fig. 1, in a uniform oncoming stream of velocity, U_∞ (Mach number M_∞) which is directed along the x -axis. Symmetry about the x,z plane is also assumed. The wing may have any small arbitrary distribution of angle of attack (symmetric about the x,z plane).

2. Governing Equations

From the conservation laws for steady irrotational flow of a perfect gas, the following linearized equation for perturbation velocity potential may be derived: (see Ref. 7 for a derivation)

$$(1-M_\infty^2)\frac{\partial^2\phi}{\partial x^2}+\frac{\partial^2\phi}{\partial y^2}+\frac{\partial^2\phi}{\partial z^2}=0 \qquad (IV-1)$$

Perturbations in velocity have been assumed small compared with U_∞ , so that the velocity components, in terms of the potential are:

$$x\ component = u+U_\infty = \frac{\partial\phi}{\partial x}+U_\infty$$

$$y\ component = v = \frac{\partial\phi}{\partial y}$$

$$z\ component = w = \frac{\partial\phi}{\partial z}$$

3. Normalizing Transformations

A linear stretching of the x coordinate by an amount

$$x = \sqrt{1-M_\infty^2}\ \bar{x} \qquad (IV-2)$$

(the Prandtl-Glauert transformation) converts Eq. (IV-1) into the three-dimensional Laplace equation. Similarly, the Ackeret transformation:

$$x = \sqrt{M_\infty^2-1}\ \bar{x} \qquad (IV-3)$$

produces a normalized wave equation

$$\frac{\partial^2 \phi}{\partial \bar{x}^2} - \frac{\partial^2 \phi}{\partial y^2} - \frac{\partial^2 \phi}{\partial z^2} = 0 \qquad (IV-4)$$

These transformations eliminate Mach number from the differential equations, and hence can be used to relate the subsonic flow over a wing to the incompressible flow over a related planform or to determine the effect of varying the Mach number of a supersonic stream.

4. Boundary Conditions

In subsonic flow, boundary conditions are applied at an infinite distance above and to the side of the wing where $\phi \to 0$ and in the plane of the wing. In supersonic flow the velocity potential is zero outside of the Mach cone bounding the disturbed region. On the surface of the wing assumed to lie in the x,y plane, the flow must follow the local slope of the wing. In the linearized approximation

$$\frac{1}{U_\infty} \left.\frac{\partial \phi}{\partial z}\right|_{z=0} = -\alpha(x,y) \qquad (IV-5)$$

where $\alpha(x,y)$ is the distribution of angle of attack. In the x,y plane, outside of the wing planform,

$$\left.\frac{\partial \phi}{\partial x}\right|_{z=0} = \text{continuous function of } z \qquad (IV-6)$$

5. Linearized Pressure Coefficient

The pressure coefficient is defined as a nondimensional difference between local pressure and free stream pressure

$$C_p = \frac{p - p_\infty}{q_\infty} \qquad (IV-7)$$

where q_∞ is the free stream dynamic pressure.

By linear theory

$$C_p = -\frac{2u}{U_\infty} = -\frac{2\left(\frac{\partial \phi}{\partial x}\right)}{U_\infty} \qquad (IV-8)$$

On a thin lifting wing at angle of attack, the expansion of the flow at a point on the upper surface will be matched by a corresponding compression at the same point on the lower surface. Hence the lifting pressure

$$\Delta C_p = C_{p_{bottom}} - C_{p_{top}} = \frac{4u}{U_\infty} = \frac{4}{U_\infty}\left(\frac{\partial \phi}{\partial x}\right)_{upper\ surface} \qquad (IV-9)$$

6. Subsonic Solutions

Solutions to the partial differential equations which satisfy the required boundary conditions are generally built up from a superposition of elementary solutions. In the subsonic case, the most commonly-used elementary solutions are the vortex and the pressure perturbation.

A differential length, $d\xi$, of a vortex of strength Γ induces at a point (x, y, z) the velocity

$$dV = \frac{\Gamma R}{4\pi\left[(x-\xi)^2+R^2\right]^{3/2}}\, d\xi \qquad (IV-10)$$

As shown on the following sketch, R is the distance from the point (x, y, z) to the axis of the vortex and $|x-\xi|$ is the distance from the differential element of the vortex to a plane through the point (x,y,z) normal to the vortex element.

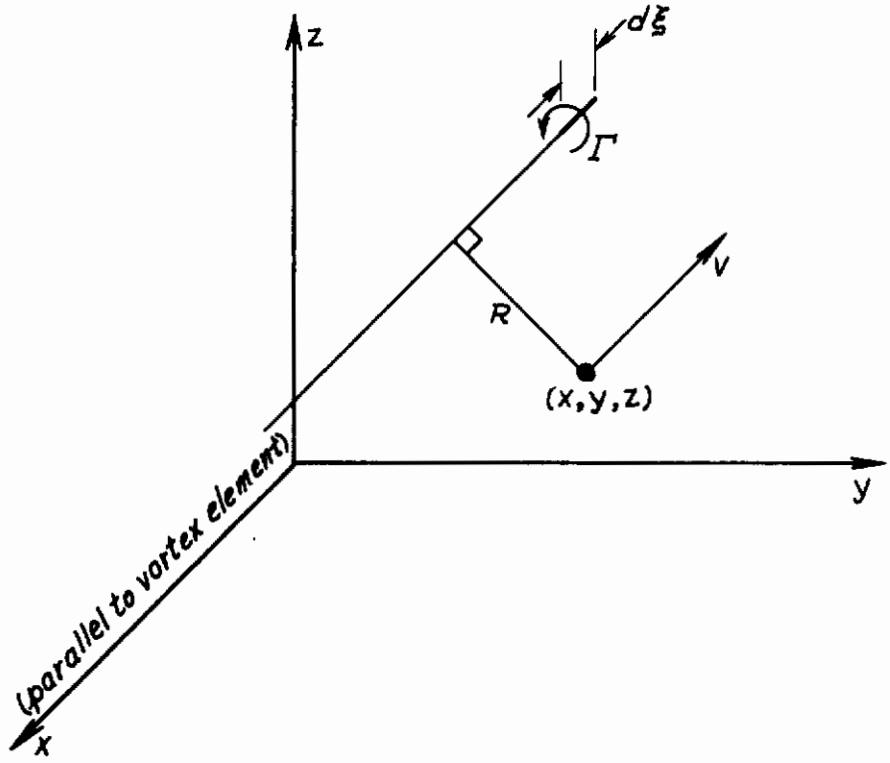

Each velocity component in a Cartesian coordinate system satisfies the Laplace equation.

As an example of the procedure of satisfying a boundary condition by a superposition of vortex solutions, consider first the vertical velocity induced at the point (x, y) by a symmetric horseshoe vortex of strength $d\Gamma$ lying in the (x, y) plane.

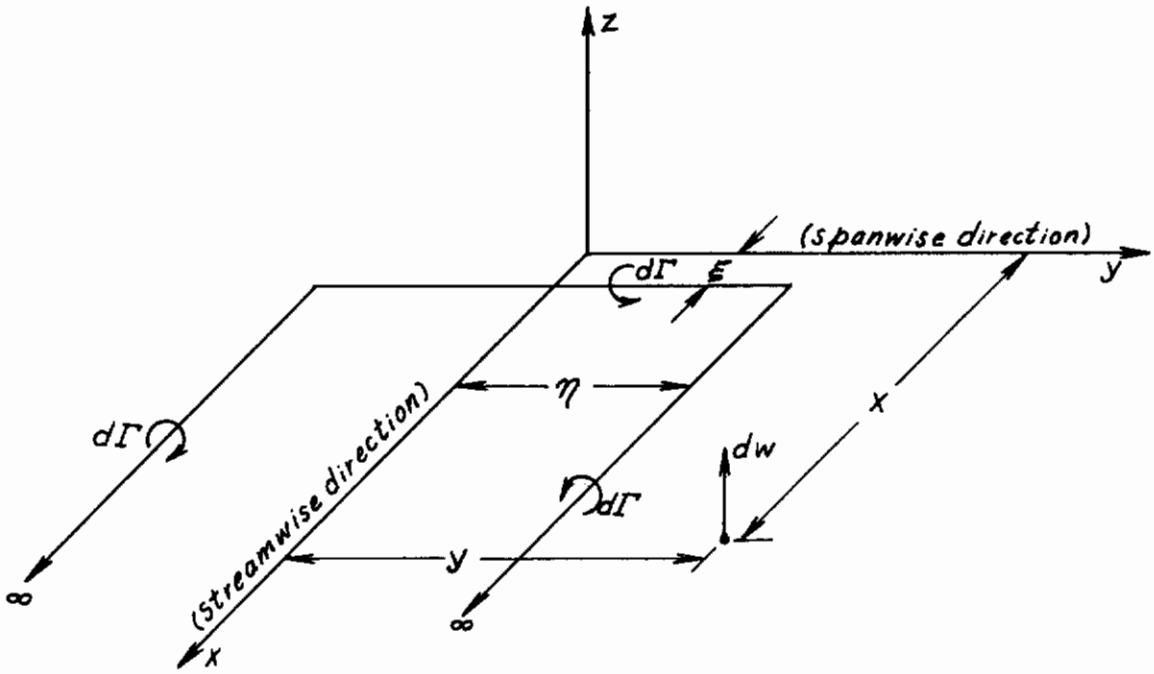

The spanwise vortex segment will induce the velocity

$$dw_{center} = \frac{d\Gamma}{4\pi} \int_{-\eta}^{\eta} \frac{(x-\xi)}{\left[(x-\xi)^2 + (y-\eta)^2\right]^{3/2}} d\eta$$

$$= \frac{d\Gamma}{4\pi(x-\xi)} \left[\frac{y-\eta}{\sqrt{(x-\xi)^2+(y-\eta)^2}} - \frac{y+\eta}{\sqrt{(x-\xi)^2+(y-\eta)^2}} \right] \qquad (IV-11)$$

Similarly, the left arm of the horseshoe $(at\ -\eta)$ will contribute the vertical velocity at (x, y)

$$dw_{-\eta} = \frac{d\Gamma}{4\pi(y-\eta)} \left[- \frac{x-\xi}{\sqrt{(x-\xi)^2 + (y+\eta)^2}} - 1 \right] \qquad (IV-12)$$

and the other arm will produce the upwash

$$dw_\eta = \frac{d\Gamma}{4\pi(y-\eta)}\left[\frac{x-\xi}{\sqrt{(x-\xi)^2+(y-\eta)^2}}+1\right] \qquad (IV-13)$$

Hence the net result of the entire horseshoe vortex is

$$dw = \frac{d\Gamma}{4\pi}\left[\frac{1}{y-\eta}\left(1+\frac{\sqrt{(x-\xi)^2-(y-\eta)^2}}{x-\xi}\right)-\frac{1}{y+\eta}\left(1+\frac{\sqrt{(x-\xi)^2+(y+\eta)^2}}{x-\xi}\right)\right] \qquad (IV-14)$$

Next, through the same station, ξ , add a large number of such symmetric horseshoe vortices of varying span and having a total strength $\frac{\partial\Gamma}{\partial\xi}$ Then the picture in the x,y plane looks as follows:

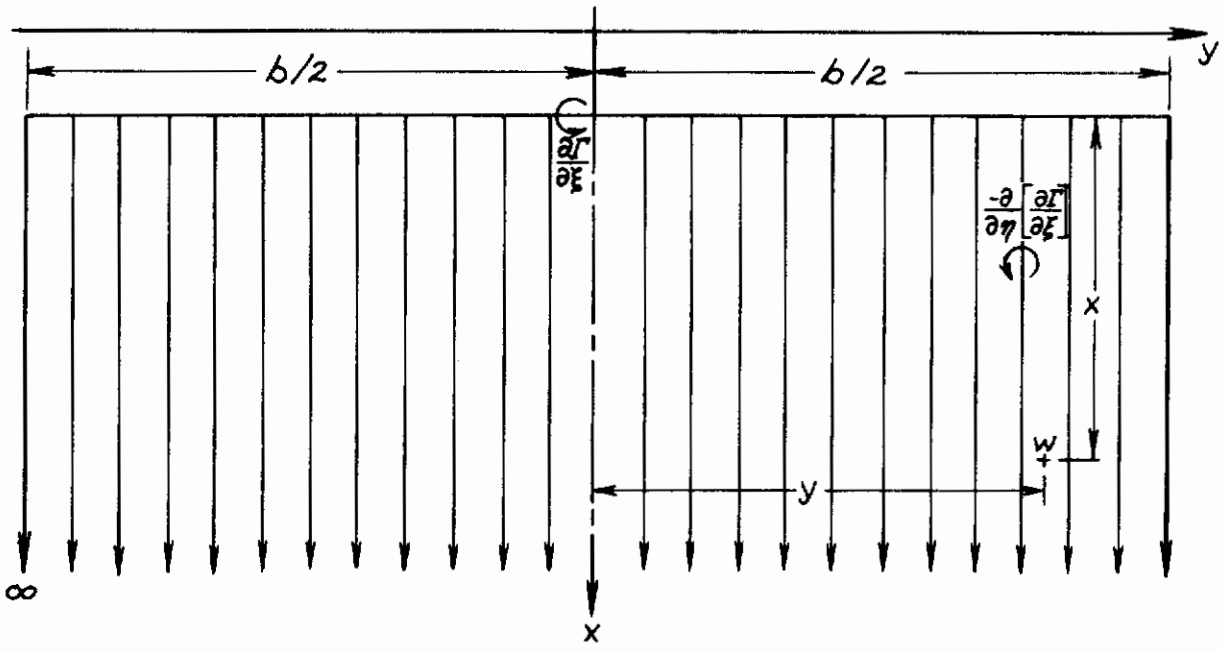

By a summation (integral) of all contributions of the form given by Eq. (IV-14) but where $d\Gamma$ is replaced by the elementary vortex of strength $-\frac{\partial}{\partial\eta}\left[\frac{\partial\Gamma}{\partial\xi}\right]$

$$\frac{\partial w(x,y)}{\partial\xi} = \frac{-1}{4\pi}\int_0^{b/2}\frac{\partial}{\partial\eta}\left(\frac{\partial\Gamma}{\partial\xi}\right)\left[\frac{1}{y-\eta}\left(1+\frac{\sqrt{(x-\xi)^2+(y-\eta)^2}}{x-\xi}\right)-\frac{1}{y+\eta}\left(1+\frac{\sqrt{(x-\xi)^2+(y+\eta)^2}}{x-\xi}\right)\right]d\eta$$

(IV-15)

And finally the planform of a wing can be covered with an array of these nets as indicated in the following sketch.

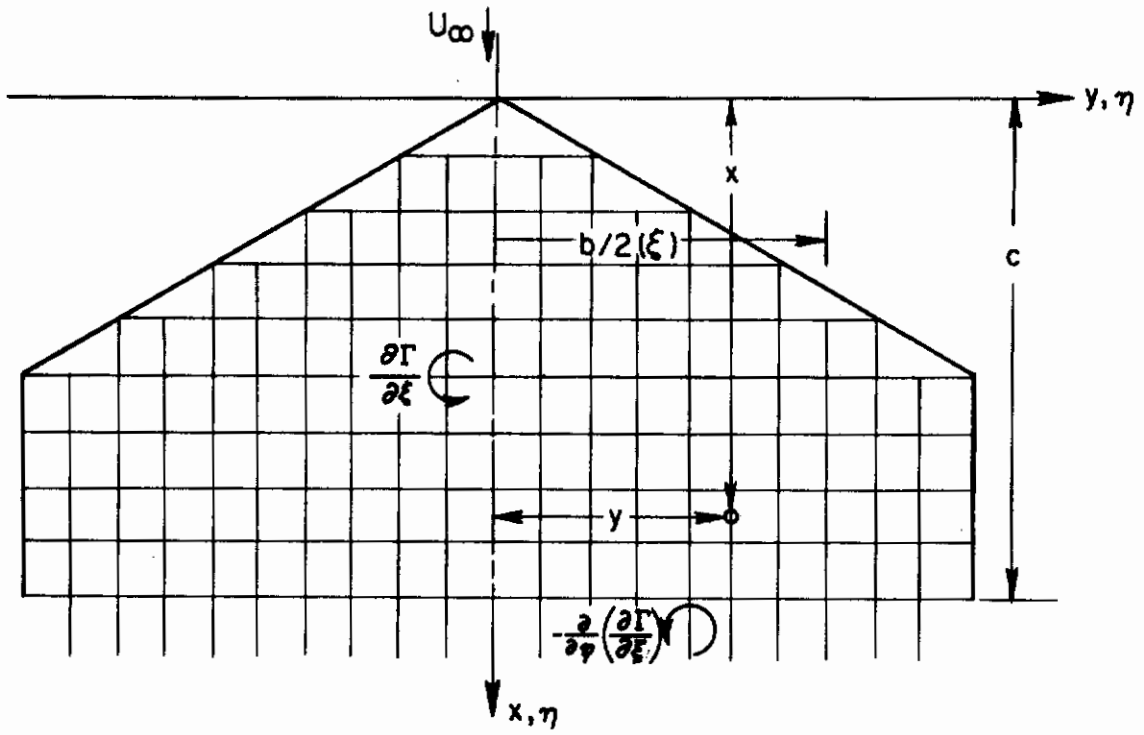

The total upwash at x, y is then

$$w(x,y) = \frac{-1}{4\pi}\int_0^c \left\{ \int_0^{\frac{b}{2}(\xi)} \frac{\partial}{\partial \eta}\left(\frac{\partial \Gamma}{\partial \xi}\right) \left[\frac{1}{y-\eta}\left(1+\frac{\sqrt{(x-\xi)^2+(y-\eta)^2}}{x-\xi}\right) - \frac{1}{y+\eta}\left(1+\frac{\sqrt{(x-\xi)^2+(y+\eta)^2}}{x-\xi}\right)\right] d\eta \right\} d\xi \qquad \text{(IV-16)}$$

This upwash is related to the wing geometry through the boundary condition of no flow through the wing surface. This condition requires that (to the linear approximation)

$$w(x,y) = -U_\infty \alpha(x,y) \qquad \text{(IV-17)}$$

where $\alpha(x,y)$ is the local slope of the wing in the streamwise direction.

The boundary conditions at $z = \infty$ and $y = \infty$ are automatically satisfied by the form of the elementary vortex solution.

The spanwise elements of vorticity constitute a vortex sheet of strength

$$\gamma(\xi,\eta) = \frac{\partial \Gamma}{\partial \xi} \qquad (IV-18)$$

which is assumed to lie in the plane of the wing. This vortex sheet produces a discontinuity in the streamwise component of velocity over the region of the x, y plane occupied by the wing planform. This component of velocity perturbation at the point ξ, η on the upper surface of the wing will be

$$u_{upper} = \frac{1}{2}\gamma(\xi,\eta)$$

An equal and opposite increment in velocity will appear on the lower surface so that the total perturbation is given by

$$\Delta u = \gamma(\xi,\eta) = \frac{\partial \Gamma}{\partial \xi} \qquad (IV-19)$$

Hence the integral equation (IV-16) may also be written

$$w(x,y) = \frac{-1}{2\pi}\int_0^c \left\{ \int_0^{\frac{b}{2}(\xi)} \frac{\partial u}{\partial \eta}\left[\frac{1}{y-\eta}\left(1+\frac{\sqrt{(x-\xi)^2+(y-\eta)^2}}{x-\xi}\right) - \frac{1}{y+\eta}\left(1+\frac{\sqrt{(x-\xi)^2+(y+\eta)^2}}{x-\xi}\right)\right] d\eta \right\} d\xi \qquad (IV-20)$$

where, by symmetry about the x -axis

$$w(x,y) = \frac{-1}{2\pi}\int_0^c \left\{ \int_{-\frac{b}{2}(\xi)}^{\frac{b}{2}(\xi)} \frac{\partial u}{\partial \eta}\left[\frac{1}{y-\eta}\left(1+\frac{\sqrt{(x-\xi)^2+(y-\eta)^2}}{x-\xi}\right)\right] d\eta \right\} d\xi \qquad (IV-21)$$

From the linear expression for pressure coefficient, Eq.(IV-9), the velocity perturbation on the upper surface is $u = \frac{U_\infty}{4}\Delta C_p$
Hence in the form given by Eq.(IV-21), the boundary conditions are to be satisfied by a superposition of pressure perturbation solutions.

7. Supersonic Solutions

The most commonly used fundamental supersonic solutions are the source and the doublet. The velocity potential for an elementary source of strength K_S is

$$\phi_S = \frac{K_S}{\sqrt{(x-\xi)^2-(y-\eta)^2-(z-\zeta)^2}} \qquad \text{(IV-22)}$$

This equation gives the velocity potential at points x, y, z generated by a source at the point ξ, η, ζ. The wave equation has been normalized to the form given in Eq. (IV-4), and corresponds to a flow at Mach number = $\sqrt{2}$. Without the normalization, the solution would be

$$\phi_S = \frac{K_S}{\sqrt{(x-\xi)^2-\beta^2(y-\eta)^2-\beta^2(z-\zeta)^2}} \qquad \text{(IV-23)}$$

where $\beta = \sqrt{M^2_\infty - 1}$

If the source lies in the plane $\zeta = 0$; then the normalized velocity potential becomes

$$\phi_S = \frac{K_S}{\sqrt{(x-\xi)^2-(y-\eta)^2-z^2}} \qquad \text{(IV-24)}$$

The vertical component, $\frac{\partial \phi}{\partial z}$, becomes

$$V_z = \frac{\partial \phi_S}{\partial z} = \frac{K_S z}{\left[(x-\xi)^2-(y-\eta)^2-z^2\right]^{3/2}} \qquad \text{(IV-25)}$$

Since V_z is antisymmetric with respect to the x,y plane, the source produces an upward component of flow above the plane and a downward flow below, thus satisfying boundary conditions typical of the thickness problem of a symmetric airfoil. Since disturbances cannot propagate forward in a supersonic flow, the flow over the top surface of an airfoil is sometimes independent of the bottom surface and then it is possible to represent the flow over a lifting wing by a superposition of source solutions.

The more obvious elementary solution for the lifting case is the doublet, which is the limit of the potential due to a source above and

one below the x,y plane as they approach each other. The doublet potential will be the vertical derivative of the source, hence for a normalized doublet of strength K_D in the x,y plane

$$\phi_D = \frac{K_D z}{\left[(x-\xi)^2 - (y-\eta)^2 - z^2\right]^{3/2}} \qquad (IV\text{-}26)$$

The corresponding vertical velocity will then be

$$V_z = \frac{\partial \phi_D}{\partial z} = \frac{K_D}{\left[(x-\xi)^2 - (y-\eta)^2 - z^2\right]^{3/2}} + \frac{3K_D z^2}{\left[(x-\xi)^2 - (y-\eta)^2 - z^2\right]^{5/2}} \qquad (IV\text{-}27)$$

which is symmetrical about $z = 0$.

To satisfy the boundary conditions in the plane of the wing, a superposition of sources or doublets may be used. The distribution of their strength is adjusted to satisfy the required boundary conditions. Thus for a distribution of doublets over the surface of a wing, the velocity potential at the point x,y,z would be $(at\ M_\infty = \sqrt{2}\,)$

$$\phi(x,y,z) = \iint_S \frac{K_D(\xi,\eta)\, z\, d\xi\, d\eta}{\left[(x-\xi)^2 - (y-\eta)^2 - z^2\right]^{3/2}} \qquad (IV\text{-}28)$$

The area of integration is the region for which the denominator is real; that is the intersection of the Mach forecone from the point x,y,z with the plane of the wing $(\zeta = 0)$ as shown below.

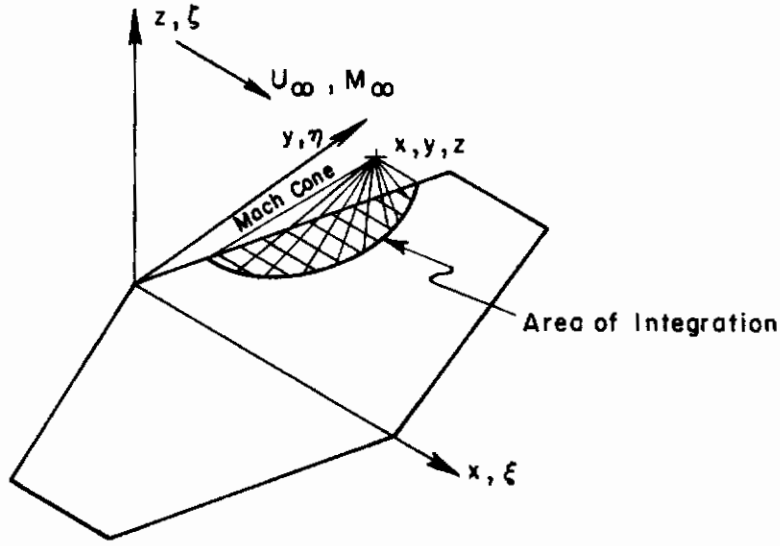

The boundary conditions require that on the wing surface

$$\left.\frac{\partial \phi(x,y,z)}{\partial z}\right|_{z=0} = \left\{\frac{\partial}{\partial z}\iint_S \frac{K_D(\xi,\eta)\, z\, d\xi d\eta}{\left[(x-\xi)^2-(y-\eta)^2-z^2\right]}\right\}_{z=0} = v_z(x;y) = -U_\infty \alpha(x,y) \qquad \text{(IV-29)}$$

where $\alpha(x,y)$ is the local slope of the wing. This integral equation for $K_D(\xi,\eta)$ has been solved directly for a few wing planforms (Ref. 7).

Similarly, source solutions may be superposed to give velocity potentials of the form (at $M_\infty = \sqrt{2}$)

$$\phi(x,y,z) = \iint_S \frac{K_S(\xi,\eta)\, d\xi\, d\eta}{\sqrt{(x-\xi)^2-(y-\eta)^2-z^2}} \qquad \text{(IV-30)}$$

The corresponding boundary condition on the top surface of the wing then becomes

$$\left.\frac{\partial \phi(x,y,z)}{\partial z}\right|_{z=0} = \left\{\frac{\partial}{\partial z}\iint \frac{K_S(\xi,\eta)\, d\xi d\eta}{\sqrt{(x-\xi)^2-(y-\eta)^2-z^2}}\right\}_{z=0} = -U_\infty \alpha(x,y) \qquad \text{(IV-31)}$$

Puckett has shown (Ref. 8), however, that this integral equation is satisfied if $K_S(\xi,\eta) = -\frac{U_\infty \alpha(\xi,\eta)}{\pi}$. Then, in the plane of the wing

$$\phi(x,y) = -\frac{U_\infty}{\pi}\iint_S \frac{\alpha(\xi,\eta)\, d\xi d\eta}{\sqrt{(x-\xi)^2-(y-\eta)^2}} \qquad \text{(IV-32)}$$

As previously mentioned, source solutions can be used to treat lift problems when the upper surface of a wing does not communicate with the lower surface, as for straight two-dimensional airfoils. Evvard (Ref. 9, 10) has extended this method to three-dimensional wings by imagining a diaphragm of unknown slope lying in the plane of the wing and preventing disturbances from one surface from propagating to the other. An additional boundary condition, zero

pressure difference, must then be applied to the diaphragm. Evvard finds that the contribution of the sources on the diaphragm to the velocity potential on the wing exactly cancels the contribution of sources on part of the wing surface, so that the boundary conditions on the top surface are all satisfied when the region of integration is modified to that shown below.

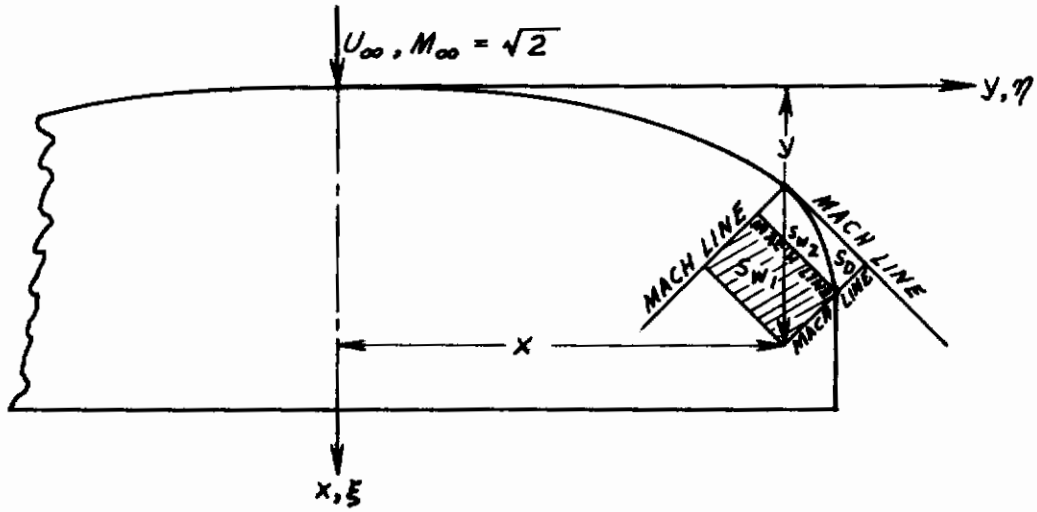

$$\phi(x,y) = -\frac{U_\infty}{\pi} \iint_{S_{W_1}} \frac{\alpha(\xi,\eta)\, d\xi\, d\eta}{\sqrt{(x-\xi)^2 - (y-\eta)^2}} \qquad \text{(IV-33)}$$

Another useful concept takes advantage of the conical similarity existing in certain regions of supersonic flow. If the boundary conditions are such that the velocity potential is a function only of $\frac{y}{x}$ and $\frac{z}{x}$, then the normalized wave equation (Eq. (IV-4)) may be reduced to the Laplace equation for the streamwise velocity.

Appropriate solutions may then be obtained by the powerful methods of complex variables. Wing pressure distributions obtained by superpositions of conical flows are given in Refs. 3 and 11. In the case of arbitrary angle of attack distribution treated here, conically similar boundary conditions are not available; hence such methods cannot be exploited.

8. Slender Wing Theory

If the wing is "slender" (low aspect ratio) as well as "thin" (small thickness ratio), then the first term of Eq.(IV-1) may be neglected since changes in ϕ with the streamwise coordinate, x, will be small compared with variations in the other directions. The remaining equation then becomes the two-dimensional Laplace equation in the cross-flow (y,z) plane. In determining solutions of this equation, functions of the x coordinate are equivalent to constants in satisfying the equation and boundary conditions in the y,z plane. Hence in such solutions each cross section of the wing is analyzed as though it were in an incompressible two-dimensional flow. Streamwise functions are used if needed to satisfy longitudinal boundary conditions.

Since the term involving Mach number does not appear, it is apparent that solutions for slender configurations hold at subsonic, transonic, and supersonic speeds. This result was first applied to low-aspect-ratio wings by Jones in Ref.12. Near $M_\infty = 1$, the first term of Eq.(IV-1) becomes negligibly small for a wider range of aspect ratio than would be true at other speeds. By writing the equation in non-dimensional form it is readily seen that, in fact, the slenderness assumption is valid when

$$\beta AR << 1$$

where $\beta = |1 - M_\infty^2|$

AR = aspect-ratio

B. HIGH ASPECT RATIO SUBSONIC WINGS

1. The Weissinger Method

Equation (IV-16), relating the upwash velocity on the wing surface to a distribution of vorticity, forms the basis of most linear subsonic lifting theories. The equation is repeated below.

$$w(x,y) = \frac{-1}{4\pi}\int_0^c \left\{ \int_0^{\frac{b}{2}(\xi)} \frac{\partial}{\partial \eta}\left(\frac{\partial \Gamma}{\partial \xi}\right) \left[\frac{1}{y-\eta}\left(1+\frac{\sqrt{(x-\xi)^2+(y-\eta)^2}}{x-\xi}\right) - \frac{1}{y+\eta}\left(1+\frac{\sqrt{(x-\xi)^2+(y+\eta)^2}}{x-\xi}\right)\right] d\eta \right\} d\xi \qquad (IV\text{-}16)$$

By equating the vertical perturbations of the flow to the local slope of the wing surface, (Eq. IV-16) becomes an integral equation for the unknown distribution of vorticity $\Gamma(\xi,\eta)$ in terms of the prescribed wing angle distribution

$$\alpha(x,y) = -\frac{w(x,y)}{U_\infty} \qquad (IV\text{-}34)$$

The incompressible case will be considered first. A Prandtl-Glauert compressibility correction will be employed later to account for Mach number effects.

Such a two-dimensional integral equation is very difficult to deal with, especially in the general case of arbitrary distribution of wing slope. Consequently, various approximations are employed to reduce the problem to a one-dimensional one. In Weissinger's lifting surface procedure, (Ref. 13), the chordwise variation of vorticity is approximated by the solution of the corresponding problem for a flat wing of infinite aspect ratio. Lawrence (Ref. 14), on the other hand, inserts the spanwise load distribution for a high aspect ratio flat wing and solves the remaining integral equation for the chordwise loading. The recommended procedure, therefore, is to use the Weissinger solution for high aspect ratio wings, and the Lawrence method, which will be described in Section IV C, for low aspect ratios. For a flat wing, both methods approach the correct loading at zero and infinite aspect ratio; hence the selection of a criterion for switching from one method to the other is not critical.

In the two-dimensional case, a vortex sheet of strength $\gamma(x) = \frac{\partial \Gamma}{\partial x}$ is assumed to lie in the plane of the wing. The flow angles induced by this

vorticity are then equated to the local slope of the wing mean camber line. The following sketch illustrates the nature of the problem:

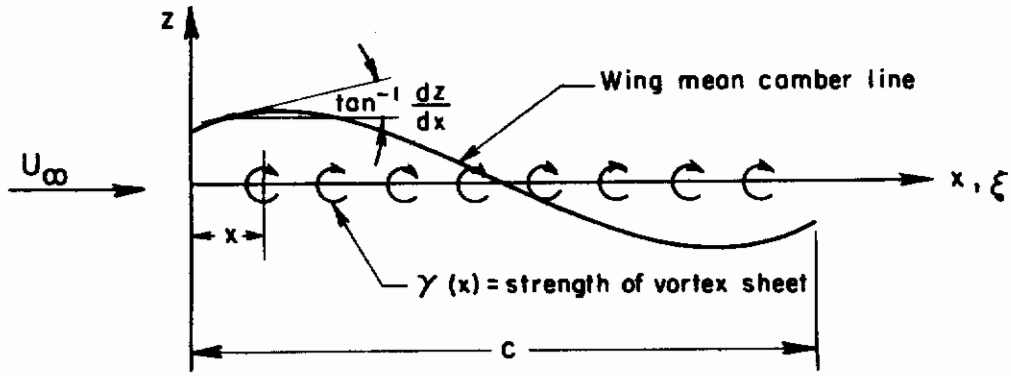

The vertical velocity induced by the distributed vorticity at $\xi = x$, $z = 0$ will be

$$w(x) = \frac{1}{2\pi}\int_0^c \frac{\gamma(\xi)\,d\xi}{\xi - x} \qquad \text{(IV-35)}$$

The boundary condition, applied in the $z=0$ plane, then requires that for a local wing slope $\frac{dz}{dx}$

$$\frac{dz}{dx} = \frac{w(x)}{U_\infty} = \frac{1}{2\pi U_\infty}\int_0^c \frac{\gamma(\xi)\,d\xi}{\xi - x} \qquad \text{(IV-36)}$$

The singularity in the integrand at the point $\xi = x$ is to be evaluated by using the Cauchy principal value.

The general solution for this equation, as given for example on page 122 of Ref. 15, is

$$\gamma(x) = \frac{2U_\infty}{\pi}\sqrt{\frac{c-x}{x}}\left[\int_0^c \frac{\frac{dz}{d\xi}}{x-\xi}\sqrt{\frac{\xi}{c-\xi}}\,d\xi + k\frac{c}{c-x}\right] \qquad \text{(IV-37)}$$

The constant of integration, k, must vanish since the vorticity is required by the Kutta condition to be zero at the wing trailing edge.

For a flat wing at angle of attack α, the boundary condition becomes

$$\frac{dz}{dx} = -\alpha$$

and Eq. (IV-37) may be integrated to give

$$\frac{\gamma(x)}{U_\infty} = 2\alpha\sqrt{\frac{c-x}{x}} \qquad \text{(IV-38)}$$

From two-dimensional airfoil theory, the lift on a unit span of the wing is proportional to the circulation, and produces a section lift coefficient of $2\pi\alpha$. Hence the angle of attack is related to the spanwise distribution of circulation by the equation

$$\frac{dL}{dy} = \rho U_\infty \Gamma = \rho U_\infty^2 \pi \alpha c$$

and thus

$$\alpha(y) = \frac{\Gamma(y)}{U_\infty \pi c} \qquad \text{(IV-39)}$$

Now, in terms of the spanwise distribution of circulation, the vorticity is given by Eq. (IV-38) as

$$\gamma(x,y) = \frac{2\Gamma(y)}{\pi c}\sqrt{\frac{c-x}{x}} \qquad \text{(IV-40)}$$

Inserting the chordwise function into the integral equation (Eq. (IV-16) gives the one-dimensional form

$$w(y) = \frac{-1}{2\pi^2 c}\int_0^c \left\{ \int_0^{\frac{b}{2}(\xi)} \sqrt{\frac{c-\xi}{\xi}}\, \frac{\partial\Gamma(\eta)}{\partial\eta} \left[\frac{1}{y-\eta}\left(1+\frac{\sqrt{(x-\xi)^2+(y-\eta)^2}}{x-\xi}\right) - \frac{1}{y+\eta}\left(1+\frac{\sqrt{(x-\xi)^2+(y+\eta)^2}}{x-\xi}\right)\right] d\eta \right\} d\xi \qquad \text{(IV-41)}$$

It is still necessary to specify a value for x in the integrand and to evaluate the remaining one-dimensional integral equation for $\Gamma(\eta)$. In his lifting surface method, Weissinger selects the three-quarter chord line as the locus at which to apply the boundary condition. That is $x = \frac{3c}{4}$. This choice will cause the approximate two-dimensional relation between local wing slope and vorticity distribution (Eq. IV-38)

to be rigorously correct not only for α =constant, but for any linear variation of α with x .

Although it is now possible to reduce Eq.(IV-41) to a one-dimensional integral equation, Weissinger indicates its solution only for the case of a rectangular wing. For a swept wing, it is more convenient to replace this spanwise integral equation by a less exact one derived by assuming that the vorticity distributed across the chord at each spanwise station is all collected into a concentrated vortex at the quarter-chord. Then when the boundary condition is applied at the three-quarter chord station, the two-dimensional (infinite wing) boundary condition is satisfied rigorously in the case of a flat wing, but no longer holds for arbitrary linear distribution of wing slope.

The geometry of the problem is illustrated in Fig. 2, where a concentrated vortex is placed on the quarter chord line which has a sweep-back angle Λ (The Weissinger "L" Method).

The strength of the bound vortex varies in an unknown manner along its length starting at zero at the right wing tip. Then at every point it is joined by an infinitesimal trailing vortex which increases the strength of the bound vortex by $d\Gamma$. The strength at the center is a maximum Γ_0 , after which the departing vortices reduce the strength to zero at the left wing tip. The loading is assumed to be symmetrical, and the bound vortex is assumed to lie in a straight line broken at the center line in the case of a swept wing. The strengths of the bound and trailing vortices are determined by requiring that at each spanwise station the downwash at the three-quarter chord point be matched to the local chordwise slope of the wing surface (mean slope if the section is cambered).* The wing slope is allowed to vary in the spanwise direction (being symmetrical about the center line, however), but at each spanwise station the wing is assumed to be at some mean angle of attack.

* The bound vortex is placed at the one-quarter chord because the two-dimensional theory indicates that this will be the moment center. Then the boundary condition is applied at the three-quarter chord to make the spanwise load correspond to the two-dimensional value in the limit of a wing of infinite span. See, for example, Chapter VIII of Ref. 16.

This matching requirement leads to an integral equation which is solved by representing the unknown vorticity distribution by a Fourier series. The coefficients of the series are determined by selecting a finite number of spanwise stations (usually 7) at which the downwash is equated to the wing slope. Then the problem reduces to that of solving the resulting linear algebraic equations for the vortex strength at the selected stations. The details of the procedure are described in Ref. 17 (as well as in Ref. 13) and are repeated below in a somewhat condensed manner.

The contribution, $-dw$, to the downwash at the point x, y due to an element of an incompressible ideal vortex of length ds is equivalent to Eq.(IV-10).

$$-dw = \frac{h\Gamma(s)\,ds}{4\pi r^3}$$

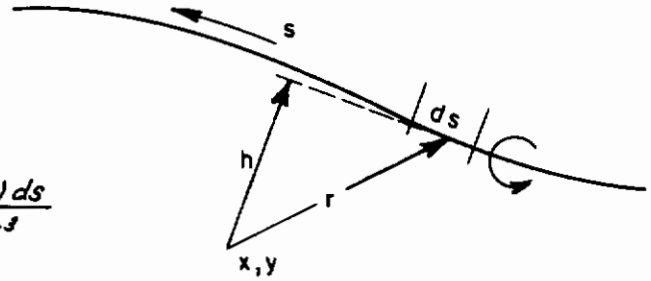

Hence the downwash at the point x, y due to the bound vortex is obtained by integrating the contributions of all of its elements giving

$$-w(x,y)_{\Gamma} = \frac{1}{4\pi}\int_{-\frac{b}{2}}^{0} \frac{(x\cos\Lambda + y\sin\Lambda)\,\Gamma(\eta)\,d\eta}{\cos\Lambda\left[(x-|\eta|\tan\Lambda)^2+(y-\eta)^2\right]^{\frac{3}{2}}} + \frac{1}{4\pi}\int_{0}^{\frac{b}{2}} \frac{(x\cos\Lambda - y\sin\Lambda)\,\Gamma(\eta)\,d\eta}{\cos\Lambda\left[(x-|\eta|\tan\Lambda)^2+(y-\eta)^2\right]^{\frac{3}{2}}} \qquad (IV\text{-}42)$$

The contribution from each trailing vortex is readily evaluated since the strength is constant. On the right side of the wing, for example,

$$-dw = -\frac{d\Gamma(\eta-y)}{4\pi}\int_{-\infty}^{x-\eta\tan\Lambda} \frac{ds}{\left[s^2+(\eta-y)^2\right]^{\frac{3}{2}}} = -\frac{d\Gamma}{4\pi(\eta-y)}\left[\frac{x-\eta\tan\Lambda}{\sqrt{(x-\eta\tan\Lambda)^2+(\eta-y)^2}}+1\right] \qquad (IV\text{-}43)$$

The downwash due to the entire trailing vortex system therefore becomes

$$-w(x,y)_{d\Gamma} = \frac{1}{4\pi}\int_{-\frac{b}{2}}^{\frac{b}{2}} \frac{1}{y-\eta}\left[1+\frac{x-|\eta|\tan\Lambda}{\sqrt{(x-|\eta|\tan\Lambda)^2+(y-\eta)^2}}\right]\Gamma'(\eta)\,d\eta \qquad \text{(IV-44)}$$

The total downwash due to all vortices results from summing the parts expressed in Eqs. (IV-42 and IV-44). If, in addition, the expressions in Eq. (IV-42) are integrated by parts, the result may be written

$$-w(x,y) = \frac{1}{4\pi}\int_{-\frac{b}{2}}^{\frac{b}{2}} \frac{\Gamma'(\eta)d\eta}{y-\eta} + \frac{1}{4\pi}\int_{-\frac{b}{2}}^{0}\left[\frac{\sqrt{(x+\eta\tan\Lambda)^2+(y-\eta)^2}}{(x+y\tan\Lambda)(y-\eta)} - \frac{1}{y-\eta}\right.$$

$$\left. + \frac{2\tan\Lambda\sqrt{x^2+y^2}}{x^2-y^2\tan^2\Lambda}\right]\Gamma' d\eta + \frac{1}{4\pi}\int_{0}^{\frac{b}{2}}\left[\frac{\sqrt{(x-\eta\tan\Lambda)^2+(y-\eta)^2}}{(x-y\tan\Lambda)(y-\eta)} - \frac{1}{y-\eta}\right]\Gamma'(\eta)d\eta \qquad \text{(IV-45)}$$

Now evaluating at the 3/4 chord line, where

$$x = \frac{c}{2} + |y|\tan\Lambda$$

the nondimensional equation for the downwash distribution is given by

$$-\frac{w(y)}{U} = \frac{1}{\pi}\int_{-1}^{1}\frac{G'(\tau)\,d\tau}{t-\tau} + \frac{\frac{b}{c}}{2\pi}\int_{-1}^{1} L(t,\tau)G'(\tau)dt \qquad \text{(IV-46)}$$

where $\tau = \frac{\eta}{\left(\frac{b}{2}\right)}$; $t = \frac{y}{\left(\frac{b}{2}\right)}$; $G = \frac{\Gamma}{b\,U_\infty}$; and on the right side of the wing where $t > 0$

$$L(t,\tau) = \frac{1}{\frac{b}{c}(t-\tau)}\left[\frac{\sqrt{\left[1+\frac{b}{c}(t+\tau)\tan\Lambda\right]^2+\frac{b^2}{c^2}(t-\tau)}}{1+2\frac{b}{c}t\tan\Lambda} - 1\right] + \frac{2\tan\Lambda\sqrt{\left[1+\frac{b}{c}t\tan\Lambda\right]^2+\frac{b^2t^2}{c^2}}}{1+2\frac{b}{c}t\tan\Lambda} \quad \cdots \tau \leq 0$$

$$L(t,\tau) = \frac{1}{\frac{b}{c}(t-\tau)}\left[\sqrt{\left[1+\frac{b}{c}(t-\tau)\tan\Lambda\right]^2+\frac{b^2}{c^2}(t-\tau)^2} - 1\right] \qquad \tau \geq 0$$

$\frac{w}{U}(t)$ on the left half of the wing may be found by symmetry with the right side. It may be noted that the expression for $L(t,\tau)$ for $\tau \leq 0$ differs in a sign within the last term from the expression given by Weissinger in Ref. 13. Weissinger's equation appears to be incorrect. The result given here agrees with that of De Young (Ref. 17), which, also has a misprint, at this point; the condition $\eta \leq 0$ being written $\eta \leq 0$

2. Computation of Spanwise Load

Equation (IV-46) is an integral equation expressing $G(\tau)$ in terms of prescribed values of $\frac{w}{U_\infty}(t)$. Weissinger solves it numerically by replacing $G(\tau)$ by the Fourier series

$$G(\phi) = \sum_{\mu=1}^{m} a_\mu \sin \mu\phi \qquad \text{(IV-47)}$$

where

$$\cos\phi = \tau$$

and, by the usual formula for Fourier coefficients

$$a_\mu = \frac{2}{\pi}\int_0^\pi G(\phi) \sin\mu\phi \, d\phi$$

Unfortunately, the unknown function $G(\phi)$ appears in the integral for determining a_μ . This difficulty is resolved by employing Multhopp's numerical integration formula (Ref. 18) which reads

$$\int_{-1}^{1} f(\eta)\, d\eta = \frac{\pi}{m+1}\sum_{n=1}^{m} f(\eta_n) \sin\theta_n \qquad \text{(IV-48)}$$

where

$$\theta_n = \frac{n\pi}{m+1} \quad ; \quad \eta_n = \cos\theta_n$$

In other words, the function $f(\eta)$ is evaluated at m points in the interval from $-1 \leq \eta \leq 1$, and the integral is (approximately) the sum of these values times appropriate weighting factors.

Using this formula on the function $G(\phi) \sin \mu \phi$ produces the following result for the coefficients a_μ

$$a_\mu = \frac{2}{m+1} \sum_{n=1}^{m} G(\theta_n) \sin \mu \theta \qquad (IV\text{-}49)$$

Then substituting these values for a_μ into Eq.(IV-47) gives

$$G(\phi) = \frac{2}{m+1} \sum_{n=1}^{m} G(\theta_n) \sum_{\mu=1}^{m} \sin \mu \theta_n \sin \mu \phi \qquad (IV\text{-}50)$$

By differentiating

$$\frac{dG(\phi)}{d\phi} = G'(\phi) = \frac{2}{m+1} \sum_{n=1}^{m} G(\theta n) \sum_{\mu=1}^{m} \mu \sin \mu \theta n \cos \mu \phi \qquad (IV\text{-}51)$$

Now Eq.(IV-46) can be integrated (with the aid of a trapezoidal integration formula) since the unknown function $G_i'(\tau)$ can be expressed through Eq.(IV-51) in terms of the m unknown constants $G_n(\theta_n)$. The result, for a symmetric wing at station ν is

$$-\left(\frac{w}{U}\right)_\nu = \left(2b_{\nu\nu} + \frac{b}{c_\nu} \bar{g}_{\nu\nu}\right) G(\theta_\nu) - \sum_{n \neq \nu}^{\frac{m+1}{2}} \left(2B_{\nu n} - \frac{b}{c_\nu} \bar{g}_{\nu n}\right) G_n(\theta_n) \qquad (IV\text{-}52)$$

$$\nu = 1, 2, 3, \ldots \frac{m+1}{2}$$

Here

$$b_{\nu\nu} = \frac{m+1}{4\sin\theta_\nu}$$

$$b_{\nu n} = \frac{\sin\theta_n}{(\cos\theta_n - \cos\theta_\nu)} \frac{1-(-1)^{n-\nu}}{2(m+1)} \qquad n \neq \nu$$

$$\bar{g}_{\nu n} = \frac{-1}{2(M+1)} \sum_{\mu=0}^{\frac{M-1}{2}} \bar{f}_{n\mu} \left(L_{\nu\mu} - L_{\nu, M+1-\mu}\right)$$

$$B_{\nu n} = \begin{cases} b_{\nu n} + b_{\nu, m+1-n} & n \neq \frac{m+1}{2} \\ b_{\nu n} & n = \frac{m+1}{2} \end{cases}$$

M = arbitrary integer defining the number of subdivisions employed in the trapezoidal integration formula of Multhopp.

$$\left.\begin{aligned} \bar{f}_{n\mu} &= 2f_{n\mu} : \quad n \neq \tfrac{m+1}{2}, \ \mu \neq 0 \\ &= f_{n\mu} : \quad n = \tfrac{m+1}{2}, \ \mu \neq 0 \\ &= f_{n\mu} : \quad n \neq \tfrac{m+1}{2}, \ \mu = 0 \\ &= \frac{f_{n\mu}}{2} : \quad n = \frac{m+1}{2}, \ \mu = 0 \end{aligned}\right\} \qquad \text{(IV-53)}$$

$$f_{n\mu} = \frac{2}{m+1} \sum_{\mu_1=1,3,5}^{m} \mu_1 \sin\mu_1\theta_n \cos\mu_1\theta_\mu \qquad \text{(IV-54)}$$

$$L_{\nu\mu} - L_{\nu, M+1-\mu} = \frac{1}{\frac{b}{c_\nu}(\tau_\nu - \tau_\mu)} \left[\sqrt{\left[1 + \frac{b}{c_\nu}(\tau_\nu - \tau_\mu)\tan\Lambda\right]^2 + \left(\frac{b}{c_\nu}\right)^2 (\tau_\nu - \tau_\mu)^2} - 1\right]$$

$$- \frac{1}{\frac{b}{c_\nu}(\tau_\nu + \tau_\mu)} \left[\frac{\sqrt{\left[1 + \frac{b}{c_\nu}(\tau_\nu - \tau_\mu)\tan\Lambda\right]^2 + \left(\frac{b}{c_\nu}\right)^2 (\tau_\nu + \tau_\mu)^2}}{1 + 2\frac{b}{c_\nu}\tau_\nu \tan\Lambda} - 1\right] - \frac{2\tan\Lambda\sqrt{\left(1 + \frac{b}{c_\nu}\tau_\nu\tan\Lambda\right)^2 + \left(\frac{b}{c_\nu}\tau_\nu\right)^2}}{1 + 2\frac{b}{c_\nu}\tau_\nu\tan\Lambda} \qquad \text{(IV-55)}$$

Also

$$\tau_\nu = \cos\left(\frac{\nu\pi}{m+1}\right)$$

$$\tau_\mu = \cos\left(\frac{\mu\pi}{M+1}\right)$$

$$\theta_n = \frac{n\pi}{m+1}$$

$$\theta_\nu = \frac{\nu\pi}{m+1}$$

$$\theta_\mu = \frac{\mu\pi}{M+1}$$

Although the final result Eq.(IV-52) appears to be fairly complicated, the equations break down into a reasonable number of simple relations which may be readily programmed for machine computation. To determine a wing loading distribution, values of $G(\theta_\nu)$ must first be determined by satisfying Eq.(IV-52) at $\frac{m+1}{2}$ points. The points fall at spanwise locations $\tau_\nu = \cos\frac{\nu\pi}{m+1} = \frac{y_\nu}{b/2}$ where $\theta_\nu = \frac{\nu\pi}{m+1}$. Generally, $m = 7$ is sufficient to establish an accurate loading curve. In that case, Eq.(IV-52) will produce four simultaneous linear equations relating the known slope of the wing $\left(\frac{w}{U}\right)_\nu$ at the spanwise locations $\tau = .924; .707; .383; 0$ to the corresponding unknowns

$$G\left(\frac{\pi}{8}\right) ; \quad G\left(\frac{\pi}{4}\right) ; \quad G\left(\frac{3\pi}{8}\right) ; \quad G\left(\frac{\pi}{2}\right)$$

The section lift coefficient, C_ℓ , is then given by

$$C_\ell(\tau_\nu) = \frac{2bG(\theta_\nu)}{c(\tau_\nu)} \qquad \text{(IV-56)}$$

where the lift on the section (per unit span) is $\ell = C_\ell \frac{\rho_\infty}{2} U_\infty^2 c$. If the lift is desired at intermediate points, then Eq.(IV-50) may be used to give $G(\phi)$ for arbitrary ϕ where $t = \cos\phi = \frac{y}{b/2}$.

The numerical procedure given above follows that of Ref. 17, which preceded the widespread use of high-speed computing machines. Although this method can be readily programmed (a FORTRAN listing

is given in Appendix A), other numerical solutions of Eq. (IV-41) might be more convenient. For example, if $G'(\tau)$ is assumed to be an unknown constant over a small interval $\Delta\tau$, then the integrations yield algebraic functions which may be evaluated at any desired number of points. The ability of high-speed computing machines to solve large numbers of simultaneous linear equations makes feasible the numerical determination of the required constant values of $G'(\tau)$. Such a procedure forms the basis of a machine program for calculating aeroelastic wing loads developed by Mason (Ref. 19).

The basic Weissinger method, as described here, does not specify the number of spanwise stations at which the downwash is to be matched to the wing slope. If seven spanwise locations are used (the root section plus three on either side), then the charts given by De Young and Harper in Ref. 17 may be used to simplify the computations. For many cases, seven stations are sufficient. Weissinger, for example, finds no advantage in using fifteen stations on a swept rectangular wing of aspect ratio 5. However, on wings with discontinuous twist, such as would appear with deflection of a partial-span flap, more stations may be required. Alternatively, the coefficients associated with the seven-station solution may be altered to account for the spanwise discontinuities. The latter procedure is adopted in Ref. 20.

3. Chordwise Load Distribution

The Weissinger "L" method gives only the spanwise loading on flat wings and assumes that the two-dimensional value is $C_\ell = 2\pi\alpha$. To determine the local pressure on an arbitrarily cambered and twisted wing it is necessary to establish also:

a. The chordwise distribution of the lift on a given section as a function of the local camber distribution; and,

b. A definition of angle of attack of a cambered airfoil section to be used to establish the proper local boundary conditions in the Weissinger procedure. That is, in Eq. (IV-46), $w(y) = -U\alpha(y)$, where $\alpha(y)$ must be defined in the case of a cambered wing.

The two properties, chordwise load distribution and $\alpha(y)$ are to be determined from the corresponding characteristics of a two-dimensional

cambered airfoil. Examining first the chordwise load distribution, let

$$\Delta C_p = \Delta C_{p_{2\text{-}dim}} \times f(y) \qquad (IV\text{-}57)$$

Now by integrating this equation across the wing chord, the spanwise loading is obtained.

$$\int_{L.E.}^{T.E.} \Delta C_p \, dx = c\, C_\ell(y)_{3\text{-}dim} = c\, C_\ell(y)_{2\text{-}dim} \times f(y)$$

Hence

$$f(y) = \frac{C_{\ell\,3\text{-}dim}}{C_{\ell\,2\text{-}dim}}$$

and the pressure distribution becomes

$$\Delta C_{p\,2\text{-}dim} \frac{C_{\ell\,3\text{-}dim}}{C_{\ell\,2\text{-}dim}} = \Delta C_p \qquad (IV\text{-}58)$$

The three-dimensional spanwise loading is obtained from Eq.(IV-56), while the solution of the two-dimensional problem was previously given by Eq.(IV-37). From that result for a wing of chordwise slope $\frac{dz}{dx}$

$$\Delta C_{p_{2\text{-}dim}} = 2\frac{\gamma(x)}{U_\infty} = \frac{4}{\pi}\sqrt{\frac{c-x}{x}}\int_0^c \frac{\frac{dz}{d\xi}}{x-\xi}\sqrt{\frac{\xi}{c-\xi}}\, d\xi \qquad (IV\text{-}59)$$

The spanwise loading is determined by integrating this expression across the wing

$$c\, C_{\ell\,2\text{-}dim} = \int_{L.E.}^{T.E.} \Delta C_{p_{2\text{-}dim}}\, dx = 2\pi c(y)\alpha(y) \qquad (IV\text{-}60)$$

By equating the spanwise loading to the form assumed in the derivation of the Weissinger equations, an effective $\alpha(y)$ is obtained. In Eq.(IV-60), the chord on the left side of the equation is the reference value used in defining the span load coefficient C_ℓ ; while $c(y)$ on the right is the local chord.

To illustrate the procedure, consider the flat two-dimensional airfoil at angle of attack α. Then $\frac{dz}{d\xi} = -\alpha$, and Eq. (IV-59) gives

$$\frac{\gamma(x)}{U_\infty} = 2\alpha\sqrt{\frac{c-x}{x}}$$

The distribution of lifting pressure over the chord is

$$\Delta p = \rho U_\infty \gamma(x) = 2\rho U_\infty^2 \alpha \sqrt{\frac{c-x}{x}} \qquad \text{(IV-61)}$$

Integrating across the chord gives the spanwise loading

$$\frac{dL}{dy} = \rho U_\infty^2 \alpha \pi c \qquad \text{(IV-62)}$$

or in coefficient form

$$c_\ell = \frac{dL}{dy} \times \frac{1}{\frac{\rho}{2} U_\infty^2 c} = 2\pi\alpha \qquad \text{(IV-63)}$$

As an additional example, the lift distribution will be calculated for an indicial angle of attack as illustrated in the following sketch. This solution may be useful in the construction of an aerodynamic matrix.

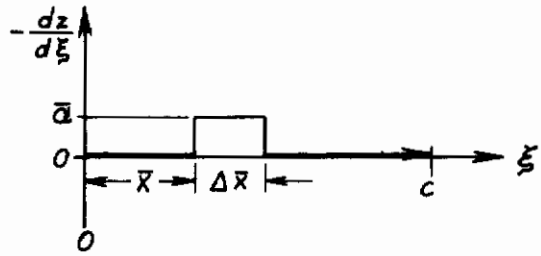

$$\left.\begin{aligned} \frac{dz}{d\xi} &= 0 && 0 \leqq \xi < x \\ \frac{dz}{d\xi} &= -\bar{\alpha} && \bar{x} \leqq \xi \leqq \bar{x} + \Delta\bar{x} \\ \frac{dz}{d\xi} &= 0 && \bar{x} + \Delta\bar{x} < \xi \leqq c \end{aligned}\right\} \qquad \text{(IV-64)}$$

The equation of the vorticity distribution Eq.(IV-59), becomes, in this case,

$$\gamma(x) = -\frac{2U_\infty}{\pi}\sqrt{\frac{c-x}{x}}\,\bar{\alpha}\left[\int_{\bar{x}}^{\bar{x}+\Delta\bar{x}} \frac{1}{x-\xi}\sqrt{\frac{\xi}{c-\xi}}\,d\xi\right] \tag{IV-65}$$

which gives, on integration,

$$\gamma(x) = \frac{2U_\infty\bar{\alpha}}{\pi}\left\{\sqrt{\frac{c-x}{x}}\left[\sin^{-1}\left(\frac{2\bar{x}+2\Delta\bar{x}-c}{c}\right)-\sin^{-1}\left(\frac{2\bar{x}-c}{c}\right)\right]\right. \tag{IV-66}$$

$$\left.+\ln\left|\frac{2\sqrt{cx-x^2}\sqrt{c\bar{x}-\bar{x}^2}+cx+(c-2x)\bar{x}}{2\sqrt{cx-x^2}\sqrt{c(\bar{x}+\Delta\bar{x})+(\bar{x}+\Delta\bar{x})^2}+cx+(c-2x)(\bar{x}+\Delta\bar{x})}\times\frac{\bar{x}+\Delta\bar{x}-x}{\bar{x}-x}\right|\right\}$$

The pressure difference between corresponding points on lower and upper wing surfaces is then given by

$$\Delta p = \rho U \gamma(x) \tag{IV-67}$$

and the corresponding pressure coefficient is

$$\Delta C_p = \frac{\Delta p}{\frac{\rho}{2}U_\infty^2} = 2\frac{\gamma(x)}{U_\infty} \tag{IV-68}$$

Now the effective angle of attack of each spanwise section may be calculated from Eq.(IV-60) and the chordwise pressure distribution obtained from Eq.(IV-58) where $C_{\ell\,3\text{-}dim}$ is the spanwise lift coefficient given by the Weissinger theory; and $\Delta C_p(x)_{2\text{-}dim}$ and $C_\ell = \frac{1}{c}\int_0^c \Delta C_p(x)_{2\text{-}dim}\,dx$ are determined by the two-dimensional theory just presented.

4. Effects of Compressibility

Compressibility may be accounted for by application of the Prandtl-Glauert rule as indicated in Ref. 17. For Mach numbers below that for which sonic speeds first appear on the airfoil, the linearized potential flow equation may be applied to indicate the effect of Mach number on pressure distribution. From this equation:

$$(1-M_\infty^2)\frac{\partial^2\phi}{\partial x^2}-\frac{\partial^2\phi}{\partial y^2}-\frac{\partial^2\phi}{\partial z^2}=0 \tag{IV-69}$$

it is apparent that increasing the x-dimension of the wing by the factor $\frac{1}{\sqrt{1-M_\infty^2}}$ will eliminate the Mach number from the equation.

Further, since the linearized pressure coefficient is proportional to $\frac{\partial \phi}{\partial x}$, the pressures should also be increased everywhere by this factor. Thus at Mach number M_∞ the pressure at a point x, y is given by

$$c_p(x,y) = \frac{c_{p_0}}{\sqrt{1-M_\infty^2}} \left(\frac{x}{\sqrt{1-M_\infty^2}}, y \right) \qquad (IV\text{-}70)$$

where c_{p_0} is the pressure coefficient at $M_\infty = 0$ at the corresponding point $\left(\frac{x}{\sqrt{1-M_\infty^2}}, y\right)$ of a wing whose planform has been altered by increasing its chordwise dimensions by the factor $\frac{1}{\sqrt{1-M_\infty^2}}$. The angle of attack distribution $\alpha(x,y)$ transforms to $\alpha\left(\frac{x}{\sqrt{1-M_\infty^2}}, y\right)$. Fig. 3 illustrates the effect of the transformation in a typical wing planform.

Since the transformed wing will have a smaller aspect ratio than the actual planform, it may be desirable to calculate its pressure distribution by the method given in Section IVC rather than by the Weissinger procedure. The low aspect ratio theory generally becomes applicable for any wing planform as $M_\infty \to 1$ since the aspect ratio of the transformed wing is smaller than that of the actual wing by a factor of $\frac{1}{\sqrt{1-M_\infty^2}}$.

5. Summary of Computational Procedure

The calculation of the pressure distribution on a wing of arbitrary twist and camber may be reduced to the following steps:

a. Convert the wing planform to an "equivalent" wing at $M_\infty = 0$ by elongating the streamwise coordinates by the factor $\frac{1}{\sqrt{1-M_\infty^2}}$

b. Subdivide the transformed wing span into m strips whose centers lie at the stations $\tau_n = \cos \frac{n\pi}{m+1}$, $n = 1, 2, 3, \ldots m$

c. At each strip find an effective angle of attack, $\alpha(\tau_n)$ from the two-dimensional analysis. That is, Eq.(IV-59) gives $\gamma(x, \tau_n)$ for any prescribed distribution of wing slope $\frac{dz}{d\xi}(\xi, \tau_n)$; and Eq.(IV-68) the corresponding chordwise pressure distribution, $\Delta c_p(x, \tau_n)$. Then the effective angle of attack at section τ_n is computed from Eq.(IV-60).

d. Solve the integral equation (IV-46) using the effective angle distribution $\alpha(\tau_n) = \frac{w(\tau_n)}{U_\infty}$. A FORTRAN program for carrying out this part of the process is given in Appendix A.*

e. Find the spanwise loading in coefficient form from Eq. (IV-56). This step is also included in the given FORTRAN program.

f. Calculate the local pressure coefficients for the transformed wing using Eq. (IV-58). In this equation $\Delta C_p(x)_{2\text{-}dim}$ and its integral $c_{\ell\ 2\text{-}dim}$ have been obtained in Step (c). The three-dimensional section lift coefficient, $c_{\ell\ 3\text{-}dim}$, is available from Step (e).

g. Apply the Mach number correction given by Eq. (IV-70). The quantity $c_{p_o}\left(\frac{x}{\sqrt{1-M_\infty^2}}, y\right)$ is the result obtained in Step (f) for the transformed wing, while the operation described by Eq. (IV-70) converts the result to the physical wing at the flight Mach number.

6. Comparison with Experiment

In order to check the range of validity of the Weissinger procedure, theoretical predictions of total lift and center of pressure have been compared with available experimental data for a variety of geometric parameters and flight conditions. Figures 4 - 9 show comparisons of measured lift curve slope (at zero angle of attack) as a function of aspect ratio with experimental data taken from Refs. 21 - 27. The use of the coordinates $\beta \frac{dc_L}{d\alpha}$ and βAR (where $\beta \sqrt{1-M_\infty^2}$) eliminates the need for separate curves at each Mach number. The wing planform is defined by the aspect ratio (AR), taper ratio (TR) and sweepback angle, $\Lambda_{L.E}$, of the leading edge. All wings have symmetrical trapezoidal shapes as sketched below.

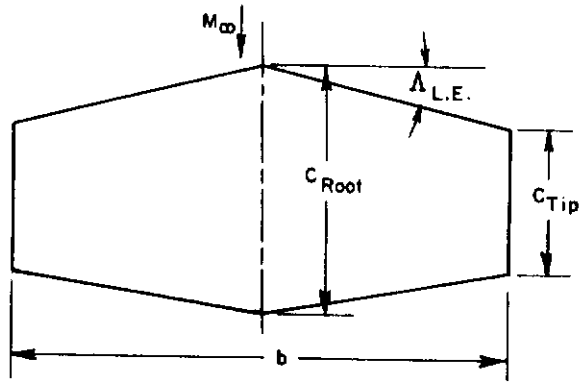

* Numerical computation reported here have been carried out, in part, at the Computation Center, Mass. Institute of Technology.

Then the aspect ratio = $\frac{2b}{c_{root} + c_{tip}}$; and the taper ratio = $\frac{c_{tip}}{c_{root}}$

The wings are also symmetric in thickness (no camber), with thickness ratios $\left(\frac{t}{c}\right)$ = $\frac{\text{maximum thickness}}{\text{chord}}$ up to about .15.

The only variable flight condition considered was the Mach number which ranged from 0 to .96. The data were taken from wind tunnel tests in which various Reynolds numbers were encountered. It has been assumed, however, that the lift is insensitive to Reynolds number in these experiments. The plots show generally good agreement between experiment and theory. The limitations of the theory implied by this comparison and other experimental checks will be discussed in the next section (Sec. IV)

Figures 10 - 16 show plots of predicted and experimental streamwise center of pressure. The ordinate in each plot is the ratio of the distance $\frac{x_{c.p.}}{c_{root}}$ where $x_{c.p.}$ is measured from the foremost point of the wing to the center of pressure; and c_{root} is the wing root chord (see sketch below), The center of pressure position is given for zero angle of attack, but the experimental values are actually obtained from the initial slopes of the lift and moment curves, since the ratio of pitching moment to lift, from which $x_{c.p.}$ is derived, is indeterminate at $\alpha = 0$

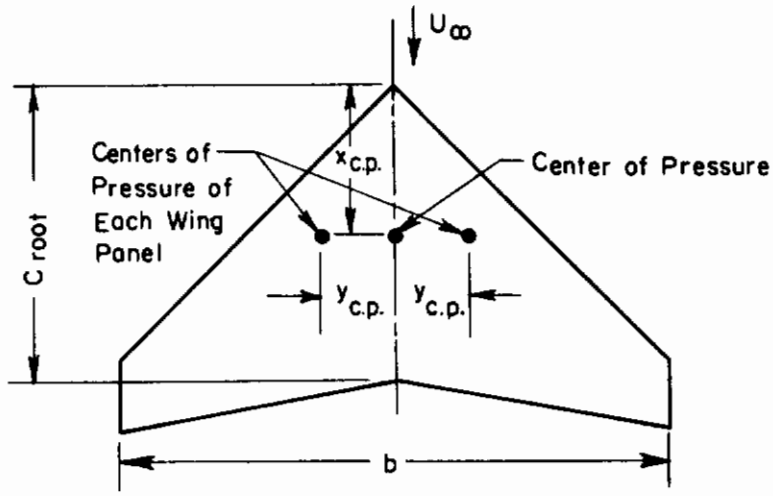

On Figs. 17 to 19, the theoretical spanwise center of pressure on an individual wing panel is compared with the experiments of Refs. 26. The plotted parameter, $\frac{y_{c.p.}}{b/2}$, is indicated on the above sketch.

The lift and center of pressure positions give only an over-all indication of the accuracy of a load distribution theory. Obviously, many distributions are possible with the same values for these integrated properties. A comparison of theoretical and experimental spanwise loading is shown in Fig. 20. The experimental data were obtained from Ref. 28.

In order to assess the effect of angle of attack on the load distribution experimental curves are presented of lift coefficient, and center of pressure location for two wing planforms in Figs. 21 - 24. The theory, being linear, predicts a constant slope of the lift curve and a constant center of pressure location. The experimental data on the wing of higher aspect ratio remain linear up to about 10°. Wing stall, evidenced by a loss of lift, seems to begin beyond this point. On the low aspect ratio wing, the lift curve slope appears to increase at angles of attack around 8° before stall begins near α = 18°. The increase in slope appears to be due to vortex separation from side edges and becomes more significant as the aspect ratio decreases since the separated vortex then influences a larger proportion of the wing surface.

7. Limitations of the Weissinger Method

The Weissinger procedure is fundamentally designed to give the spanwise loading on thin, uncambered wings of high aspect ratio in incompressible flow. Its range of validity may be estimated from the trends indicated by the comparisons with experiment shown in Figs. 4 to 23. The following table summarizes the range of geometrical and flight parameters over which the method gives load distributions which are of acceptable accuracy, as defined in Section III.

Table 1

Range of Applicability of Weissinger Theory

PARAMETER	RANGE OF VALIDITY	COMMENTS
βAR $(\beta = \sqrt{1-M_\infty^2})$	2 - ∞	At a given aspect ratio, the procedure is probably less accurate on a cambered wing than on a flat wing.
$\Lambda_{L.E.}$	0 - 60°	More highly swept wings could probably be treated more accurately by the Lawrence Method (Sec.IVC)
TR	0 - 1	Works well on tapered wings since largest errors probably occur in the vicinity of the wing tips.
$\frac{t}{c}$	0 - .12	Probably is satisfactory to t/c → .15 on high aspect ratio wings.
$\lvert\alpha\rvert$	0 - 8°	Holds over greater range of angle of attack if stall or vortex separation do not become significant.
M_∞	0 - .9	The limitation on βAR restricts the Mach number range.
$\frac{h}{c}$ (h = maximum height of mean camber line)	0 - .1	Consistent with angle of attack and thickness limitations.

8. Comparison with Other Theories

In degree of complication, the Weissinger method as presented here stands between the simpler lifting-line theories and the more complicated complete lifting surface theories. Several other methods have also been proposed which are approximately equivalent to the Weissinger method in ease and versatility of application and hence might be substituted, but do not seem to offer any particular advantage. Other variations are available in the literature but none appears significantly superior. A brief discussion will indicate the major distinctions between the competing lifting-line methods. The basic principles of lifting surface methods will also be described. While they might give improved accuracy in predicting effects of camber, the small difference in result does not seem to justify the extra labor.

The older lifting line theories, based on Prandtl's analysis (Ref. 29) were designed to give the spanwise load distribution on unswept wings. If the wing is replaced by a straight vortex, as indicated below, whose strength is $\Gamma(\eta)$, then the trailing vortices of strength $\frac{d\Gamma}{d\eta}$ induce an upwash velocity $w(y)$ at the point y on the lifting line. Following the derivation beginning on page 137 of Ref. 30, for example:

$$w(y) = -\frac{1}{4\pi}\int_{-\frac{b}{2}}^{\frac{b}{2}} \frac{\frac{d\Gamma}{d\eta}\,d\eta}{y-\eta} \qquad (IV\text{-}71)$$

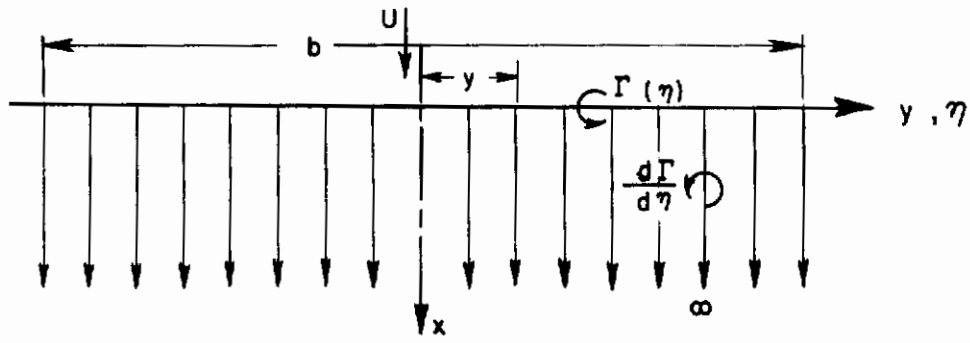

The wing, at the station y, is at an effective angle of attack $\alpha_o(y)$ which is the sum of the geometric angle, $\alpha(y)$ (referred to the local zero lift angle in the case of cambered wings), and the upwash angle $\frac{w(y)}{U_\infty}$ induced by the trailing vortices. Hence,

$$\alpha_0(y) = \alpha(y) + \frac{w(y)}{U_\infty} \qquad (IV\text{-}72)$$

The Prandtl lifting line theory assumes that the lift carried by the section at y is equal to the two-dimensional lift curve slope multiplied by the effective angle, α_0. Using the theoretical value of 2π for the section lift coefficient then gives for the lift per unit span

$$\frac{dL}{dy}(y) = 2\pi \times \frac{\rho_\infty}{2} U_\infty^2 c(y) \left[\alpha(y) - \frac{w(y)}{U_\infty}\right] \qquad (IV\text{-}73)$$

The lift is also proportional to the circulation:

$$\frac{dL}{dy}(y) = \rho_\infty U_\infty \Gamma(y) \qquad (IV\text{-}74)$$

Hence, combining Eqs.(IV-71), (IV-73), and (IV-74), produces the following integral equation for the circulation

$$\Gamma(y) = \pi U_\infty \alpha(y) c(y) - \frac{c(y)}{4} \int_{-\frac{b}{2}}^{\frac{b}{2}} \frac{\frac{d\Gamma}{d\eta}\, d\eta}{y - \eta} \qquad (IV\text{-}75)$$

Various methods have been proposed for solving this integral equation. The one given by Glauert (and which Prandtl attributes to E. Trefftz), makes the substitution $\eta = \frac{b}{2}\cos\theta \quad (0 \leq \theta \leq \pi)$. Then the circulation may be expressed as a Fourier series in θ

$$\Gamma(\eta) = \sum_{n=1}^{\infty} B_n \sin n\theta \qquad (IV\text{-}76)$$

When this series is inserted in Eq.(IV-75), the integration may be performed, and the following equation relating the coefficients results.

$$\sum_{n=1}^{\infty} \left[B_n \sin n\theta \left(\sin\theta + \frac{n\pi c}{2b}\right)\right] = \pi U_\infty c \alpha \sin\theta \qquad (IV\text{-}77)$$

Matching the boundary conditions at m points on the semi span (m values of $\theta°$ between 0 and $\frac{\pi}{2}$) produces m linear equations from which the first m values of B_n can be determined.

An improved method of solution by Irmgard Lotz (Ref. 31), simplifies the calculation considerably and is the procedure recommended in

ANC-1 (Ref. 31). She expresses $\alpha_0 \sin\theta$ and $\frac{\sin\theta}{c(\theta)}$ by Fourier series so that $\sin\theta$ cancels out of the equation, and also results in more rapid convergence. A modification by Multhopp (Ref. 18) further simplified the numerical procedure.

The integral in Eq. (IV-71) becomes infinite in the case of a swept wing, hence the Weissinger procedure, and others, were introduced to circumvent this difficulty. In the Weissinger method, the boundary condition is applied on the 3/4 chord line instead of on the lifting vortex so that a bent lifting line does not result in infinite downwash. Various other such devices have been proposed; a few examples will be described.

Truckenbrodt (Ref. 32) presents a theory very similar to Weissinger's, but in his analysis the boundary conditions may be applied at arbitrary locations on the wing. Then, if the two-dimensional section lift coefficient is $c_\ell = k\alpha$, the downwash at a distance Δx from a vortex of strength Γ is

$$-w = \frac{\Gamma}{2\pi\Delta x} = \frac{\frac{1}{2} c_\ell c U_\infty}{2\pi\Delta x} = \frac{\frac{k}{2} c U_\infty \alpha}{2\pi\Delta x} \qquad (IV-78)$$

In order that the downwash angle, $-\frac{w}{U_\infty}$, match the angle of attack

$$\frac{\Delta x}{c} = \frac{k}{4\pi}$$

The theoretical value of lift curve slope, k, is 2π, which leads Weissinger to apply his boundary condition at the 3/4 chord, where the distance $\frac{\Delta x}{c} = \frac{1}{2}$. For smaller values of section lift coefficient (obtained experimentally), $\frac{\Delta x}{c} < \frac{1}{2}$. Truckenbrodt can thus incorporate a correction for the difference between theoretical and experimental section lift coefficient. In the Weissinger procedure, such a correction would be accomplished by multiplying the calculated pressure distribution by the ratio of experimental to theoretical section lift. Truckenbrodt presents a graphical method of finding the downwash at any point on (or off of) the wing. Hence the boundary conditions may be applied at any stations.

A more versatile procedure is proposed by Küchemann in Ref. 33. By separating the contributions of chordwise and spanwise vortices, he obtains directly a solution for the pressure distribution over the wing similar to that given for the Weissinger procedure. However, he then introduces the parameter, n , such that the vorticity distribution due to a uniform angle of attack is written:

$$\gamma(x) = C\left(\frac{c-x}{x}\right)^n \qquad (IV\text{-}80)$$

where, by comparison with Eq. (IV-60), $C = 2U_\infty Q$ and $n = \frac{1}{2}$. By empirically adjusting these constants, correction for the experimental two-dimensional lift coefficient can be incorporated:

$$C = \frac{U_\infty \sin n\pi}{n} \cdot \frac{c_l}{2\pi} \qquad (IV\text{-}81)$$

and also an adjustment made which accounts for the fact that $n \to 1$ as $AR \to 0$:

$$n = 1 - \frac{1}{2\left[1+\left(\frac{2}{AR}\right)^2\right]^{1/4}} \qquad (IV\text{-}82)$$

These modifications (and others introduced by Küchemann) produce a theory of great versatility. In the present report, two simpler methods are proposed instead; namely those of Weissinger for high aspect ratio wings, and Lawrence (Ref. 14) for low aspect ratios. Since both theories work well at intermediate aspect ratios, Küchemann's refinements appear to be unnecessary. The Lawrence method will be discussed in Section IVC.

Various lifting surface methods have been proposed, all based essentially on the two-dimensional vortex system leading to Eq. (IV-16). All procedures for solving this two-dimensional integral equation make use of some assumed form for the variation of vorticity in one direction, in order to reduce the problem to a one-dimensional integral equation. The Weissinger method and the Lawrence method thus constitute particular choices of vorticity variation in the chordwise and spanwise directions respectively. Other choices may give superior accuracy for certain planforms or angle of attack distributions, but might then be less accurate in other cases. Where the boundary conditions are satisfied at 15 points on the wing surface, the Weissinger procedure seems to give as accurate a prediction of spanwise loading on a high aspect

ratio wing as any other. A comparison made by Schneider (Ref. 28) of calculations of span loading by Weissinger's lifting line method and the lifting surface methods of Falkner (Ref. 34) and Multhopp (Ref. 35), show equally good agreement with experiment. Falkner's method, however, required a larger number of control points to achieve the accuracy of the Weissinger method. The comparison, it should be noted, was for a 45° swept wing of AR = 8.02 and a taper ratio of .45. The airfoil section (NACA 63, A012) was 12% thick and uncambered.

A brief description of these lifting surface theories will be given in which the method of distributing the chordwise vorticity will be identified but not the numerical procedure for solving the resulting integral equations.

In Falkner's model, six concentrated vortices are placed on lines $\frac{C}{24}$, $\frac{5C}{24}$, $\frac{9C}{24}$, $\frac{13C}{24}$, $\frac{17C}{24}$, and $\frac{21C}{24}$. Boundary conditions are satisfied at several spanwise locations along the three chordwise lines $\frac{15C}{24}$, $\frac{19C}{24}$, and $\frac{23C}{24}$. Multhopp uses a distributed vorticity of the form $a_0 \cot \theta/2$ where a_0 = constant and $\cos\theta = 1 - \frac{x}{c/2}$. Control points are selected along the 3/4 chord line. In a higher order approximation, the vorticity is assumed to vary as $a_0 \cot \frac{\theta}{2} + a_1 \sin\theta$. In this case, boundary conditions are satisfied along lines at .3455C and .9045C.

Weissinger and Truckenbrodt also describe lifting surface theories in Refs. 13 and 36, respectively. The Weissinger method, described earlier, uses the chordwise distribution of vorticity dictated by the solution of the corresponding two-dimensional airfoil problem. Truckenbrodt uses the same chordwise distribution but adds another distribution which gives no lift but a pitching moment about the quarter chord. Thus, if the two-dimensional lift and pitching moment are known for the prescribed wing section, approximate proportions of the two distributions of vorticity may be incorporated.

In these methods the chordwise distribution of vorticity is always assumed, and the spanwise variation determined by solving an integral equation relating the vorticity to the wing slope. The chordwise vorticity and boundary conditions are so chosen that the results should approach the proper limits in the case of a flat wing of infinite or

vanishingly small aspect ratio. However, since the chordwise distribution of vorticity is prescribed, the methods may not accurately predict the load distribution on cambered low aspect ratio wings. Therefore, in such cases, a desirable procedure would be to prescribe the spanwise variation of vorticity and solve for the chordwise function by matching the local wing slopes. Such a procedure is described in the next section.

C. LOW ASPECT RATIO SUBSONIC WINGS

1. The Lawrence Method

In Weissinger's procedure, the chordwise variation of vorticity is prescribed, and the spanwise distribution is determined by solution of the appropriate integral equation. Lawrence, (Ref. 14), on the other hand, prescribes the spanwise distribution and solves a chordwise integral equation which satisfies a boundary condition on local wing slope. Both methods approach the correct limits for flat wings at infinite and zero aspect ratio. But for low aspect-ratio wings, Lawrence's method would be expected to account more accurately for arbitrary camber distribution. As in the presentation of the Weissinger method, the incompressible case will be treated first, then a correction for compressibility will be given.

Lawrence uses the pressure distribution rather than the vorticity as his elementary solution. These are related, as indicated by Eqs.(IV-9) and (IV-19). From Eq.(IV-21), then, the integral equation expressing the local upwash velocity in terms of the streamwise velocity perturbation (which is proportional to the pressure) is, for a wing with spanwise symmetry

$$w(x,y) = \frac{-1}{2\pi}\int_0^c \left\{ \int_{-\frac{b}{2}(\xi)}^{\frac{b}{2}(\xi)} \frac{\partial u}{\partial \eta}\left[\frac{1}{y-\eta}\left(1 + \frac{\sqrt{(x-\xi)^2+(y-\eta)^2}}{x-\xi} \right) \right] d\eta \right\} d\xi \qquad (IV\text{-}21)$$

Using an integration by parts, this equation may also be written

$$w(x,y) = \frac{-1}{2\pi}\frac{\partial}{\partial y}\int_0^c \left\{ \int_{-\frac{b}{2}(\xi)}^{\frac{b}{2}(\xi)} \frac{u(\xi,\eta)}{y-\eta}\left[1 + \frac{\sqrt{(x-\xi)^2+(y-\eta)^2}}{x-\xi} \right] d\eta \right\} d\xi \qquad (IV\text{-}83)$$

This is the form which Lawrence generally uses. It is an integral equation for the two-dimensional unknown $u(\xi,\eta)$ in terms of a prescribed vertical

velocity $w(x,y) = -U_\infty \alpha(x,y)$. As in the procedure of Weissinger and others, the solution is effected by expressing $u(\xi,\eta)$ as a given function of one variable multiplied by an unknown function of the other variable. Unlike the techniques primarily derived for high aspect ratio application, however, Lawrence chooses the spanwise variation as the one which is prescribed. The appropriate spanwise function is the elliptic distribution of lift experienced by a flat rectangular wing. It is incorporated mathematically by multiplying both sides of Eq. (IV-83) by the elliptical spanwise variation and integrating over the wing span.

$$\int_{-\frac{b}{2}(x)}^{\frac{b}{2}(x)} w(x,y)\sqrt{\left(\frac{b}{2}(x)\right)^2-y^2}\,dy = \frac{-1}{2\pi}\int_{-\frac{b}{2}(x)}^{\frac{b}{2}(x)}\sqrt{\left(\frac{b}{2}(x)\right)^2-y^2}\left\{\frac{\partial}{\partial y}\left[\int_0^c\left(\int_{-\frac{b}{2}(\xi)}^{\frac{b}{2}(\xi)}\frac{u(\xi,\eta)}{y-\eta}\left[1+\frac{\sqrt{(x-\xi)^2+(y-\eta)^2}}{(x-\xi)}\right]d\eta\right)d\xi\right]\right\}dy \qquad \text{(IV-84)}$$

After integrating by parts with respect to y and interchanging the order of integration

$$\int_{-\frac{b}{2}(x)}^{\frac{b}{2}(x)} w(x,y)\sqrt{\left(\frac{b}{2}x\right)^2-y^2}\,dy = \frac{-1}{2\pi}\int_0^c\left\{\int_{-\frac{b}{2}(\xi)}^{\frac{b}{2}(\xi)} u(\xi,\eta)\left[\int_{-\frac{b}{2}(x)}^{\frac{b}{2}(x)}\frac{y}{\sqrt{\left(\frac{b}{2}(x)\right)^2-y^2}}\left(\frac{1}{y-\eta}\right)\left(1+\frac{\sqrt{(x-\xi)^2+(y-\eta)^2}}{(x-\xi)}\right)dy\right]d\eta\right\}d\xi$$

(IV-85)

The integration with respect to y can, in principle, be evaluated. Lawrence approximates it in the following way. First, the integral is written in the form

$$\int_{-\frac{b}{2}(x)}^{\frac{b}{2}(x)}\frac{y}{\sqrt{\left(\frac{b}{2}(x)\right)^2-y^2}}\left(\frac{1}{y-\eta}\right)\left(1+\frac{\sqrt{(x-\xi)^2+(y-\eta)^2}}{(x-\xi)}\right)dy = \int_{-\frac{b}{2}(x)}^{\frac{b}{2}(x)}\frac{y}{(y-\eta)\sqrt{\left(\frac{b}{2}(x)\right)^2-y^2}}\left(1+\frac{|x-\xi|}{x-\xi}\right)dy$$

$$+\int_{-\frac{b}{2}(x)}^{\frac{b}{2}(x)}\frac{y}{\sqrt{\left(\frac{b}{2}(x)\right)^2-y^2}}\left[\frac{\sqrt{(x-\xi)^2+(y-\eta)^2}-|x-\xi|}{(x-\xi)(y-\eta)}\right]dy \qquad \text{(IV-86)}$$

The first term then yields

$$\int_{-\frac{b}{2}(x)}^{\frac{b}{2}(x)} \frac{y}{(y-\eta)\sqrt{\left(\frac{b}{2}(x)\right)^2-y^2}}\left(1+\frac{|x-\xi|}{x-\xi}\right)dy = \pi\left(1+\frac{|x-\xi|}{x-\xi}\right) \qquad (IV\text{-}87)$$

while introducing the low-aspect ratio approximation

$$\sqrt{(x-\xi)^2+(y-\eta)^2} \sim \sqrt{(x-\xi)^2+\left(\frac{b}{2}(x)\right)^2} \qquad (IV\text{-}88)$$

makes the second term become

$$\int_{-\frac{b}{2}(x)}^{\frac{b}{2}(x)} \frac{y}{\sqrt{\left(\frac{b}{2}(x)\right)^2-y^2}}\left[\frac{\sqrt{(x-\xi)^2+(y-\eta)^2}-|x-\xi|}{(x-\xi)(y-\eta)}\right]dy = \int_{-\frac{b}{2}(x)}^{\frac{b}{2}(x)} \frac{y}{(x-\xi)^2\sqrt{\left(\frac{b}{2}(x)\right)^2-y^2}}\left[\frac{y-\eta}{\sqrt{(x-\xi)^2+(y-\eta)^2}+|x-\xi|}\right]dy$$

$$\sim \int_{-\frac{b}{2}(x)}^{\frac{b}{2}(x)} \frac{y}{(x-\xi)^2\sqrt{\left(\frac{b}{2}(x)\right)^2-y^2}}\left[\frac{y-\eta}{\sqrt{(x-\xi)^2+\left(\frac{b}{2}(x)\right)^2}-|x-\xi|}\right]dy$$

$$= \frac{\pi\left(\frac{b}{2}(x)\right)^2}{2(x-\xi)}\left[\frac{1}{\sqrt{(x-\xi)^2+\left(\frac{b}{2}(x)\right)^2}+|x-\xi|}\right] \qquad (IV\text{-}89)$$

Then, combining the two terms

$$\int_{-\frac{b}{2}(x)}^{\frac{b}{2}(x)} \frac{y}{\sqrt{\left(\frac{b}{2}(x)\right)^2-y^2}}\left(\frac{1}{y-\eta}\right)\left(1+\frac{\sqrt{(x-\xi)^2+(y-\eta)^2}}{x-\xi}\right)dy = \frac{\pi}{2}\left[1+\frac{|x-\xi|}{x-\xi}\right]-\frac{\pi}{2}\left[1+\frac{\sqrt{(x-\xi)^2+b^2}}{x-\xi}\right] \qquad (IV\text{-}90)$$

This result is then inserted into Eq. (IV-85) giving

$$-\int_{-\frac{b}{2}(x)}^{\frac{b}{2}(x)} w(x,y)\sqrt{\left(\frac{b}{2}(x)\right)-y^2}\,dy = \frac{1}{2}g(x)+\frac{1}{4}\int_0^c g'(\xi)\left[1+\frac{\sqrt{(x-\xi)^2-\left(\frac{b}{2}(x)\right)^2}}{x-\xi}\right]d\xi \qquad (IV\text{-}91)$$

where $$g'(x) = \int_{-\frac{b}{2}(x)}^{\frac{b}{2}(x)} u(x,\eta)\,d\eta \qquad (IV\text{-}92)$$

2. Pressure Distribution

Equation (IV-91) is an integral equation for the one-dimensional unknown function $g(x)$. Since $u(x,\eta)$ is proportional to the pressure coefficient, $g'(x)$ is proportional to a chordwise load distribution, and $g(x) = \int_0^x g'(x)\,dx$ is proportional to the total load on the wing back to the x-station. More precisely, the relation between chordwise load, $\frac{dL}{dx}$ and $g'(x)$ would be

$$g'(x) = \int_{-\frac{b}{2}(x)}^{\frac{b}{2}(x)} u(x,\eta)\,d\eta = \frac{U_\infty}{4}\int_{-\frac{b}{2}(x)}^{\frac{b}{2}(x)} \Delta c_p(x,\eta)\,d\eta = \frac{U_\infty}{4}\int_{-\frac{b}{2}(x)}^{\frac{b}{2}(x)} \frac{\Delta p(x,\eta)}{\frac{\rho_\infty}{2}U_\infty^2}$$

$$= \frac{1}{2\rho_\infty U_\infty}\,\frac{dL}{dx} \qquad \text{(IV-93)}$$

By analogy with the Weissinger procedure in which the chordwise loading is determined by the distribution for an infinite airfoil, in the Lawrence method the required spanwise loading is that of a wing of infinitesimal span. For this case, $\frac{b}{2}(x)$ is negligible compared with $x-\xi$, and hence Eq. (IV-91) reduces to

$$g_{AR\to 0}(x) = -\int_{-\frac{b}{2}(x)}^{\frac{b}{2}(x)} w(x,y)\sqrt{\left(\frac{b}{2}(x)\right)^2 - y^2}\;dy \qquad \text{(IV-94)}$$

In general, (from Eq. (IV-93),

$$\int_{-\frac{b}{2}(x)}^{\frac{b}{2}(x)} \Delta c_p(x,y)\,dy = \frac{4\,g'(x)}{U_\infty}$$

while in the special case of extremely small aspect ratio, using Eq. (IV-94) to express $g(x)$,

$$\Delta c_{p\,AR\to 0} = -\frac{4}{U_\infty}\,\frac{\partial}{\partial x}\left[w(x,y)\sqrt{\left(\frac{b}{2}(x)\right)^2 - y^2}\right]$$

Now representing the general case by

$$\Delta c_p = \Delta c_{p_{AR \to 0}} \times f(x)$$

from the preceding relations, it is apparent that

$$f(x) = \frac{g'(x)}{\int_{-\frac{b}{2}(x)}^{\frac{b}{2}(x)} \frac{\partial}{\partial x} w(x,y) \sqrt{\left(\frac{b}{2}(x)\right)^2 - y^2}}$$

and hence

$$\Delta c_p = \frac{4 g'(x) \frac{\partial}{\partial x} \left[w(x,y) \sqrt{\left(\frac{b}{2}(x)\right)^2 - y^2} \right]}{U_\infty \int_{-\frac{b}{2}(x)}^{\frac{b}{2}(x)} \frac{\partial}{\partial x} \left[w(x,y) \sqrt{\left(\frac{b}{2}(x)\right)^2 - y^2} \right] dy} \qquad (IV\text{-}95)$$

The procedure is not strictly applicable for wings with swept trailing edges. For such wings, the spanwise integration should include the velocity perturbations in the downwash field as illustrated below. Such an operation is assumed when the order of integration is changed to give Equation (IV-85). Here, the left side of Equation IV-91 will be assumed to be zero behind the section of maximum width of the wing. This assumption gives reasonable results if the wing trailing edge is not greatly swept.

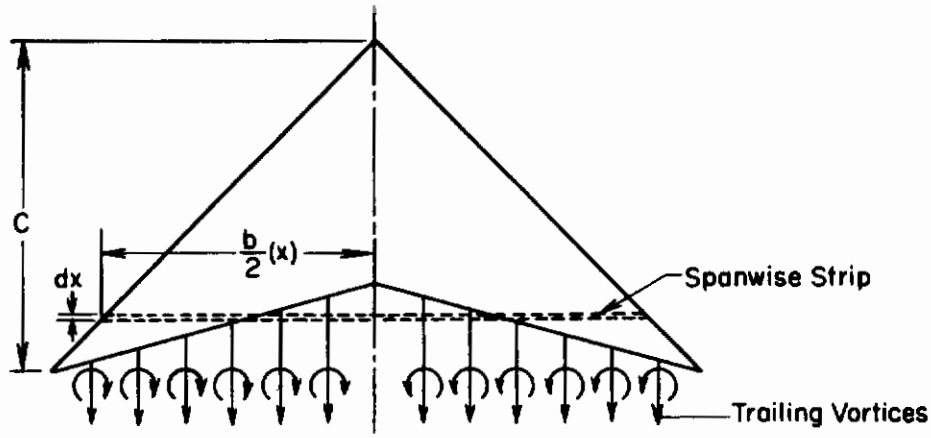

3. Solution of Integral Equation

To find the chordwise load parameter, $g'(x)$, a solution of the integral equation (IV-91) is required. Lawrence begins by rewriting the equation as follows

$$4k(x) = 2g(x) + g(c) + \frac{b}{2}(x)\int_0^c \frac{g'(\xi)\,d\xi}{x-\xi} + \int_0^c g'(\xi)\left[\frac{\sqrt{(x-\xi)^2 + \left(\frac{b}{2}(x)\right)^2} - \frac{b}{2}(x)}{x-\xi}\right] d\xi \qquad (IV\text{-}96)$$

where

$$k(x) = -\int_{-\frac{b}{2}(x)}^{\frac{b}{2}(x)} w(x,y)\sqrt{\left(\frac{b}{2}(x)\right)^2 - y^2}\;\; dy \qquad (IV\text{-}97)$$

Then making the transformations

$$x = \frac{c}{2}(\cos\theta + 1)$$
$$\xi = \frac{c}{2}(\cos\tau + 1) \qquad (IV\text{-}98)$$

$$4k(\theta) = 2g(\theta) + g(0) + \frac{b(\theta)}{c}\int_0^\pi \frac{g'(\tau)\,d\tau}{\cos\tau - \cos\theta} + \int_0^\pi g'(\tau)\,H(\theta,\tau)\,d\tau \qquad (IV\text{-}99)$$

where

$$H(\theta,\tau) = \frac{\sqrt{(\cos\tau - \cos\theta)^2 - \frac{b^2(\theta)}{c^2}} - \frac{b(\theta)}{c}}{\cos\tau - \cos\theta} \qquad (IV\text{-}100)$$

Equation (IV-99) is solved by expanding $g(\theta)$ in a Fourier series and determining the coefficients by satisfying the equation for each harmonic. Lawrence gives the following result which satisfies a Kutta

condition and makes $g(\theta) = 0$ at the leading edge.

$$g(\theta) = (\pi-\theta)(A_0 + A_1) + \sum_{r=1}^{N-1} (A_{r-1} - A_{r+1}) \frac{\sin r\theta}{r} \qquad \text{(IV-101)}$$

where, by definition, $A_{N-1} = A_N = 0$.
Then

$$\frac{4}{\pi} k(\theta) = \left[F_1(\theta) - F_0(\theta)\right] A_0 + \sum_{r=1}^{N-2} \left[F_{r+1}(\theta) - F_{r-1}(\theta)\right] A_r \qquad \text{(IV-102)}$$

where

$$F_0(\theta) = \frac{2\theta}{\pi} + H_0(\theta, b(\theta)) - 3$$

$$F_r(\theta) = \frac{2\sin r\theta}{\pi r} + \frac{b(\theta)\sin r\theta}{\sin\theta} + H_r(\theta, b(\theta)) \qquad r = 1, 2 \ldots \qquad \text{(IV-103)}$$

and

$$H_r(\theta, b(\theta)) = \frac{1}{\pi}\int_0^{\pi} \cos(r\tau)\, H(\theta, b(\theta), \tau)\, d\tau \qquad \text{(IV-104)}$$

By matching coefficients of the various harmonics of the Fourier series, the following set of simultaneous equations is obtained.

$$\frac{4}{\pi} k_n = (F_{1n} - F_{0n}) A_0 + \sum_{r=1}^{N-2} (F_{r+1,n} - F_{r-1,n}) A_r \qquad n = 1, 2 \ldots N-1 \qquad \text{(IV-105)}$$

where

$$k_n = k\left(\frac{n\pi}{N}\right) \quad \text{and} \quad F_{r,n} = F_r\left(\frac{n\pi}{N}\right)$$

The most difficult part of the procedure is the evaluation of $H_{r,n}$ using Equation (IV-104) at each value of n. By the trapezoidal rule

$$H_{r,n}(b_n(\theta)) = \frac{1}{\pi}\int_0^{\pi} \cos(r\tau)\, H(\theta_n, b_n(\theta), \tau)\, d\tau$$

$$= \frac{1}{M}\left[\frac{H(\theta_n, b_n(\theta), 0) + (-1)^r H(\theta_n, b_n(\theta), \pi)}{2} - \sum_{m=1}^{M-1} \cos\frac{M\pi r}{M} H\left(\theta_n, b_n(\theta), \frac{m\pi}{M}\right)\right] \qquad \text{(IV-106)}$$

where M is the number of subdivisions of the interval of integration. Lawrence gives plots of $H_{r,n}$ for r = 0, 1, 2, 3 and n = 1, 2, 3 as functions of b (θ)/ c. If more values are required (and according to Lawrence such is the case) then the procedure would be tedious for a hand calculation, but the numerical evaluation of the integrals for $H_{r,n}$ would present no difficulty for a high-speed computer.

4. Effects of Compressibility

As in the Weissinger method, the Prandtl-Glauert transformation is applied to correct for compressibility. The procedure is described in Section IV B 4.

In the transonic speed range, $\beta = \sqrt{1-M_\infty^2} \to 0$. Consequently, the transformed wing becomes one of vanishingly small aspect ratio. The pressures on the transformed wing, as calculated by the Lawrence method, will also approach zero with the aspect ratio. When converted back to the physical plane, however, the local pressure is obtained by multiplying this small calculated pressure by $\frac{1}{\sqrt{1-M_\infty^2}}$ which can be a large number as $M_\infty \to 1$. The pressure distribution on a wing thus approaches a finite limit as $M_\infty \to 1$. This limit is given by slender wing theory which will be discussed further in Section IV D.

5. Summary of Computational Procedure

The pressure distribution may be obtained by the following procedure

(a) Subdivide the chord of the wing into m spanwise strips whose centers lie at the stations $\theta_n = \frac{c}{2}\left(\cos\frac{n\pi}{m+1}+1\right)$, $n = 1, 2, 3, \ldots, m$

(b) At each strip find an effective span load parameter

$$\frac{1}{\left[\frac{b}{2}(\theta_n)\right]^2} k(\theta_n) = \frac{-1}{\left[\frac{b}{2}(\theta_n)\right]^2} \int_{-\frac{b}{2}(\theta_n)}^{\frac{b}{2}(\theta_n)} w(\theta_n, y) \sqrt{\left(\frac{b}{2}(\theta_n)\right)^2 - y^2}\, dy$$

Here $w(\theta_n, y) = -U_\infty \alpha(\theta_n, y)$ is obtained from the spanwise distribution of wing slope at the chordwise station θ_n. $w(\theta_n, y)$ is assumed to be zero off of the wing.

(c) Solve the integral equation (IV-99). A FORTRAN program for carrying out this solution is given in Appendix B for wings of the general shape sketched below.

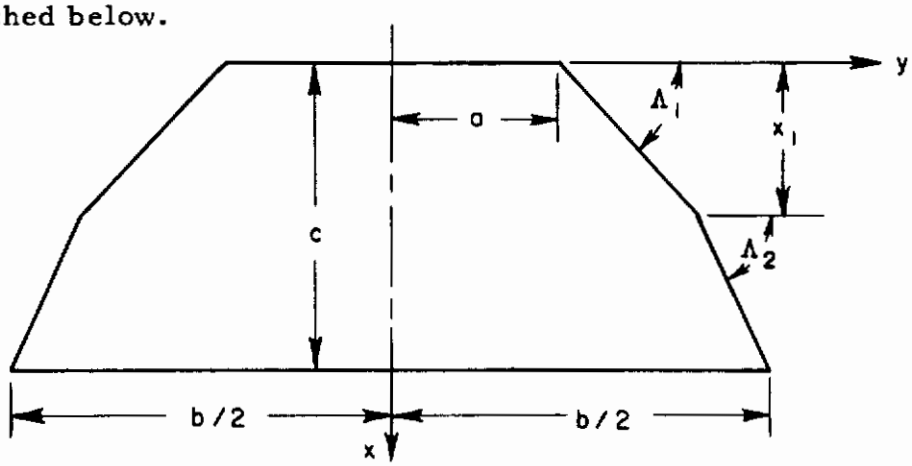

The program incorporates the compressibility correction, and its output gives $g'(x)$.

(d) Find the local pressure coefficients from Equation (IV-95). Thus

$$\Delta c_p = \frac{4 g'(x) \frac{\partial}{\partial x} \left[w(x,y) \sqrt{\left(\frac{b}{2}(x)\right)^2 - y^2} \right]}{U_\infty \int_{-\frac{b}{2}(x)}^{\frac{b}{2}(x)} \frac{\partial}{\partial x} \left[w(x,y) \sqrt{\left(\frac{b}{2}(x)\right)^2 - y^2} \right] dy}$$

6. Comparison With Experiment

The initial slope of the lift coefficient predicted by Lawrence is compared with experiments on a number of flat wings in Figures 25 to 28. The agreement is satisfactory although the data tends to scatter somewhat. The lift as a function of angle of attack is quite nonlinear in

some of these cases, making it difficult to determine the initial slope of the curve. This effect, rather than shortcomings of the theory, is believed to be responsible for the scatter in the data. The experimental information was found in Reference 37.

The chordwise center of pressure predictions are compared with experiment in Figures 29 to 32. There again, the agreement is satisfactory, but, as in the case of the lift, the data scatters a little, probably due to the difficulty in reading the initial slopes of the nonlinear lift and moment curves.

The nonlinearity of the variation of lift with angle of attack is illustrated on Figures 21 and 22. Here lift coefficient is plotted against angle of attack for two different wings. The predicted initial slopes are also shown according to the Lawrence theory and the Weissinger theory. Since the nonlinearity is partly caused by vortex separation from the wing side edges, the effects are more pronounced at the lower aspect ratios.

Figures 23 and 24 show the variations of center of pressure with angle of attack for the same two wings. Again the Weissinger and Lawrence theories are indicated. The trailing edges of these wings were swept back somewhat in excess of the limits of validity of the Lawrence theory.

7. Limitations of the Lawrence Method

The Lawrence method might be expected to fail when applied to cambered wings of high aspect ratio although it approaches the correct limit as $AR \rightarrow \infty$ for a flat wing. In addition, the assumption of zero load on parts of the wing lying in its own downwash field is only a crude approximation. Hence, the formulas are valid only for wings with nearly zero sweep of the trailing edge.

The following Table summarizes the range of geometrical and flight parameters over which the method gives load distributions of acceptable accuracy. The limitations are estimated from comparisons between theory and experiment.

Table 2

Range of Applicability of Lawrence Theory

Parameter	Range of Validity	Comments
βAR	$0 < \beta AR \leq 2$	At $\beta \to 0$ the Lawrence theory approaches the limit given by Jones' theory. (Ref.12)
$\Lambda_{L.E.}$	$0 < \Lambda_{L.E.} < 85°$	
$\Lambda_{T.E.}$	$-10° < \Lambda_{T.E.} < 10°$	
TR	$0 \leq TR \leq 1$	
$\frac{t}{c}$	$0 < \frac{t}{c} < .12$	The data shows no consistent effect of thickness.
α	$0 \leq \lvert\alpha\rvert < 3° AR$	For AR up to about 5, the range of linearity increases with AR.
M_∞	$0 < M_\infty < .95$	At $\beta AR < .25$ Jones' theory gives a simpler result of adequate accuracy.
$\frac{h}{c}$	$0 \leq \frac{h}{c} \leq 0.1$	

8. Comparison With Other Theories

The position of the Lawrence method with respect to other lifting line and lifting surface theories was described in Section IV B 8. Unlike most of the other theories, Lawrence prescribes the spanwise variation of load in order to reduce his two-dimensional integral equation to a function of only the chordwise direction. Thus, his theory should be more accurate than the others for low aspect ratio cambered wings. Küchemann (Ref. 33), develops an empirical bridge between the Lawrence method and the Weissinger approach. Since both methods give accurate load distributions on flat wings over the entire range of aspect ratios, the necessity for Küchemann's complication is difficult to establish without systematic pressure measurements on cambered and twisted wings.

Consequently, for present purposes the Lawrence theory replaces the Weissinger method at a reduced aspect ratio of two $(\beta AR=2)$ an empirical choice.

At extremely low aspect or at $M_\infty \to 1$ $(\beta AR < .25)$ the Lawrence method approaches the finite limit given by the Jones theory (Ref. 12), which has the advantage of being simpler than any of the other procedures. Since it is the limiting form when sonic speed is approached from either direction, Jones' theory is valid at transonic speeds above or below the speed of sound. The Jones method is described in the next Section.

D. TRANSONIC WINGS

1. The Jones Theory

The transonic theory of R. T. Jones (Ref. 12) is based on the assumptions of slender wing theory mentioned previously in Section IV A7. In non-dimensional form, the linearized equation for velocity potential may be written

$$\pm(\beta AR)^2 \phi_{\bar{x}\bar{x}} + \phi_{\bar{y}\bar{y}} + \phi_{\bar{z}\bar{z}} = 0 \qquad \text{(IV-107)}$$

The equation represents a subsonic flow when $\beta = \sqrt{1-M_\infty^2}$ and the first term is accompanied by a positive sign. In supersonic flow, $\beta = \sqrt{M_\infty^2-1}$ and the negative sign is used. $\bar{x} = \frac{x}{\bar{c}}$ where $\bar{c}$ is the mean chord. $\bar{y} = \frac{y}{b}$ where b is the wing span. In either case, for $\beta AR << 1$, the first term becomes neglibibly small, and the equation reduces to the two-dimensional Laplace equation. In solving the equation, the boundary conditions are satisfied in each cross plane (y, z - plane) and the x-location of the plane appears only as a parameter.

Although Jones derives solutions of Eq. (IV-107) in a different manner, it will be simplest here to determine the low aspect ratio limit of the Lawrence theory since almost all of the needed results are available in Section IV C. The Jones result then becomes a special case of

Lawrence's theory, where instead of the approximation

$$\sqrt{(x-\xi)^2+(y-\eta)^2} \sim \sqrt{(x-\xi)^2+\left(\tfrac{b}{2}(x)\right)^2}$$

(See Eq. (IV-88), Jones uses

$$\sqrt{(x-\xi)^2+(y-\eta)^2} \sim |x-\xi| \qquad (IV\text{-}108)$$

Then the integral equation (IV-91) would become

$$g(x) = -\int_{-\frac{b}{2}(x)}^{\frac{b}{2}(x)} w(x,y)\sqrt{\left(\tfrac{b}{2}(x)\right)^2-y^2}\,dy \qquad (IV\text{-}109)$$

As before

$$g'(x) = \frac{1}{2\rho U_\infty}\frac{dL}{dx} \qquad (IV\text{-}110)$$

In this case, then (as shown on page 60),

$$\Delta c_p = -\frac{4}{U_\infty}\frac{\partial}{\partial x}\left[w(x,y)\sqrt{\left(\tfrac{b}{2}(x)\right)^2-y^2}\right] \qquad (IV\text{-}111)$$

Jones gives the solution for constant angle of attack $\alpha = -\frac{w}{U_\infty}$ which is

$$\Delta c_p = \frac{2a\,\frac{b}{2}(x)}{\sqrt{\left(\tfrac{b}{2}(x)\right)^2-y^2}}\frac{db}{dx} \qquad (IV\text{-}112)$$

This equation indicates that a negative lift will appear when the span is decreasing. As Jones points out, however, sections of the wing behind its maximum span will lie in a downwash field which is not considered by the theory. Application of a Kutta condition to swept trailing edges leads to the approximation that the wing carries no lift behind its maximum section.

2. Effect of Compressibility

Applying the Prandtl - Glauert transformation at subsonic speeds or the corresponding Ackert transformation in the supersonic case does not effect Eq. (IV-111) since both sides would be multiplied by $\beta = \sqrt{|1 - M_\infty^2|}$ Here the relation is independent of Mach number. This result is not surprising since the original assumption that $\beta AR << 1$ eliminates the Mach number from the linearized partial differential equation for velocity potential.

3. Summary of Computational Procedure

For wings in which $\beta AR << 1$, Eq. (IV-111) gives the pressure distribution directly. The formula is

$$\Delta C_p = -\frac{4}{U_\infty} \frac{\partial}{\partial x} \left[w(x,y) \sqrt{\left(\frac{b}{2}(x)\right)^2 - y^2} \right] \qquad 0 \leq x \leq x\left(\frac{b}{2}_{max}\right)$$

$$\Delta C_p = 0 \qquad x > x\left(\frac{b}{2}_{max}\right)$$

where $x\left(\frac{b}{2}_{max}\right)$ is the location of the maximum span station.

No compressibility correction is required.

4. Comparison with Experiment

The curves comparing the Lawrence theory with experiment (Figs. 25 to 32) show that Jones' theory for a flat wing becomes identical to Lawrence's when the aspect ratio has been reduced to about 1.5. Since the data happens to be transonic, the reduced aspect ratio corresponding to 1.5 would be $\beta AR \sim .3$. At low aspect ratio, then, the agreement exhibited between Lawrence's theory and experimental data on flat wings would also apply to Jones' theory.

At supersonic speeds Jones gives a comparison of his theory with measurements on a flat triangular wing of aspect ratio = .75 at M_∞ = 1.75. The theoretical and experimental lift curve slope and pitching moment agree near $\alpha = 0$ within the accuracy of the experiment.

Additional comparisons are given in Figs. 33 to 37 which are described in Section IV-E. The lift data were obtained from Refs. 38-47.

5. Limitations of Jones' Theory

The following Table gives the range of geometrical and flight parameters over which the method appears to give load distributions of acceptable accuracy.

Table 3

Range of Applicability of Jones Theory

Parameter	Range of Validity	Comments
βAR $(\beta = \sqrt{\lvert 1-M_\infty^2 \rvert})$	0 - .25	Although the theory is probably accurate over a wider range, the Lawrence theory or Evvard's method may be better for cambered wings.
$\beta \tan \Lambda_{L.E.}$	>10	This criterion is consistent with $\beta AR \leq .25$ On unswept wings, the Jones theory concentrates all of the lift on the leading edge.
$\lvert \Lambda_{T.E.} \rvert$	0 - 10°	
TR	0 - .2	Jones theory does not give reliable pressure distribution information if $db/dx \leq 0$ or discontinuous.
t/c	0 - .12	
$\lvert \alpha \rvert$	0° - 3° AR	The lift on slender wings becomes nonlinear at quite low angles of attack.
M_∞	.8 - 1.2	Provided $\beta AR \leq .25$
h/c	0 - .1	

6. Comparison With Other Theories

The Jones theory was derived here as a special case of the Lawrence theory. It is possible also to show that it represents the low aspect ratio or transonic limit of linearized supersonic wing theory. For example, the lift curve slope of a low aspect ratio triangular

wing in coefficient form is (See page 199 of Ref. 3.)

$$\frac{dC_L}{d\alpha} = \frac{2\pi \cot \Lambda_{L.E.}}{E\left(\sqrt{1-(\beta \cot \Lambda_{L.E.})^2}\right)} = \frac{\pi AR}{2E\left(\sqrt{1-\left(\frac{\beta AR}{4}\right)^2}\right)}$$

where E is the complete elliptic integral of the second kind. The Jones theory applies when $\beta AR << 1$. Then

$$E\left(\sqrt{1-\left(\frac{\beta AR}{4}\right)^2}\right) \longrightarrow E(1) = 1 .$$

Hence $\frac{dC_L}{d\alpha} \longrightarrow \frac{\pi}{2} AR$

This result is identical to that obtained by integrating the pressure coefficient given by Eq. (IV-112) for the case of a triangular wing.

Section IV E gives a more complete description of linear supersonic wing theory. The Jones result is equivalent to a low aspect ratio limit of the general theory.

E. SUPERSONIC WINGS

1. Linear Wing Theory

Linear theory (Ref. 48) is the basis of most calculations of pressure distribution on wings in supersonic flow. In this method, the partial differential equation for velocity potential is linearized by assuming perturbations in velocity are small compared with the flight speed (and also with the speed of sound). As in the subsonic case, solutions are determined by applying boundary conditions in the plane of the wing, and the pressure distribution is given by a simple linearized relation. By virtue of the linearity of the theory with flow deflection angle, the calculated pressure difference between top and bottom surfaces is assumed to be independent of wing thickness. The lift load computation, therefore, is carried out for a thin plate lying midway between upper and lower wing surfaces.

The linearized equation for velocity potential, ϕ, is (see Ref. 48):

$$-(M_\infty^2 - 1)\frac{\partial^2\phi}{\partial x^2} + \frac{\partial^2\phi}{\partial y^2} + \frac{\partial^2\phi}{\partial z^2} = 0 \qquad (IV\text{-}113)$$

The wing, moving in the negative x-direction at velocity U_∞ (Mach No. M_∞) is represented by the surface $z = f(x,y)$ It is assumed to lie nearly in the $z = 0$ plane as sketched below:

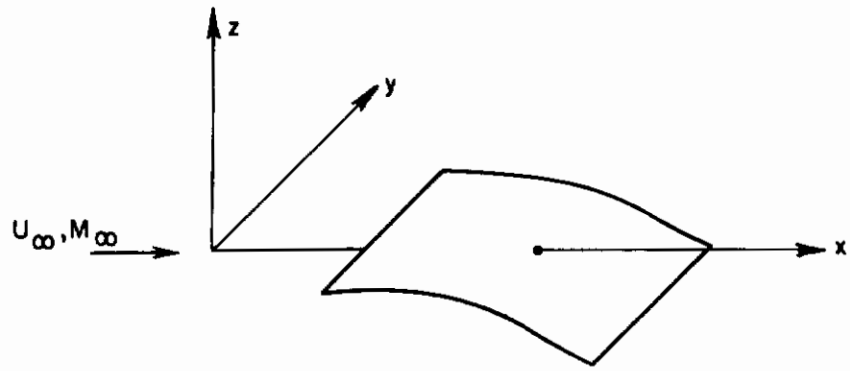

The boundary condition on the wing requires that the flow be deflected to become tangent to the wing surface. In the linearized analysis then, the following condition is applied in the plane of the wing ($z = 0$):

$$v_z = \frac{\partial\phi}{\partial z} = U_\infty \frac{\partial f(x,y)}{\partial x} \qquad (IV\text{-}114)$$

Off of the wing in the $z = 0$ plane, the pressure must be continuous; hence, since the pressure perturbation is proportional to $\frac{\partial\phi}{\partial x}$:

$\frac{\partial\phi}{\partial x}$ continuous in the plane $z = 0$ outside of the wing. $(IV\text{-}115)$

A Kutta condition (finite velocity) must be satisfied at a trailing edge.

Ahead of the Mach lines issuing back from the wing, the free stream is undisturbed by the presence of the wing. In addition, all

disturbances must die out as $z \to \infty$ or $y \to \infty$

As indicated above, the linearized pressure difference is proportional to the perturbation of the streamwise component of velocity on the upper surface of the wing.

Specifically $\Delta C_p = \frac{4}{U_\infty} \frac{\partial \phi}{\partial x}\Big|_{\text{upper surface}}$ (IV-116)

where $C_p = \frac{p - p_\infty}{\frac{\rho}{2} U_\infty^2}$

The linear theory provides a basic method for computing lift distribution which can be modified or corrected, if necessary, to account for nonlinear effects. Therefore, a good deal of effort has been expended to produce tractable mathematical solutions for many general classes of wings. The solution to be described here is based on a method first proposed by Evvard. His procedure, derived in Ref. (10), takes advantage of the fact that the distribution of source solutions of the wave equation (IV-113) may be expressed in terms of the local flow inclinations in the plane $z=0$. On the wing surface, of course, the flow inclination is known. Evvard succeeds in expressing the integrated effect of the unknown sources off of the wing in terms of the known distribution on the wing surface. An equivalent derivation is given in Ref. 48 by a different mathematical process.

The source solution of the wave equation in the plane $z=0$ for a source of unit strength at the point $x=\xi$, $y=\eta$, $z=0$ is a special case of the general source solution given by Eq. IV-23. Here

$$\phi_s(x,y) = \frac{1}{\sqrt{(x-\xi)^2 - \beta^2 (y-\eta)^2}} \qquad \text{(IV-117)}$$

where $\beta = \sqrt{M_\infty^2 - 1}$

The velocity potential at the point x, y due to an integration of infinitesimal sources of strength $f(\xi, \eta)$ will then be

$$\phi(x,y) = \iint \frac{f(\xi,\eta)\,d\xi\,d\eta}{\sqrt{(x-\xi)^2 - \beta^2(y-\eta)^2}} \qquad (IV\text{-}118)$$

If the strengths of the sources are taken proportional to the local flow inclinations, and the area of integration includes all sources in the Mach forecone from the point x, y (where the denominator of the integrand is real) then the velocity potential will satisfy the boundary conditions as well as the differential equation. Then

$$\phi(x,y) = \frac{U_\infty}{\pi} \iint_S \frac{\alpha(\xi,\eta)\,d\xi\,d\eta}{\sqrt{(x-\xi)^2 - \beta^2(y-\eta)^2}} \qquad (IV\text{-}119)$$

is the velocity potential on the top surface of a lifting wing with a local distribution of flow inclination equal to $\alpha(\xi,\eta)$. The area of integration is shaded in the sketch below

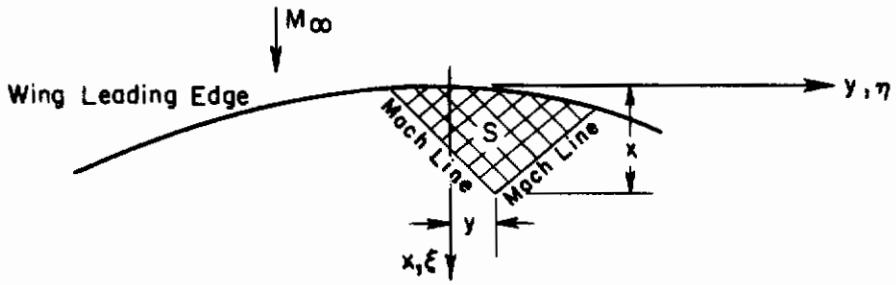

When the area of integration includes a region not on the wing, so that the flow inclination is not known, then Evvard demonstrates that the proper result is obtained by omitting the integration over the regions S_1 and S_2 shown on the following page:

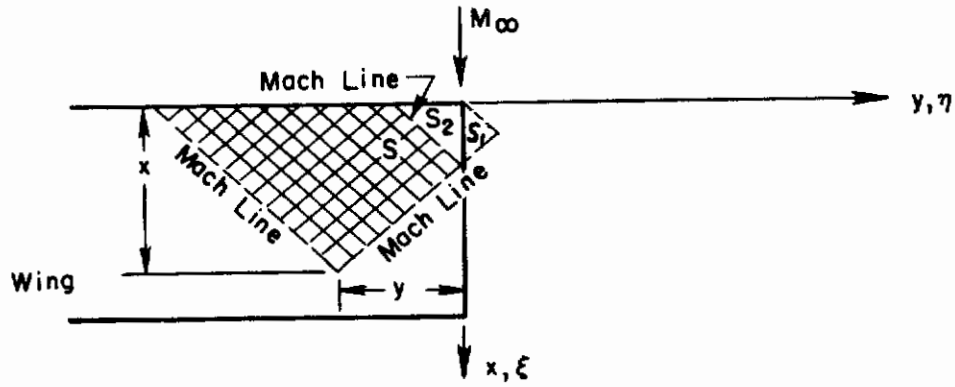

If more than one side edge is involved, such as on a triangular wing swept behind the Mach line, then the region of integration becomes a set of parallelograms, A_1 , A_2 ... as indicated on the next sketch. The set terminates when a reflected Mach line would lie outside of the wing; or continues indefinitely to a pointed leading edge

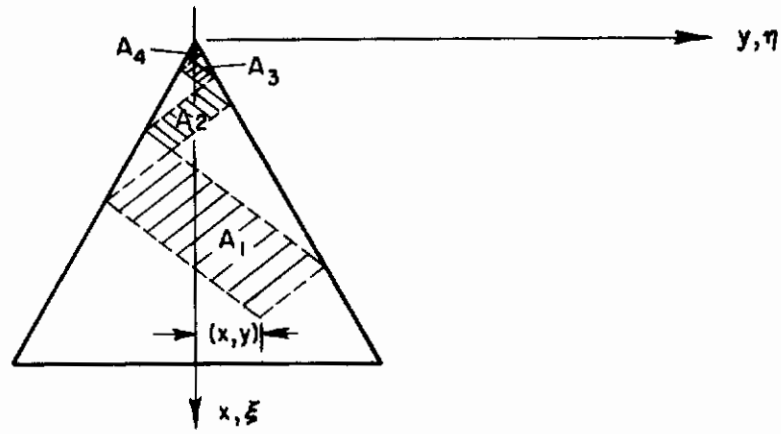

Equation IV-119 when integrated with alternating signs over the indicated regions is then capable of giving the velocity potential distribution for wings of general planform.

"Subsonic" trailing edges (swept behind the Mach lines) require special treatment to insure that a Kutta condition is satisfied. The necessary extension of the procedure for this case is given in Ref. 10. The complicated equations which result will not be repeated here; hence this procedure does not provide a means of calculating pressures in regions influenced by the wing's own wake.

Although the numerical solution of Eq. (IV-119) may become quite tedious when the wing is warped and twisted in some prescribed manner,

the process is usually a straightforward one requiring only a numerical integration to obtain $\phi(x,y)$, and a subsequent differentiation to obtain the pressure coefficient. A computer program of considerable versatility is under development by Ralph Carmichael of the Ames Laboratory, NASA.

In the case of wings with continuously interacting side edges, such as the triangular wing sketched above, the region of integration becomes an infinite set of parallelograms. It is then necessary, in practice, to terminate the numerical process after including some finite number of such regions. Etkin and Woodward (Ref. 49) have demonstrated that the use of two regions gives a decided improvement over the result of using just one, and is usually sufficiently close to the exact linear theory result. Using this approximation, the velocity potential at the point x, y on the triangular wing in question would be

$$\phi(x,y) = \frac{U_\infty}{\pi} \iint_{A_1} \frac{\alpha(\xi,\eta)\,d\xi\,d\eta}{\sqrt{(x-\xi)^2 - \beta^2(y-\eta)^2}} - \frac{U_\infty}{\pi} \iint_{A_2} \frac{\alpha(\xi,\eta)\,d\xi\,d\eta}{\sqrt{(x-\xi)^2 - \beta^2(y-\eta)^2}} \qquad (IV\text{-}120)$$

2. Summary of Computational Procedure

Since the calculation of pressure distribution on a supersonic wing by Evvard's method does not require the inversion of an integral equation, the computational procedure is quite simple, although sometimes very tedious. The following steps outline the process.

(a) Determine the areas of integration for each point x, y, by forming the forward Mach lines reflecting from side edges where necessary. Usually it is convenient to subdivide the wing plan form into regions requiring 0, 1, 2, . . . side-edge reflections.

(b) For a given wing slope distribution, $\alpha(\xi,\eta)$ calculate the velocity potential distribution from Eq. (IV-119). Where multiple

side edge reflections are encountered, the approximation given by Eq. (IV-120) may be used. For simple functions $\alpha(\xi,\eta)$ the integration can usually be carried out analytically. Otherwise a numerical integration is required.

(c) Compute the lift distribution from Eq. (IV-116) Any numerical computations in step b should provide accurate results at small intervals to avoid large errors in determining the derivative, $\frac{\partial \phi}{\partial x}$.

A FORTRAN program is given in Appendix C for calculating the pressure distribution on a wing of the following geometry with arbitrary angle of attack variation in the spanwise direction only.

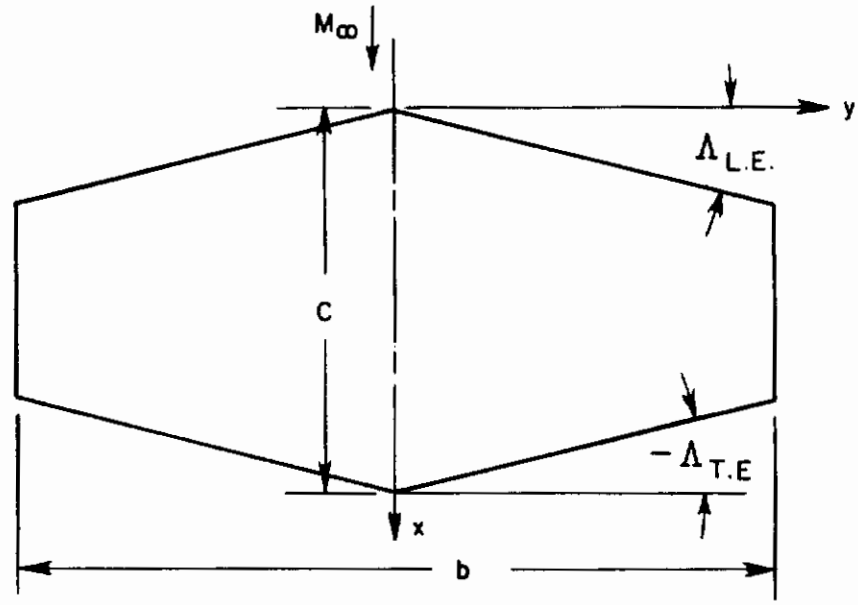

The program is limited to subsonic leading edges $(\tan \Lambda_{L.E.} > \beta)$ and supersonic trailing edges $(|\tan \Lambda_{T.E.}| < \beta)$

3. Comparison With Experiment

Figures 33 to 37 show comparisons of computed lift curve slope with experimental data for a number of flat wings of different plan forms. The agreement between theory and experiment is generally satisfactory except for geometries in which the wing leading edge is nearly sonic

($M_\infty \cos \Lambda_{LE} \sim 1$). Ulmann and Bertram (Ref. 50) attribute the discrepancy to an effect of wing thickness and propose a semi-empirical correction procedure. Since the application of such a correction has not been studied in the case of wings of arbitrary camber, it is not incorporated here. However, it is significant to note that this thickness effect was treated with apparent success by applying a two-dimensional analysis to highly-swept wings.

Comparisons of theoretical and experimental chordwise and spanwise centers of pressure shown in Figs. 38 to 42 also show agreement except when the wing leading edges are nearly sonic. The streamwise center of pressure data for rectangular wings scatter badly. The theory seems to predict a position somewhat too far back (by about 4 percent). Wing thickness will cause a forward shift which probably accounts for the major discrepancy between theory and experiment. In some cases forces on model support stings may cause the experimental center of pressure to shift rearward.

Plots of lift and centers of pressure against angle of attack, for a delta and a rectangular wing are shown in Figs. 43 to 46. The region of linearity seems to be greater on supersonic wings than in the subsonic case. The same type of increase of lift with angle of attack, probably due to vortex separation, again occurs on the low-aspect-ratio wing. The theoretical lift curve slope is in error in this case of a wing with nearby sonic leading edge.

Direct comparisons of theoretical and experimental pressure distributions are available for certain flat and warped rectangular and triangular wings.

Data were obtained in Ref. 51 on the flat rectangular and triangular semi-span models shown in Figs. 47 and 48. Figs. 49 and 50 show comparisons taken from Ref. 52 between linear theory and measured load distributions on these two wings at $\alpha = 5°$ and $M_\infty = 2$. The agreement is generally good. Application of shock-expansion theory (see, for example, Ref. 7) indicates that the discrepancies near the leading and trailing edges on the inboard section of the rectangular wing are due to thickness effects.

Cambered models of these wings were also tested. Tables 4 and 5 show the angle of attack distributions on the cambered rectangular and triangular wings.

Table 4

Midplane Angle of Attack Distribution for Rectangular Wing

y/b/2 \ x/c	0.000	0.071	0.214	0.286	0.429	0.571	0.714	0.786	0.929	1.000
					Degrees					
0.000	0.00	0.00	0.00	0.00	0.00	0.00	0.00	0.00	0.00	0.00
0.286	- 0.92	- 0.77	- 0.49	- 0.33	- 0.03	0.30	0.64	0.82	1.12	1.20
0.486	- 1.60	- 1.38	- 0.89	- 0.63	- 0.11	0.44	1.02	1.30	1.66	1.78
0.629	- 2.08	- 1.79	- 1.19	- 0.87	- 0.23	0.43	1.11	1.43	2.02	2.25
0.771	- 2.49	- 2.18	- 1.50	- 1.13	- 0.36	0.39	1.13	1.48	2.11	2.39
0.829	- 2.59	- 2.27	- 1.58	- 1.22	- 0.45	0.35	1.13	1.50	2.23	2.52
0.914	- 2.85	- 2.48	- 1.73	- 1.35	- 0.54	0.26	1.03	1.42	2.19	2.55
0.971	- 2.87	- 2.52	- 1.79	- 1.42	- 0.62	0.17	0.95	1.33	2.13	2.52
1.000	- 2.89	- 2.55	- 1.83	- 1.45	- 0.67	0.11	0.90	1.29	2.09	2.48

Table 5

Midplane Angle of Attack Distribution for Triangular Wing

y/b/2 \ x/c	.077	.154	.231	.269	.385	.500	.615	.731	.769	.827	.885	.942
						Degrees						
.05	3.07	3.03	2.94	2.89	2.69	2.42	2.08	1.63	1.46	1.14	0.68	0.13
.20	2.96	2.90	2.78	2.73	2.50	2.21	1.87	1.43	1.24	0.89	0.50	0.11
.35	2.75	2.64	2.51	2.45	2.20	1.91	1.59	1.18	0.99	0.73	0.37	0.00
.50	2.40	2.28	2.14	2.06	1.79	1.52	1.26	0.93	0.78	0.58	0.34	0.05
.65	1.94	1.83	1.70	1.61	1.31	1.14	0.91	0.66	0.61	0.46	0.37	0.23
.85	1.18	1.18	1.09	1.01	0.79	0.71	0.63	0.57	0.56	0.55	0.54	0.54

The cambered wing test data is compared with experiment in Figs. 51 and 52. In both the rectangular and triangular wings, the agreement between theory and experiment is about as good for cambered wings as for flat wings. As may be seen from Tables 4 and 5, however, the range of angle of attack on the cambered wings is a little less than the 5° on the flat wings.

4. Limitations of the Method

On the basis of comparison with experiment and examination of higher order terms in Mach number and angle of attack, the estimated limitations on the linear theory are given in the following table.

Table 6

Range of Applicability of Linear Supersonic Wing Theory

Parameter	Range of Validity	Comments
βAR $(\beta=\sqrt{M_\infty^2-1})$	$.25<\beta AR<\infty$	At transonic speeds $\beta\to 0$, the Jones theory becomes more convenient
$\Lambda_{L.E.}$	$0 \leq \Lambda_{L.E.} \leq 85°$	Vortex separation on highly swept wings introduces nonlinearities
$\frac{1}{\beta}\tan\Lambda_{T.E.}$	$-1<\frac{\tan\Lambda_{T.E.}}{\beta}<1$	Method does not apply to wings with subsonic trailing edge
$\frac{t}{c}$	$0<\frac{t}{c}<.1$	The center of pressure is sensitive to wing thickness. To keep the wave drag low, the thickness ratio will generally be small on supersonic wings.
$\lvert\alpha\rvert$	$0<\lvert\alpha\rvert<5°AR$	At high AR--stall causes nonlinear effects beginning at about 20°
M_∞	$1.2<M_\infty<4.5$	Approaches the Jones limit at transonic speeds
$\frac{h}{c}$	$0\leq\frac{h}{c}\leq .1$	
TR	$0\leq TR\leq 1$	

5. Comparison With Other Theories

Since, as explained in Section II, this report is concerned only with linear operations on the local angle of attack, an appropriate basis for calculations of load distribution is the linear supersonic wing theory. For certain planforms and angle of attack distributions (delta wings at uniform α for example) this theory, results in simple solutions of the load calculation problem. However, Evvard's method, as suggested here, gives a solution for arbitrary plan form and angle of attack distribution which, if not simple, is at least straightforward except possibly for wings with subsonic trailing edges.

Evvard actually writes his solution in terms of the slopes of the upper and lower wing surfaces, so that wing thickness effects are partially taken into account. However, on a thick wing, the local Mach number will differ from the free stream Mach number even at zero angle of attack, thereby modifying the lift distribution at small angles of attack. This effect of thickness, which would still lead to a linear aerodynamic load distribution, might, with further development, be incorporated in the analysis of supersonic wings.

At transonic speeds, or for low aspect ratio wings ($\beta AR \ll 1$) linear supersonic theory approaches the simpler Jones result given previously.

F. EFFECT OF BODY INTERFERENCE ON WING LIFT DISTRIBUTION

1. The Procedure of Gray and Schenk

The calculation of the load distribution on a wing-body combination requires a solution of the appropriate partial differential equation for the flow field which satisfies the boundary condition of no flow through the surfaces of the configuration. A superposition of the separate solutions for wing and body will not be correct because the wing solution will produce a flow through the body and vice versa. Since a complete solution of the wing-body problem is obtainable only in rare special cases, such as a conical wing on a conical body, the following approximation is employed.

The load distribution and flow fields are calculated for wing and body separately. Then the flow about the body in the presence of the wing is applied to the wing, giving a load distribution which must be added to the wing-alone value. The force on the body due to the wing is obtained by immersing the body in the wing flow field. In principle, improved results might be obtained by repeating the process using the revised load distributions to compute the required flow fields, but such a refinement is not justified in view of other approximations in the procedure.

The wing-body interference problem is thus divided into two parts. The procedure for calculating the interference pressures produced on the wing due to the presence of the body will be specified using the method of Gray and Schenk (Ref. 2). The calculation of the influence of the wing on the body loads will be discussed in the section of the report dealing with loads on bodies (Section V).

The procedure of Gray and Schenk is based on the work of Lennertz (Ref. 53). It assumes that the spanwise loading on the wing alone is known along with the corresponding center of pressure distribution. The wing alone is defined to be the "exposed" wing as shown in the sketch below:

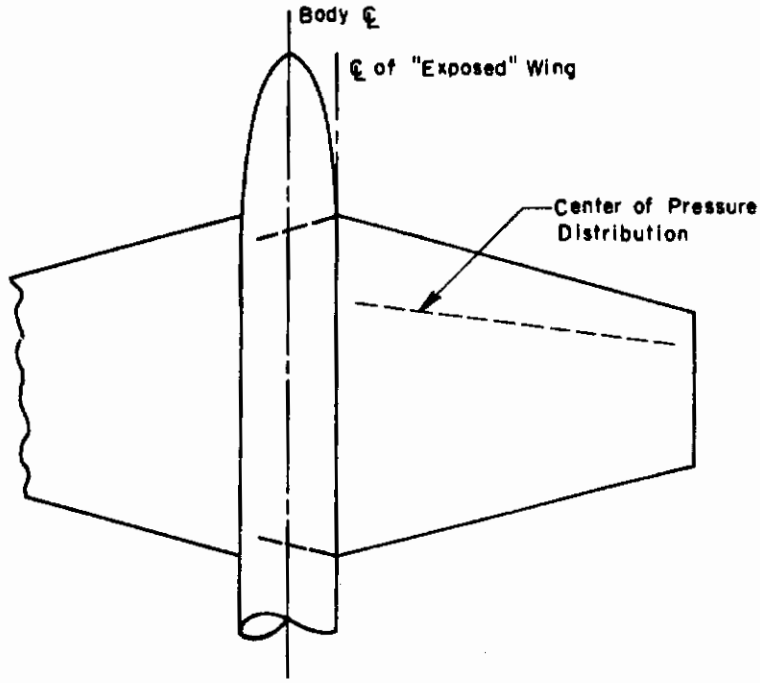

The following sketch shows typical plots of a wing spanwise loading and center of pressure.

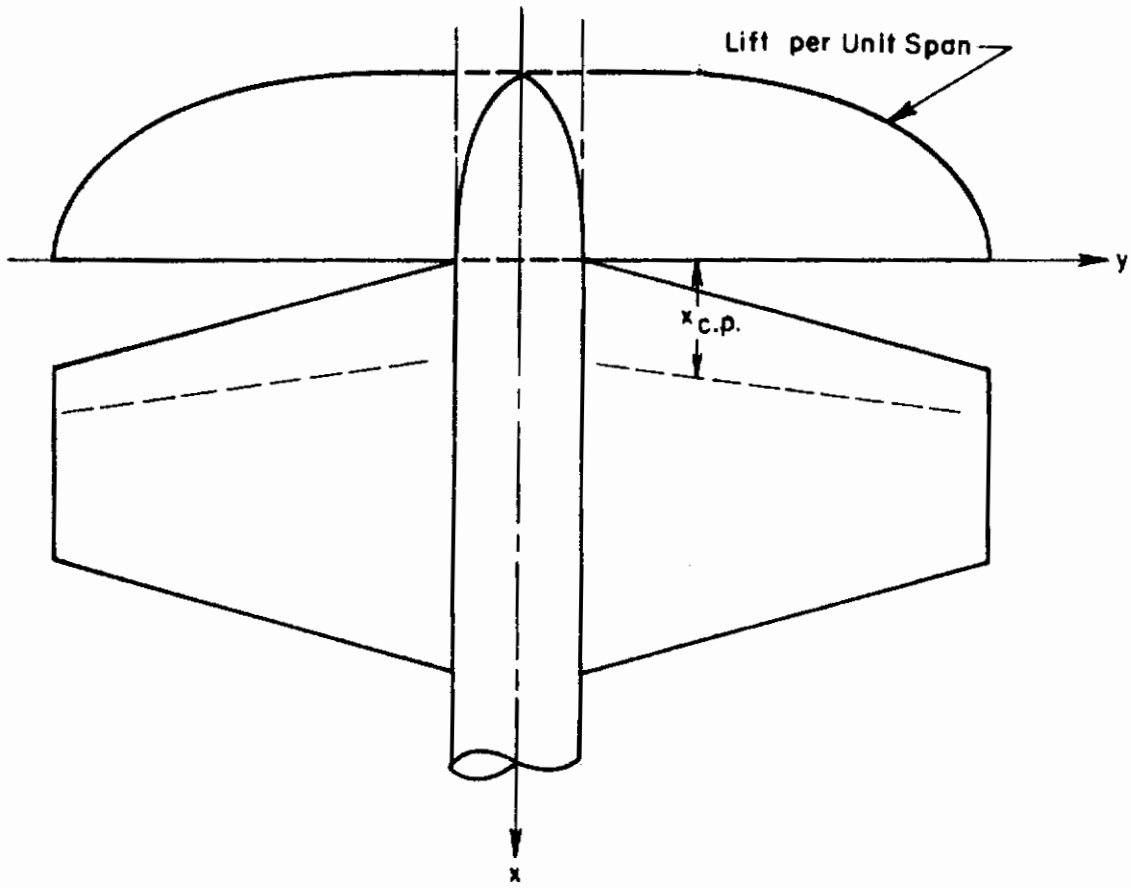

The calculation of wing load due to fuselage interference is carried out in six steps.

a. Subdivide the spanwise load distribution on the wing alone into a number of load increments.

b. Replace these step increases in load by lifting horseshoe vortices.

c. Locate the image vortices within the body.

d. Calculate the upwash distribution at control points on the wing due to these image vortices.

e. Add the upwash due to fuselage angle of attack (if any)

f. Compute the wing load due to the total distribution of upwash at the control points on the wing.

2. Calculation Of Upwash Distribution On The Wing

In the first step, the spanwise loading may be subdivided arbitrarily as illustrated below. The number of subdivisions must be sufficient to obtain a good representation of the image vortex system.

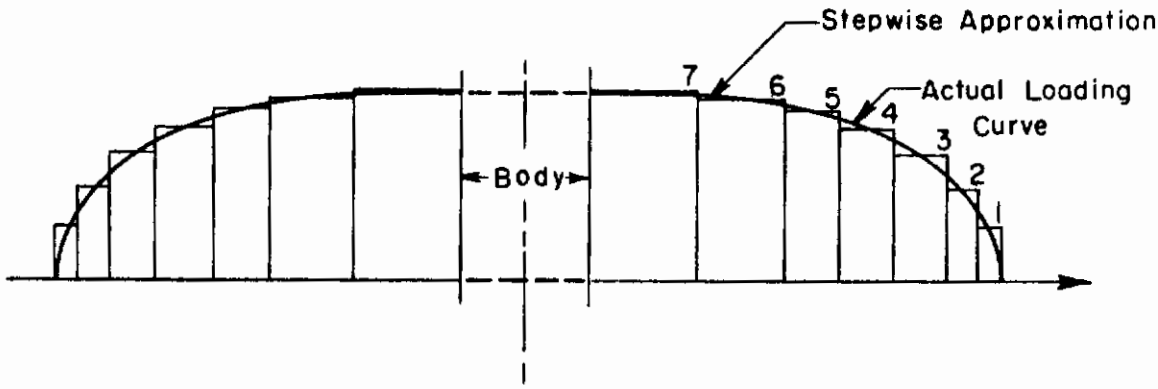

Now, in step two, each increment in spanwise loading is replaced by a horseshoe vortex. The bound portion of the horseshoe is taken parallel to the spanwise coordinate and located approximately on the center of pressure curve. The trailing portions extend to infinity in the streamwise direction (see sketch).

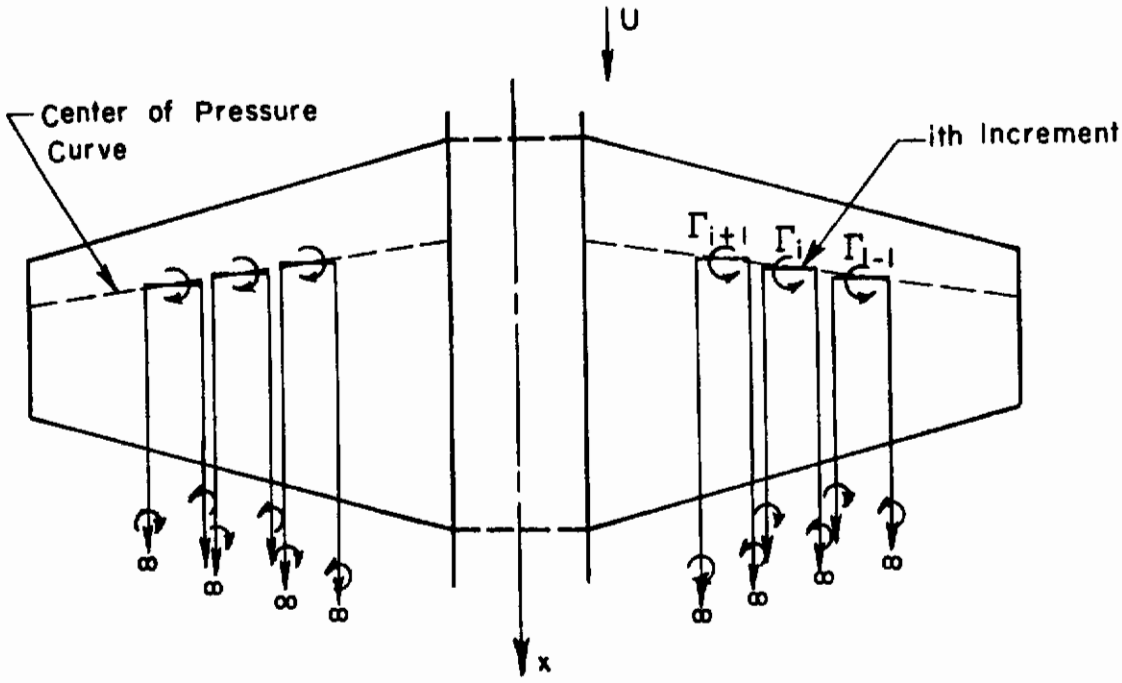

The strength of each vortex Γ_i , is proportional to the corresponding value of the spanwise loading

$$\Gamma_i = \frac{1}{\rho_\infty U_\infty}\left(\frac{dL}{dy}\right) \qquad \text{(IV-121)}$$

where ρ_∞ = free stream density
U_∞ = free stream velocity

Note that an inboard trailing vortex lying adjacent to the body is canceled by its image and is omitted from the computation.

The next step is to locate image vortices within the body so as to satisfy the boundary condition of no flow normal to the body surface.

For a circular body of radius a, the image is a vortex of equal strength and opposite sign located on a line joining the vortex to the center of the circular body. The image is at a distance r_j from the center of the body.

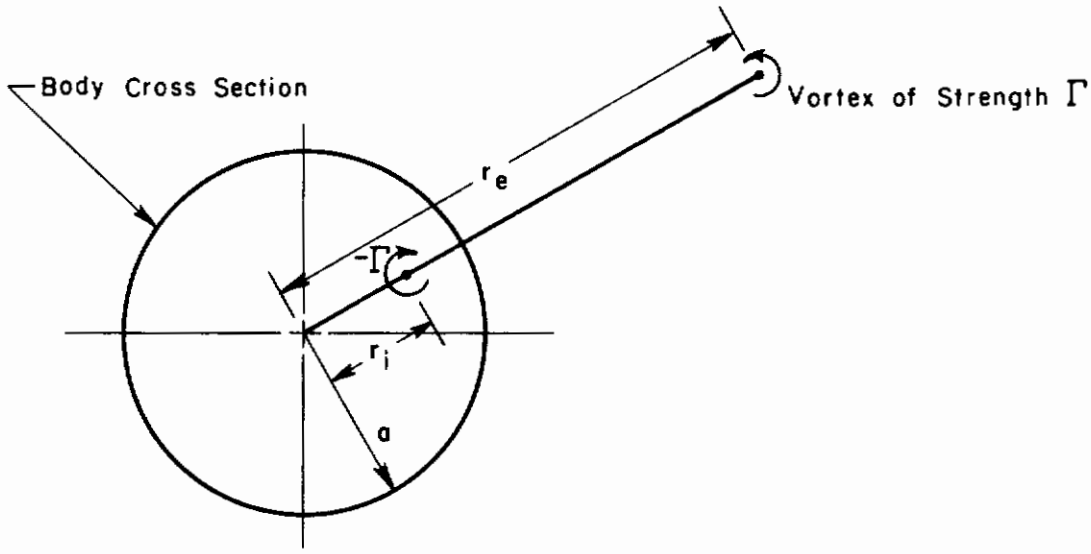

$$r_j = \frac{a^2}{r_e} \qquad (IV\text{-}122)$$

The image vortex is assumed to begin at the same axial station as the external wing vortex. The image of a complete horseshoe vortex is assumed to consist of the images of the two trailing vortices whose starting points are joined by a straight vortex segment approximating the image of the bound lifting vortex.

Step 4 requires the calculation of upwash distribution over the wing due to the image vortex system. The following sketch shows the geometrical relation between a high wing and a typical image horseshoe vortex.

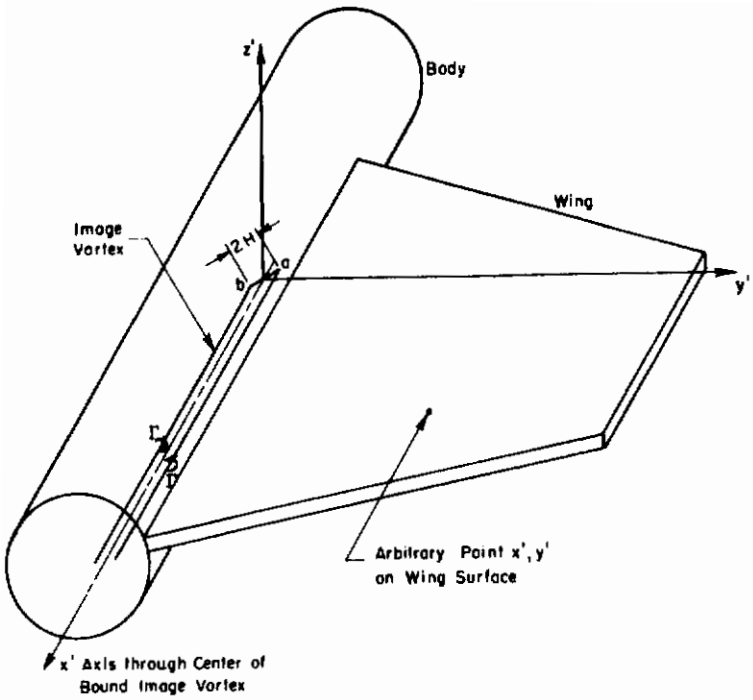

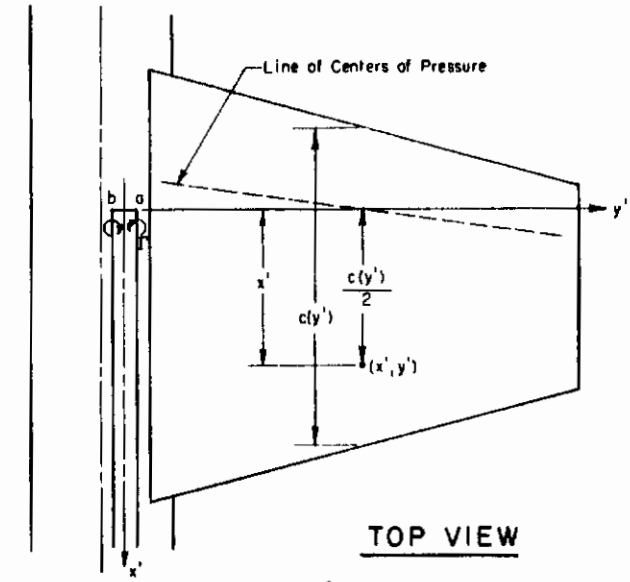

TOP VIEW

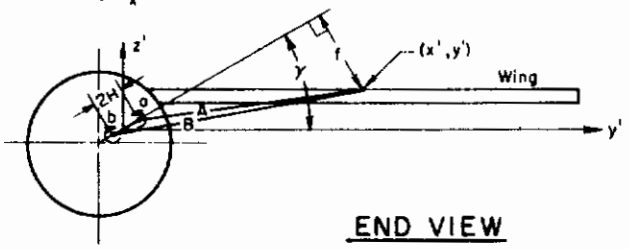

END VIEW

The upwash at the control point (x', y') due to the trailing vortex through a is (from Ref. 2).

$$w_a = \frac{\Gamma}{4\pi A^2}\left(1 + \frac{x'}{\sqrt{(x')^2 + A^2}}\right)\left(y' - H\cos\gamma\right) \qquad \text{(IV-123)}$$

The trailing vortex through b induces an upwash

$$w_b = \frac{-\Gamma}{4\pi B^2}\left(1 + \frac{x'}{\sqrt{(x')^2 + B^2}}\right)\left(y' + H\cos\gamma\right) \qquad \text{(IV-124)}$$

while the image of the bound vortex joining a and b induces the upwash

$$w_{ab} = \frac{-\Gamma}{4\pi}\,\frac{x'\cos\gamma}{f^2 + x'^2}\left(\frac{\sqrt{B^2 - f^2}}{\sqrt{B^2 + (x')^2}} - \frac{\sqrt{A^2 - f^2}}{\sqrt{A^2 + (x')^2}}\right) \qquad \text{(IV-125)}$$

The fuselage angle of attack induces an upwash on the wing of magnitude

$$w_f = U_\infty \alpha \frac{a^2}{R^2}\cos 2\theta \qquad \text{(IV-126)}$$

where R and θ are defined by the following sketch

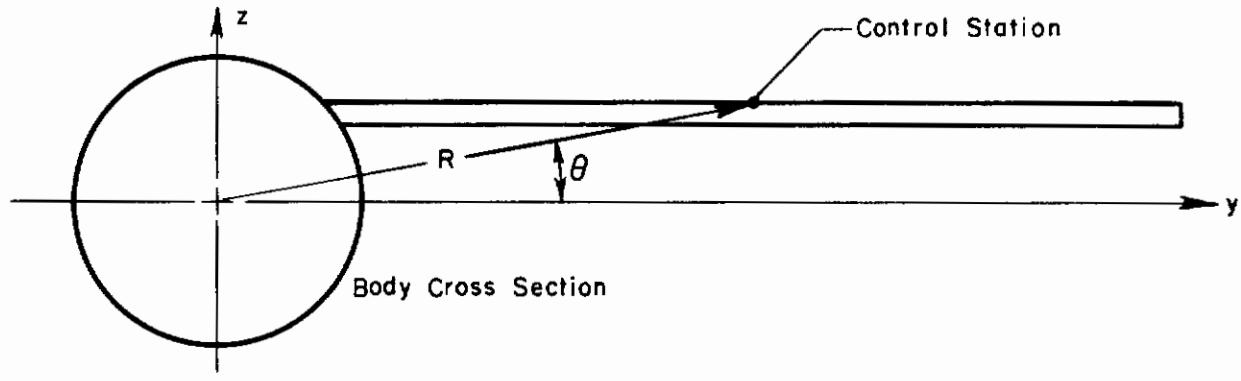

3. Calculation of Wing Load Due to Wing-Body Interference

The control points (x' , y') are chosen along a line which is one half of the local chord behind the center of pressure at each spanwise station. The local flow angles are then determined by adding the contributions of all image vortices from equations (IV-123) - (IV-125) plus the body upwash from Eq. (IV-126). The spanwise angle distribution, resulting from the downwash divided by the free stream velocity, is assumed to be uniform in the chordwise direction. Hence, the additional distribution of wing load due to wing body interference is obtained by applying one of the previously determined procedures (Section IV B, Section IV C, Section IV D, or Section IV E) to this effectively twisted wing.

4. Effects of Compressibility

Compressibility effects would be incorporated in the wing-alone loading before it is subdivided to initiate the computation of wing body interference and also in the computation of load due to the body-induced angle distribution. However, it should be noted that the incompressible vortex solution has been used to determine the angle of attack distribution. Placing the control points at one-half chord length behind the center of pressure line is also justifiable only for subsonic wings. In the supersonic case, the point at which a bound lifting vortex induces a downwash angle matching the local wing slope will depend on Mach number and wing geometry. Since the effects of the image of the lifting vortex will not be large, the extension of the subsonic rule to the supersonic case should not introduce a significant error.

5. Summary of Computational Procedure

The steps in the computation may now be rewritten including reference to the appropriate equations.

(a) Calculate the spanwise load distribution for the wing alone (by the methods of Section IV B, IV C, IV D, or IV E depending on Mach

number and aspect ratio), and subdivide the load into a number of increments.

(b) Replace these step increases in load by lifting horseshoe vortices whose strength is given by Eq. (IV-121). The vortices are placed with spanwise element located at the local center of pressure, and spanning the width of the load step, and with the arms of the "horseshoe" trailing back in the plane of the wing. The trailing element at the body junction is omitted.

(c) Locate image vortices inside of the body at positions given by Equation (IV-122).

(d) Calculate the upwash distribution due to the image vortices, at control points on the wing (one-half of the local chord behind the center of pressure line.) The total upwash is the sum of the contributions of Equations (IV-123), (IV-124) and (IV-125).

(e) Add the upwash due to fuselage angle of attack from Equation (IV-126). The total upwash is assumed to be constant in the chordwise direction.

(f) Compute the wing load due to this spanwise upwash distribution.

For high-aspect ratio subsonic wings, the Weissinger procedure may be used as outlined in Section IV B 5. For low-aspect-ratio subsonic wings, the Lawrence method, summarized in Section IV C5, applies. Transonic wings may be treated by Jones' theory which reduces to Equation (IV-112) where $\left[\alpha = \alpha(y) = -\frac{w(y)}{U_\infty}\right]$. Supersonic wings require application of the method given in Section IV E 2.

The load calculated by these methods is that due to the effect of the body interference. To obtain the total load on the wing, the interference load is added to that of the wing alone. Appendix D gives a FORTRAN program for calculating the pressure distribution on a twisted subsonic wing by the Weissinger procedure including the effect of body interference. Another FORTRAN program is listed for calculating the pressure distribution on a twisted supersonic wing with subsonic leading edges using Etkin's method. Again the pressure includes the effects of wing alone as well as the wing-body interference.

6. Comparison With Experiment

Systematic experiments on effects of wing-body interference are rare. Considering the number of possible variations of wing, body, and flight parameters, a comprehensive experimental program could be an ambitious undertaking. Furthermore, in model breakdown force tests, it is not possible to separate the interference of the body on the wing from the force on the body due to wing interference. It is necessary, therefore, to obtain interference data from pressure measurements or from force measurements on an individual wing panel.

Figure 53 shows a wing body configuration on which extensive Mach number 2 pressure data are reported in Ref. 54. Figure 54 shows theoretical and experimental wing load distributions for the model at 4° angle of attack. The theory seems to account correctly for the effect of the body on the wing pressure. The pressure differences on the front of the wing are higher than theory, while the rear stations are low. The discrepancies appear to be explainable by the effect of wing thickness ($t/c = .1$). The data appears to be sufficiently linear with angle of attack up to at least 10°.

Other experimental data are discussed in Section V, where, after including the effect of the wing on the body, force data can be used as a basis of comparison.

7. Limitations of the Theory

Several restrictive assumptions have been explicitly or implicitly incorporated in the derivation of this procedure. These include:

(a) The body is approximated by an infinite circular cylinder.

(b) The plane of the wing (in which the boundary conditions are applied) is parallel to the body axis.

(c) The downwash induced on the wing by its image vortices has only a spanwise variation and is constant in the chordwise direction.

(d) The vortex image model is assumed to represent adequately the boundary condition at the body surface. Actually, the model is exact only at the plane of the lifting line and at infinity. At other stations a small cross flow will exist at the body surface.

(e) The alteration of wing spanwise loading due to the presence of the body is not taken into account when finding the image vortex system.

(f) The trailing vortices are parallel to the body axis.

(g) Although compressibility effects are included in the wing-alone loading and when computing the load distribution in the interference downwash field, it should be noted that the incompressible vortex solution has been used to determine the angle of attack distribution.

Because of these assumptions, and by comparison with the small amount of available test data, application of the theory is approximately limited to the range of parameters given in the following Table:

Table 7

Range of Applicability of Image Vortex Theory for Calculating the Effect of the Body on the Wing Load Distribution

Parameter	Range of Validity	Comments
body cross section	circular	Body must be nearly a circular cylinder from the wing leading edge to about one chord length behind the trailing edge.
ℓ/d (body fineness ratio)	$\frac{\ell}{d} > 5$	
$\frac{d}{b} = \frac{\text{body diam.}}{\text{wing span}}$	$0 \leq \frac{d}{b} \leq \infty$	
AR	$1 < AR < \infty$	Since chordwise variations in downwash are neglected, theory may be inadequate at low AR.
M_∞	$0 < M_\infty < 4$	May be less accurate at high Mach numbers
$\Lambda_{L.E.}$	$0 < \Lambda_{L.E.} < 75°$	Since chordwise variations in downwash are neglected, theory may be inadequate at low AR.
TR	$0 < TR < 1$	
t/c	$0 < \frac{t}{c} < .1$	Theory may be satisfactory for thicker wings at subsonic speeds.
$\lvert\alpha\rvert$	linear range for wing alone	
i = wing incidence angle	$\lvert\alpha+i\rvert$ in linear range for wing alone	
$\frac{h}{c}$	$0 < \frac{h}{c} < .1$	

8. Comparisons With Other Theories

The simplest methods for handling wing-body interference are probably those based on slender body (and slender wing) theory. In such theories, as given for example in Ref. 55, the flow in each cross section is treated locally as a solution of the two-dimensional Laplace equation. Then conformal mapping may be used to transform the wing-body combination into a more convenient geometry for which solutions are known. Although much of the wing-body interference phenomenon takes place near the wing-body juncture where slender-body theory should be valid, such a theory gives an inadequate approximation of the pressure on a high-aspect-ratio wing.

Pitts, Nielsen, and Kaattari (Ref. 56) have achieved considerable success by using slender body theory to find a factor representing the ratio of the lift of a wing in the presence of a body to that of the wing alone. This factor is then multiplied by the wing-alone lift - obtained by any appropriate method--to account for the effect of the body interference. While this procedure gives a satisfactory representation of the total lift on the wing, it does not directly indicate how the lift is to be distributed; hence the image vortex theory is recommended here. Other studies, Refs. 57 and 58, for example, invoke reverse flow relationships to calculate the total force on supersonic wing-body configurations. Additional methods are reviewed in Ref. 59.

The present result is limited to circular bodies of revolution for which the proper vortex image location is known. It may be possible to generalize these results to nearly circular ellipses by finding approximate image vortex positions for such a body. Or a generalization of the slender body theory, which is given in Ref. 60 for elliptical bodies, might be developed. At present, no method satisfactorily gives complete load distributions for a combination of general body shape and wing aspect ratio.

SECTION V

BODY LOAD DISTRIBUTIONS

A. GENERAL THEORETICAL BACKGROUND

1. Description of the Problem

A body of general shape in a stream of velocity U_∞ is represented in Figure 55. The body is assumed to be symmetric about the x, z plane and to lie approximately in the x, y plane where the free stream velocity is in the x- direction. The centroids of the cross sections form a "mean camber line" which makes a local angle $\alpha(x)$ with the x-axis.

In the present study, it will be assumed that the body behaves structurally as a beam bending in the x, z plane, so that the distribution of normal aerodynamic load, $\frac{dL}{dx}$ is required. The angular distribution of pressure around the body cross sections is not needed except possibly as an intermediate step toward determining the lift on the cross section. A few of the basic mathematical tools used to analyze the lift distribution will be summarized first.

2. Slender Body Theory

As in the slender wing theory discussed in Chapter IV, the slender body theory assumes that the two-dimensional cross flow satisfied the Laplace equation for the velocity potential.

$$\frac{\partial^2 \phi}{\partial y^2} + \frac{\partial^2 \phi}{\partial z^2} = 0 \qquad (V\text{-}1)$$

The assumption is valid when $\frac{\beta}{(\ell/d)} << 1$ where $\beta = \sqrt{|1-M_\infty^2|}$ and (ℓ/d) = fineness ratio of the body. A simple example will illustrate the physical principles involved.

Consider first the flow about a cambered body of revolution as sketched on the following page.

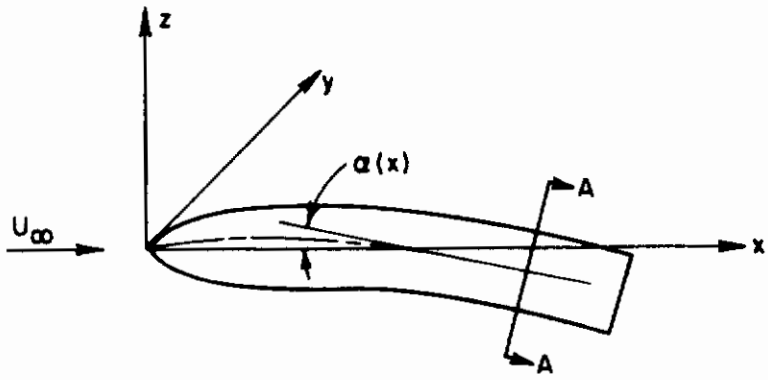

The flow pattern in the cross-sectional plane A-A would then appear as:

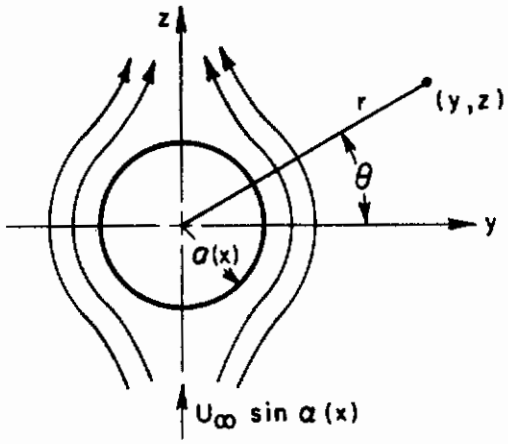

The velocity potential for the flow around the cylinder would be

$$\phi = U_\infty \sin \alpha(x)\, z \left(1 + \frac{[a(x)]^2}{y^2+z^2}\right) \qquad (V\text{-}2)$$

with velocities

$$v = \frac{\partial \phi}{\partial y} = -2 U_\infty \sin \alpha \frac{a^2 y z}{(y^2+z^2)^2} \qquad (V\text{-}3)$$

$$w = \frac{\partial \phi}{\partial z} = U_\infty \sin \alpha \left(1 + \frac{a^2}{y^2+z^2}\right) - 2 U_\infty \sin \alpha \frac{a^2 z^2}{(y^2+z^2)^2} \qquad (V\text{-}4)$$

The total energy in the cross flow stream is then

$$\int_{-\infty}^{\infty}\int \frac{\rho_\infty}{2} (v^2 + w^2)\, dy\, dz = \int_{-\infty}^{\infty}\int \frac{\rho_\infty}{2} U_\infty^2 \sin^2 \alpha\, dy\, dz + \frac{1}{2} U_\infty^2 \sin^2 \alpha\, m' \qquad (V\text{-}5)$$

That is, the total energy consists of the undisturbed free stream energy

plus that associated with the disturbance caused by the flow about the cylinder. The cylinder energy is then represented by an "apparently mass", m' per unit length multiplied by $\frac{1}{2} U_\infty^2 \sin^2\alpha$. The momentum associated with the cylinder disturbance can be readily calculated when the apparent mass has been determined. The energy due to the pressure of the cylinder is

$$E_{cyl.} = \int_a^\infty \left\{ \int_0^{2\pi} r \left[\frac{\rho_\infty}{2} (v^2 + w^2) - \frac{\rho_\infty}{2} U_\infty^2 \sin^2\alpha \right] d\theta \right\} dr \qquad (V\text{-}6)$$

where

$$y = r \cos\theta$$
$$z = r \sin\theta$$

Evaluating the integral gives the energy as

$$E_{cyl.} = \frac{\rho_\infty}{2} \pi a^2 U_\infty^2 \sin^2\alpha = \frac{1}{2} U_\infty^2 \sin^2\alpha \, m' \qquad (V\text{-}7)$$

It is evident that

$$m' = \rho_\infty \pi a^2 \qquad (V\text{-}8)$$

The steady potential flow produces no force on the cylinder, but as the flow changes from cross-section to cross-section of a body the motion imparted to the apparent mass of air will result in a reaction on the body.

The downward momentum over an axial element Δx of the body will be

$$U_\infty \sin\alpha \, m' \Delta x = \rho_\infty \pi U_\infty \sin\alpha(x) \left[a(x) \right]^2 \Delta x \qquad (V\text{-}9)$$

The lift force on the element will be equal to the rate of change of momentum:

$$\Delta L = \frac{d}{dt} \left\{ \rho_\infty \pi U_\infty \sin\alpha(x) \left[a(x) \right]^2 \right\} \Delta x$$

$$= U_\infty \cos\alpha \frac{d}{dx} \left\{ \rho_\infty \pi U_\infty \sin\alpha(x) \left[a(x) \right]^2 \right\} \Delta x \qquad (V\text{-}10)$$

For small angles of attack, then,the streamwise distribution of lift will be

$$\frac{dL}{dx} = \rho_\infty \pi U_\infty^2 \frac{d}{dx} \left[\alpha(x)\, a^2(x)\right] \qquad (V\text{-}11)$$

Although this derivation is given here for the case of a body of revolution, slender bodies of more general cross-section including thin wings, may be similarly analyzed. This was, in fact, the procedure followed by Jones in his low-aspect-ratio wing theory (Ref. 12).

3. Exact Solutions for Supersonic Potential Flow

Because of its simplicity, the slender body theory can be applied to bodies of very general shape. However, the approximations in the theory sometimes produce results of questionable accuracy. In certain special cases, it is possible to obtain more exact solutions of the load distribution problem. These solutions may then be used to check the range of validity of the slender body theory, and also form a basis for other approximate methods. Two exact solutions of the nonlinear equation for supersonic potential flow will be discussed since they prove useful for these purposes.

The governing partial differential equation for velocity potential in steady irrotational supersonic flow is given on page 124 of Ref. 48 as

$$\phi_{xx}(a^2-\phi_x^2) + \phi_{yy}(a^2-\phi_y^2) + \phi_{zz}(a^2-\phi_z^2) = 2\phi_{yz}\phi_y\phi_z + 2\phi_{xz}\phi_x\phi_z + 2\phi_{xy}\phi_x\phi_y \qquad (V\text{-}12)$$

where a is the local speed of sound. Special solutions in two and three - dimensions of particular interest will be cited here.

In two dimensions (x and z), the equation becomes

$$\phi_{xx}(a^2-\phi_x^2) + \phi_{zz}(a^2-\phi_z^2) = 2\phi_{xz}\phi_x\phi_z = (\phi_{xz}+\phi_{zx})\phi_x\phi_z \qquad (V\text{-}13)$$

The "Prandtl-Meyer" solution of this equation results by considering the consequences of the assumption that the total velocity, V, is a function only of the flow direction θ. Then, by definition, $V = \sqrt{u^2+w^2}$ and $\theta = \tan^{-1}\frac{w}{u}$ where $u = x$-component of velocity $= \frac{\partial \phi}{\partial x}$, and $w = z$-component of velocity $= \frac{\partial \phi}{\partial z}$. In terms of V and θ,

$$\left.\begin{aligned}
\phi_{xx} &= \frac{\partial u}{\partial x} = \frac{\partial}{\partial x}(V\cos\theta) = \left(\frac{dV}{d\theta}\cos\theta - V\sin\theta\right)\frac{\partial\theta}{\partial x} \\
\phi_{xz} &= \frac{\partial u}{\partial z} = \left(\frac{dV}{d\theta}\cos\theta - V\sin\theta\right)\frac{\partial\theta}{\partial z} \\
\phi_{zx} &= \frac{\partial w}{\partial x} = \left(\frac{dV}{d\theta}\sin\theta + V\cos\theta\right)\frac{\partial\theta}{\partial x} \\
\phi_{zz} &= \frac{\partial w}{\partial z} = \left(\frac{dV}{d\theta}\sin\theta + V\cos\theta\right)\frac{\partial\theta}{\partial z}
\end{aligned}\right\} \quad (V\text{-}14)$$

Then Eq. (V-13) becomes

$$\left(a^2 - V^2\cos^2\theta\right)\left(\frac{dV}{d\theta}\cos\theta - V\sin\theta\right)\frac{\partial\theta}{\partial x} + \left(a^2 - V^2\sin^2\theta\right)\left(\frac{dV}{d\theta}\sin\theta + V\cos\theta\right)\frac{\partial\theta}{\partial z}$$

$$-V^2\sin\theta\cos\theta\left(\frac{dV}{d\theta}\cos\theta - V\sin\theta\right)\frac{\partial\theta}{\partial z} - V^2\sin\theta\cos\theta\left(\frac{dV}{d\theta}\sin\theta + V\cos\theta\right)\frac{\partial\theta}{\partial x} = 0 \quad (V\text{-}15)$$

or

$$\left[(1-M^2)\cos\theta\frac{dV}{d\theta} - V\sin\theta\right]\frac{\partial\theta}{\partial x} + \left[(1-M^2)\sin\theta\frac{dV}{d\theta} - V\cos\theta\right]\frac{\partial\theta}{\partial z} = 0 \quad (V\text{-}16)$$

and, since $\phi_{xz} = \phi_{zx}$

$$\left[\sin\theta\frac{dV}{d\theta} + V\cos\theta\right]\frac{\partial\theta}{\partial x} - \left[\cos\theta\frac{dV}{d\theta} - V\sin\theta\right]\frac{\partial\theta}{\partial z} = 0 \quad (V\text{-}17)$$

where $M = \frac{V}{a}$ = local Mach number.

These two equations in $\frac{\partial\theta}{\partial x}$ and $\frac{\partial\theta}{\partial z}$ have the trivial solution $\frac{\partial\theta}{\partial z} = \frac{\partial\theta}{\partial x} = 0$ everywhere unless the determinant of the coefficients is zero. This latter condition requires

$$\left[\frac{dV}{d\theta}\right]^2 (1-M^2) + V^2 = 0 \qquad (V\text{-}18)$$

Hence

$$\frac{dV}{d\theta} = \pm \frac{V}{\sqrt{M^2-1}} \qquad (M>1) \qquad (V\text{-}19)$$

The one-dimensional isentropic flow relations provide an expression for V in terms of M:

$$\frac{V^2}{a_0^2} = \frac{M^2}{1+\frac{\gamma-1}{2}M^2} \qquad (V\text{-}20)$$

where a_0 is the velocity of sound at stagnation conditions, and γ is the ratio of specific heats. It is then possible to integrate Eq. (V-19) giving

$$\theta = \text{constant} \pm \left[\sqrt{\frac{\gamma+1}{\gamma-1}}\tan^{-1}\sqrt{\frac{\gamma-1}{\gamma+1}(M^2-1)} - \tan^{-1}\sqrt{M^2-1}\right] \qquad (V\text{-}21)$$

Thus, a relation between local Mach number and flow angle is established. The one-dimensional isentropic flow relations, given, for example, in Ref. 61 may be used to determine other properties in terms of the local Mach number.

By a similar procedure, an exact solution to the three-dimensional equation is also attainable. However, in that case, the resulting ordinary differential equation does not have a closed form solution. Numerical results are tabulated in Ref. 62, and elsewhere.

4. Method of Characteristics

The Prandtl-Meyer solution may be applied directly to the determination of the flow around a corner; while the three-dimensional analog solves the cone problem. In addition these solutions form the basis of the numerical "method of characteristics" which may be applied to a wide class of

flows. The two-dimensional method of characteristics is described in Ref. 61. A more complete treatment, including the three-dimensional analysis is given in Ref. 63.

The two-dimensional procedure is indicated in the following sketch

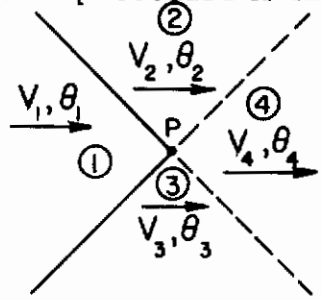

If, at the point P in an irrotational flow field, the properties are known in regions 1, 2, and 3, then the properties in region 4 can be determined by turning the flows from regions 2 and 3 in such a way that each arrives at the same flow direction and velocity in region 4. The boundaries of the regions are the characteristic lines (local Mach lines) which divide the flow field into a mesh of constant-property cells. By increasing the fineness of the mesh, the numerical solution thus obtained comes closer to an exact solution of Eq. (V-13). Other numerical procedures are also possible; all becoming identical in the limit of infinitesimal mesh size.

The three-dimensional method of characteristics is in many respects analogous to the two-dimensional case; but differs fundamentally in that properties immediately behind a straight characteristic line will be the same everywhere in a two-dimensional flow but in general will vary in the three-dimensional flow.

A shock wave in the flow may be treated by the normal or oblique shock relations given in Ref. 61 or 64.

5. Effects of Boundary Layer and Flow Separation

The nonviscous theories, such as slender body theory, can be improved by assuming that the potential flow field surrounds the body plus its boundary layer displacement thickness. This modification is particularly important in boattailed bodies . Slender body theory predicts zero lift on

an inclined body which is pointed at both ends. The growth and separation of the axial boundary layer, however, will cause an outward displacement of the potential flow over the aft end of the body, which then behaves as though it had a finite base area. This refinement will not be incorporated in the present report.

Of greater significance is the effect of vortex separation. As the angle of attack increases, a pair of vortices separate from the lee side of the body in a manner similar to the separation from side edges of low-aspect-ratio wings. On bodies, however, the separation causes such a rapid increase in lift that at about 5° angle of attack the actual lift may already be twice the linear value. In fact it is sometimes difficult to measure the initial slope of the lift curve since the nonlinear contribution increases so quickly.

In Ref. 65, Allen proposed a cross-flow drag theory to account for the nonlinear variation of lift with angle of attack. Since then, several improvements in his concept have been proposed, but all rely to some extent on empirically determined parameters. In keeping with the scope of the present report, the nonlinear theories will not be incorporated here.

B. SLENDER BODY THEORY

1. Review of the Theory

The slender body theory described in the first section of this chapter was first proposed by Munk (Ref. 66) as a means of calculating the lift on airships. Tsien later showed that this incompressible theory might also be applied at supersonic speeds (Ref. 67). Here it will be recommended for use primarily at subsonic and transonic speeds since a more accurate supersonic method is available. However, since the improved supersonic theory applies only to bodies of revolution, the slender body method is also useful for noncircular bodies throughout the speed range from subsonic to supersonic.

The extension to elliptic bodies is given in Ref. 68, where the apparent mass associated with an ellipse is given as

$$m' = \rho_\infty \pi \left(\frac{b}{2}\right)^2 \qquad (V\text{-}22)$$

Here b is the horizontal axis of the ellipse (normal to the cross-flow). Then the streamwise distribution of lift becomes, by analogy to Eq. (V-11)

$$\frac{dL}{dx}_{ellipse} = \rho_\infty \pi U_\infty^2 \frac{d}{dx}\left\{\alpha(x)\left(\frac{b}{2}(x)\right)^2\right\} \qquad (V\text{-}23)$$

Of course, for a wing, which is the limiting case of a flat ellipse, Eq. (V-23) is equivalent to Eq. (IV-111) given by Jones' theory for slender wings. Also, for bodies of revolution, the expression reduces to that given by Eq. (V-11).

2. Summary of Computational Procedure

The calculation of the lift distribution on a body of general shape is carried out by the use of Eq. (V-23) although the derivation is strictly valid only for elliptical cross sections. Thus,

$$\frac{dL}{dx} = \rho_\infty \pi U_\infty^2 \frac{d}{dx}\left\{\alpha(x)\left(\frac{b}{2}(x)\right)^2\right\}$$

According to this formula there will be no lift on cylindrical portions of the body. A force will appear only where the shape is changing, such as over the nose region; or where the angle of attack is changing as on a cambered body.

3. Comparison with Experiment

Figure 56 shows a comparison of theoretical and experimental lift curve slopes for circular ogive-cylinders. The slope, $\frac{dC_L}{d\alpha}$ at $\alpha = 0$, is plotted against Mach number for bodies of various fineness ratio. In the subsonic case the nose of the body is a two-caliber secant ogive

followed by a cylindrical afterbody. The supersonic bodies have tangent-ogive noses of varying lengths. The data are taken from Ref. 69. The theory gives $\frac{dC_L}{d\alpha} = 2$ (per radian) for all cases as may be easily seen from integration of Eq. (V-11). The coefficient is defined in terms of the area of the body cross section at the base. The centers of pressure are plotted in Fig. 57.

Although the agreement between theory and experiment is reasonably good for short bodies, the data show a rearward movement of center of pressure with increasing fineness ratio which is not predicted by the theory. The growth of boundary layer displacement thickness would explain the presence of a force on the cylindrical portion of the body.

The variation of lift coefficient with angle of attack is shown in Fig. 58 for a few cases. The nonlinearity of the experimental data is evident on the figure.

4. Limitations of the Method

The theory produces erroneous results due to the approximations in its representation of the potential flow and also due to the effects of viscosity and flow separation. The slender body approximation limits the range of applicability of the result to smooth bodies of high fineness ratio. The angle of attack must also be small. Further, as in the slender wing theory, the slenderness assumption may be relaxed somewhat at transonic speeds, while at high Mach numbers the approximation will be poorer.

Boundary layer growth will introduce significant errors on long cylindrical or boattailed bodies. Vortex separation will also become important on long bodies and will cause a nonlinear increase of lift with angle of attack.

The following table summarizes the limitations of slender body theory

Table 8

Range of Validity of Slender Body Theory

Parameter	Range of Validity	Comments
$\frac{l}{d}$	$5 < \frac{l}{d} < 8$	Lower fineness ratio is acceptable if $M_\infty \to 1$. May be applied to higher fineness ratio if nose is long.
$\frac{A\ base}{A\ max.} = \frac{base\ area}{max.\ cross\ sect.}$	$> .8$	Boundary layer separation causes errors on boattailed bodies.
$\alpha(x)$	$< 3°$	Vortex separation causes errors at higher angles of attack.
$\delta_o = $ semi-vertex angle of nose	$< 15°$	
M_∞	$0 < M_\infty < 2$	Accuracy is poorer at high supersonic speeds.

5. Comparison with other Theories

The slender body theory can obviously be improved in two directions. First, a more accurate solution of the potential flow problem may be employed; and second, boundary layer growth and vortex separation may be included in the analysis. More accurate potential flow theories are indicated in Ref. 70 based on linear and higher order equations. However, these extensions have not been developed for bodies of general cross section at angle of attack. It is possible, in principle, to resort to the three-dimensional method of characteristics (see Ref. 63) in the supersonic range but the numerical labor is enormous, particularly since a bow shock must appear in the flow.

Since these more complicated theories do not take into account vortex separation or boundary layer growth their use is not recommended. The latter effects will usually cause greater errors than the approximations to the potential flow. Vortex separation introduces a force distribution which is nonlinear in angle of attack as explained in Section VA5. Such nonlinear forces are excluded from the present investigation. The

effect of boundary layer growth is not difficult to estimate in the case of cylindrical body sections, but the correction does not seem to have been generally mentioned in the literature. A procedure is given in Ref. 71.

An improved potential flow analysis has been proposed by Syvertson and Dennis (Ref. 72). This procedure, which will be described in the next Section, is particularly useful in the speed range around $M_\infty \sim 3$ where the slender body theory is often inadequate.

C. SUPERSONIC BODIES OF REVOLUTION

1. Shock Expansion Theory

Syvertson and Dennis (Ref. 72) assume that at very small angles of attack the streamlines next to a body of revolution lie along meridians. They then calculate the pressure perturbation on each meridian due to angle of attack,

The procedure begins by simulating the contour of the axisymmetric body by tangent conical frustrums as indicated below:

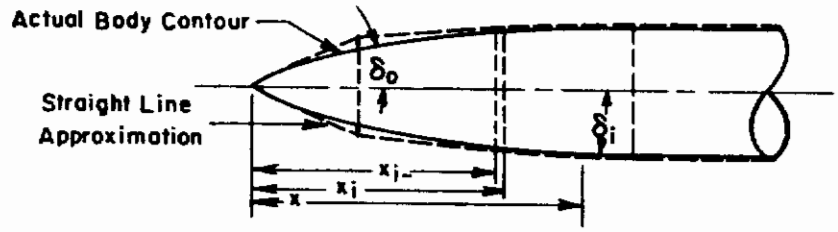

If the pressure is known everywhere on the surface of the zero-angle-of-attack body, then the normal force coefficient generated by a small angle at station x would be

$$\frac{dC_N}{dx} = \frac{2\pi}{A} \Lambda r \qquad (V\text{-}24)$$

where A is the reference area (generally the base area of the body), and Λ is the nondimensional loading on a thin disk of unit radius normal to the body axis and at angle of attack α. Λ is defined by the following equation:

$$\Lambda = \frac{\alpha}{\pi q_\infty} \int_0^\pi \frac{dp}{d\alpha} \cos\phi \, d\phi \qquad (V\text{-}25)$$

where ϕ is an azimuthal angle measured from the bottom element of the body cross section.

The next step in the process, then, is the evaluation of $\frac{dp}{d\alpha}$

This quantity is obtained by differentiating the pressure distribution on the axisymmetric (zero-angle-of-attack) body. Syvertson and Dennis assume that this pressure distribution is of the form

$$p = p_c - (p_c - p_i) e^{-\eta} \qquad (V-26)$$

where

$$\eta = \left(\frac{\partial p}{\partial s}\right)_i \frac{x - x_i}{(p_c - p_i) \cos \delta_i} \qquad (V-27)$$

Here p_c is the pressure on a cone (at zero angle of attack) of semi-vertex angle δ_i ; p_i is the pressure just past the corner at x_i obtained by a Prandtl-Meyer expansion of the flow from the condition just upstream of the corner through the angle $(\delta_{i-1} - \delta_i)$. The distance along an element of the conical frustrum is designated by s. Equation (V-26) has been chosen to give the correct change in pressure at each corner where the flow is locally equivalent to a two-dimensional Prandtl-Meyer expansion. At large distance from the corner the pressure must approach the value for a cone of semi-vertex angle δ_i . The particular form of Eq. (V-26) results from the fact that the rate of change of pressure with distance along the conical frustrum is proportional to the pressure; hence an exponential appears when the differential variation is integrated.

Differentiation with respect to angle of attack would give

$$\frac{dp}{d\alpha} = \frac{dp_c}{d\alpha}(1 - e^{-\eta}) + e^{-\eta} \frac{dp_i}{d\alpha} + (p_c - p_i) e^{-\eta} \frac{d\eta}{d\alpha} \qquad (V-28)$$

However, at $\eta = 0$ $(x = x_i)$, $\frac{dp}{d\alpha} = \frac{dp_i}{d\alpha}$; hence the last term must be zero. The rate of change of p_i with angle is obtained from the Prandtl-Meyer equation. For example Eq. (V-21) gives the variation of Mach number with flow angle. Then, the one-dimensional isentropic

flow relations can be applied to give the variation of pressure with Mach number. The flow angle varies from a compression angle α at $\phi = 0$ (bottom of body) to an expansion at the top surface. Then

$$\theta = -\alpha \cos \phi \tag{V-29}$$

Finally, the integral of cone pressure must be evaluated in order to compute the first term of Eq. (V-28). The normal force on a cone is the normal component of the integral of the pressure over the area. Thus, in coefficient form, the slope of the normal force is

$$\left.\frac{dC_N}{d\alpha}\right|_{cone} = \frac{1}{q_\infty \pi \tan \delta_i} \int_0^\pi \frac{dp_c}{d\alpha} \cos \phi \, d\phi \tag{V-30}$$

where δ_i = cone semi-vertex angle and the coefficient is normalized by the base area of the cone.

When these results are introduced into Eq. (V-25), the nondimensional loading becomes

$$\Lambda = \alpha \tan \delta_i \, (1 - e^{-\eta}) \left.\frac{dC_N}{d\alpha}\right|_{cone} + \frac{\alpha}{\pi q_\infty} e^{-\eta} \int_0^\pi \frac{dp_i}{d\alpha} \cos \phi \, d\phi \tag{V-31}$$

Syvertson and Dennis note that from the Prandtl-Meyer relations

$$\frac{dp_i}{d\alpha} = \frac{p_i M_i \sqrt{M_i^2 - 1}}{p_{i-} M_{i-} \sqrt{M_{i-}^2 - 1}} \tag{V-32}$$

where p_{i-} and M_{i-} refer to the pressure and Mach number on the non-lifting body at the point just upstream of the corner x_i. Furthermore, from the definition of Λ,

$$\Lambda_{i-} = \frac{\alpha}{\pi q_\infty} \int_0^\pi \frac{dp_{i-}}{d\alpha} \cos \phi \, d\phi \tag{V-33}$$

Hence,

$$\Lambda = \alpha \tan \delta_i \, (1 - e^{-\eta}) \left.\frac{dC_N}{d\alpha}\right|_{cone} + \frac{p_i M_i \sqrt{M_i^2 - 1}}{p_{i-} M_{i-} \sqrt{M_{i-}^2 - 1}} \Lambda_{i-} \tag{V-34}$$

To evaluate this expression, it is necessary to determine $\left(\frac{\partial p}{\partial s}\right)_i$ in order to obtain η from Eq. (V-27). The function is derived in Ref. 72 by calculating the change of pressure along a general streamline in a Prandtl-Meyer flow and then determining the limit as the streamline approaches the surface of the body, The result is approximately

$$\left(\frac{\partial p}{\partial s}\right)_i = \frac{\gamma p_i M_i^2}{2 r_i (M_i^2 - 1)} \left(\frac{\Omega_{i-}}{\Omega_i} \sin\delta_i - \sin\delta_i\right) + \frac{p_i M_i^2 (M_{i-}^2 - 1) \Omega_{i-}}{p_{i-} M_{i-}^2 (M_i^2 - 1) \Omega_i} \left(\frac{\partial p}{\partial s}\right)_{i-} \qquad (V\text{-}35)$$

where

$$\Omega = \frac{1}{M} \left[\frac{1 + \frac{\gamma - 1}{2} M^2}{\frac{\gamma - 1}{2}}\right]^{\frac{\gamma + 1}{2(\gamma - 1)}} \qquad (V\text{-}36)$$

and γ = ratio of specific heats = 1.4 for air at ordinary temperatures.

2. Summary of Computational Procedure

The necessary tools have now been assembled by means of which the load distribution is to be constructed. The procedure may be carried out in the following manner:

(a) The calculation begins with the determination of the pressures on the non-lifting segmented body starting from the conical tip. The pressure, p_{1-} and Mach number, M_{1-}, on the surface of the nonlifting cone are constant and are tabulated (Ref. 64, for example).

(b) The next step is to compute the pressure p_1 and Mach number M_1 on the nonlifting body at the point x_1 just past the first turn of the segmented body. The Prandtl-Meyer relations are employed (tabulated in Ref. 64) to calculate the new pressure and Mach number obtained by expanding from p_{1-} and M_{1-} (on the cone) through the angle $\delta_{1-} - \delta_1$ to the new values p_1 and M_1.

(c) The pressure gradient just past the corner is also needed and can be obtained from Eq. (V-35) where $\left(\frac{\partial p}{\partial s}\right)_{1-}$ is the gradient of

pressure on the cone and is zero.

(d) The pressures along the conical frustrum joining station x_1 and x_2 are found from Eq. (V-26) where η is given as a function of x by Eq. (V-27). In particular, p_{2-} (at the end of the frustrum where $x = x_{2-}$) is needed.

(e) The Mach number corresponding to this pressure is obtained from one-dimensional flow tables (Ref. 64), or by the equation

$$\frac{p_{2-}}{p_1} = \left[\frac{1 + \frac{\gamma-1}{2} M_1^2}{1 + \frac{\gamma-1}{2} M_{2-}^2}\right] \qquad (V\text{-}37)$$

(f) The gradient $\left(\frac{\partial p}{\partial s}\right)_{2-}$ is obtained by differentiating Eq. (V-26). Thus

$$\left(\frac{\partial p}{\partial s}\right)_{2-} = \frac{p_{c-} - p_{2-}}{p_c - p_1} \left(\frac{\partial p}{\partial s}\right)_1 \qquad (V\text{-}38)$$

Here p_c is the surface pressure on the cone of semi-vertex angle δ_i. $\left(\frac{\partial p}{\partial s}\right)_1$ has been found in step (c); p_{2-} in step (d); and p_1 in step (b).

(g) Now step (b) is repeated to find p_2 and M_2 by turning the flow through the angle $\delta_1 - \delta_2$. Also step (c) is repeated to give $\left(\frac{\partial p}{\partial s}\right)_2$. But this time $\left(\frac{\partial p}{\partial s}\right)_{2-}$ used in Eq. (V-35) is not zero but is the value found in step (f). Continuing along the body, the pressure (and Mach number) are determined at all points on the nonlifting body.

(h) The normal force distribution is also calculated by proceeding rearward from the conical nose. First, the slope of the normal force on the conical tip is obtained from available numerical solutions of the exact three-dimensional potential flow equations. These numerical results are tabulated in Ref. 73.

(i) The loading parameter Λ_o can now be found, where, on the cone,

$$\Lambda_o = \alpha \tan \delta_o \left.\frac{dC_N}{d\alpha}\right|_{cone-\delta_o} \qquad (V\text{-}39)$$

Then the normal force distribution is given by Eq. (V-24). The angle of attack may be a function of x in this expression for Λ_0.

(j) On the first conical frustrum, having angle δ_0, the loading parameter is obtained from Eq. (V-34) where $\frac{dC_N}{d\alpha}\Big|_{cone}$ is the slope of the normal force for a cone of semi-vertex angle δ_1. Λ_1 is the loading parameter at the end of the conical tip. All other quantities are available from the nonlifting solution.

(k) The normal force distribution in the region from $x_1 < x < x_2$ is now obtained from Eq. (V-24)

(l) The process is continued for the remaining conical frustrums.

Forces on the external surfaces of ducted bodies may be computed in a similar manner, assuming that the internal flow is "swallowed" with no spill-over. In this case the initial flow consists of a cylinder of the free stream, and the first section of the body will compress the flow by turning it through a concave corner. The compression may be treated by oblique shock theory or, unless the turning angle is large (more than 20°), it may be approximated by an isentropic (Prandtl-Meyer)analysis.

3. Comparison With Experiment

Extensive checks presented in Ref. 72 show very good agreement between theory and experiment on cone-cylinder and ogive-cylinder bodies. Some of the lift data are reproduced in Figs. 59 and 60. Corresponding centers of pressure are shown in Figs. 61 and 62. Slender body theory would predict $\frac{dC_N}{d\alpha} = 2$ for all cases. The data show that the slender body theory fails to account for the lift on the cylindrical after body; while the shock-expansion method predicts this extra lift quite accurately.

4. Limitations of the Theory

The shock-expansion method was developed for application to bodies for which $\frac{M_\infty}{fn} \sim 1$ where fn is the nose fineness ratio. It appears to be accurate at least through the range $.4 \leq \frac{M_\infty}{fn} \leq 2$.

As presented here, the Prandtl-Meyer solution is used to find the changes in properties as the flow is turned around segments of the body contour. In the case of a concave corner, oblique shock relations should, in principle, be used instead. Equations corresponding to such cases are included in Ref. 72. However, the flow will often separate in the neighborhood of a concave corner, therefore, the solution may then be seriously in error. Consequently, if the shock wave is so strong that the Prandtl-Meyer relations are inapplicable, the oblique shock formulas are probably equally erroneous.

Although the shock-expansion method seems to predict accurately the lift distribution on cylindrical portions of the body, it still does not account for possible effects of boundary layer growth or separation. Therefore, unless a correction to body shape is made to account for the growth of the boundary layer displacement thickness, the method will be inaccurate when such effects are important, as, for example, on boat-tailed bodies. Vortex separation will also limit the applicable angle of attack range.

The following table shows estimated ranges of validity of the method.

Table 9

Range of Validity of Shock-Expansion Theory

Parameter	Range of Validity	Comments
$\frac{M_\infty}{fn}$	$.4 \leqq \frac{M_\infty}{fn} \leqq 2$	Probably applies over an even wider range
$\frac{\ell}{d}$	$3 \leqq \frac{\ell}{d} \leqq 20$	
M_∞	$2 \leqq M_\infty \leqq 6$	Subject to the limits on M_∞/fn
$\alpha(x)$	$< 3°$	
δ_o = semi-vertex angle of nose	< shock detachment angle	
$\frac{A_{base}}{A_{max.}}$	$> .75$	
body cross section	circular	

5. Comparison With Other Theories

The data plotted in Figs. 59-62 indicate that the slender body theory gives reasonably accurate load distributions over the expanding body nose. On cylindrical sections, where the slender body theory predicts no lift, the shock expansion method gives much better results. If boundary layer growth is significant, then neither theory will be correct, but, in the data shown here, the lift on the cylindrical portion of the body was explainable by an entirely nonviscous analysis.

On the other hand, besides being more cumbersome to use, the shock-expansion theory applies only to circular bodies; therefore it would be desirable to somehow extend or improve the slender body theory. One such extension has been proposed by Beverly Beane in Ref. 74. She adds the loading due to camber computed by slender body theory to an experimentally determined load distribution on an uncambered lifting body. The perturbation in load due to body camber is successfully predicted by slender body theory. In view of this success, it may be possible to develop a theory which would account for non-circular cross section as well as camber by perturbations of a more accurate basic theory.

In some respects this procedure is related to the "hybrid" theory of Van Dyke (Ref. 75). After deriving a second order theory for bodies of revolution, he finds that the determination of lift distribution is practical only for a cone. He then suggests that the axial pressure distribution be determined to second order or by some other accurate method and then be combined with a linear cross flow analysis. Syvertson and Dennis show by comparisons with experiment that their shock-expansion theory is generally more accurate than the hybrid analysis.

The method of characteristics would give greater accuracy than the shock-expansion procedure, but requires very lengthy calculations. On a cone, since the shock-expansion procedure uses the exact solutions, the results would be identical. Improvements on other body shapes are expected to be too small to warrant the additional labor especially when boundary layer growth and vortex separation will limit the applicability of both procedures.

D. EFFECT OF WING INTERFERENCE ON BODY LOAD

1. Slender Body Theory

The addition of a wing tends to block the flow of high pressure air from the windward side of a body to the leeward surface; hence the body carries more lift in the vicinity of the wing. This increment in lift has been calculated by Spreiter (Ref. 55) using slender body theory. In spite of its limitations, slender body theory appears to be a reasonable method of calculating the body carry-over. effect for the following reasons.

(a) The theory is simple and versatile.

(b) The interference effects of interest lie near the x - axis where slender body theory should be valid.

(c) Experimental data in which the interference of the body on the wing is separated from that of the wing on the body is rarely available. Consequently, it is difficult to compare the accuracy of different theories.

In this method, each cross section of the flow is analyzed as though it were independent of all other cross sections. Consequently a midwing mounted on a circular body would appear at some axial station (x-coordinate) as shown below

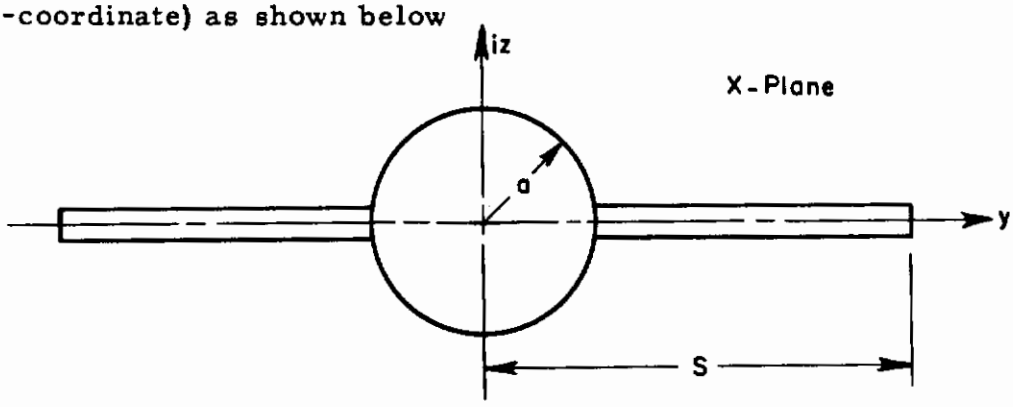

The conformal transformation $\zeta = X - \frac{a^2}{X}$ maps the wing-body in the X-plane, where $X = y + iz$, into a straight horizontal line of width $d = 2\left(s - \frac{a^2}{s}\right)$ in the ζ plane. The flow about this line may be

calculated from known potential solutions (Ref. 76, for example). Then the pressure distribution on the body may be determined when the solution is transformed back to the X-plane. The chordwise load distribution on the body in the presence of the wing is given by Spreiter for a configuration at uniform angle of attack.

$$\frac{1}{q_\infty}\frac{dL}{dx} = 4\alpha s\left\{\left(1-\frac{a^2}{s^2}\right)\frac{da}{dx}+\left[\left(1-\frac{a^4}{s^4}\right)\frac{ds}{dx}+2\frac{a}{s}\left(1+\frac{a^2}{s^2}\right)\frac{da}{dx}+\frac{s}{2a}\left(1+\frac{a^2}{s^2}\right)\frac{da}{dx}\right]\sin^{-1}\left(\frac{\frac{2a}{s}}{1+\frac{a^2}{s^2}}\right)\right\} \qquad (V\text{-}41)$$

An angle of attack variation will produce an additional lift distribution. For the case where the angle of attack varies with x but at each station is the same for both wing and body, the carryover lift would be given by

$$\frac{1}{q_\infty}\frac{dL}{dx} = 4\alpha s\left\{\left(1-\frac{a^2}{s^2}\right)\frac{da}{dx}+\left[\left(1-\frac{a^4}{s^4}\right)\frac{ds}{dx}+2\frac{a}{s}\left(1+\frac{a^2}{s^2}\right)\frac{da}{dx}+\frac{s}{2a}\left(1+\frac{a^2}{s^2}\right)\frac{da}{dx}\right]\sin^{-1}\left(\frac{\frac{2a}{s}}{1+\frac{a^2}{s^2}}\right)\right\}$$

$$+8a^2\left\{\frac{s}{2a}\left(1-\frac{a^2}{s^2}\right)+\left[\frac{s}{2a}\left(1+\frac{a^2}{s^2}\right)\right]^2\sin^{-1}\left(\frac{\frac{2a}{s}}{1+\frac{a^2}{s^2}}\right)\right\}\frac{da}{dx}-2\pi\frac{d}{dx}(a^2\alpha) \qquad (V\text{-}42)$$

The last term represents the lift on the body alone as given by Eq. (V-23).

Lift is developed until the station of maximum wing span is reached. Beyond this point, Eq. (V-42) would indicate a negative contribution where $ds/dx < 0$, but the effect of the downwash field from the wing on more rearward areas tends to invalidate the theory beyond the station of maximum span. Spreiter gives an approximate method of estimating the force distribution induced on the body behind the maximum span station, but this relatively small correction will not be included here. Instead, the interference load on the wing is assumed to be negligible behind the section at which $\frac{dL}{dx} = 0$ by analogy with Jones' argument for slender wings.

The derivation given by Spreiter covers only the case of a horizontal mid-wing on a circular body. By making other conformal trans-

formations, more general configurations might be handled (elliptical bodies, for example). However, in view of the inherent limitations of slender-body theory, the additional complication is not introduced here. In application, the cross sections of noncircular bodies might be approximated either by circles or by vertical or horizontal lines. Certain generalizations are given in Refs. 59 and 60.

Pitts, Nielsen, and Kaattari (Ref. 56) have integrated Eq.(V-41) to give the total lift carryover on a cylindrical body. They propose a method in which all component forces are normalized by the wing-alone lift coefficient. Therefore, although the ratio of interference lift to wing lift is calculated by slender-body theory, a more accurate determination of wing-alone lift can be incorporated. Their method does not give the load distribution however.

2. Summary of Computational Procedure

For a mid-wing on a circular body the additional load on the body due to the presence of the wing is given by Eq. (V-42). This result holds only if both wing and body have the same angle of attack at each station. Although no general method is available for calculating the effect of wing incidence, Pitts, Nielsen, and Kaattari suggest an approximate procedure. They would multiply the load on the body given by Eq. (V-42) by the ratio of wing lift due to body interference for a wing at incidence to that for a wing at angle of attack. Then

$$\left(\frac{dL}{dx}\right)_i = \left(\frac{dL}{dx}\right)_\alpha \frac{\left(\frac{dL}{dx}\right)_{w(B)i}}{\left(\frac{dL}{dx}\right)_{w(B)\alpha}} \qquad (V\text{-}43)$$

Here $\left(\frac{dL}{dx}\right)_\alpha$ is obtained from Eq. (V-42); while the load on a wing at incidence in the presence of a body $\left(\frac{dL}{dx}\right)_{w(B)i}$ and the interference load for wing and body at angle of attack $\left(\frac{dL}{dx}\right)_{w(B)\alpha}$ are obtained by the procedures given in Section IV F. The expression approximates

reciprocity relations derived in Ref. 77 where, by slender body theory, the lift on the body due to wing incidence is equal to the lift on the wing due to the body on a configuration at angle of attack minus the lift on the wing due to body incidence.

3. Comparison with Experiment

In order to measure the force on a body due to wing interference, either separate balances may be used on each component of a model or a pressure distribution model may be tested. Either experiment is difficult and such data are rare. Figure 63 shows a comparison of theoretical and experimental streamwise distribution of body carryover lift. The data are obtained by integrating the lift component of pressure measured around the circumference of the body. The pressure distributions are given in Ref. 54. Since the model had from three to eight pressure taps at each axial station, the integration of circumferential pressures is inaccurate.

The discrepancy between theory and experiment is typical of the supersonic case. Disturbances cannot propagate forward of characteristic lines, hence the effect of the wing appears on aft stations of the body. The slender body theory, on the other hand, applies the wing carryover at the wing stations. In the present case, a small wing on a long body, the error is not as great as might occur on large-winged configurations.

Figures 64 to 67 show comparisons between experimental and theoretical lift curve slopes and centers of pressure on wing-body combinations. Since the interference between wing and body is not a large percentage of the total force, this comparison is not a sensitive test of the accuracy of the theoretical calculation of interference effects.. However, the agreement between theory and experiment indicates that the combined methods satisfactorily predict the overall structural loads. The difference between theoretical and experimental lift on Fig. 64 is primarily due to the inaccuracy of slender body theory which predicts zero lift on the doubly pointed body. The data were obtained from Refs. 56

and 78; while the theoretical methods are indicated on Figs. 64 and 66.

4. Limitations of the Method

Slender body theory gives a reasonable approximation of the carryover lift induced by a wing on a body; but the distribution of the lift is not accurately predicted. In subsonic configurations, the body begins to pick up a load ahead of the wing leading edge because the circulation around a lifting wing results in an upwash in the oncoming flow field. In the supersonic case, on the other hand, discrepancies can still occur since the effect of the wing appears on aft body stations. Wings with unswept leading edges present difficulties in the slender body theory, since in such cases $\frac{ds}{dx} \rightarrow \infty$. The prediction of total load is not necessarily inaccurate, however, since the integral is finite.

It is difficult to accurately assess the quantitative effect of these errors since systematic experimental data are unavailable. The following table gives a general indication of the limitations of slender body theory for the prediction of body carryover lift.

Table 10

Range of Validity of Slender Body Theory
for Prediction of Body Carryover Force

Parameter	Range of Validity	Comments
M_∞	$0 \leq M_\infty < 2$	Predicts force too far forward at supersonic speeds
$\frac{l}{d}$	$3 \leqq \frac{l}{d} \leqq 20$	Theory not sensitive to body fineness ratio
$\frac{s}{d}$	$1 \leqq \frac{s}{d} \leqq 3$	At subsonic and transonic speeds a wider wing span might be acceptable.
$\lvert\alpha\rvert$	$< 3^\circ$	Vortex separation can lead to large errors at higher angles of attack

5. Comparison With Other Theories

No other method can match the simplicity and versatility of the slender-body-theory. It is possible to extend it to wing-body combinations of any cross-sectional shape for which the transformation to a straight horizontal line is known (for example, see Ref. 60 and pages 323-324 of Ref. 79). However, as illustrated by the comparison with experiment shown in Fig. 63 the prediction of load distribution may leave something to be desired.

Surveys of the wing-body interference problem have been presented in Refs. 59 and 79. Some of the available methods which might be superior to slender-body theory do not give load distributions (Trefftz plane solutions, for example). Others have been carried through only for uniform angle of attack. Two promising methods will be described here, however, since they may be useful in cases in which slender-body theory is inadequate. The first method, an extension of the Lawrence procedure discussed in Section IV C is appropriate for subsonic speeds. The second procedure, based on a supersonic theory by Ferrari has been derived only for certain special geometries.

If the Lawrence theory, presented in Ref. 14, is regarded as an extension of the Jones slender-wing theory; then an analogous result might be derived for subsonic slender wing-body combinations. In Ref. 59 Lawrence and Flax show that in fact an integral equation of form similar to Eq. (IV-91) results

$$k(x) = \frac{1}{2} g(x) + \frac{1}{4} \int_{L.E.}^{T.E.} g'(\xi) \left[1 + \frac{\sqrt{(x-\xi)^2 + \left(\frac{b}{2}(x)\right)^2}}{x-\xi} \right] d\xi \qquad (V\text{-}44)$$

where $g'(x) = \frac{1}{2\rho U_\infty} \frac{dL}{dx}$

= chordwise load parameter for the wing-body combination.

The only differences between this expression and Eq. (IV-91) is in the definition of k(x). Here k(x) is the chordwise loading parameter for the wing-body combination obtained from slender body theory. That is

$$K'(x) = \frac{1}{2\rho U_\infty}\left(\frac{dL}{dx}\right)_{\text{slender body theory}} \qquad (V\text{-}45)$$

$$K'(x) = \int_{-\frac{b}{2}(x)}^{\frac{b}{2}(x)} \left[\alpha(x,y) + \alpha_B f(y)\right] \sqrt{\left(\frac{\bar{b}}{2}(x)\right)^2 - \bar{y}^2}\; dy \qquad (V\text{-}46)$$

where $\frac{\bar{b}}{2}(x)$ is the semi-span of the transformed wing, which results from a transformation of the wing-body combination into a horizontal wing plus vertical line body. $\bar{y}$ is the transformed spanwise coordinate. $\alpha_B f(y)$ is the vertical velocity induced along the wings by an isolated body in two-dimensional flow at an angle α_B. The body is omitted from the region of integration. This integral equation can be solved by methods similar to those used in Section IV C.

In the supersonic regime, Ferrari proposes an iterative solution of the linearized equations of motion without invoking the slender-body assumption. His procedure, given in Ref. 79, begins with the following definition of a velocity potential:

$$\phi = U_\infty \frac{b}{2}\left\{\xi + (\phi_b)_1 + \alpha_w\left[(\phi_b)_2 - \zeta + \phi_w + \phi^{(w)} + \phi^{(b)}\right]\right\} \qquad (V\text{-}47)$$

where

$\xi = \frac{2x}{b}$

$\zeta = \frac{2z}{b}$

b = tip-to-tip wing span (including body)

$U_\infty \frac{b}{2}(\xi - \alpha_w \zeta)$ = free stream velocity potential

$U_\infty \frac{b}{2}\left[(\phi_b)_1 + \alpha_w (\phi_b)_2\right]$ = perturbation of potential produced by body alone.

$U_\infty \frac{b}{2} \alpha_w \phi_w$ = perturbation of potential produced by wing alone (wing extends through body)

$U_\infty \frac{b}{2} \alpha_w \phi^{(w)}$ = perturbation representing the interference of the body on the wing.

$U_\infty \frac{b}{2} \alpha_w \phi^{(b)}$ = perturbation representing interference of the wing on the body.

Ferrari proceeds to establish boundary conditions and find integral relations for the interference potentials. By expanding in Fourier series, he is able to obtain solutions and corresponding forces for certain wing plan forms. Numerical results have been obtained only for rectangular wings at uniform angle of attack.

A modification of Ferrari's procedure introduced by Rae in Ref. 80 gives a simple solution for the carryover lift on a body due to a rectangular wing of infinite aspect ratio at uniform angle of attack. Lawrence and Flax suggest that this procedure might be extended to finite aspect ratio wings by calculating a correction term by slender body theory.

On the whole, the problem of calculating the load distributions due to wing-body interference is not yet satisfactorily resolved; particularly to the degree of generality required for aeroelastic analysis. Solutions in the supersonic range especially are inadequate. Some suggestions by Lagerstrom and Van Dyke (Ref. 81) for reducing the wing-body to a planar problem might help in development of a more accurate procedure.

Suggestions for further investigation in this area, and other recommendations are discussed in the next session.

Contrails

SECTION VI

RECOMMENDATIONS FOR IMPROVEMENTS AND EXTENSIONS

A. GENERAL CONSIDERATIONS

The present investigation attempts to select, from available methods, theoretical procedures for calculating the aerodynamic loads required for structural design. Since the aerodynamic forces are eventually to be incorporated in an aeroelastic computation, the methods must be versatile enough to provide loads on wings and bodies with arbitrary angle of attack distributions. The program is restricted at present to the linear range, since the results are intended for use in a linear aeroelastic analysis. Procedures have been described for calculating loads on wings and bodies and for mutual interference between the two components. Where necessary, different theoretical methods have been prescribed for different ranges of Mach number or geometrical parameters.

In some categories the available methods for treating the linear wing-body problem are inadequate or may be simplified or improved by further development. Desirable improvements of this type are described in the next section. Where possible, suggestions are advanced for pursuing such development. Also experimental programs are recommended where data are needed to aid in the promulgation or verification of analytical procedures.

In Section VI C possible developments are indicated which would extend the scope of the investigation beyond the simple airplane type of wing-body configurations considered here. Such geometric extensions as unsymmetric loads, wing-tail interference, and affects of engine nacelles and other external mountings are discussed. In addition, mention is made of the special problems involved in determining the loads on missiles, helicopters, and other unconventional configurations.

Extensions to nonlinear aerodynamic forces are projected in Section VID. In order to apply a nonlinear theory for predicting load distributions, it is first necessary to establish a suitable framework of nonlinear aeroelasticity. After a discussion of possible procedures for treating the nonlinear aeroelastic problem, three sources of nonlinear aerodynamic loads are discussed.

Sections VI E and VIF briefly indicate aerodynamic load problems which involve flow regimes entirely excluded from the present work. In one case, dynamic problems are discussed; while in the latter section hypersonic phenomena are described.

B. IMPROVEMENTS IN LINEAR ANALYSES

1. Specialization of Aeroelastic Problems

In Section II, typical matrix formulations of the aeroelastic problem are presented. In the present investigation, loads are given, where available for arbitrary angle of attack distribution. In this way the required aerodynamic information is made available for input to any linear aeroelastic operation. If, however, a particular form is chosen for the solution of the aeroelastic problem, then the load distribution theories might be simplified by carrying out the indicated operations for the corresponding specialized angle of attack distributions. Two examples may be cited to illustrate this point .

Consider first a typical "box" method in which a wing planform is subdivided into a number of small boxes. The aeroelastic problem, as outlined in Section II, may then be reduced to a matrix equation in which the elements of an aerodynamic matrix represent the pressure at the center of the ith box due to a unit angle of attack of box j. In this case, the computation of load distribution may be specialized to the particular case of a unit angle of attack of the ith box with zero angle elsewhere. The theories can then be applied to this case instead of being written in more general form. If the box size approaches zero then particularly simple solutions will sometimes result. This procedure, unfortunately, may re-

quire the use of hundreds of boxes. The resulting large matrices can be handled only by high speed computing machines, and can even tax the capacity of big machines. An alternative procedure would be to make use of a series of smooth angle distributions.

A series of normal mode shapes of a flexible wing, for example, would provide a basis on which to formulate an aeroelastic analysis . The elastic deformations and aerodynamic forces may still be related by a matrix equation (see, for example, Ref. 82 which includes dynamic terms). The advantages of this representation are

(a) Compared to box methods, a very small matrix will give a good approximation of the loads.

(b) The use of mode shapes facilitates extension to dynamic problems.

However, since the mode shapes depend on structural as well as geometric properties of the wing, the required angle of attack distributions cannot be prescribed. Even if some general form such as a Fourier series is established, the corresponding load distributions may be difficult to calculate.

Regardless of the choice of method of aeroelastic analysis, considerable progress can be made in unifying and extending the procedures for calculating aerodynamic loads if the form in which they are to be used is established. If possible, the aeroelastic analysis should be designed to include the entire wing-body combination.

2. Generalization of Weissinger Lifting Surface Solution

Within the framework of a specified linear aeroelastic theory, several improvements might be developed in the procedures recommended in this report. One such improvement would be the further development of the Weissinger lifting surface method. In this solution of the subsonic wing load problem, Weissinger reduces his two-dimensional integral equation for vorticity distribution by assuming that the chordwise vorticity is distributed in accordance with the result of a two-dimensional analysis.

The solution of the resulting one-dimensional integral equation for general plan form and camber is somewhat more complicated than the Weissinger lifting line method which is presented in Section IVB.

Although by comparison with flat wing data, the Weissinger "L" method seems to give adequate load predictions, it may be less reliable when applied to cambered wings. Therefore, further development of the lifting surface or "F" method might be useful. If a particular angle of attack distribution is prescribed by the previously-mentioned specialization of the aeroelastic problem, then generalization of the "F" method may be significantly simplified.

3. Modifications Due to Wing Thickness

Another way in which the calculation of wing loads might be improved is by allowing for the effect of wing thickness. If the variation of load with angle of attack were everywhere truly linear, then wing thickness would not affect the difference in pressure between upper and lower surfaces. However, although arising from a nonlinear phenomenon, the effect of thickness can be included in a linear theory by examining the perturbations of the flow about the thick wing with zero load instead of perturbations of the free stream flow.

One possible approach to the calculation of thickness effects would begin with known nonlinear solutions for the two-dimensional pressure distributions. For example, in supersonic flow, shock-expansion methods (combining oblique shock and Prandtl-Meyer solutions)can be used to obtain exact nonviscous solutions for the flow over two-dimensional airfoils. The problem remains, however, of extending the analysis to three-dimensional problems. Some success has been achieved (Ref. 83), in the supersonic case, by solving the three-dimensional wing problem in the usual manner, but using in the linear formulas the local value of Mach number determined by the two-dimensional exact solution rather than the free stream value. It may be possible to develop an analogous procedure for subsonic wings.

4. Improvements in Slender Body Theory

The attractions (simplicity and versatility) of slender body theory are somewhat offset by its limited range of applicability. Van Dyke has pointed out, however (Ref. 75), that in the prediction of load distributions the accuracy of the longitudinal flow is more important than that of the cross flow. This principle is the basis of his "hybrid" theory, and might be further exploited. Then, if the pressure distribution can be accurately predicted for a non-lifting body of general shape, the variation around the cross-section may be adequately represented by the sectional cross flow. Further development along this line requires accurate solutions for bodies of general shape aligned with the free stream flow. The shock-expansion method, given for bodies of revolution in Section VC, is based on an accurate solution of the zero-lift problem. An extension of this method to more general body shapes would improve the situation in the supersonic speed range. Simple subsonic methods of comparable accuracy do not appear to be available.

For smooth bodies, the local ratio of body height to width seems to adequately characterize the shape of the cross section. Consequently extension of theories to elliptic cross sections would represent a very valuable generalization of currently available methods.

5. Improvement and Extension of Wing-Body Interference Analysis

Perhaps the most significant inadequacy of available methods of predicting load distributions is in the calculation of wing-body interference effects. Slender body theory often gives insufficient accuracy; while more elaborate representations of the flow, such as the vortex model described in Section IV F, have been developed only for bodies of revolution.

An extension of the vortex model to bodies of elliptic cross section would require a derivation of the two-dimensional flow about an ellipse in the presence of a vortex. A solution to this problem, although not explicitly available in the literature, can be obtained by a conformal mapping of the flow about a vertical plate in the presence of a symmetrical pair of

vortices. Although such a flow field is quite complicated, only the normal velocities in its own plane are required to establish the interference forces on the wing.

The extension of the Lawrence theory to the wing-body combination appears to offer the most likely prospect for improving the prediction of body load due to wing interference. Such a procedure would not be valid behind the wing-body junction. On the aft sections of the body, the wing influence would be manifested by an angle of attack distribution induced by the wing downwash field. The vertical velocities in the vicinity of the body can be estimated by assuming that the flow field behind the wing is represented by a pair of concentrated lifting vortices. The force distribution on the aft part of the body is then calculated by the best available theory for a cambered body.

6. Effects of Viscosity

On the whole, viscosity has little effect on the lift distribution. In the Reynolds number range in which boundary layer theory is valid (Reynolds No. > 10,000 for example), the displacement thickness creates the effect of an increase in thickness of wing or body. Since, in the linear theory, thickness has little influence on lift distribution (but, see Section VI B-3), it is usually unnecessary to apply a correction for viscosity. However, in some situations boundary layer growth and separation can cause noticeable alterations in the load within the linear range of angles of attack.

One such condition arises in the case of cylindrical lifting bodies where slender body theory predicts no load. Even the more accurate shock expansion method predicts only a small force on long cylindrical sections of the body. The growth of the boundary layer displacement thickness can then result in a normal force and pitching moment of significant proportions compared to the nonviscous result.

Separation of the flow from the rear of boattailed models can also invalidate a nonviscous analysis.

If the flow does not follow the body contour, then the loads will not follow the nonviscous theoretical analysis. It is, at present, difficult to estimate the possible influence of boundary layer separation in such cases. Supersonic experiments reported in Refs. 84, 85 and 86 indicate a negative lift over the converging part of a boattailed body but not as much as indicated by theory. On subsonic bodies, due to the unfavorable pressure gradient, the boundary layer is even more likely to separate over a boattail. The pitching moment data reported in Ref. 87 indicate that the predicted download on the aft end of such bodies is not fully realized.

Another situation in which viscosity affects the linear load distribution arises in connection with boundary layer separation at a wing trailing edge. Because of this separation the full circulation does not develop around subsonic airfoils. The effect is often taken into account by empirically approximating the section lift coefficient by 6 instead of the theoretical value of 2π. The overestimate of lift curve slope given by the Weissinger theory for rectangular wings (see Fig. 5) would be reduced by this correction.

Other types of separation result in side edge vortices and stall. These produce nonlinear forces and will be discussed in Section VI D.

7. Empirical Corrections

In the present study, empirical methods, such as the correction mentioned above, have been avoided. After all, an empirical relation, even when based on a large amount of accumulated experience, may fail when applied in a new situation. However, when the physical conditions are understood qualitatively if not quantitatively, then an empirical formula may provide a simple and reliable result. Therefore improved methods of computing load distributions may incorporate empirical relations or correction terms.

The thickness correction proposed by Ulmann and Bertram (Ref. 50) for supersonic wings with leading edges lying nearly along Mach lines is

an example of an empirical correction based on a qualitative assessment of the physical situation.

8. Recommendations for Experimental Investigations

Data are available against which almost any load prediction theory may be tested. However, the range of validity of a theoretical procedure cannot be established by comparison with a scattered sampling of experimental information. A systematic program is needed, in which the important parameters are varied over the range of interest. It is sometimes possible to assemble a systematic set of data collected from a variety of sources. The lift curves of flat wings, for example, are available over wide ranges of geometric and flight conditions. In several other categories, however, only isolated data are available. Such categories will be enumerated together with suggested test programs.

(a) Effect of twist and camber on load distribution.

The subsonic theories, in particular, favor flat wings. Hence, tests employing a systematic variation of twist and camber might reveal unexpected limitations of the methods. Wind tunnel tests on models with linear symmetric twist and with varying amounts of circular arc camber are recommended, although other parameters, such as camber shape and distribution might also be added. The following Table illustrates a suggested range of parameters:

Table 11

Study of Effects of Twist and Camber on Wing Load Distributions

Parameter	Range of Interest
Twist of wing tip	0 - 15°
Camber = $\frac{h}{c}$	0 - .2
AR	.5 - 6
TR	0 - 1
Λ	0 - 60°
M_∞	0 - 4
α	-20° to +30°

In spite of the large number of variables, a satisfactory program would require fewer than 50 models. The effect of aspect ratio, for example, could be demonstrated by testing a low aspect ratio model and a high aspect ratio model at each value of taper ratio, sweep, etc. Then at one condition, two extra models could be added to fill in the intermediate points.

At a minimum,measurements of lift, and chordwise and spanwise center of pressure positions would be needed, hence sidewall mounted half-wing models, or equivalent, would be required. One or two pressure distributions would also be desirable to aid in determining the cause of any discrepancies between theory and experiment.

The suggested program is quite extensive, particularly in its investment in wind tunnel models. The model size should thus be selected for minimum construction cost, probably resulting in maximum dimensions on the order of 6" - 12". The wind tunnel (or tunnels) should then be selected to efficiently accommodate such models.

(b) Loads on non-circular and cambered bodies

Forces have been measured on a large variety of bodies of revolution under various flight conditions, but experimental data on noncircular or cambered bodies tends to be fragmentary. Consequently, a systematic series of wind tunnel tests on bodies of elliptic cross section--straight as well as cambered--would help in the evaluation of theories predicting the loads on such configurations.

Of fundamental importance is the onset and development of vortex separation resulting in nonlinear lift loads on bodies. Any program embodying measurements of body loads should include investigation of vortex separation. This point is again mentioned in SectionVI D5.

(c) Investigation of wing-body interference

Ref. 54 reports one part of an extensive experimental investigation by Cornell Aero. Lab. of effects of wing-body interference. Wind tunnel tests at subsonic and supersonic speeds include many measurements of pressure distributions on wings and bodies for a variety of configurations. However, for many conditions of interest, experimental information is

unavailable. In particular, the effects of noncircular bodies and of wing locations above and below the body midplane seem worthy of further study. Accepting the Cornell data as providing intensive information on relatively few representative configurations, its value could be enhanced by the addition of force data expanding the range of the test variables to include additional geometric parameters. The following table suggests such a supplementary program

Table 12

Experiments on Wing-Body Combinations

Parameter	Range of Interest
$\frac{\text{body width}}{\text{body height}}$ (elliptical cross sections)	1/2 to 2
$\frac{\text{position of wing junction above body mid plane}}{\text{body height}}$	- 1/2 to + 1/2
wing plan form	delta and rectangular
$\frac{\text{wing span}}{\text{body width}}$	1 to 5
M_∞	0 to 4
α	- 20° to + 30°
i_w = wing incidence	- 10° to + 10°

To separate effects of wing on body from the interference of the body on the wing, separate balances would measure the forces and moments on the entire configuration and on a single wing panel. It will also be necessary to have data on the body alone and on a sidewall mounted wing panel. The program represented in Table 12 would require about four wing models and four or five bodies with provision for mounting the wing at several different heights on the body and at various incidence angles.

Models on the order of 12" long should be satisfactory, although larger dimensions might simplify the design of the balance needed for measuring wing panel loads. Wind tunnels of appropriate dimensions to accommodate such models should cover subsonic and supersonic speeds.

To keep the force levels within the range of balance sensitivity, it may be desirable to omit low speed tests. Compressibility effects are not large below $M_\infty \sim .5$ and can be estimated analytically when necessary.

C. GEOMETRIC EXTENSIONS OF THE LINEAR ANALYSIS

1. Cruciform and other Non-Planar Lifting Surfaces

In supersonic flow, where cruciform wings are more likely to be encountered, the linear theory (Ref. 88)may be applied to the derivation of load distributions. Recent extensions of Evvard's method (see Ref. 89) may be applied to end plates and other non-planar geometries.

At subsonic or transonic speeds, solutions to flows about interfering surfaces may often be obtained by slender body theory. For more accurate results, the general flow field due to a nonplanar vortex distribution might first be determined, then, by matching the appropriate boundary conditions, forces on the various surfaces could be calculated. Such an extension of the Weissinger procedure is included in the computer program of Ref. 19.

2. Ring Wings

A particular non-planar configuration which has received some attention because of its ability to cancel wave drag is the ring-wing-body combination. The linear theory of supersonic ring-wing configurations - including full and partial rings--is quite thoroughly discussed in Ref. 90. Linear theory, in fact, does not give a sufficiently accurate description of the mutual interference between wing and central body to give reliable designs of drag-cancelling configurations; however, the lift load is more satisfactorily predicted.

Since wave drag is not a problem, the ring wing would not often be encountered in subsonic flow. Annular stabilizing surfaces are sometimes used on bombs or torpedoes, however. The wing load can perhaps be adequately estimated by considering each section as a part of a two-dimensional airfoil with angle of attack varying sinusoidally around the cir-

cumference. The body then would be responsible primarily for producing a radial load on the wing which can be estimated on the basis of an induced camber computed by slender body theory.

3. Ducted Bodies

Removing the central body from a ring-wing-body configuration leaves a ducted body. The force distribution on such a body might be computed, then, by the same principles as the ring wing. However, when the body is of high fineness ratio, perturbations of the internal flow undergo many internal reflections in the length of the body. Ref. 91 gives a review and development of theories for the force distribution on axisymmetric ducted bodies. The linear theory for supersonic ducted bodies is given in Ref. 92.

In most instances, ducted bodies serve as engine inlets and hence the internal pressures are intimately dependent on heat addition and engine performance. The internal structure then becomes a part of the engine. As mentioned previously (Section VC2), the external pressures on a supersonic engine inlet operating in its supercritical regime may be calculated by an extension of shock-expansion theory.

Development of theories for other operating regimes could proceed as for a solid body, if the dividing streamtube between internal and external flow can be identified. This streamline is then treated as a part of the body surface but, by definition, carries no load.

4. Unsymmetric Loads

The methods described in the present report have been specialized to the case of configurations which are symmetric about the x, z plane. If it becomes necessary to calculate structural loads in unsymmetric conditions, such as yawed flight, then considerable additional labor is required. Any of the procedures presented here can be extended to unsymmetrical situations. For example, Evvard's method of calculating pressures on supersonic wings remains unchanged when applied to an un-

symmetrical plan form or angle of attack distribution, but changes in the regions of integration introduce additional numerical complication. In other procedures, such as the Weissinger method, terms have been simplified or cancelled completely by the symmetry condition. The basic concept is not so limited, however.

5. Wing-Tail Interference

Wing-tail interference computations require, first, a representation of the wing downwash field in the region of the tail, followed by a calculation of the force on the tail in this downwash field. In most cases, the wing can be represented by a large horseshoe vortex whose strength and location are determined by the span load distribution on the wing.

In subsonic configurations, the wing lifting line may lie close to the tail and account for most of the downwash. In the supersonic case where the wing span is likely to be smaller, the trailing tip vortices may be more important.

Since methods are available, and already presented in Section IV, for computing the load distribution on lifting surfaces in an arbitrary downwash (or angle of attack) field, extensions to cover wing and tail interference can proceed in a straightforward manner.

The effect of the wing on the tail is inherently nonlinear, even when linearized theories are used in the calculation. The motion of the wing tip vortices with respect to the plane of the tail, as the vehicle angle of attack changes, introduces nonlinear variations of tail load with angle of attack of the configuration. The problem becomes geometrically more complicated when the tail does not lie in the plane of the wing or if yaw angles or unsymmetric control deflections are introduced. Some of these problems are considered in Ref. 93, for example. Although other solutions of this problem are available, for the most part they are intended to provide integrated forces and moments for performance calculations and do not emphasize the load distribution.

6. Effects of Engine Nacelles

Engine nacelles and external stores alter the load distribution on nearby lifting surfaces. Such effects seem to be treated primarily by correlations of experimental data and previous experience. Refs. 94 and 95, for example, show the measured effect of store and nacelle location on wing lift but do not attempt a quantitative analysis.

Development of a theoretical treatment of wing-store interference would thus be desirable, and might be regarded as an extension of wing-body interference theories. Most successful analytical treatments of wing-body interference treat the body as an infinite cylinder (slender-body-theory is the major exception). It might be possible, however, to derive a vortex theory in which the image vortex in the body is curved to better match the boundary condition on the surface of a short nacelle-type of body with changing diameter.

7. Slipstream Effects

Besides the geometric interference of nacelles, another disturbance is created by jet engine or propeller slipstreams. The higher velocity exhaust air can produce local changes in the condition of the "free stream" impinging on a lifting surface. In addition the expanding or contracting geometry of the streamtube separating exhaust air from free stream induces local angle of attack variations.

An extensive treatment of slipstream interference is included in Ref. 79. Further development is required, however, to adapt this analysis to the solution of structural load problems.

8. Axial Loads

The present report treats only load distributions in the lift (or "normal force") direction. Even when the structural problem can be separated into normal and tangential components, the drag may sometimes contribute to the aeroelastic lift load. For example the drag on a high horizontal tail will apply a bending moment to the fuselage. In addition,

of course, the complete structural analysis must include all components of aerodynamic load.

A substantial body of literature is available concerning the calculation of drag. However, the review and evaluation of the drag calculation procedures constitutes a project in itself.

9. Extension to "Unconventional" Aircraft

The concept of a "conventional" airplane is becoming increasingly elusive; but, for example, missiles, helicopters, ground effects machines, and vertical take-off configurations have been neglected in the present treatment. Most of the procedures included here are applicable to missiles, and, when in level flight, a vertical take-off airplane is not much different from any other. However, in its own peculiar flight regime each specialized vehicle encounters aerodynamic loads which require specialized methods of analysis.

Procedures for calculating loads have been developed as needed for each type of aircraft, and improvements are continually forthcoming. It may be desirable, at some future time, to combine these separate results into a unified treatment of the structural loads problem.

10. Experimental Investigations

In most of the areas in which geometrical extensions have been suggested, a substantial body of experimental data is already available. Although information is not usually complete on the detailed effect of variation of every possible parameter, in most cases the data would be sufficient to judge the validity of a proposed extension. For example low speed measurements of unsymmetric forces are reported in Refs. 21 and 29 and the results of an extensive investigation of wing-tail interference are available in Refs. 96 and 97.

On the other hand, where the development of new techniques or applications involves assumptions of unsubstantiated validity, supplementary data may be required. The areas most likely to suffer from insufficient

experimental information are expected to be in the interference effects of engine nacelles and other stores; and the influence of jet engine slipstream.

No specific experimental programs are recommended at this time since, unlike the situation covered in Section VI B, the limitations of present theories and available data have not been evaluated.

D. NONLINEAR EFFECTS

1. Nonlinear Aeroelasticity

The aeroelastic analysis presented in Section II assumes linear relations between pressure and angle of attack and between load and deflection.

In order to make use of a nonlinear relation between angle of attack and resulting aerodynamic load, it is first necessary to revise the aeroelastic analysis so as to accommodate such a nonlinear function.

If Eq. (II-12) is replaced by the relation

$$\left[\Delta p_j\right] = \alpha^* \left[A^*_j\right] + \left[A_{ij}\right]\left[\alpha_i - \alpha^*\right] \qquad (VI\text{-}1)$$

where α^* = some constant average angle of attack and $\left[A^*_j\right]$ = matrix giving the corresponding pressure distribution, then the new aerodynamic matrix $\left[A_{ij}\right]$ gives a relation between pressure distribution and perturbation in angle of attack linearized about the average angle α^*. In this case the final load distribution becomes

$$\left[\Delta p_j\right] = \left[\left[I\right] - \left[A_{ij}\right]\left[c_{ij}\right]\right]^{-1} \left\{\left[A_{ij}\right]\left[\alpha_{0_i} - \alpha^*\right] + \alpha^*\left[A^*_j\right]\right\} \qquad (VI\text{-}2)$$

In addition to this approach, more general iterative methods might also be investigated.

Assuming that a suitable expression, such as Eq. (VI-2), is found to take account of the aeroelastic effects of nonlinear aerodynamic forces, it then becomes necessary to determine the elements of the new aero-

dynamic matrices. In Eq. (VI-2) $[A_j^\circ]$ is a column matrix which gives the pressure distribution due to the uniform angle of attack α°. For example, if the following sketch represents the variation of pressure at station j with angle of attack, then the element $A_j^\circ = \Delta p_j^\circ / \alpha^\circ$.

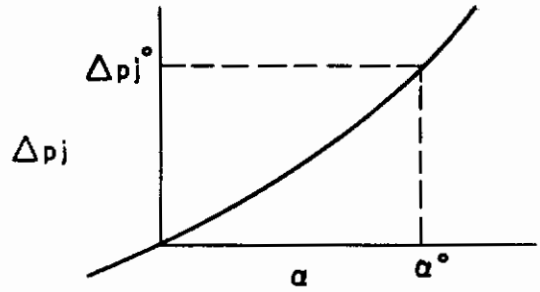

For wings, the nonlinearities at moderate angles of attack appear to be due primarily to vortex separation from side edges. The values of A_j° may then be determined by methods such as those given in Refs. 98 and 99. The elements of the aerodynamic matrix Aij require a knowledge of the lift distribution on arbitrarily cambered and twisted wings in the presence of vortex separation. Such information is not currently available and must be developed. It appears possible to solve this problem by extensions of linear wing theory, provided the camber distribution does not effect the location of vortex separation.

2. Nonlinear Unseparated Flow

The equation for velocity potential in compressible flow is nonlinear (see Eq. (V-12). Exact solutions indicate a nonlinear dependence of pressure coefficient on flow angle. Although the pressure difference between top and bottom surfaces of an airfoil remains linear to second order in angle, eventually higher order terms affect the lift and, to a greater extent, the pitching moment. Correction for this nonlinearity is possible in some cases based on approximate extensions of known exact solutions. However, the need for such corrections is practically nonexistent.

A correction for the effect of wing thickness only, as suggested in Section VI B 3, does not result in a nonlinear aeroelastic problem.

When, on the other hand, the angle of attack becomes so large that the lift would become nonlinear with angle of attack, flow separation effects predominate, and the entire analytical problem must be revised. The separation, from bodies as well as wings, takes two forms. Vortex separation from side edges usually produces an increase in lift. The nature and present status of this phenomenon will be discussed in the next section (Section VI D 3).

Stall is manifested by a forward movement of boundary layer separation from the trailing edge of a wing (or body) until a large part of the surface is in the separated region (although, in some cases, the leading edge separates first). A reduction of lift below the linear value accompanies the onset of stall. The problem of determining load distributions under such conditions is briefly discussed in Section VI D 4.

3. Effects of Vortex Separation

Concentrated vortices separate from side edges of thin lifting wings and result in local increases in lift. Figure 22 shows a noticeable departure from linearity beginning at about 8° angle of attack on a swept wing of AR = 2. An analytical treatment of this problem is given by Brown and Michael in Ref. 98 for triangular wings and by Cheng in Ref. 99 for rectangular plan forms. Although other procedures have been developed, the method advanced in these reports seems to be based on the simplest physical representation of the important observed features of the flow.

In this model a pair of separated vortices appears on the lee side of the wing connected to the side edges by vortex sheets of infinitesimal strength.

An analogous treatment of conical and cylindrical bodies of revolution has been proposed by Bryson in Ref. 100. However, unlike the wing problem in which the equivalent of a Kutta condition requires that the feeding sheets separate from the side edges, the separation points on circular bodies are established empirically. In addition, the axial station at which the vortex pair first leaves the surface of the body cannot always be pre-

dicted. Further studies of this problem (now in progress) are directed at deriving analytical methods of determining separation points and extending the solutions to bodies of more general shape.

Even if conditions can be found for completely specifying the two-vortex model of the flow, the calculation of load distributions may depend on a more refined physical model. The prediction of lift by Brown and Michael, for example, agrees with experiment, but they calculate negative pressures over some areas of low-aspect-ratio wings.

The wing or body with vortex separation would thus be treated by the best and most general available analysis for flat wings or uncambered bodies. Aeroelastic (or initial) deformations are then to be analyzed by linear perturbations of this result.

4. Effects of Stall

The problem of stall has been treated primarily by correlation of experimental data (see, for example, Ref. 101). For swept wings, according to a recent survey by Harper and Maki (Ref. 102), the state of knowledge is even worse since two-dimensional data on the onset of stall does not apply to the three-dimensional swept wing. Since the maximum load under some flight conditions will occur at maximum lift, it is important to be able to estimate, at least qualitatively, the change in load distribution accompanying the onset of stall.

While an empirical approach appears at present to offer the most attractive short-range solution to the problem, some benefit would be derived from a physical model of the flow, leaving a few parameters to be experimentally determined. According to the description given by Harper and Maki, wing stall is accompanied by a separation of the flow from the leading edge or forward of the trailing edge, or both, and a vortex separation from side edges. It may be possible, therefore, to correlate experimental data on the basis of the location and extent of separated areas.

5. Experimental Investigations

Data are available for comparison with nonlinear theories, but is probably inadequate for illustrating the phenomena on the basis of which a

new theory is to be developed. Therefore, the type of experiment most needed at present would show details of flow field and pressure distribution rather than total force and moment. Such information is being obtained in the course of other investigations of nonlinear forces. An example is the pressure and flow studies reported in Ref. 103.

Data on noncircular and cambered bodies would, however, be immediately useful. Although measurements of load distribution would meet some requirements, flow visualization techniques showing vortex locations and separation points on the body would be of even greater significance. With the aid of such data, present methods of predicting nonlinear forces on circular bodies might be extended to more general shapes. Tests on two families of bodies would be desirable: - a group of about three circular bodies of varying camber, and an equal number of uncambered bodies of elliptical cross section. Data of the type obtained in Ref. 103 would be desirable, but to repeat such a program on six different bodies is perhaps unwarranted. Pressure distributions on all bodies with only a few flow field studies might be adequate.

E. DYNAMIC PROBLEMS

1. Maneuver Loads

The calculation of load distribution during a maneuver requires solution of the partial differential equation for unsteady flow. General methods of approach and some particular solutions are given in Ref. 48. Further investigation is required to obtain the results appropriate to particular maneuvers and configurations.

In Ref. 1, the lift during maneuver is claimed to be proportional to angle of attack up to values well above the steady-state maximum. An investigation of this point, which cannot be settled purely on the basis of a linear analysis, would also appear important.

2. Gust Loads

A particular type of maneuver is the response to a gust. A maneuver might be defined by prescribing a distribution of angle of attack as a function of time. A gust load, on the other hand, fundamentally, results from the response of an airplane to a particular upwash distribution in the "free stream." Since the airplane's flight path will be altered by the gust load, the variation with time of the relative angle of attack will not exactly duplicate the imposed upwash distribution. An integral equation for the gust load on a two-dimensional non-pitching airfoil is given on page 294 of Ref. 48. Further discussions are contained in Refs. 104 and 105. However, results for general plan form and flight conditions do not appear to be available.

3. Flutter

Some success has been achieved recently (Refs. 106-109) in attempts to reduce the dynamic problem of high speed wing flutter to the determination of a combination of static loadings. Calculations by this method require the load distributions associated with several normal deflection modes of the structure. Hence the procedure is simplified if these distributions have been made available in the static aeroelastic analysis. However, the loads induced by the waving motion of the wing are also required in the analysis so that a solution for the normal modes is not sufficient for the flutter calculation .

The results of a wind tunnel test reported in Ref. 109 show good agreement between predicted and measured flutter speed on a wing where the prediction is based on direct measurement of the load distributions on wings deflected to simulate normal and induced mode shapes. Further development may provide a reliable procedure for calculating flutter speed on an entirely theoretical basis.

F. CONSIDERATIONS AT HYPERSONIC SPEEDS

1. Effects of Entropy Layer

The procedures for calculating load distributions on supersonic vehicles cannot be applied to indefinitely high Mach numbers. At hypersonic speeds ($M_\infty > 5$) new physical phenomena violate the assumptions underlying the derivation of the supersonic equations of motion as well as the mathematical processes involved in their linearization. The relation of some of these new physical conditions to the aerodynamic load problem will be briefly mentioned here with little or no indication of the procedures available for their treatment. Details may be found in texts such as Ref. 110. Reference 111 is directed more particularly to aeroelastic problems.

One phenomenon not predicted by supersonic linear theory, which assumes isentropic flow, is the entropy layer appearing behind a strong shock wave. In this region the temperature of the air increases above the isentropic value and other properties change also. However, the pressure on a wedge behind a strong oblique shock is not much different from the value that would be calculated by isentropic theory, as may be inferred from the chart on page 385 of Ref. 70.

2. Real Gas Effects

The rapid heating of air by passage through a strong shock wave can cause excitation of new degrees of freedom of the molecules in the air and eventually cause dissociation, ionization and other chemical reactions. These changes in the properties of air, which in general will not be in equilibrium everywhere over a hypersonic body, directly effect the temperature and internal energy. The pressure is influenced to a lesser extent.

3. Effects of Aerodynamic Heating

Aerodynamic heating, especially severe at high Mach numbers, introduces its own structural problems. The coupling of aerodynamic

and thermal loads, sometimes termed "aerothermoelasticity," has been extensively investigated over the past fifteen years. An extensive treatment of the subject may be found in Ref. 112.

4. Effects of Viscosity

Viscous effects are, of course, always present to some degree; but they have increased significance in some areas of hypersonic flight. In reentry, or other high-altitude vehicles, the flight regime includes regions of extremely low density (and hence low Reynolds number) where viscous forces can predominate.

5. Noncontinuum Effects

Other low density phenomena, depending on the Knudsen number, appear when the air acts more like a collection of molecules than like a continuous medium. At the extreme of free molecule flow, so-called "Newtonian impact" theory provides a simple basis for calculating loads. At intermediate Knudsen number, more complicated modifications may be required. The flow regimes were first defined by Tsien in Ref. 113.

Contrails

REFERENCES

1. Spanwise Air-Load Distribution, ANC-(1) Army-Navy-Commerce Committee on Aircraft Requirements, Washington, 1938

2. Gray, W. L., and Schenk, K. M., A Method for Calculating the Subsonic Steady-State Loading on an Airplane with a Wing of Arbitrary Plan Form and Stiffness, NACA Tech. Note 3030, 1953.

3. Jones, R. T. and Cohen, Doris, "Aerodynamics of Wings at High Speeds," Section A. of Aerodynamic Components of Aircraft at High Speeds Vol. VII of High Speed Aerodynamics and Jet Propulsion, Edited by A. F. Donovan and H. R. Lawrence, Princeton University Press, 1957

4. Bisplinghoff, R. L., Ashley, H., and Halfman, R. L., Aeroelasticity, Addison-Wesley, Reading, Mass., 1958.

5. Strength of Metal Aircraft Elements, MIL-HDBK-5, March, 1959.

6. Pugsley, A. G., Airworthiness (Air), A Philosophy of Aeroplane Strength Factors, ICAO Circular 2-AN/2, 1948.

7. Ferri, A., Elements of Aerodynamics of Supersonic Flows, MacMillan Company, New York, 1949.

8. Puckett, A. E., "Supersonic Wave Drag of Thin Airfoils," Journal Aero Science, Vol. 13, No. 9, September 1946.

9. Evvard, J. C., Distribution of Wave Drag and Lift in the Vicinity of Wing Tips at Supersonic Speeds, NACA Tech. Note 1382, 1947.

10. Evvard, J. C., Use of Source Distributions for Evaluating Theoretical Aerodynamics of Thin Finite Wings at Supersonic Speeds, NACA Report 951, 1950.

11. Lagerstrom, P. A., Linearized Supersonic Theory of Conical Wings, NACA Tech. Note 1658, 1948.

12. Jones, R. T., Properties of Low-Aspect Ratio Pointed Wings at Speeds Below and Above the Speed of Sound, NACA Report 835, 1946.

13. Weissinger, J., The Lift Distribution of Swept-Back Wings, NACA TM1120, 1947, Translation of "Uber die Auftriebsverteilung von Pfeilflugeln," ZWB, Forschungsbericht, Nr. 1553, Berlin - Adlershof, 1942.

14. Lawrence, H. R., "The Lift Distribution on Low Aspect Ratio Wings at Subsonic Speeds," Journal of Aero Sci., Vol. 18, No. 10, Oct., 1951.

REFERENCES (Continued)

15. Thwaites, B. (Editor), Incompressible Aerodynamics, Oxford, Clarendon Press, 1960.

16. Rauscher, M., Introduction to Aeronautical Dynamics, Wiley and Sons, New York, 1953.

17. De Young, J., and Harper, C. W., Theoretical Symmetric Span Loading at Subsonic Speeds for Wings Having Arbitrary Planform, NACA Report 921, 1948.

18. Multhopp, H., "Die Berechnung der Auftriebsverteilung von Tragflugeln", Luftf.-Forschg. Bd. 15, p. 153, 1938.

19. Mason, J. S., and Dickie, R. E., Subsonic Aeroelastic Loads, Ryan Aeronautical Co., Aerospace Div. Computer Program 1150, Oct. 1963.

20. DeYoung, J., Theoretical Span Loading Due to Flap Deflection for Wings of Arbitrary Planform at Subsonic Speeds, NACA Report 1071, 1952.

21. Purser, P. E., and Spearman, M. L., Wind-Tunnel Tests at Low Speed of Swept and Yawed Wings Having Various Plan Forms, NACA TN 2445, 1951.

22. Fisher, L. R., and MacLachlan, R., Wind-Tunnel Investigation at Low Speeds of the Pitching Derivatives of Untapered Swept Wings, NACA RM L8G19, 1948.

23. Johnson, B. H., Jr., Investigation of a Thin Wing of Aspect Ratio 4 in the Ames 12-Foot Pressure Wind Tunnel. I - Characteristics of a Plain Wing, NACA RM A8D07, 1948.

24. McCormack, G. M., and Stevens, U. I., Jr., An Investigation of the Low-Speed Stability and Control Characteristics of Swept-Forward and Swept-Back Wings in the Ames 40-by-80-Foot Wind Tunnel, NACA RM A6K15, 1947.

25. Kelly, M. W., Low Speed Aerodynamic Characteristics of a Large-Scale 60° Swept-Back Wing with High Lift Devices, NACA RM A52A14a, 1952.

26. Cahill, J. F., and Gottlieb, S. M., Low-Speed Aerodynamic Characteristics of a Series of Swept Wings having NACA 65A006 Airfoil Sections, NACA RM L50F16, 1950.

REFERENCES (Continued)

27. Kolbe, C. D., and Boltz, F. W., The Forces and Pressure Distribution at Subsonic Speeds on a Plane Wing Having 45° of Sweepback, an Aspect Ratio of 3, and a Taper Ratio of 0.5, NACA RM A51G31, 1951.

28. Schneider, W. C., A Comparison of the Spanwise Loading Calculated by Various Methods with Experimental Loadings Obtained on a 45° Sweptback Wing of Aspect Ratio 8:02 at a Reynolds Number of 4.0×10^6, NACA Report 1208, 1954.

29. Prandtl, L., "Tragflügeltheorie, I. Mitteilung," Nachrichten der Königlichen Gesellschaft der Wissenschaften zu Göttingen, Math. Phys. Klasse, p. 451, 1918

30. Glauert, H. The Elements of Aerofoil and Airscrew Theory, Macmillan Co., New York, 1943.

31. Lotz, I., "Berechnung der Auftriebsverteilung beliebig geformter Flügel," Zeitschr. f. Flugtechnik u. Motorluftschiffahrt, Vol. 22, No. 7, April 1931.

32. Truckenbrodt, E., "Beiträge zur erweiterten Traglinientheorie," Zeitschr. f. Flugwiss. Bd 1, Heft 2, p. 31, 1953.

33. Küchemann, D., A Simple Method for Calculating the Span and Chordwise Loading on Straight and Swept Wings of any Given Aspect Ratio at Subsonic Speeds, Aero. Res. Counc. Reports and Memoranda No. 2935, 1956.

34. Falkner, V. M., The Calculation of Aerodynamic Loading on Surfaces of Any Shape, R and M No. 1910, British A. R. C., 1943.

35. Multhopp, H., Methods for Calculating the Lift Distribution of Wings (Subsonic Lifting Surface Theory), Report No. Aero 2353, British R. A. E., January, 1950.

36. Truckenbrodt, E., Theoretical and Experimental Investigations on Swept and Delta Wings in Symmetrical Flow, Inst. of Fluid Mech., Tech. Univ., Braunschweig, Germany, Report No. 54/7a, 1954.

37. Emerson, H. F., Wind-Tunnel Investigation of the Effect of Clipping the Tips of Triangular Wings of Different Thickness, Camber, and Aspect Ratio - Transonic Bump Method, NACA TN 3671, June, 1956.

REFERENCES (Continued)

38. Kaattari, G. E., Pressure Distributions on Triangular and Rectangular Wings to High Angles of Attack-Mach. Numbers 1.45 and 1.37, NACA RMA54019, 1954.

39. Kaattari, G. E., Pressure Distributions on Triangular and Rectangular Wings to High Angles of Attack-Mach. Numbers 2.46 and 3.36, NACA RM A54J12, 1955.

40. Schindel, L. H., Wind Tunnel Force and Moment Tests of Rectangular, Triangular, and Trapezoidal Wings at M = 2.0, M. I. T. Naval Supersonic Laboratory, Analysis and Research Report No. 100/TR-1, 1951.

41. Middleton, W. D. and Sorrells, R. B., Off Design Aerodynamic Characteristics at Mach Numbers of 1.61 and 2.20 of a Series of Highly Swept Arrow Wings Designed for Mach Numbers 2.0 Employing Various Degrees of Twist and Camber, NASA TN D-1630, March, 1963.

42. Mueller, J., and Grimaud, J., Effect of Twist and Camber and Thickness on the Aerodynamic Characteristics of a 75° Swept Arrow Wing at a Mach Number of 2.91, NASA TM X-138, December, 1959.

43. Clarkson, M. H., and Ettlinger, H. J., Normal Force and Moment Data Obtained on the JHU Wing Series 3, 4, 10B, , 16, and 25 at the Lone Star Laboratory at a Mach Number of 1.5, Defense Research Laboratory, Report CF-874/DRL-143, 1948.

44. Clarkson, M. H., and Ettlinger, H. J., Lift, Drag, and Pitching Moment Data Obtained on the JHU Wing Series 1, 3, and 4 at the Ordnance Aerophysics Laboratory at a Mach Number of 1.73, Defense Research Laboratory, Report CF-954/DRL-159, 1948.

45. Thompson, M. J., Preliminary Analysis of Airfoil Test Data Obtained in the OAL Wind Tunnel at a Mach Number of 1.73, Defense Research Laboratory, Report CF-1004/DRL-171, 1948.

46. Pitts, W. C., Force, Moment, and Pressure Distribution Characteristics of Rectangular Wings at High Angles of Attack and Supersonic Speeds, NACA RM A55K09, 1956

47. Dunning, R. W. and Ulman, E. F., Aerodynamic Characteristics at Mach Number 4.04 of a Rectangular Wing of Aspect Ratio 1.33 having a 6 percent thick Circular-Arc. Profile and a 30-Percent Chord Full-Span Trailing-Edge Flap, NACA RML53D03, 1953.

REFERENCES (Continued)

48. Heaslet, M. A., and Loma, H., "Supersonic and Transonic Small Perturbation Theory", Section D, of General Theory of High Speed Aerodynamics, Edited by W. R. Sears., Vol. VI of High Speed Aerodynamics and Jet Propulsion. Princeton University Press, 1954

49. Etkin, B., and Woodward, P. A., "Lift Distribution on Supersonic Wings with Subsonic Leading Edges and Arbitrary Angle of Attack Distribution", Proceedings, Second Canadian Symposium on Aerodynamics, held at the Institute of Aerophysics, University of Toronto, February 1954.

50. Ulmann, E. F., and Bertram, M. H., Aerodynamic Characteristics of Low-Aspect Ratio Wings at High Supersonic Mach Numbers, NACA RM L53I23, 1953.

51. Durgin, F. H. and Tilton, E. L. III, The Effect of Camber and Twist on Wing Pressure Distributions for Mach Numbers from 2 to 7.6, Part I: Experimental Data, Aero Sys. Div. Report ASD-TDR-62-557, Part I, December, 1962

52. Beane, B. J. The Effect of Camber and Twist on Wing Pressure Distribution for Mach Numbers from 2 to 7.6, Part II: Comparisons with Theory, Aero Sys. Div. Report ASD-TDR-62-557, Part II, May 1963.

53. Lennertz, J., On the Mutual Reaction of Wings and Body, NACA Tech Memo 400, 1927

54. Nichols, S., Interference between Wing and Body at Supersonic Speeds, Part VIII Data Report, Pressure Distribution Tests of Wing Body Interference Models at Mach No. of 2.0, Phase IV Tests of March 1950, Cornell Aero. Lab. Report No. CAL/CF1571, July 1951.

55. Spreiter, J. R., Aerodynamic Properties of Slender Wing-Body Combinations at Subsonic, Transonic, and Supersonic Speeds, NACA Tech Note 1662, 1948.

56. Pitts, W. C., Nielsen, J. N. and Kaattari, G. E., Lift and Center of Pressure of Wing-Body-Tail Combinations at Subsonic, Transonic and Supersonic Speeds, NACA Report 1307, 1957.

57. Flax, A. H. Integral Relations in the Linearized Theory of Wing-Body Interference, Cornell Aero. Lab. Report CAL-45, 1952.

58. Clarke, J. H., Reverse Flow and Supersonic Interference, Brown Univ., Div. of Engineering Report AFOSRTN-58-625, 1958.

59. Lawrence, H. R. and Flax, A. H., "Wing-Body Interference at Subsonic and Supersonic Speeds-Survey and New Development." Journal of Aero. Sci., Vol. 21, No. 5, May 1954.

60. Kahane, A., The Lift and Moment of Slender Elliptical Cross-Section, Body-Wing and Fin Combinations, Republic Aviation Corp., Report EDR-57-:52, 1952.

61. Liepmann, H. W., and Puckett, A. E., Introduction to Aerodynamics of a Compressible Fluid, John Wiley & Sons, New York, 1947.

62. Kopal, Z., Tables of Supersonic Flow Around Cones, Mass. Inst. of Tech., Center of Analysis, Tech. Report No. 1, 1947.

63. Ferri, A., "The Method of Characteristics," Section G of General Theory of High Speed Aerodynamics, Edited by W. R. Sears, Vol. VI of High Speed Aerodynamics and Jet Propulsion, Princeton University Press, Princeton, 1954.

64. Ames Research Staff, Equations, Tables, and Charts for Compressible Flow, NACA Report 1135, 1953.

65. Allen, H. J., Estimation of the Forces and Moments on Inclined Bodies of Revolution, NACA RM A9 I 26, 1949.

66. Munk, M. M., The Aerodynamic Forces on Airship Hulls, NACA Report 184, 1924.

67. Tsien, H. S., "Supersonic Flow Over an Inclined Body of Revolution," Journal of Aero Sci., Vol. 5, No. 12, Oct. 1938,

68. Brown, C. E., "Aerodynamics of Bodies at High Speeds," Section B of Aerodynamic Components of Aircraft at High Speeds, Edited by A. F. Donovan and H. R. Lawrence, Vol. VII of High Speed Aerodynamics and Jet Propulsion, Princeton University Press, Princeton, 1957.

69. Kelly, H. R., The Estimation of Normal-Force and Pitching Moment Coefficients for Blunt-Based Bodies of Revolution at Large Angles of Attack, U. S. Naval Ordnance Test Station Report TM-998, 1953.

70. Lighthill, M. J., "Higher Approximations", Section E of General Theory of High Speed Aerodynamics, Edited by W. R. Sears, Vol. VI of High Speed Aerodynamics and Jet Propulsion, Princeton Univ. Press, Princeton, 1954

REFERENCES (Continued)

71. Preston, J. H., The Calculation of Lift Taking Account of the Boundary Layer, Aeronautical Research Council, R and M 2725, 1949.

72. Syvertson, C. A., and Dennis, D. H., A Second-Order Shock-Expansion Method Applicable to Bodies of Revolution near Zero Lift, NACA Report 1328, 1957.

73. Kopal, Z., Tables of Supersonic Flow Around Yawing Cones, Mass. Inst. of Tech., Center of Analysis, Tech. Report No. 3, 1947.

74. Beane, B. J., The Effects of Body Camber on Body Pressure Distributions and Wing Forces for M=2 to 7.6, Part II: Comparisons with Theory, Mass. Inst. of Tech., Aerophysics Lab., Tech. Report No. 3, ASD Tech Report 61-295 Part II, June, 1961.

75. Van Dyke, M. D., "First-and Second-Order Theory of Supersonic Flow Past Bodies of Revolution," Journal of Aero. Sci., Vol. 18, No. 3, March 1951.

76. Glauert, H., The Elements of Aerofoil and Airscrew Theory, Cambridge University Press, Second Ed., 1947.

77. Heaslet, M. A., and Spreiter, J. R., Reciprocity Relations in Aerodynamics, NACA Tech. Note 2700, 1952.

78. Johnson, B. H., Jr. and Rollens, F. W., Investigation of a Thin Wing of Aspect Ratio 4 in the Ames 12-Foot Pressure Wind Tunnel. V-Static Longitudinal Stability and Control Throughout the Subsonic Speed Range of a Semispan Model of a Supersonic Airplane, NACA Research Memo A9101, 1949.

79. Ferrari, C., "Interaction Problems" Section C of Aerodynamic Components of Aircraft at High Speeds, Edited by A. F. Donovan and H. R. Lawrence, Vol. VII of High Speed Aerodynamics and Jet Propulsion, Princeton University Press, 1957.

80. Rae, W. J., Generalized Distribution along the Body Axis of the Increment in Lift Produced by Interference from the Wing, Cornell AeroLab. Report CAL/CM-794, 1953.

81. Lagerstrom, P. A., and Van Dyke, M. D., General Considerations about Planar and Non-Planar Lifting Systems, Douglas Aircraft Co., Report SM-13432, 1949.

82. Pearce, B. F., Topics on Flexible Airplane Dynamics, Part I. Residual Stiffness Effects in Truncated Modal Analysis, Systems Technology, Inc., Report ASD-TDR-63-334, July, 1963.

83. Schindel, L. H., Notes on the Mach Number Method, Mass. Inst. of Tech., Aerophysics Lab., Memorandum AR 100-78, 1951.

84. Leupold, M. J., and Covert, E. E., Investigation of External Store Shapes for Supersonic Speeds, Mass. Inst. of Tech., Naval Supersonic Lab. Report WTR 42, 1953 (Confidential)

85. Covert, E. E., Supersonic Wind Tunnel Investigation to Determine the Interference Effects of the Sting Used to Support the Model in the Tunnel, Mass. Inst. of Tech., Naval Supersonic Lab., Report WTR 124, 1956.

86. Cohen, R. J., Aerodynamic Characteristics of Four Bodies of Revolution Showing Some Effects of Afterbody Shape and Fineness Ratio at Free Stream Mach Numbers from 1.50 to 1.99, NACA Research Memo., E51C06, 1951.

87. Hopkins, E. J. and Carel, H. C., Experimental and Theoretical Study of the Effects of Body Size on the Aerodynamic Characteristics of an Aspect Ratio 3.0 Wing-Body Combination, NACA Research Memo. A51G24, 1951.

88. Spreiter, J. R., The Aerodynamic Forces on Slender Plane and Cruciform - Wing and Body Combinations, NACA Report 962, 1950.

89. Ashley, H., Some Recent Developments in Interference Theory for Aeronautical Applications, Fluid Dynamics Res. Lab., Mass Inst. of Tech. Report No. 63-3, July, 1963.

90. Beane, B. J., Supersonic Drag Characteristics of Partial-Ring Wings, Naval Supersonic Lab., Mass. Inst. of Tech., Report No. TR444, 1960.

91. Hough, G. R., The Aerodynamic Loading on Streamlined Ducted Bodies, Therm Advanced Research Div., Report TAR-TR625, Dec. 1962.

92. Brown, C. E., and Parker, H. M., A Method for the Calculation of External Lift, Moment, and Pressure Drag of Slender Open Nose Bodies of Revolution at Supersonic Speeds. NACA Report 808, 1945.

93. Spreiter, J. R., and Sacks, A. H., "The Rolling-Up of the Trailing Vortex Sheet and Its Effect on Downwash Behind Wings," Journal of Aero Sci., Vol. 18, No. 1, Jan. 1951.

REFERENCES (Continued)

94. Coe, C. F., The Effects of Tip-Mounted Jet Nacelles on the Transonic Characteristics of Low-Aspect Ratio Wings, NACA, Research Memo A52J21, 1952

95. Jacobsen, C. R., Effects of the Spanwise, Chordwise, and Vertical Location of an External Store on the Aerodynamic Characteristics of a 45° Sweptback Wing of Aspect Ratio 4 at Mach Numbers of 1.41, 1.62, and 1.96, NACA Research Memo L52J27, 1953.

96. Schindel, L. H., and Durgin, F. H., Survey of the Downwash Field Behind Rectangular, Trapezoidal and Delta Wings at Mach Nos. 1.71, 1.99, and 2.50, Naval Supersonic Lab., Mass. Inst. of Tech. Report WTR 29, 1953 (Confidential)

97. Schindel, L. H. and Durgin, F. H., Forces on Tails in A Measured Supersonic Downwash Field, Naval Supersonic Lab., Mass. Inst. of Tech. Report WTR 33, 1953 (Confidential)

98. Brown, C. E., and Michael, W. H., Jr., " Effect of Leading-Edge Separation on the Lift of a Delta Wing!' Journal of Aero. Sci., Vol. 21, No. 10, Oct. 1954.

99. Cheng, H. K., " Remarks on Nonlinear Lift and Vortex Separation", Journal of Aero. Sci., Vol. 21, No. 3, Mar. 1954.

100. Bryson, A. E., Jr., " Symmetric Vortex Separation on Circular Cylinders and Cones," Journal of Applied Mech., Vol. 26, No. 4, Dec. 1959.

101. Soule, H. A., and Anderson, R. F., Design Charts Relating to the Stalling of Tapered Wings, NACA Report 703, 1940.

102. Harper, C. W., and Maki, R. L., A Review of the Stall Characteristics of Swept Wings, NASA Tech. Note D-2373, July 1964.

103. Rodgers, E. J., Real Flow Over a Body of Revolution at Angle of Attack, Ordnance Res. Lab., Penn State Univ., Tech. Memo. 5.2420-13, March 1963.

104. Heaslet, M. A., and Lomax, H., Two-dimensional Unsteady Lift Problems in Supersonic Flight, NACA Report 945, 1949.

105. Lomax, H., Lift Developed on Unrestrained Rectangular Wings Entering Gusts at Subsonic and Supersonic Speeds, NACA Tech. Note 2925, 1953.

106. Mollo - Christensen, E., and Martuccelli, J. R., A Study of the Feasibility of Experimental Determination of Aerodynamic Forces for Use in Flutter Calculation. Part I: Direct and Inferential Determination of Unsteady Aerodynamic Forces, Aeroelastic and Structures Res. Lab., Mass. Inst. of Tech., Tech. Report 66-1, 1957.

107. Mollo - Christensen, E., A Study of the Feasibility of Experimental Determination of Aerodynamic Forces for Use in Flutter Calculation. Part II: Determination of Unsteady Aerodynamic Forces from Steady State Measurements, Aeroelastic and Structures Res. Lab., Mass. Inst. of Tech., Tech. Report 66-2, 1957.

108. Mollo-Christensen, E., and Martuccelli, J. R., A Study of the Feasibility of Experimental Determination of Aerodynamic Forces for Use in Flutter Calculation. Part III: Summary and Conclusions, Aeroelastic and Structures Res. Lab., Mass. Inst. of Tech., Tech. Report 66-3, 1957.

109. Beane, B. J., and Durgin, F. H., An Example of Flutter Calculation Using Experimentally-Determined Quasi-Steady Aerodynamic Forces, Aerophysics Lab., Mass. Inst. of Tech. Report TR 9, 1961 (Confidential)

110. Hayes, W. D., and Probstein, R. F., Hypersonic Flow Theory, Academic Press, New York, 1959.

111. Bisplinghoff, R. L. "Some Structural and Aeroelastic Considerations of High-Speed Flight" (Nineteenth Wright Brothers Lecture), Journal of Aero. Sci., Vol. 23, No. 4, April 1956.

112. Batt, J. R. et al, Thermoelastic Effects on Hypersonic Stability and Control, Parts I, II, and III, Air Force Aeronautical Systems Division Reports ASD-TR-61-287, May 1963.

113. Tsien, H. S., "Superaerodynamics, Mechanics of Rarefied Gases," Journal of Aero. Sci. Vol. 13, No. 12, Dec. 1946.

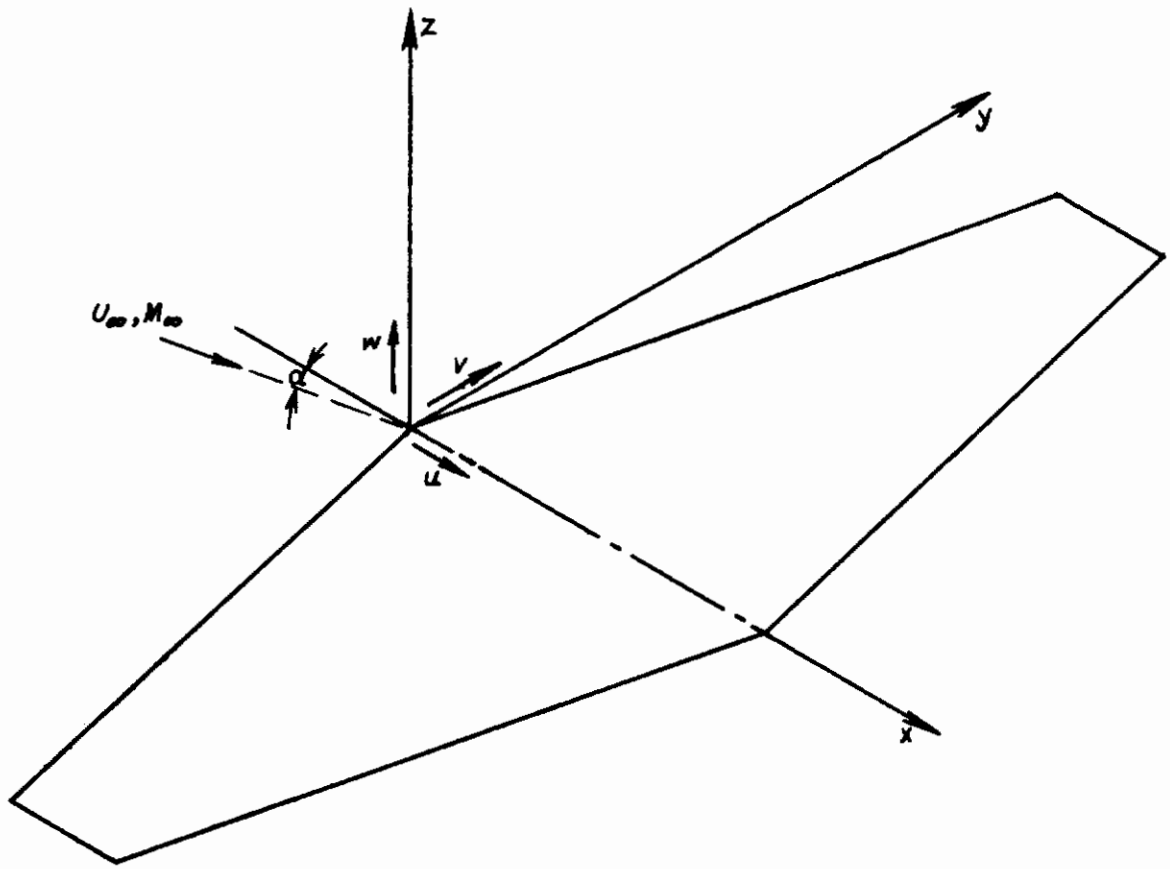

Figure 1. Wing coordinate system

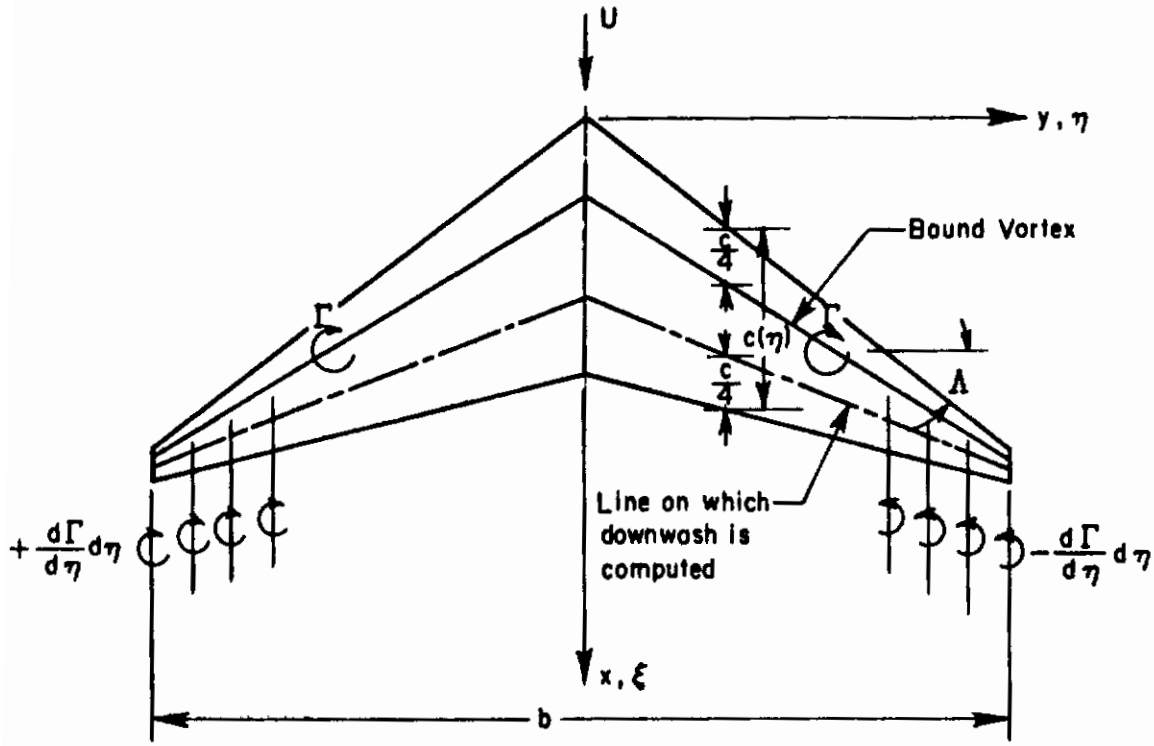

Figure 2. Weissinger's wing - vortex model

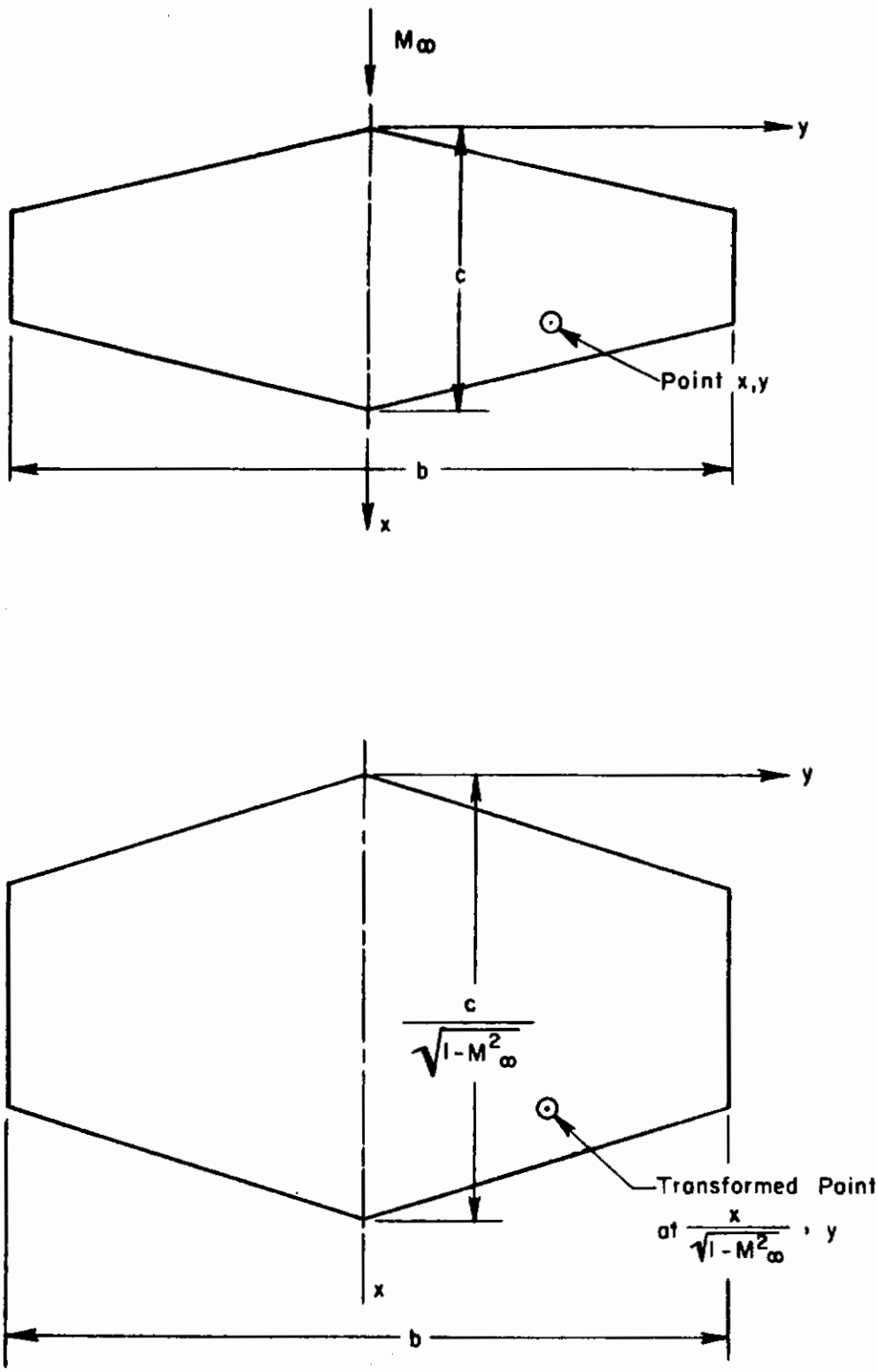

Figure 3. Application of Prandtl-Glauert transformation

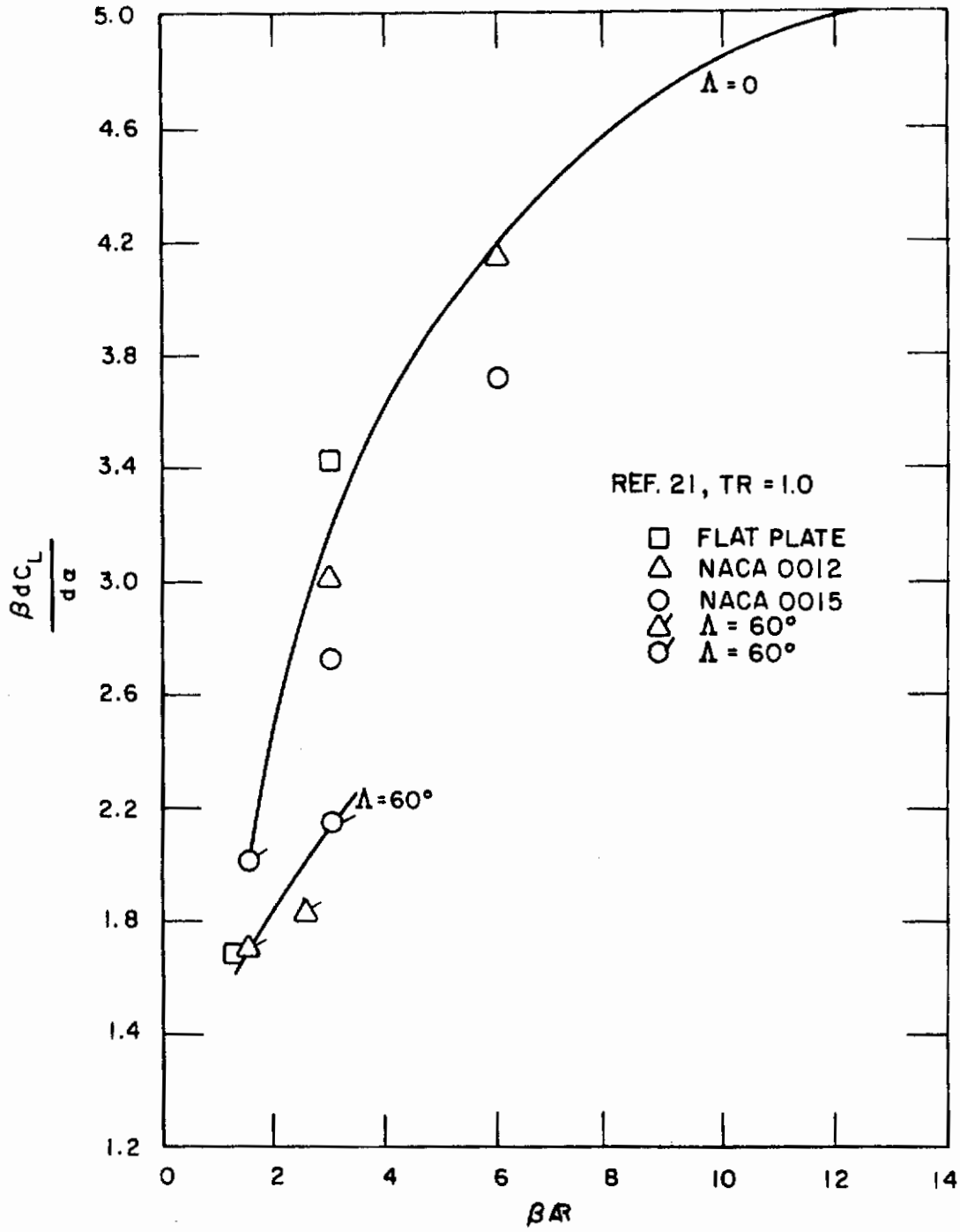

Figure 4. Lift curve slope for swept and unswept wings at $M_\infty \sim 0$. Comparison with Weissinger theory

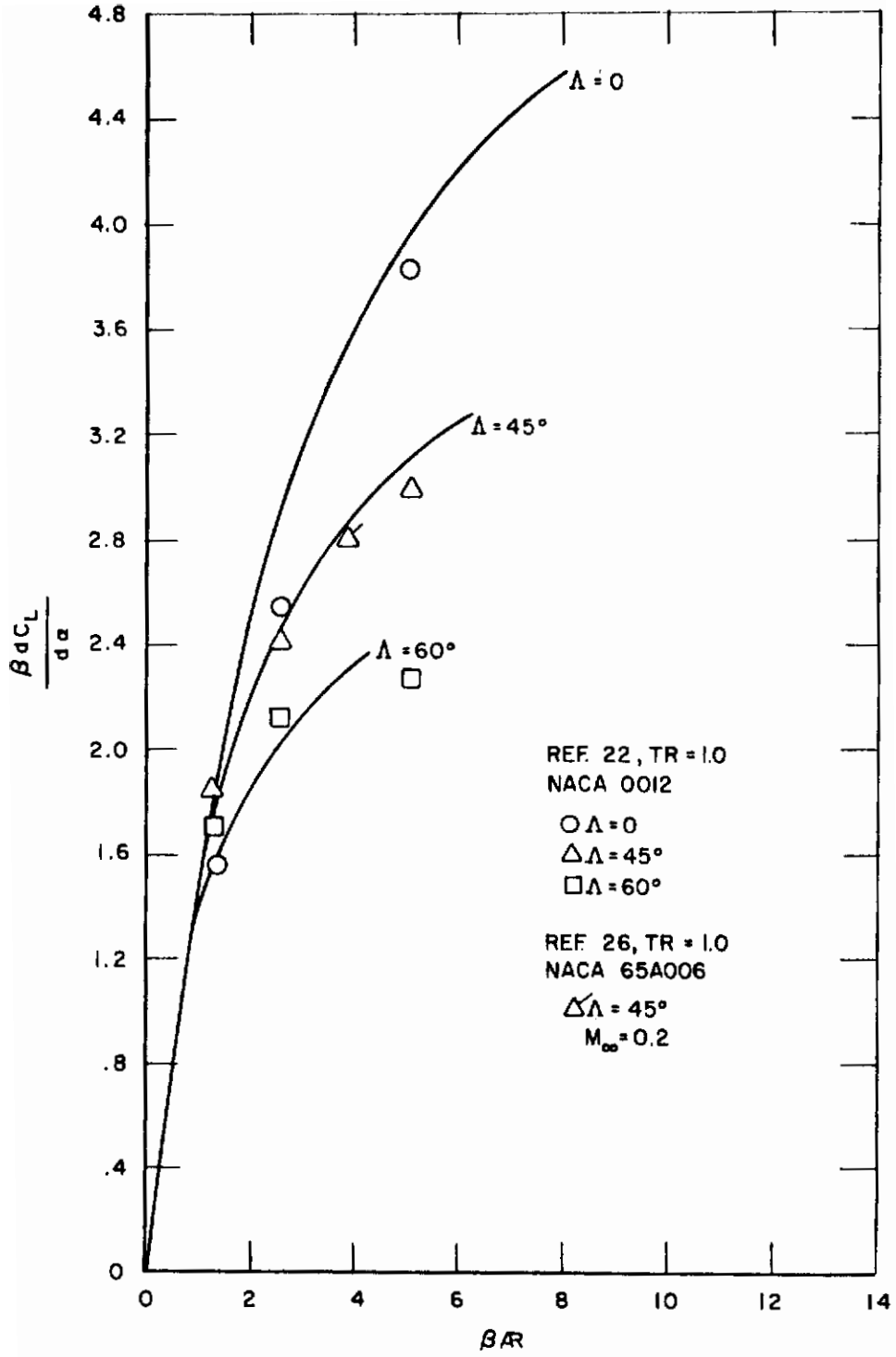

Figure 5. Lift curve slope for swept and unswept wings at Mach$_\infty$ ~ 0. Comparison with Weissinger theory

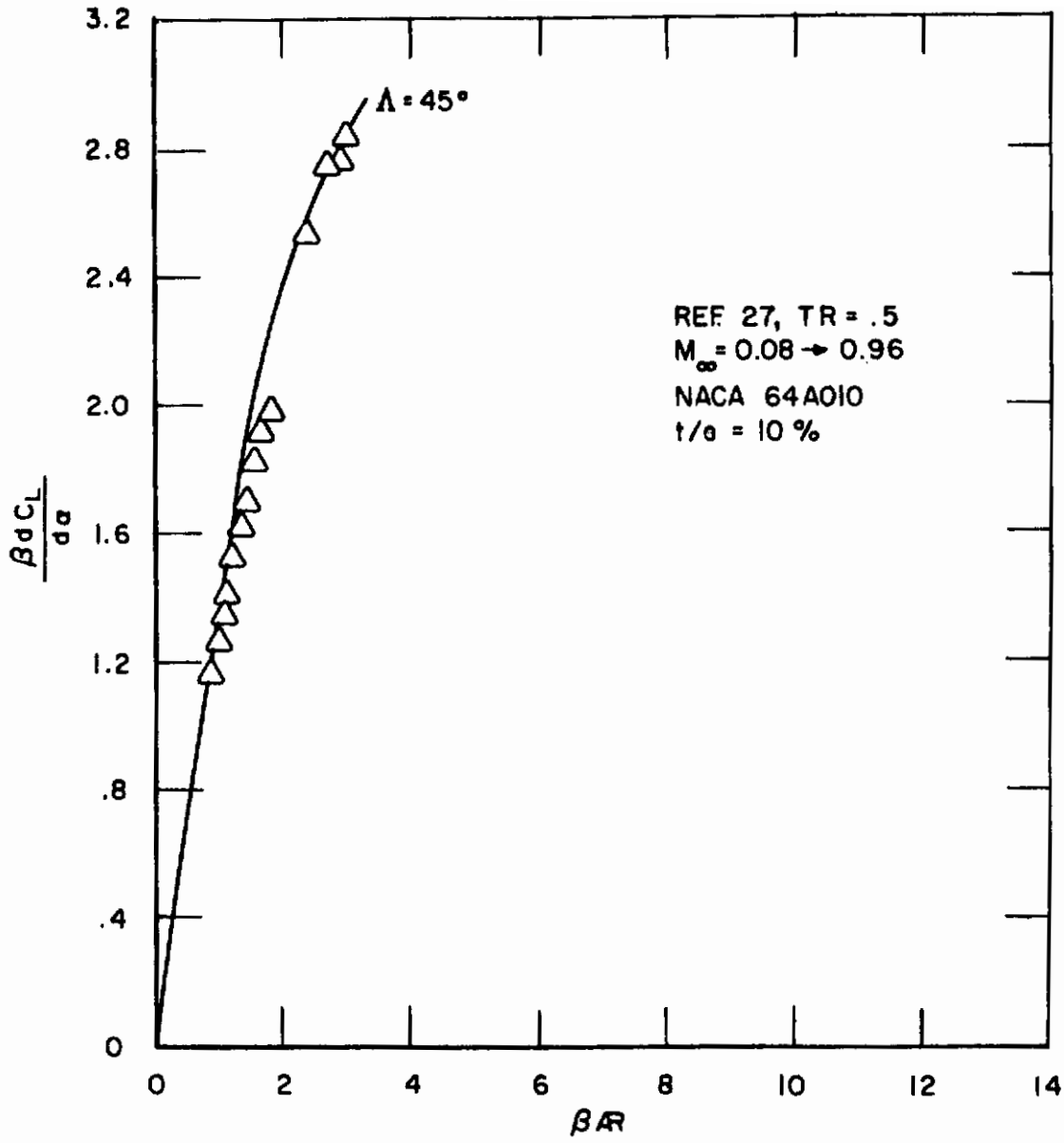

Figure 6. Lift curve slopes for aspect ratio 3 trapezoidal wing at various Mach numbers. Comparison with Weissinger theory

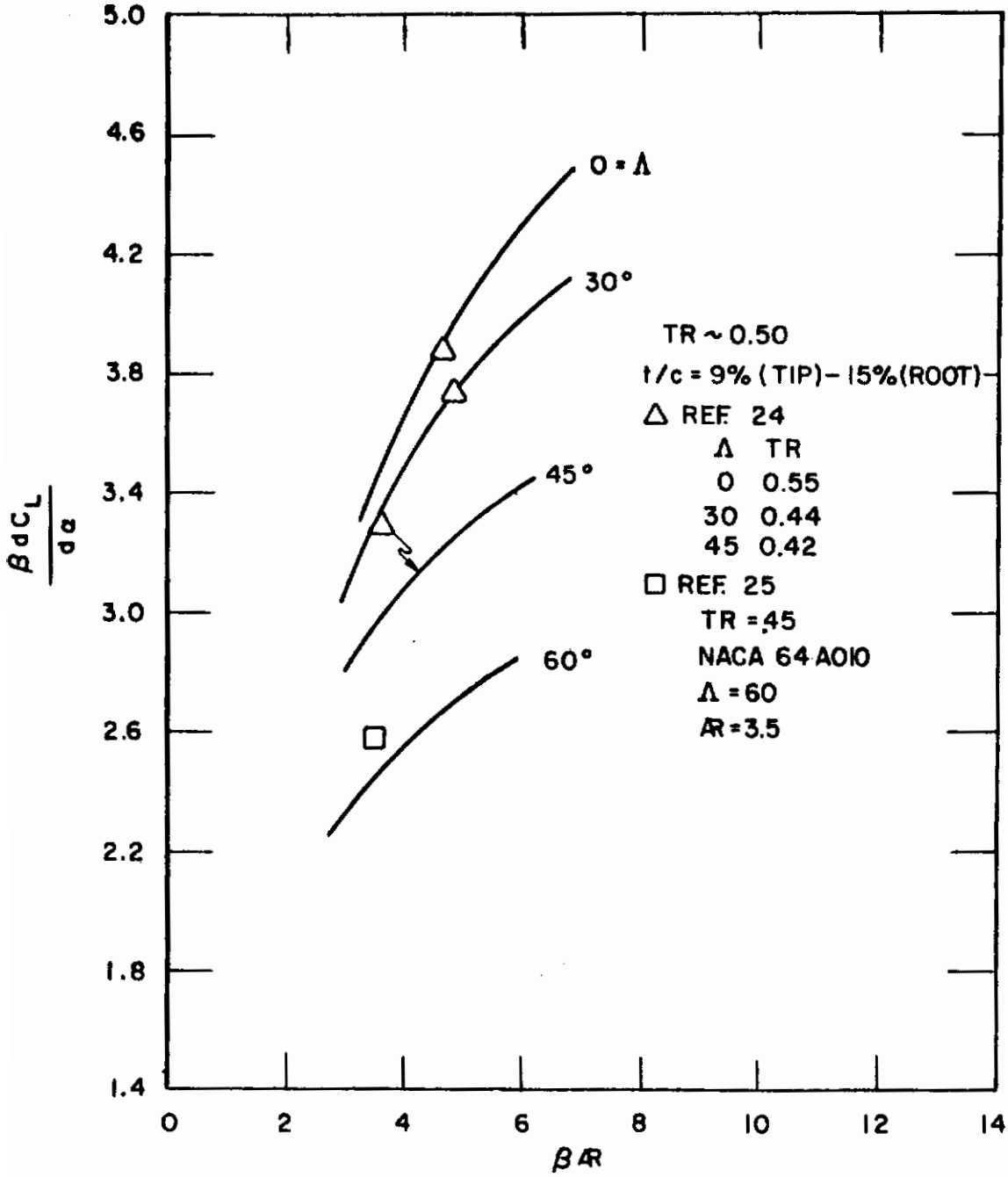

Figure 7. Lift curve slopes for swept and unswept trapezoidal wings at $M_\infty \sim 0$. Comparison with Weissinger theory

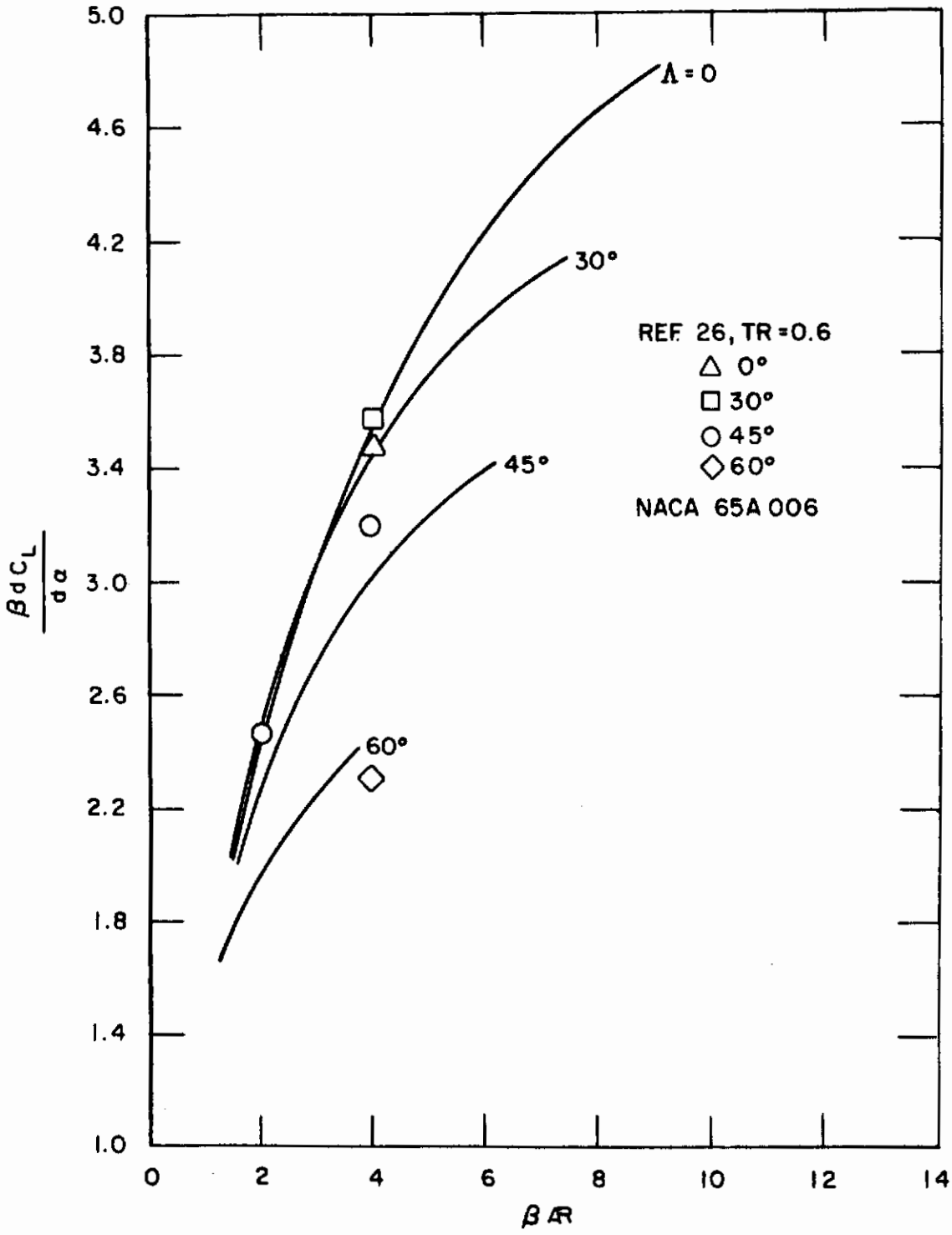

Figure 8. Lift curve slopes for swept and unswept trapezoidal wings at $M_\infty = 0.2$. Comparison with Weissinger theory

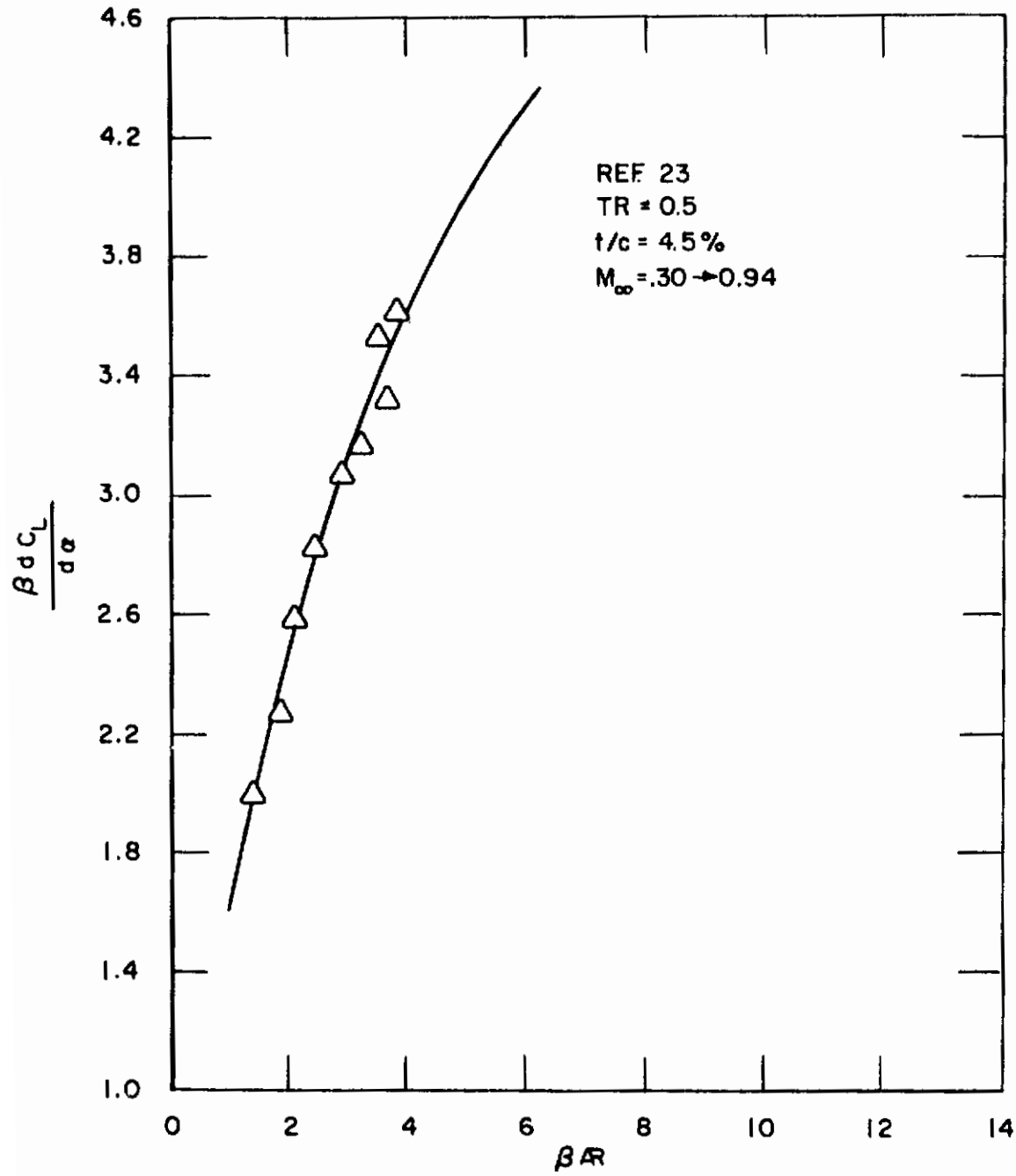

Figure 9. Lift curve slopes for unswept aspect ratio 4 trapezoidal wing at various Mach numbers. Comparison with Weissinger theory

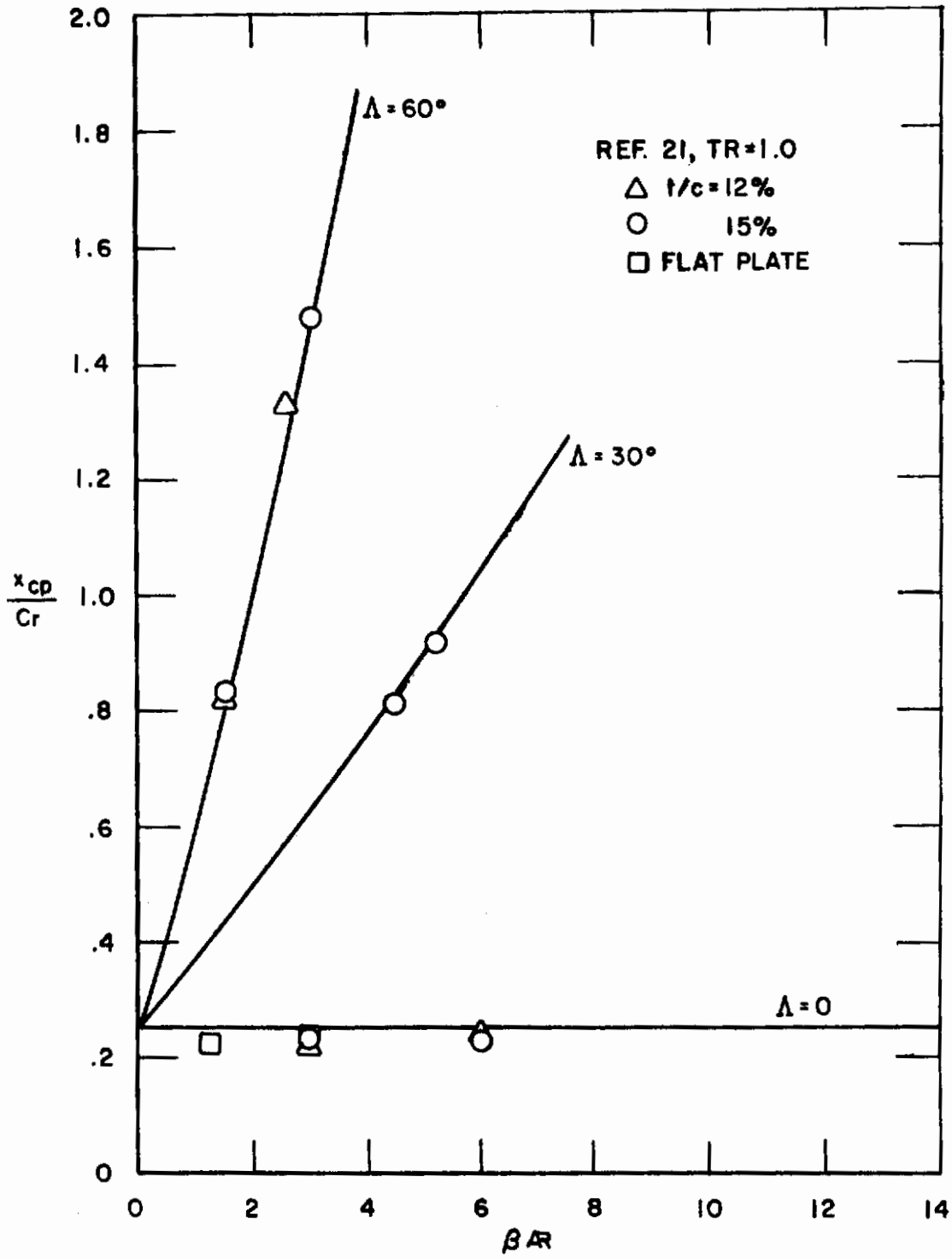

Figure 10. Streamwise center of pressure for swept and unswept wings at $M_\infty \sim 0$. Comparison with Weissinger theory

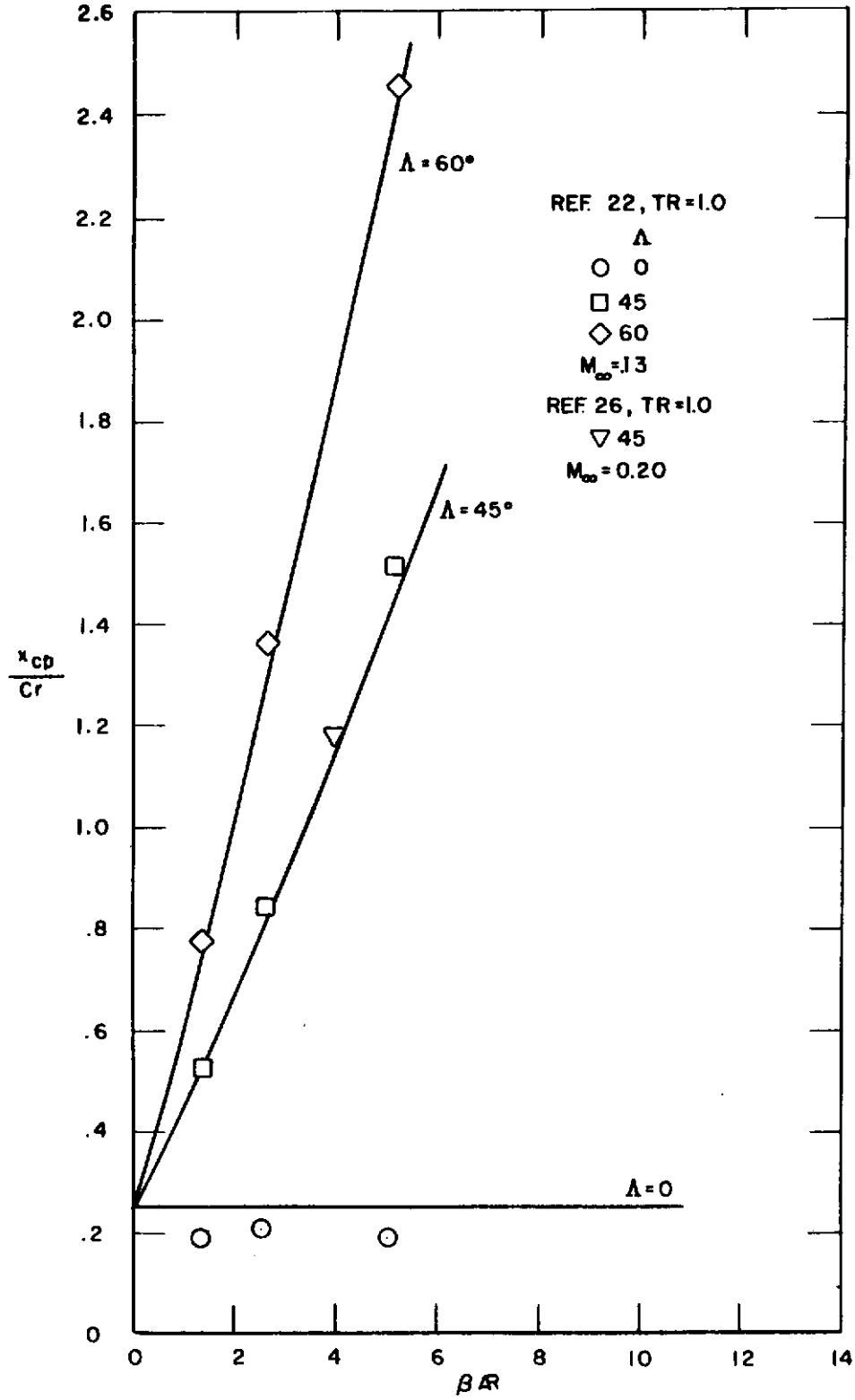

Figure 11. Streamwise center of pressure for swept and unswept wings at $M_\infty \approx 0$. Comparison with Weissinger theory

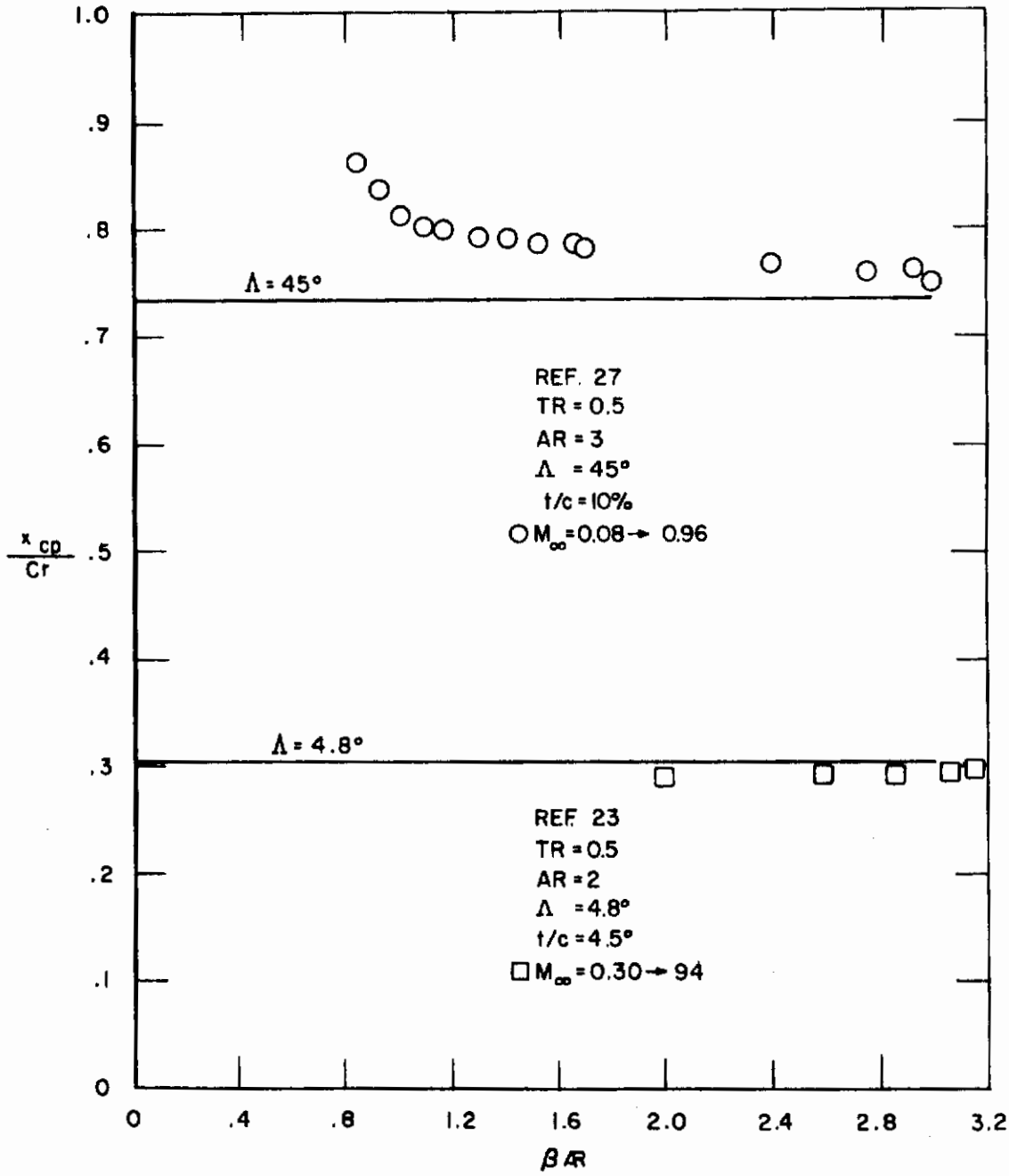

Figure 12. Streamwise center of pressure for trapezoidal wing at various Mach numbers. Comparison with Weissinger theory

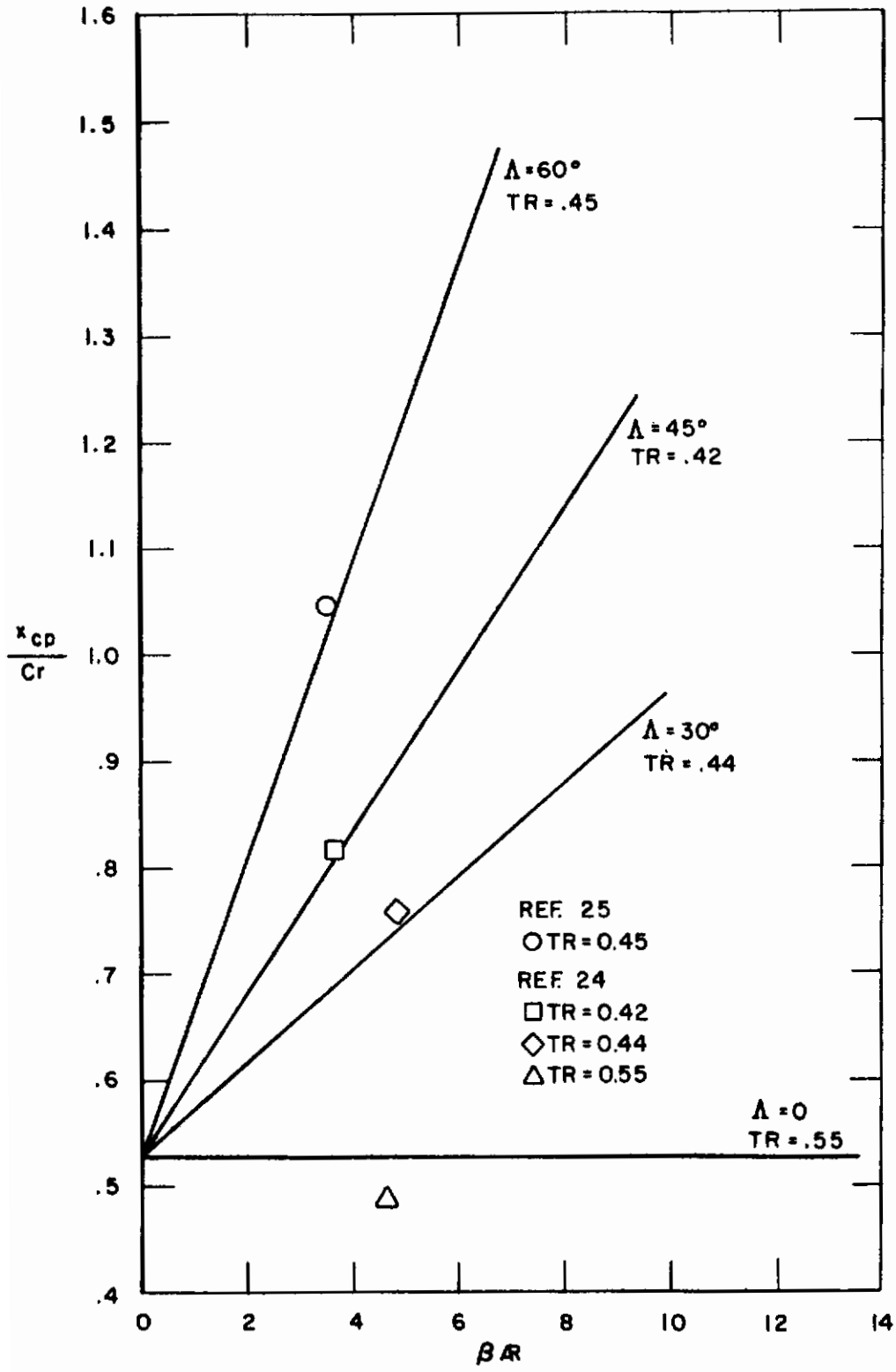

Figure 13. Streamwise center of pressure for swept and unswept trapezoidal wings at $M_\infty \sim 0$. Comparison with Weissinger theory

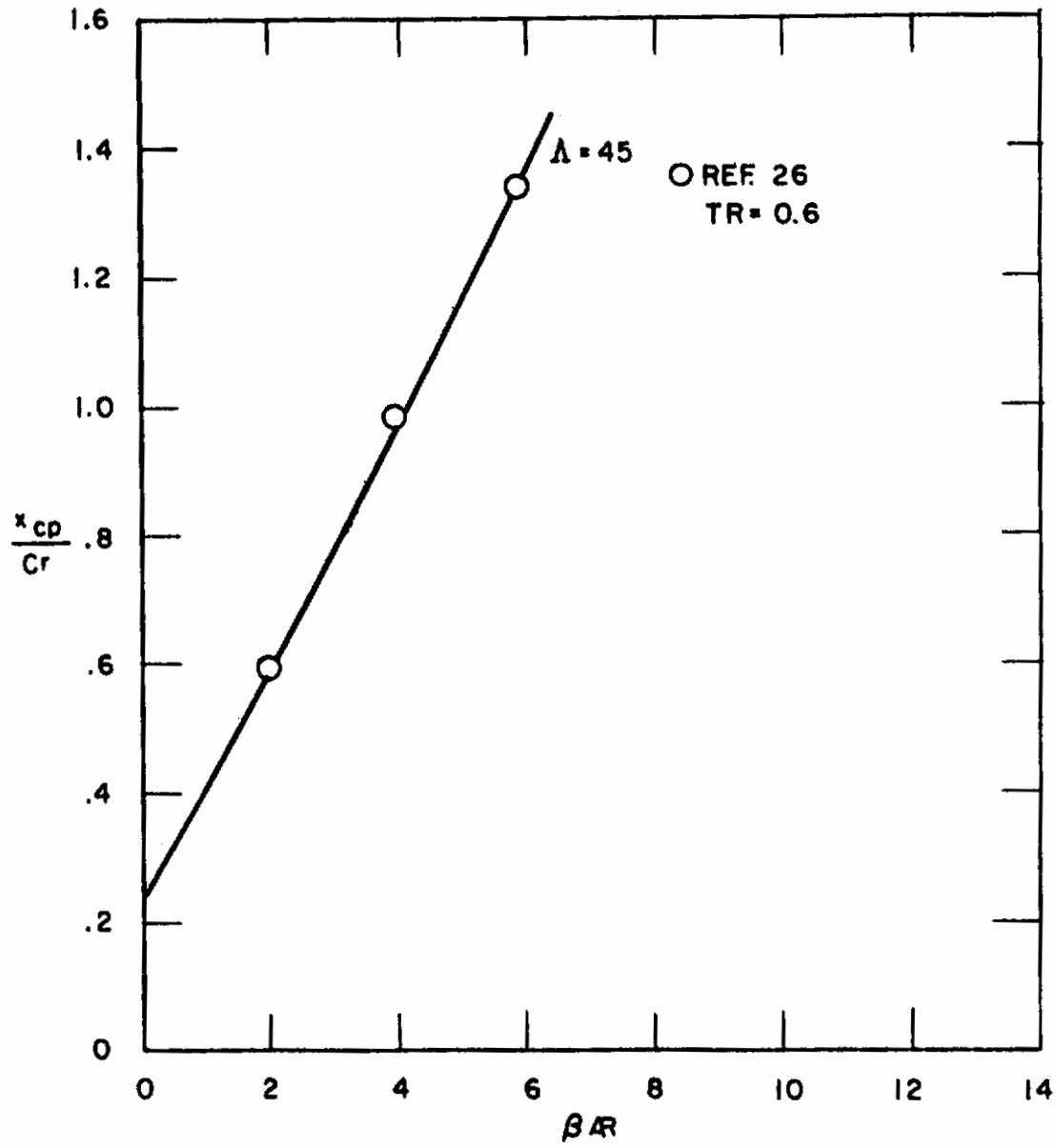

Figure 14. Variation of streamwise center of pressure with aspect ratio for swept trapezoidal wings at M_∞ = .2. Comparison with Weissinger theory

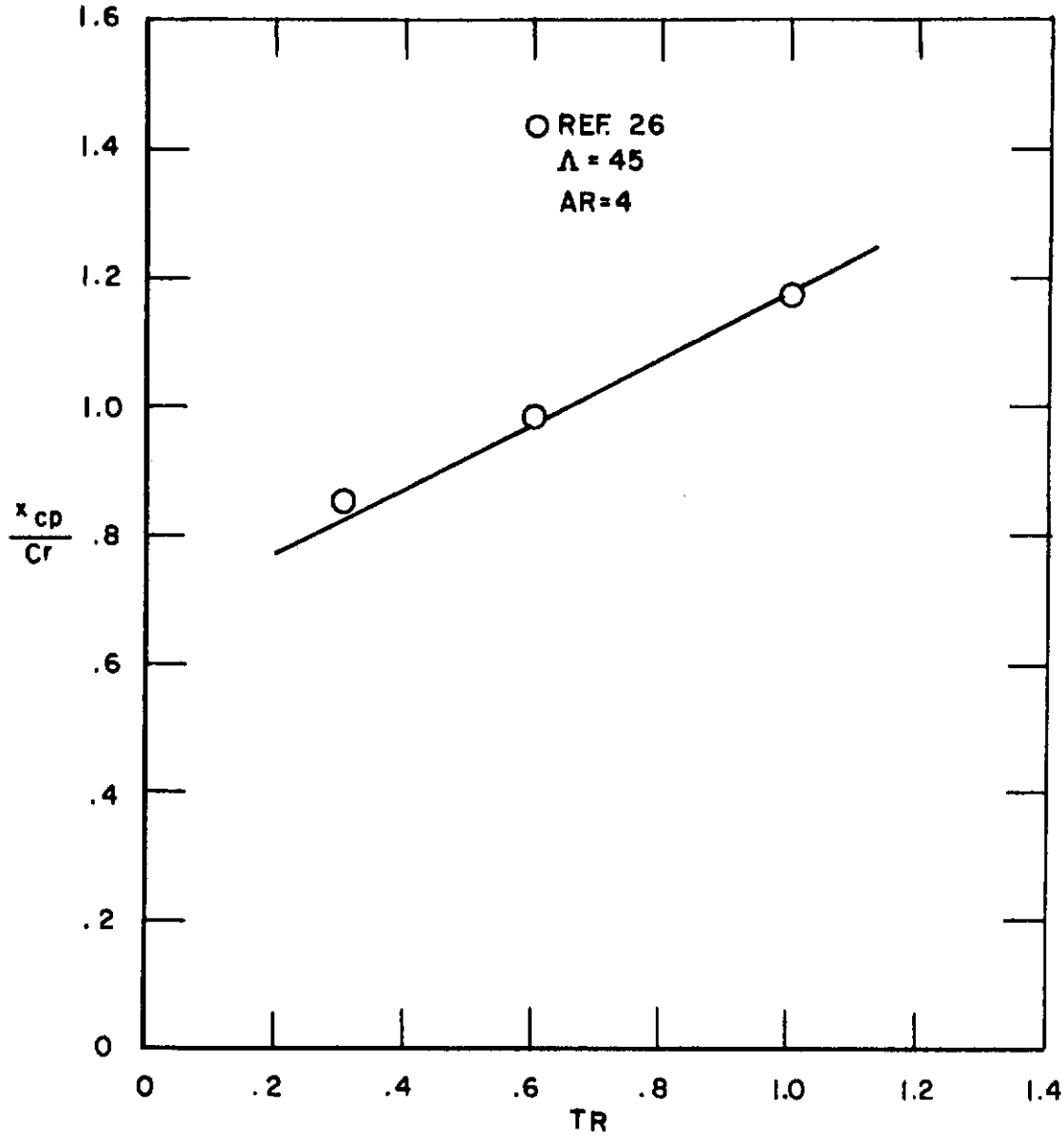

Figure 15. Variation of streamwise center of pressure with taper ratio for swept trapezoidal wings at M_∞ = 0.2. Comparison with Weissinger theory

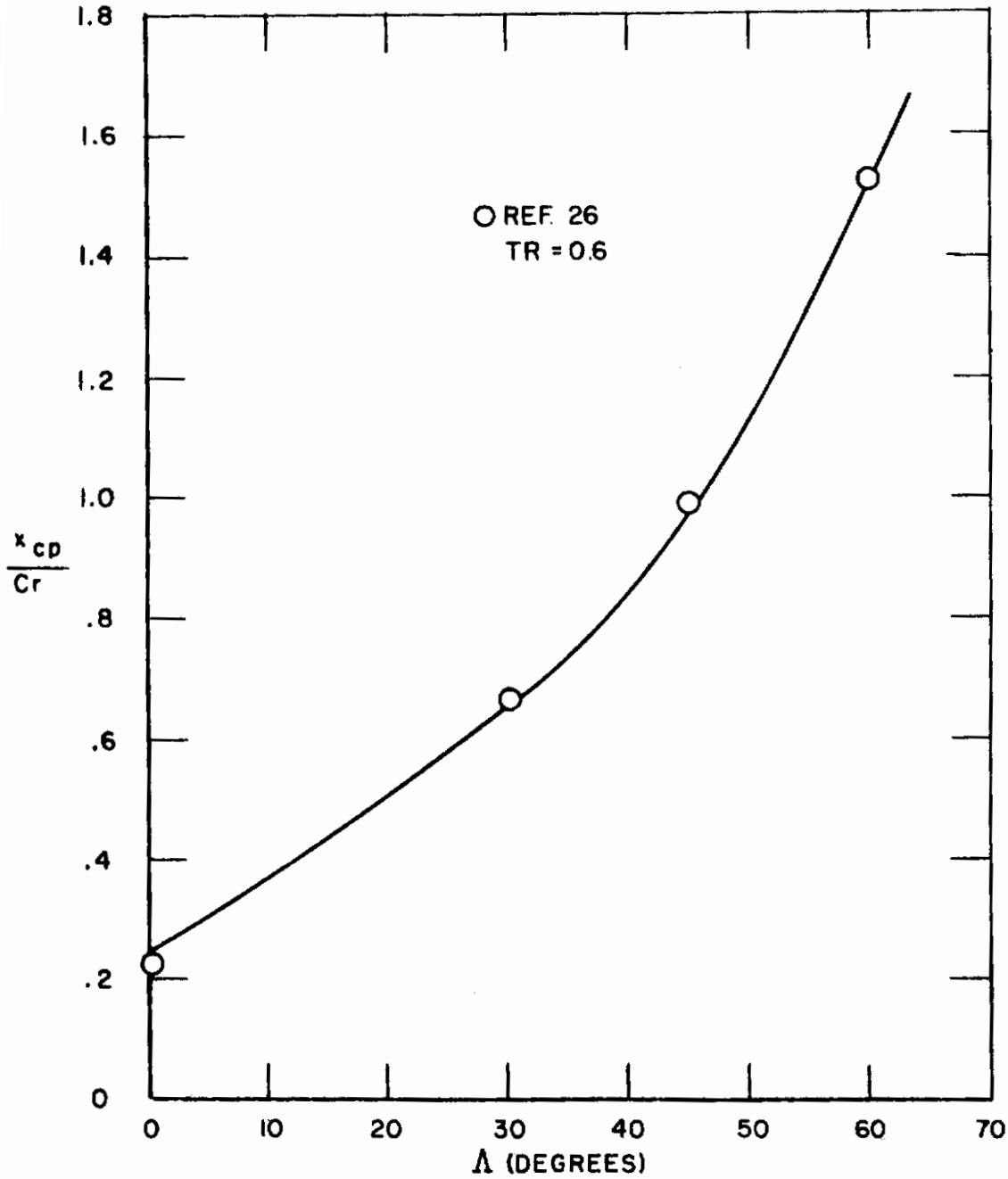

Figure 16. Variation of streamwise center of pressure with sweep back of quarter chord for aspect ratio 4 trapezoidal wings at $M_\infty = 0.2$. Comparison with Weissinger theory

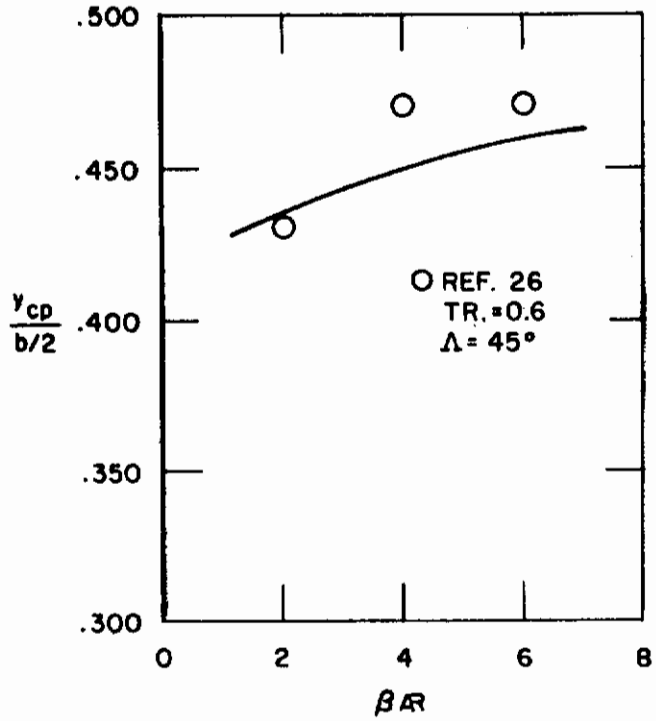

Figure 17. Variation of spanwise center of pressure aspect ratio for swept trapzeoidal wing panels at $M_\infty = 0.2$. Comparison with Weissinger theory

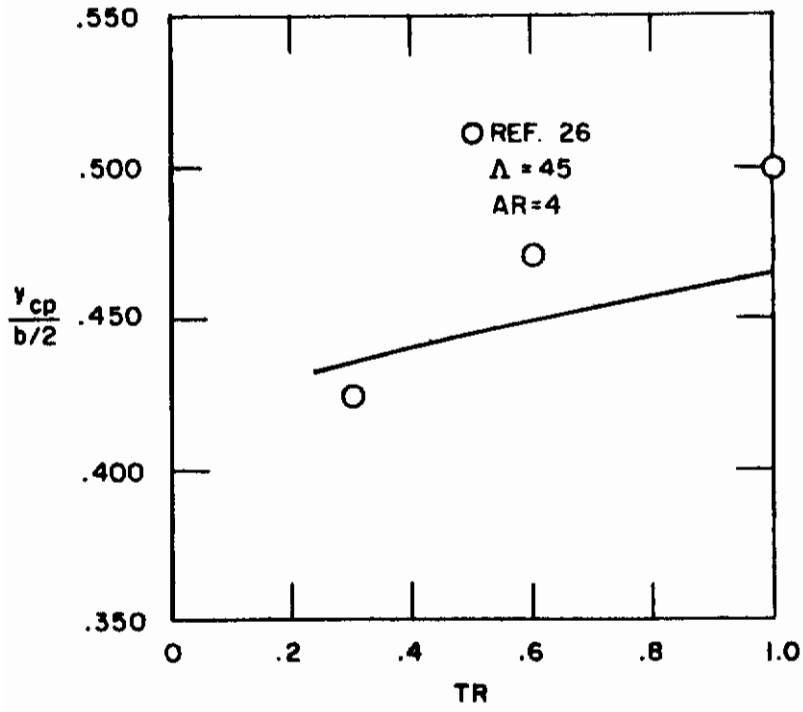

Figure 18. Variation of spanwise center of pressure with taper ratio for swept trapezoidal wing panels at $M_\infty = 0.2$. Comparison with Weissinger theory

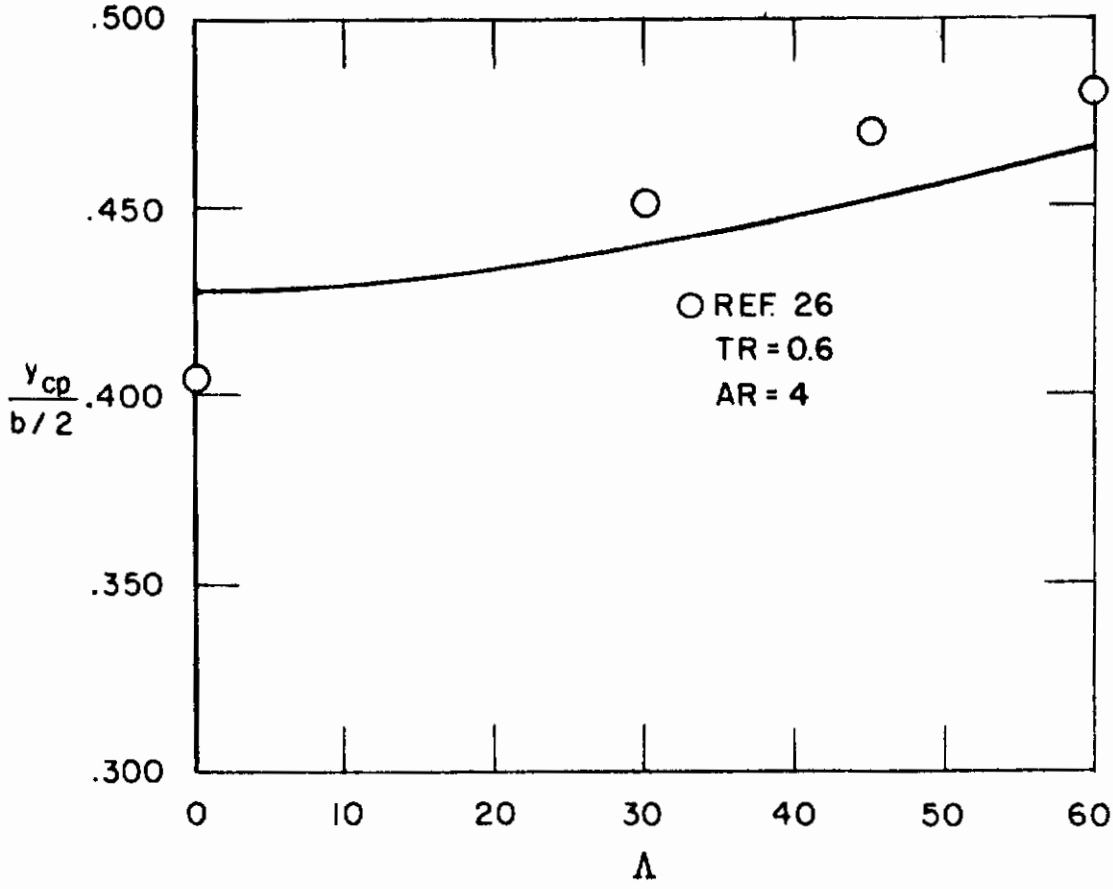

Figure 19. Variation of spanwise center of pressure with sweepback of quarter chord for trapezoidal wing panels at M_∞ = 0.2. Comparison with Weissinger theory

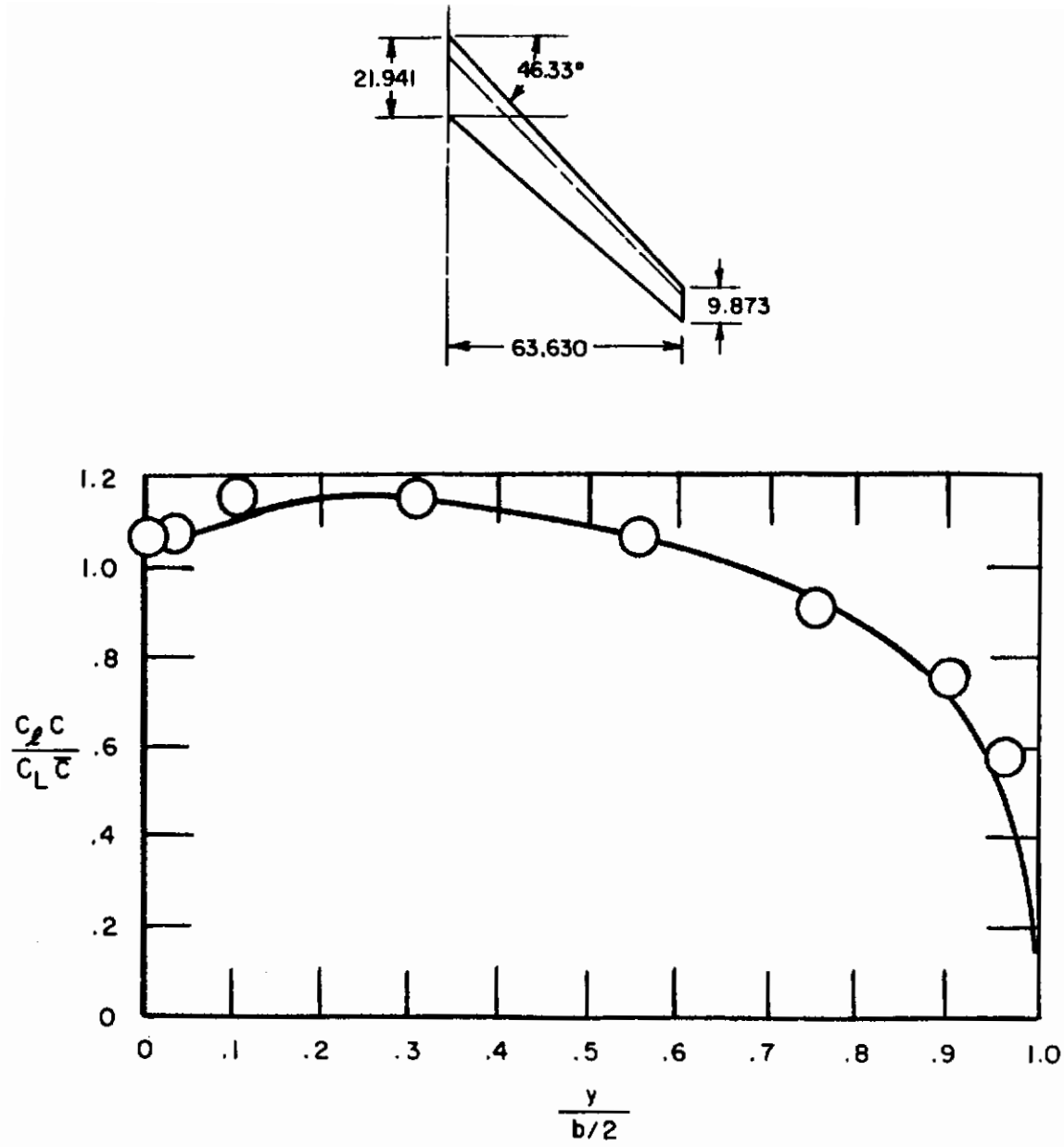

Figure 20. Comparison of theoretical and experimental spanwise load distribution on a flat wing at $M_\infty \sim 0$. Angle of attack = 4.7°

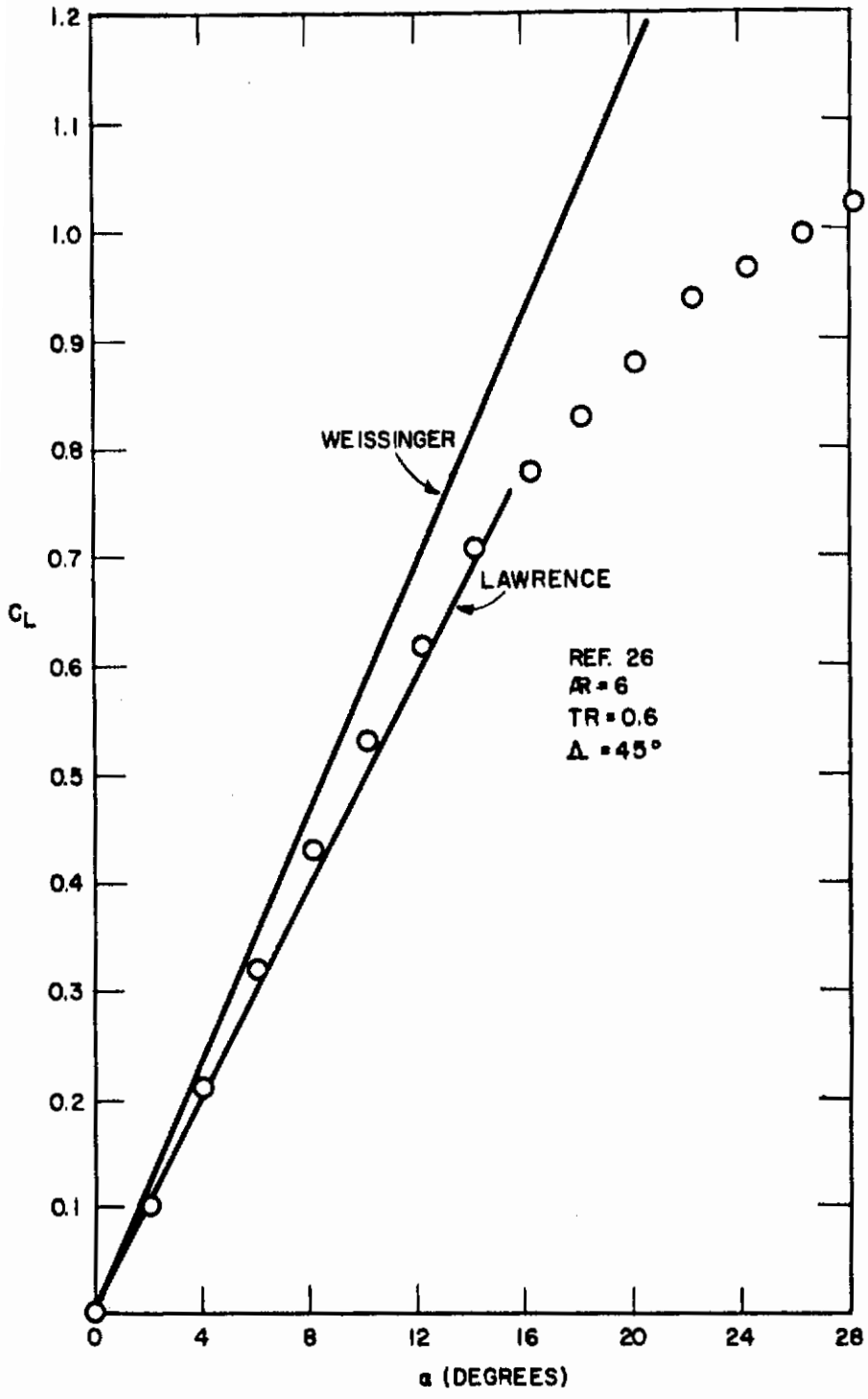

Figure 21. Lift curve for aspect ratio 6 trapezoidal wing at $M_\infty = 0.2$. Comparison with Weissinger theory and Lawrence theory

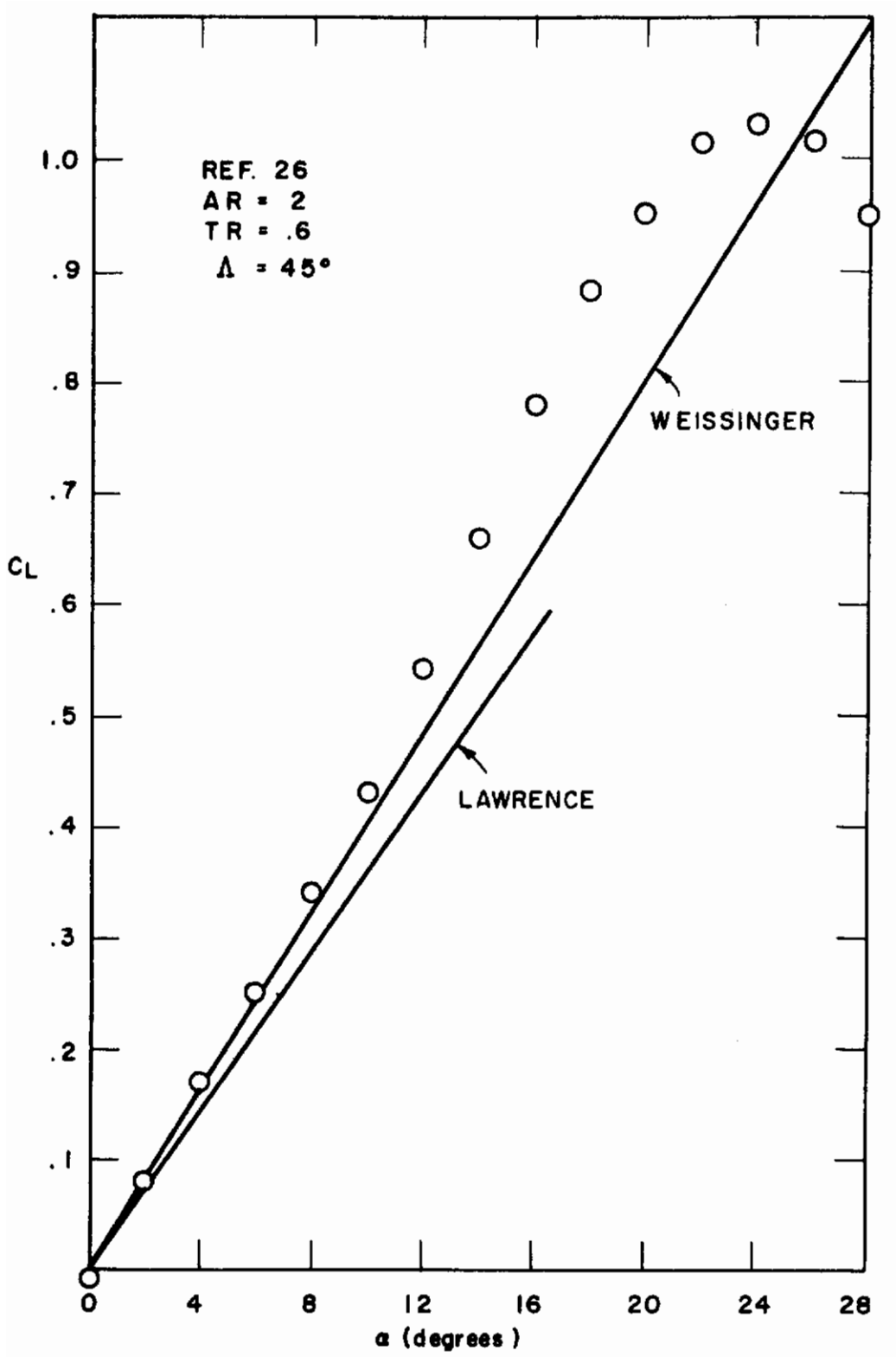

Figure 22. Lift curve for aspect ratio 2 trapezoidal wing at $M_\infty = 0.2$. Comparison with Weissinger theory and Lawrence theory.

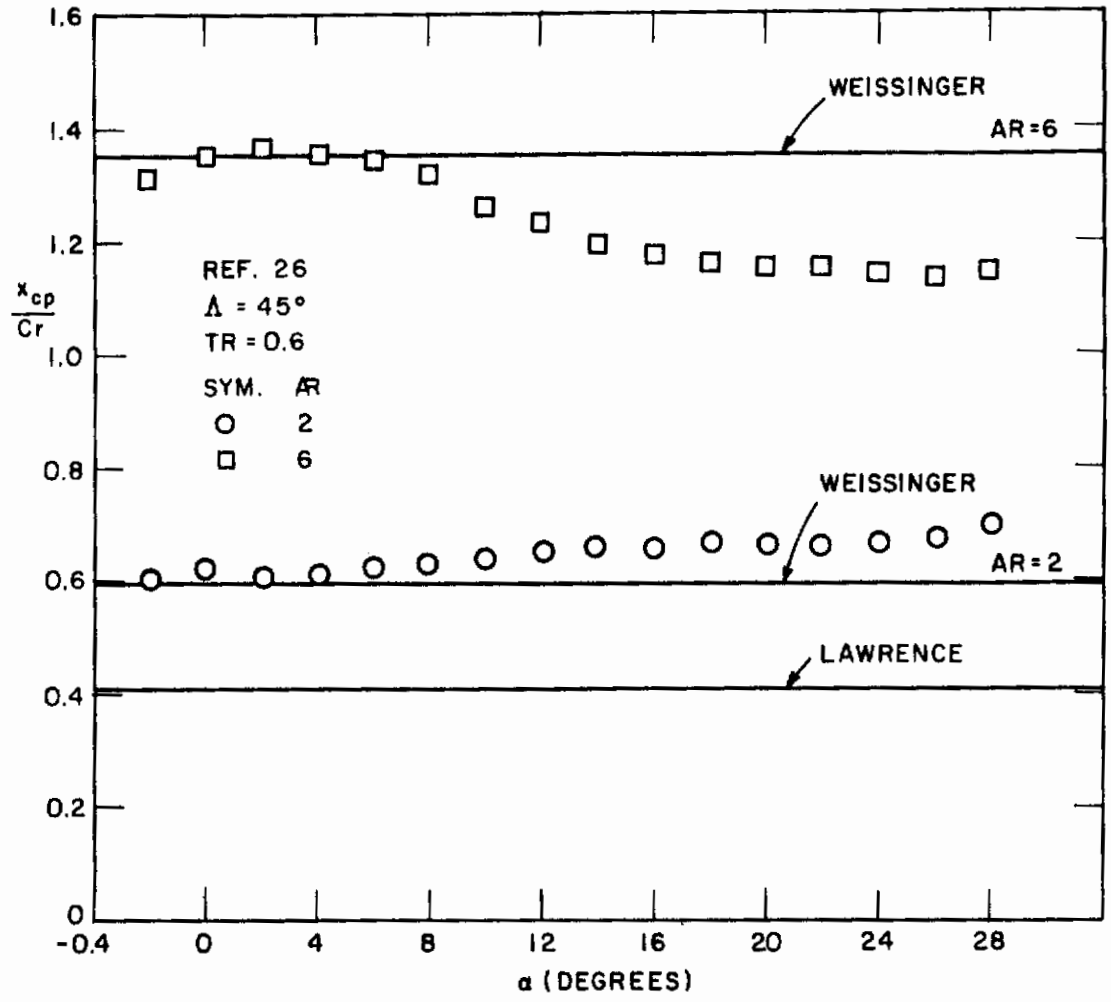

Figure 23. Streamwise centers of pressure for swept trapezoidal wings at $M_\infty = 0.2$. Comparison with Weissinger theory and Lawrence theory

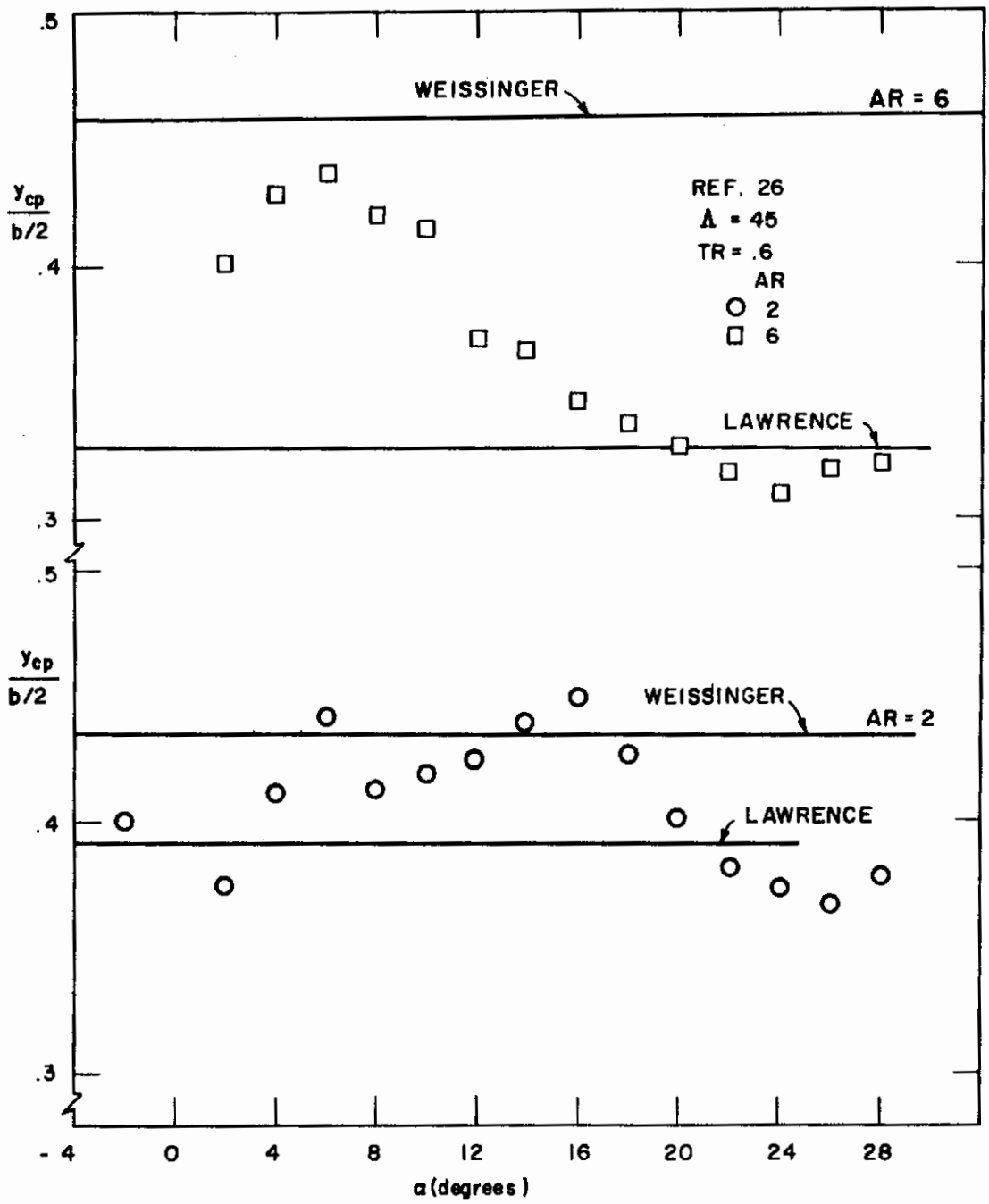

Figure 24. Spanwise centers of pressure for swept trapezoidal wings at $M_\infty = 0.2$. Comparison with Weissinger theory and Lawrence theory

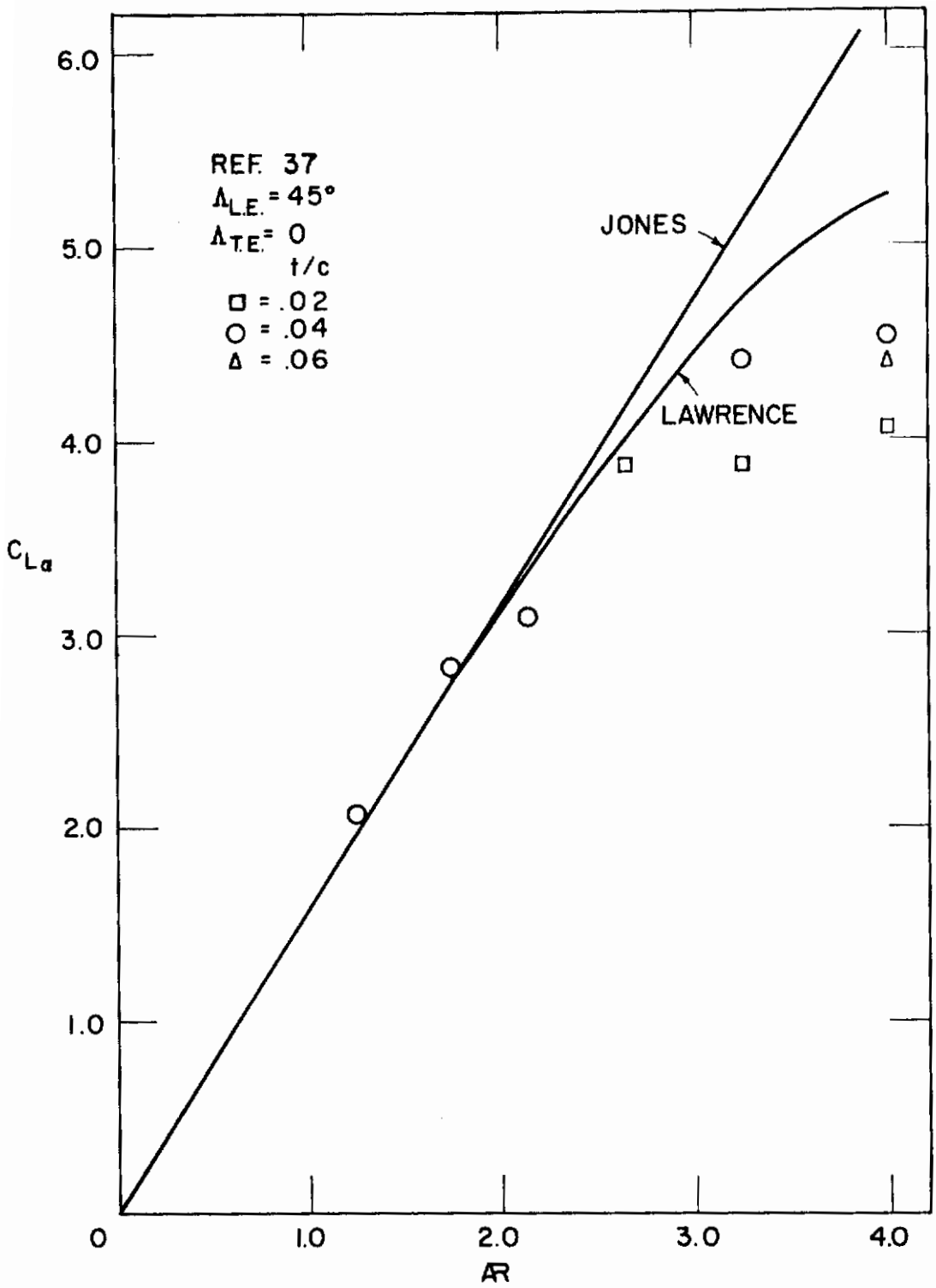

Figure 25. Lift curve slopes for swept trapezoidal wings at M_∞ = .98. Comparison with Lawrence theory and Jones theory

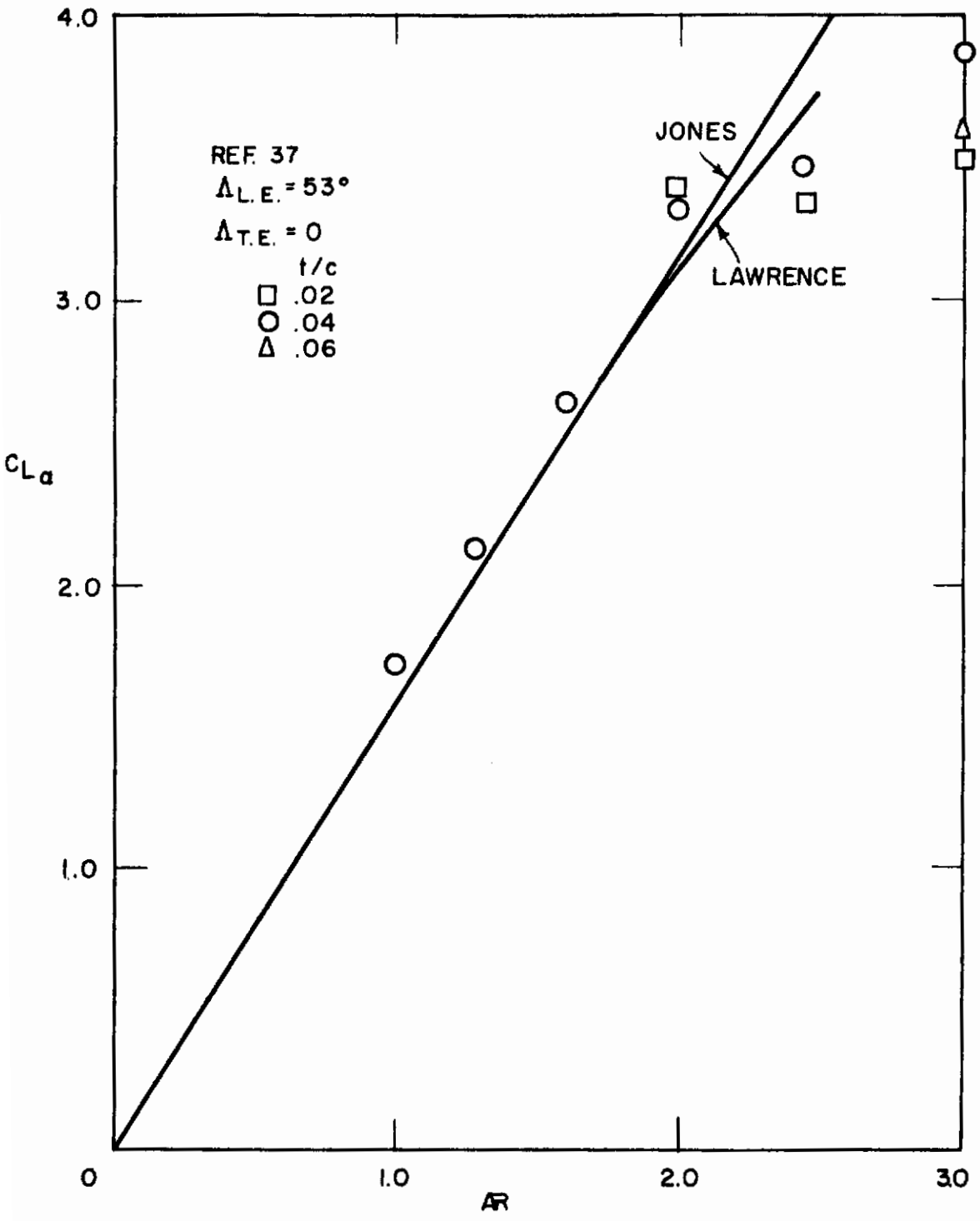

Figure 26. Lift curve slopes for swept trapezoidal wings at $M_\infty = .98$. Comparison with Lawrence theory and Jones theory

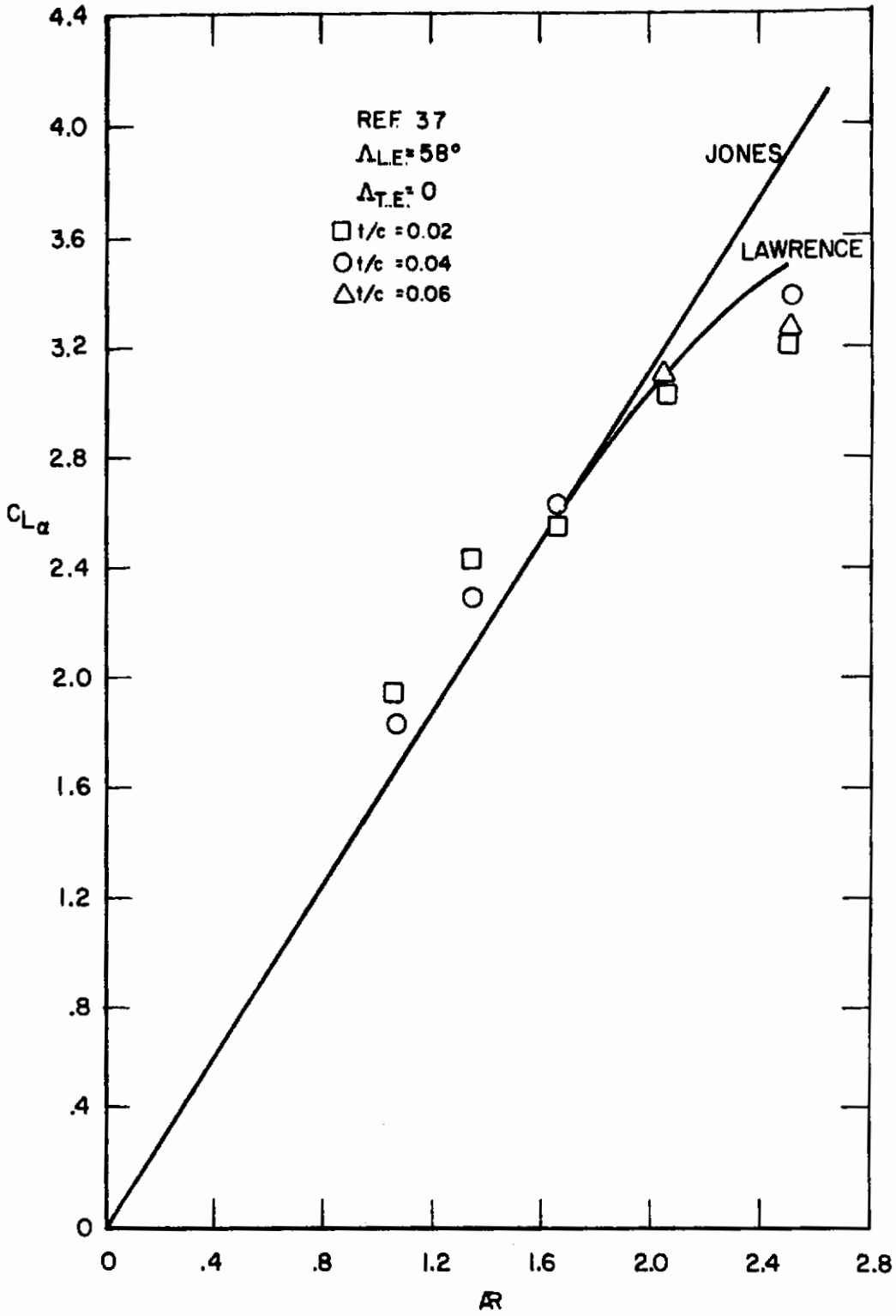

Figure 27. Lift curve slopes for swept trapezoidal wings at M_∞ = .98. Comparison with Lawrence theory and Jones theory

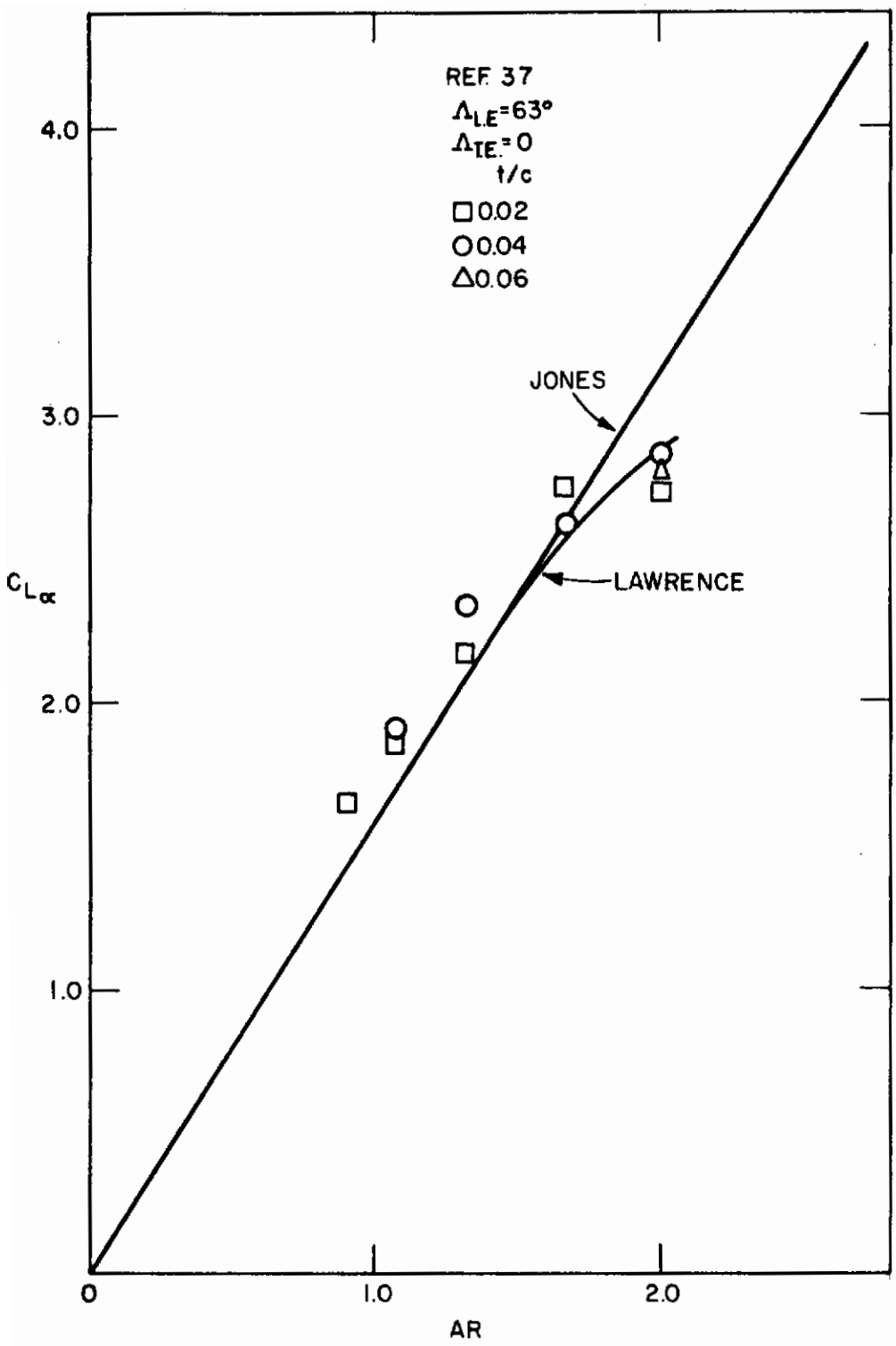

Figure 28. Lift curve slopes for swept trapezoidal wings at M_∞ = .98. Comparison with Lawrence theory and Jones theory

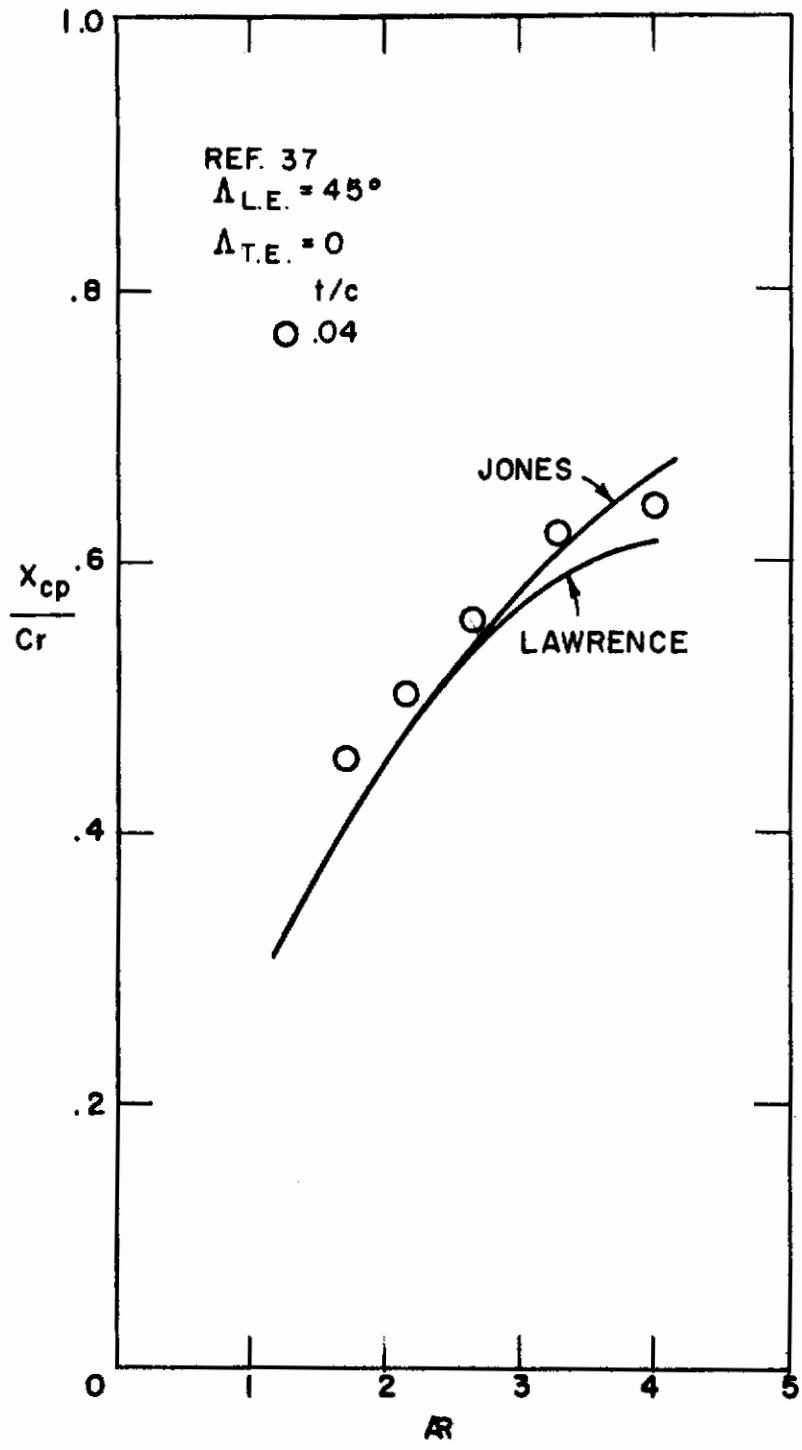

Figure 29. Streamwise center of pressure for swept trapezoidal wings at $M_\infty = .98$. Comparison with Lawrence theory and Jones theory

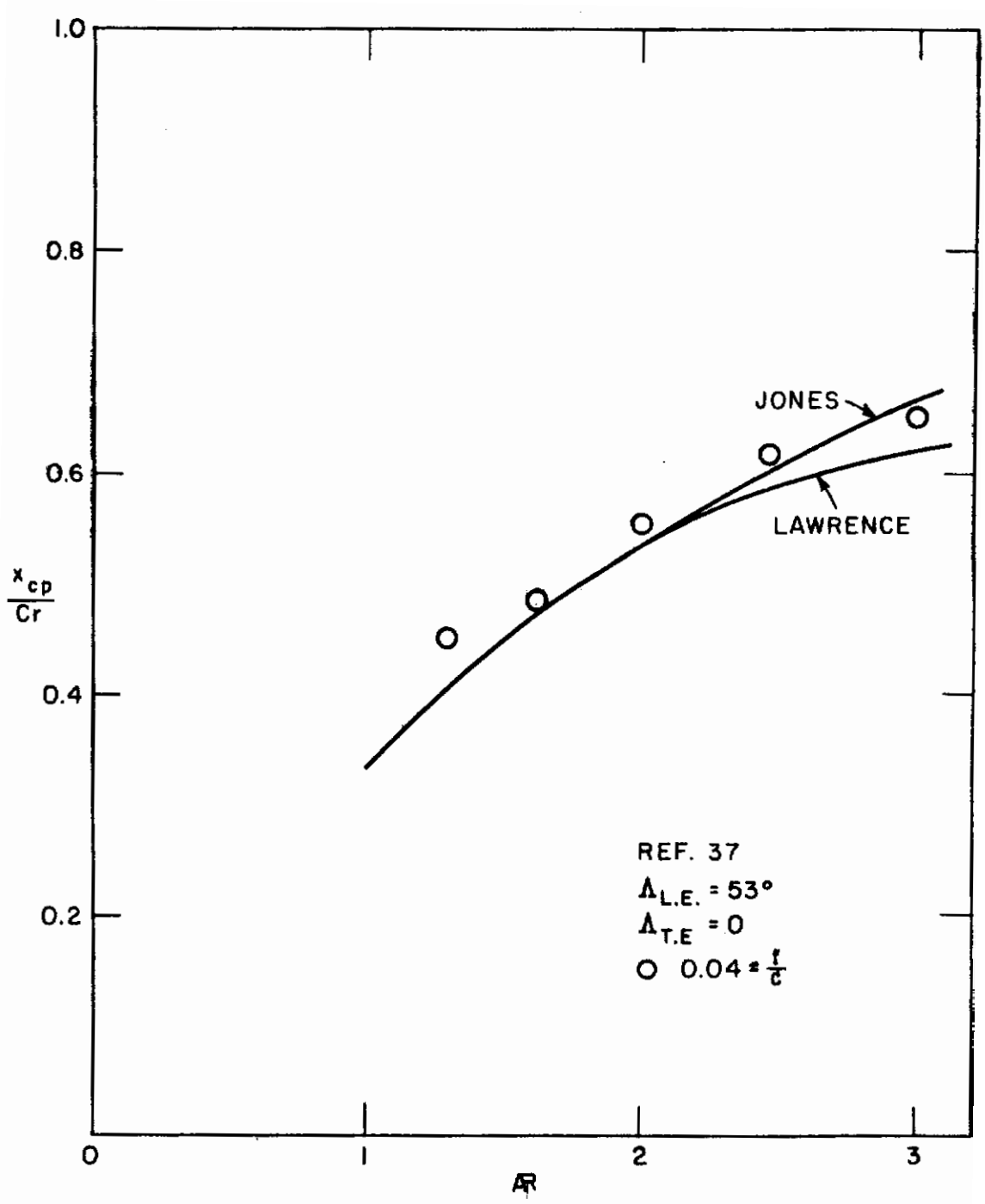

Figure 30. Streamwise center of pressure for swept trapezoidal wings at $M_\infty = .98$. Comparison with Lawrence theory and Jones theory

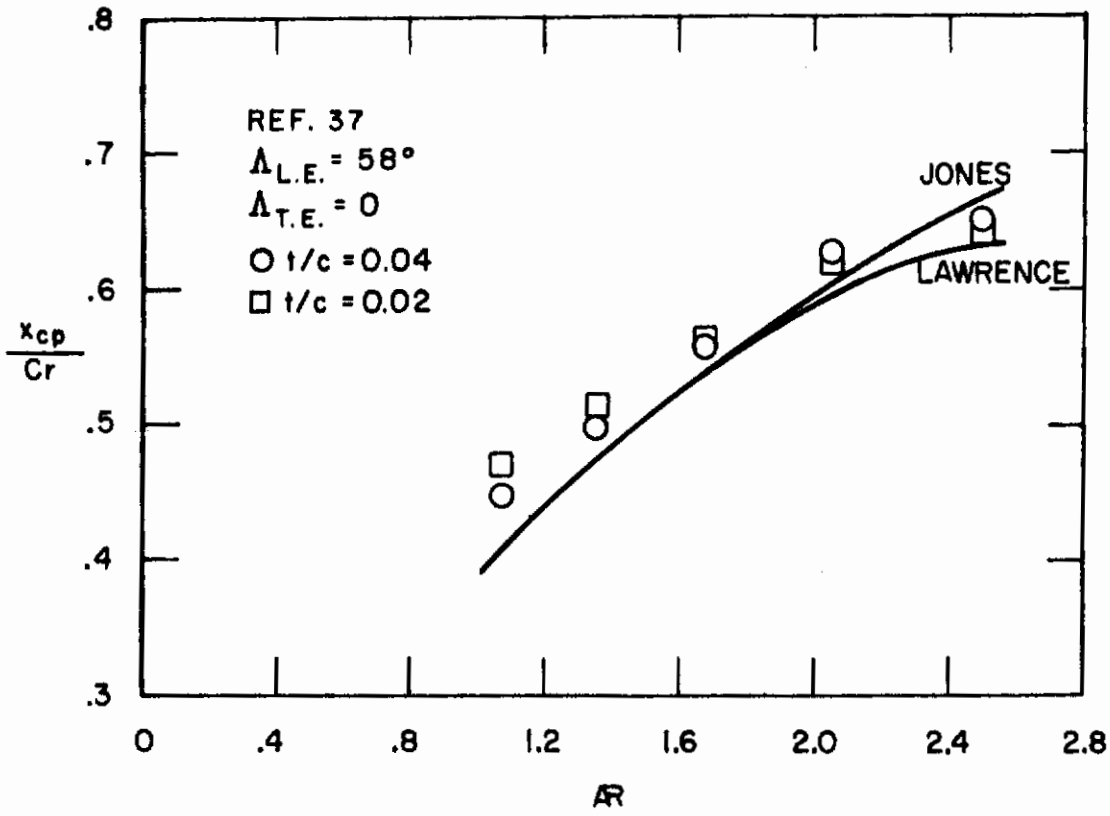

Figure 31. Streamwise center of pressure for swept trapezoidal wings at M_∞ = .98. Comparison with Lawrence theory and Jones theory

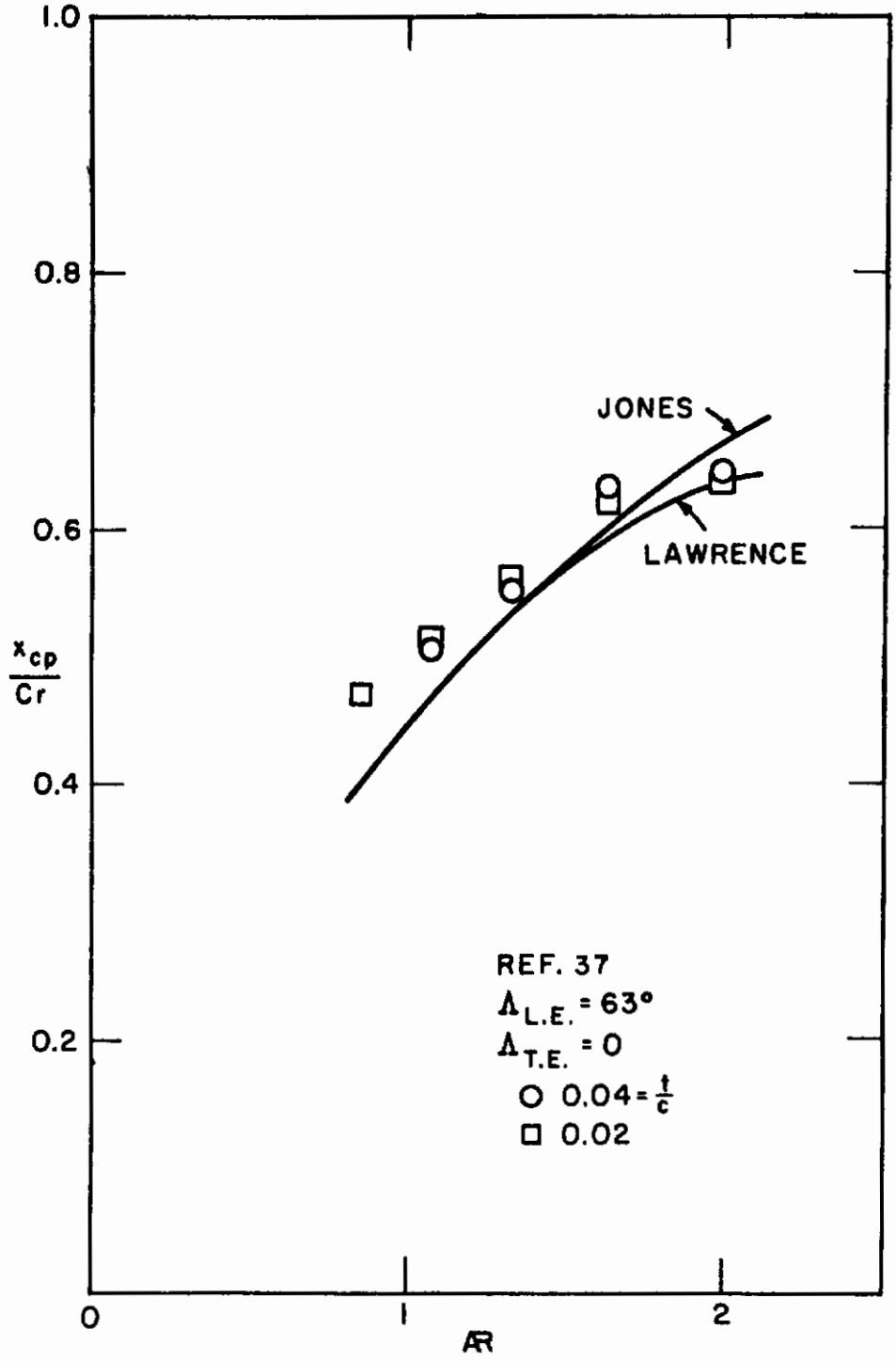

Figure 32. Streamwise center of pressure for swept trapezoidal wings at $M_\infty = .98$. Comparison with Lawrence theory and Jones theory

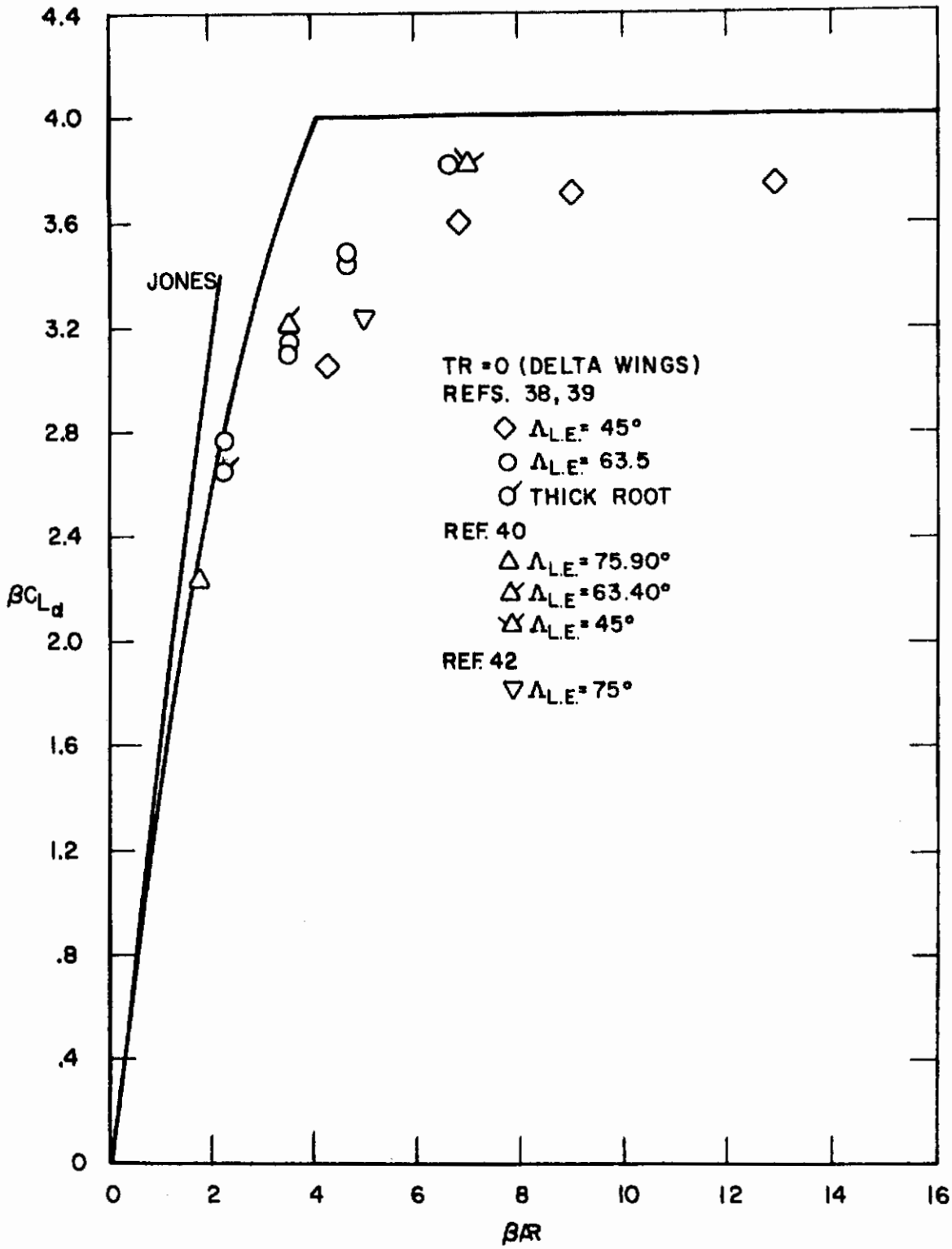

Figure 33. Lift curve slopes for delta wings at supersonic speed. Comparison with linear wing theory and Jones theory

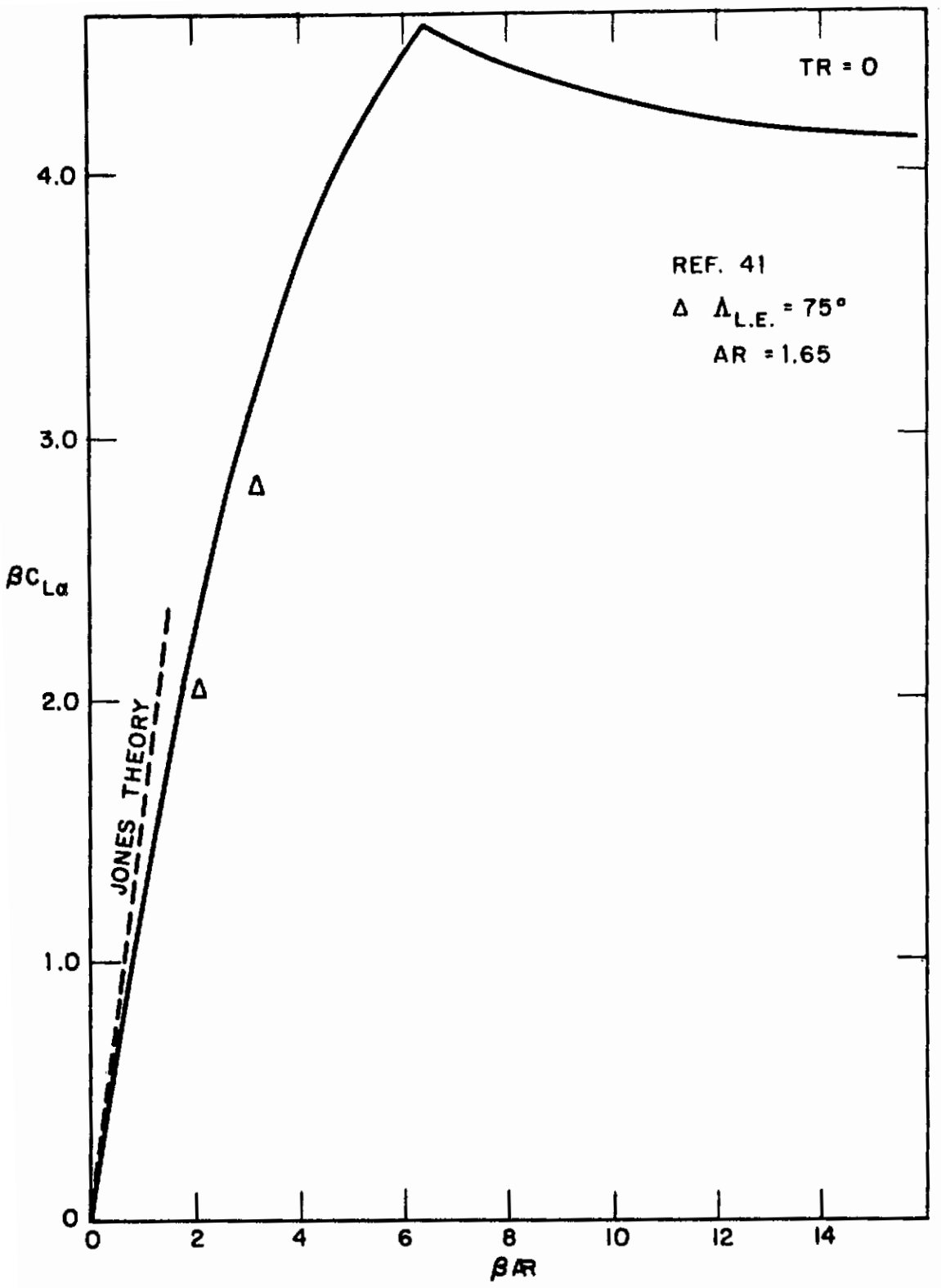

Figure 34. Lift curve slopes for arrow wings of AR = 1.65 at supersonic speed. Comparison with linear wing theory and with Jones theory

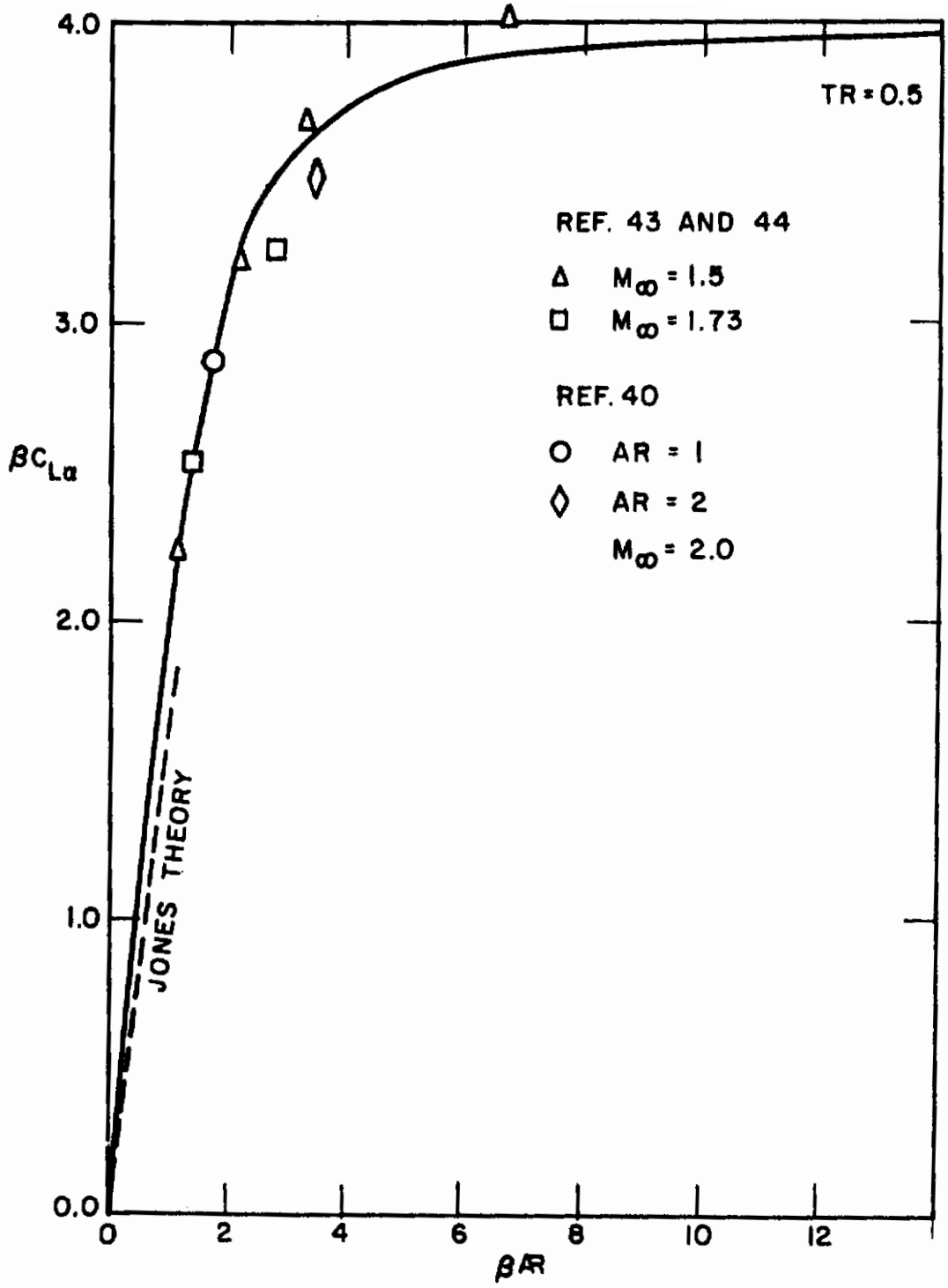

Figure 35. Lift curve slopes for symmetric trapezoidal wings at supersonic speed. Comparison with linear wing theory and with Jones theory

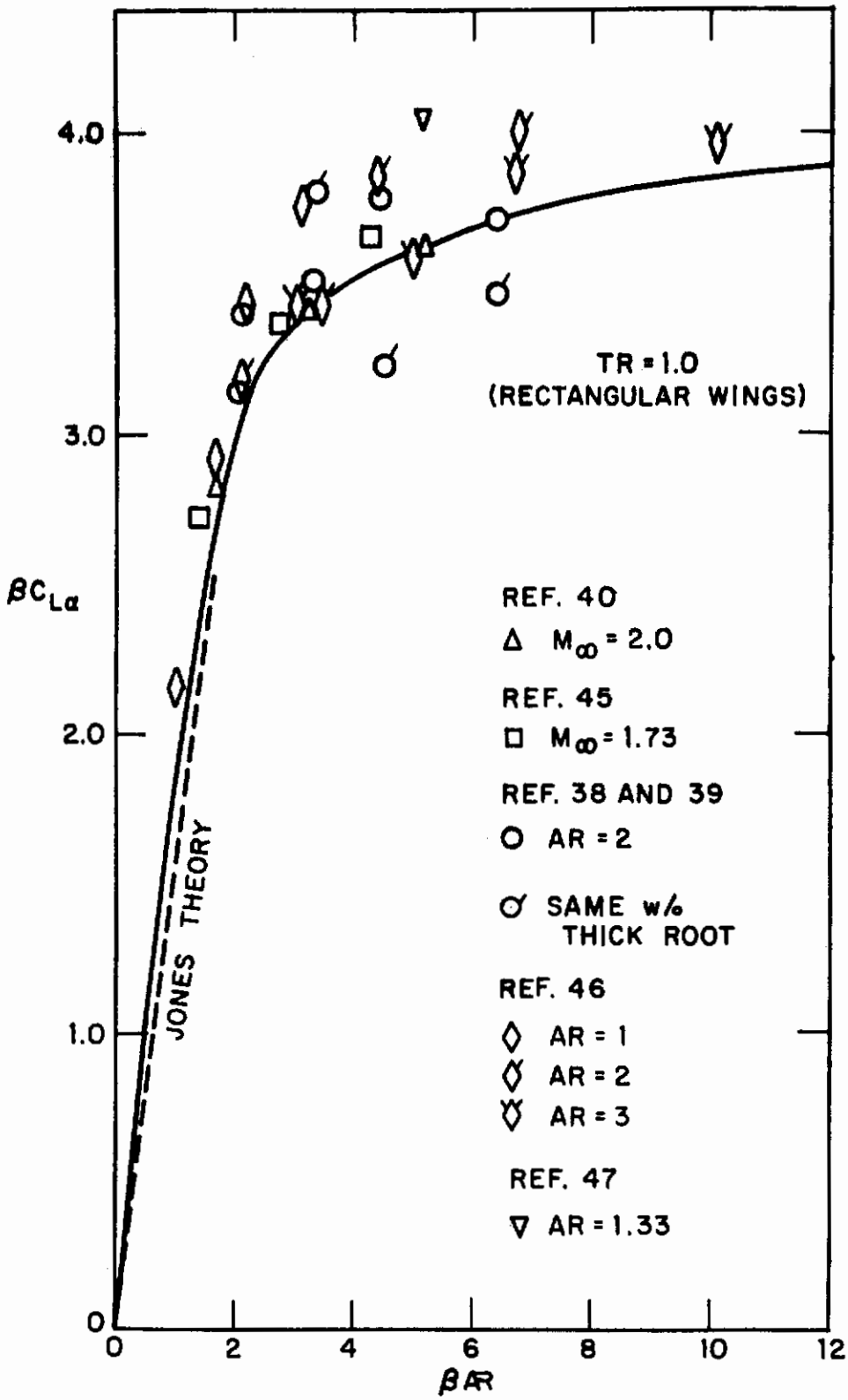

Figure 36. Lift curve slopes for rectangular wings at supersonic speed. Comparison with linear wing theory and with Jones theory

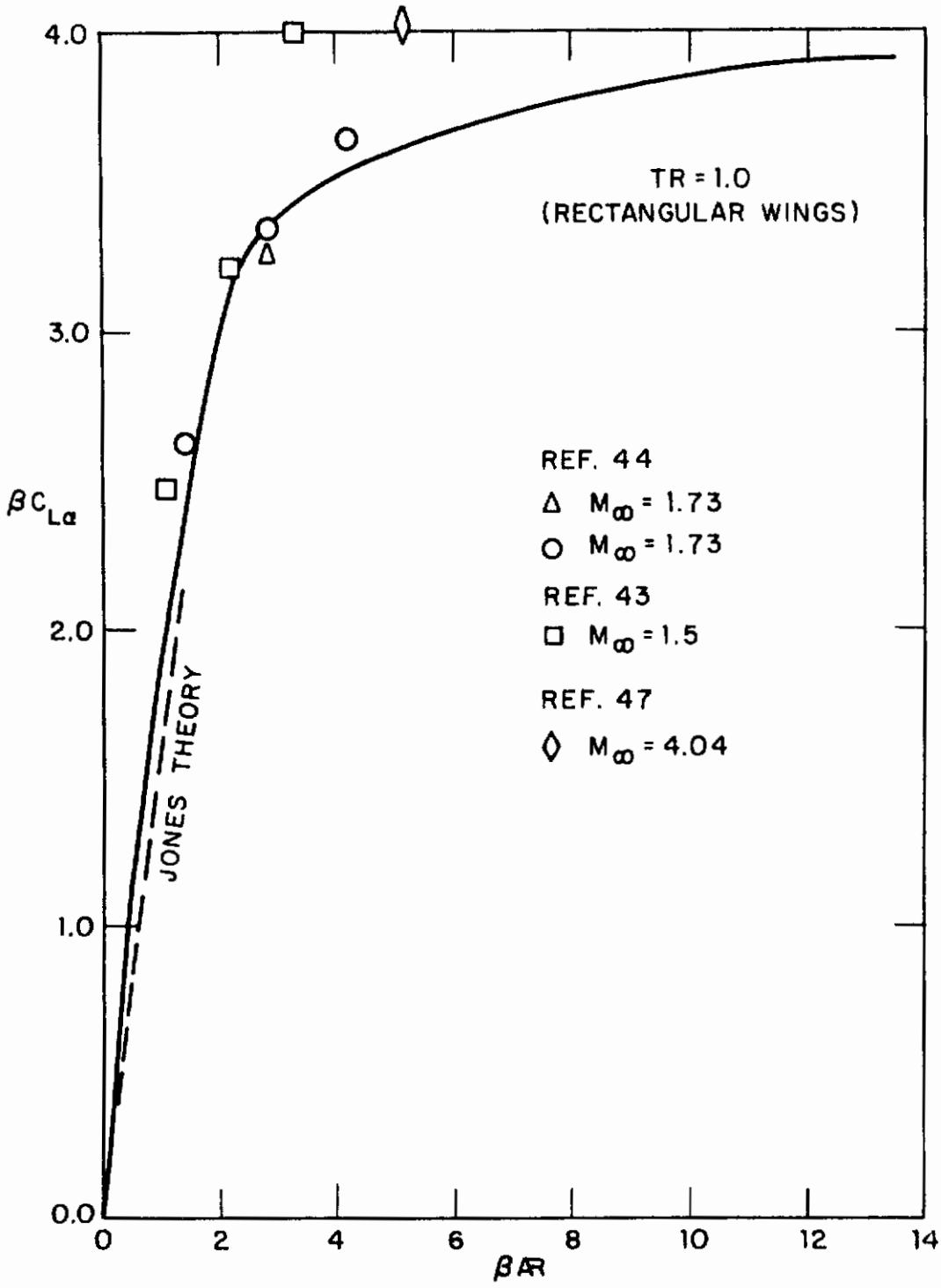

Figure 37. Lift curve slopes for rectangular wings at supersonic speed. Comparison with linear wing theory and with Jones theory

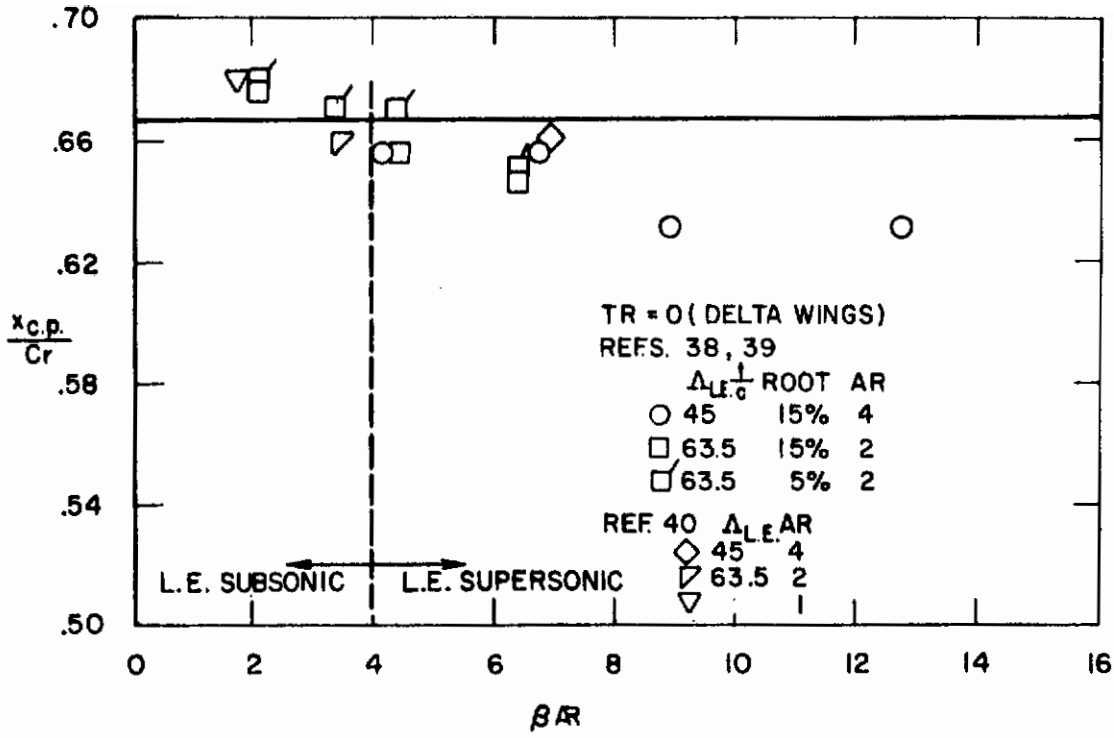

Figure 38. Streamwise center of pressure for delta wings at supersonic speed. Comparison with linear theory

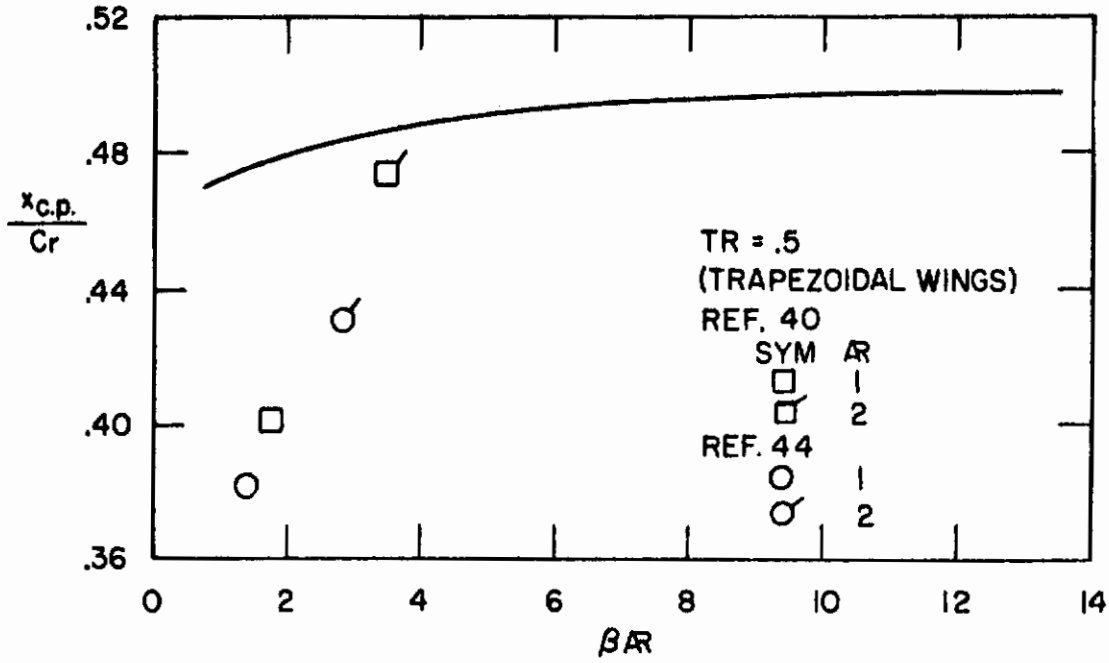

Figure 39. Streamwise center of pressure for symmetric trapezoidal wings at supersonic speed. Comparison with linear theory

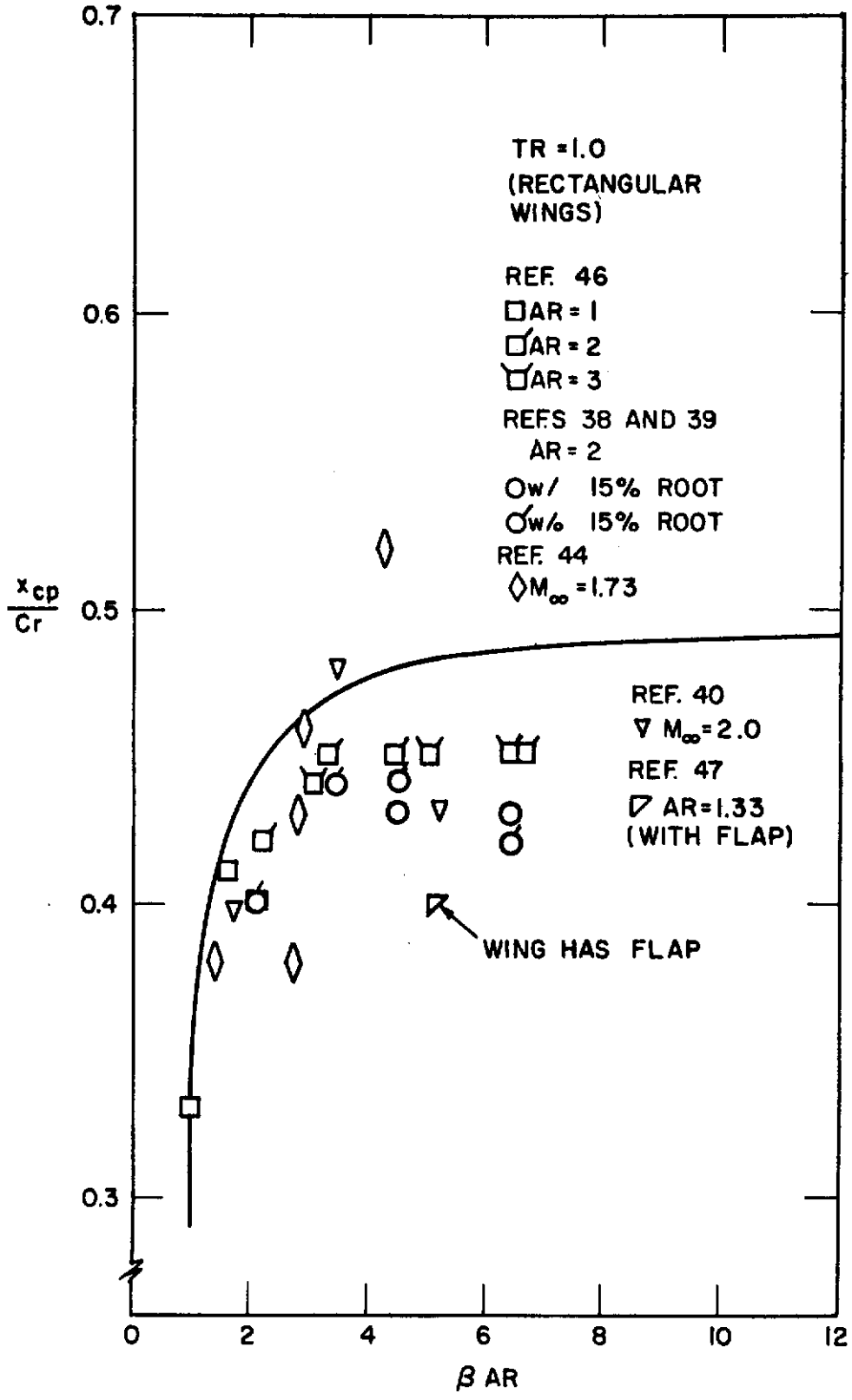

Figure 40. Streamwise center of pressure for rectangular wings at supersonic speed. Comparison with linear theory

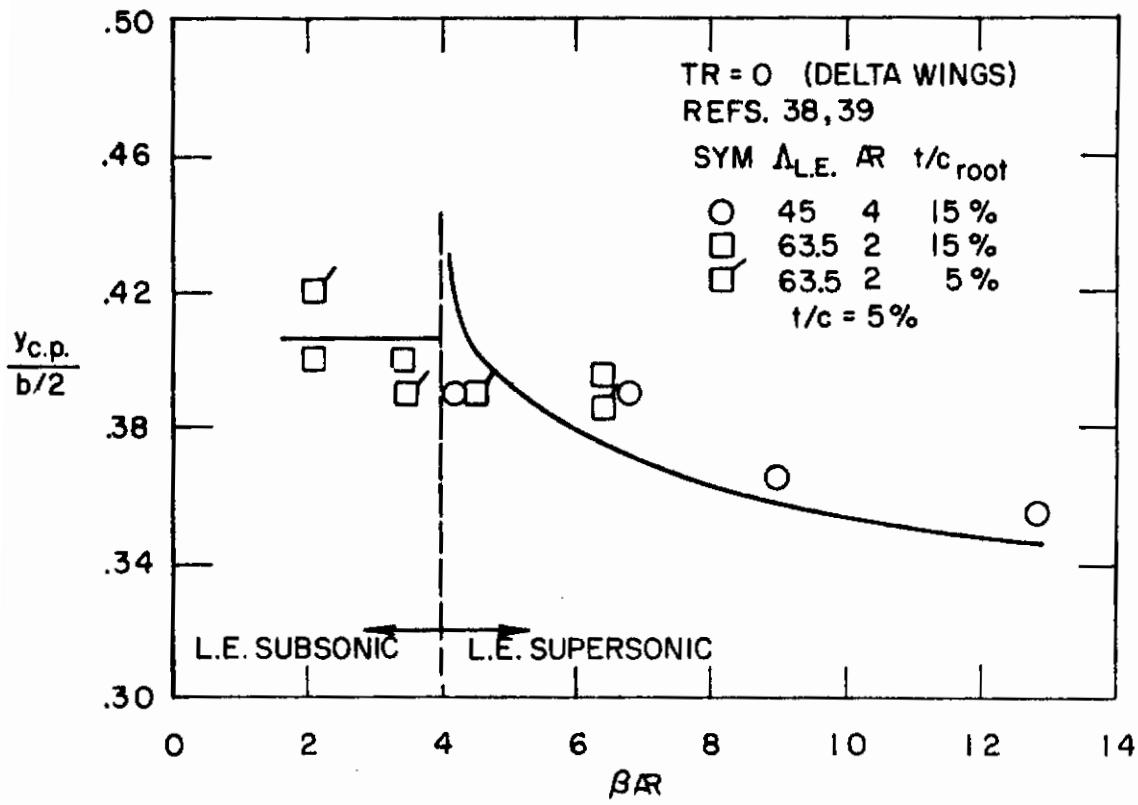

Figure 41. Spanwise center of pressure for delta wings at supersonic speeds. Comparison with linear theory

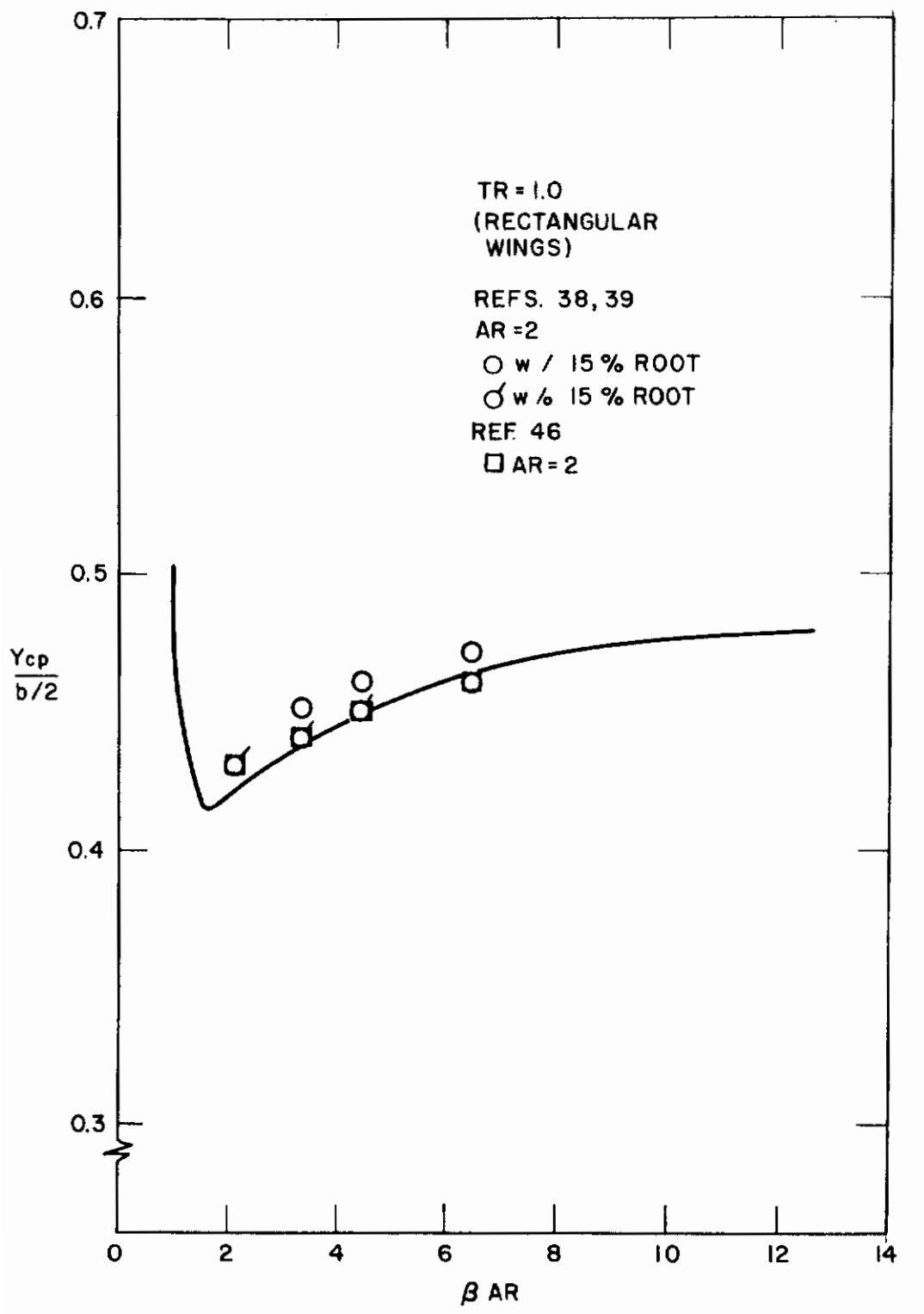

Figure 42. Spanwise center of pressure for rectangular wings at supersonic speeds. Comparison with linear theory

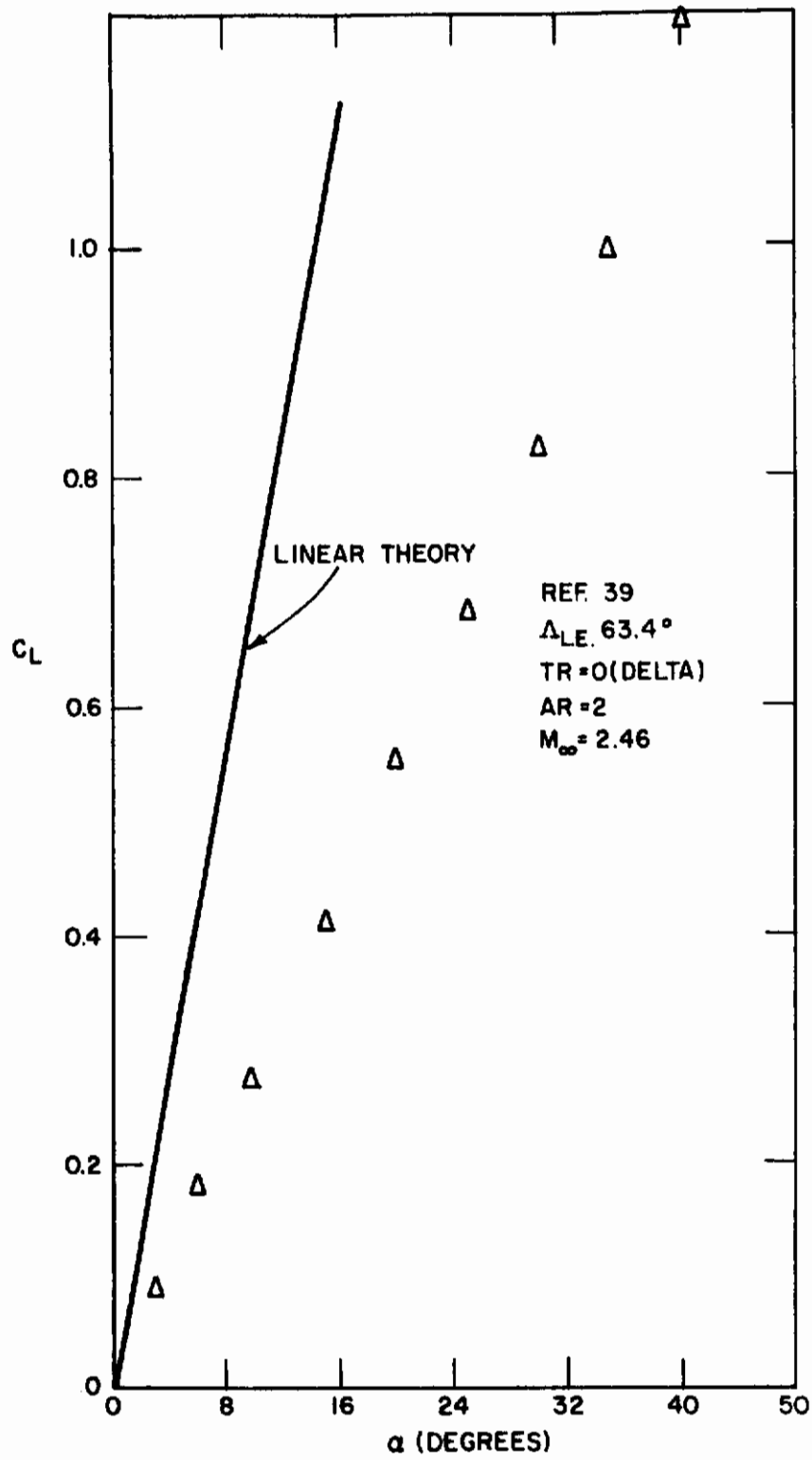

Figure 43. Lift curve for delta wing at M_∞ = 2.46. Comparison with linear theory

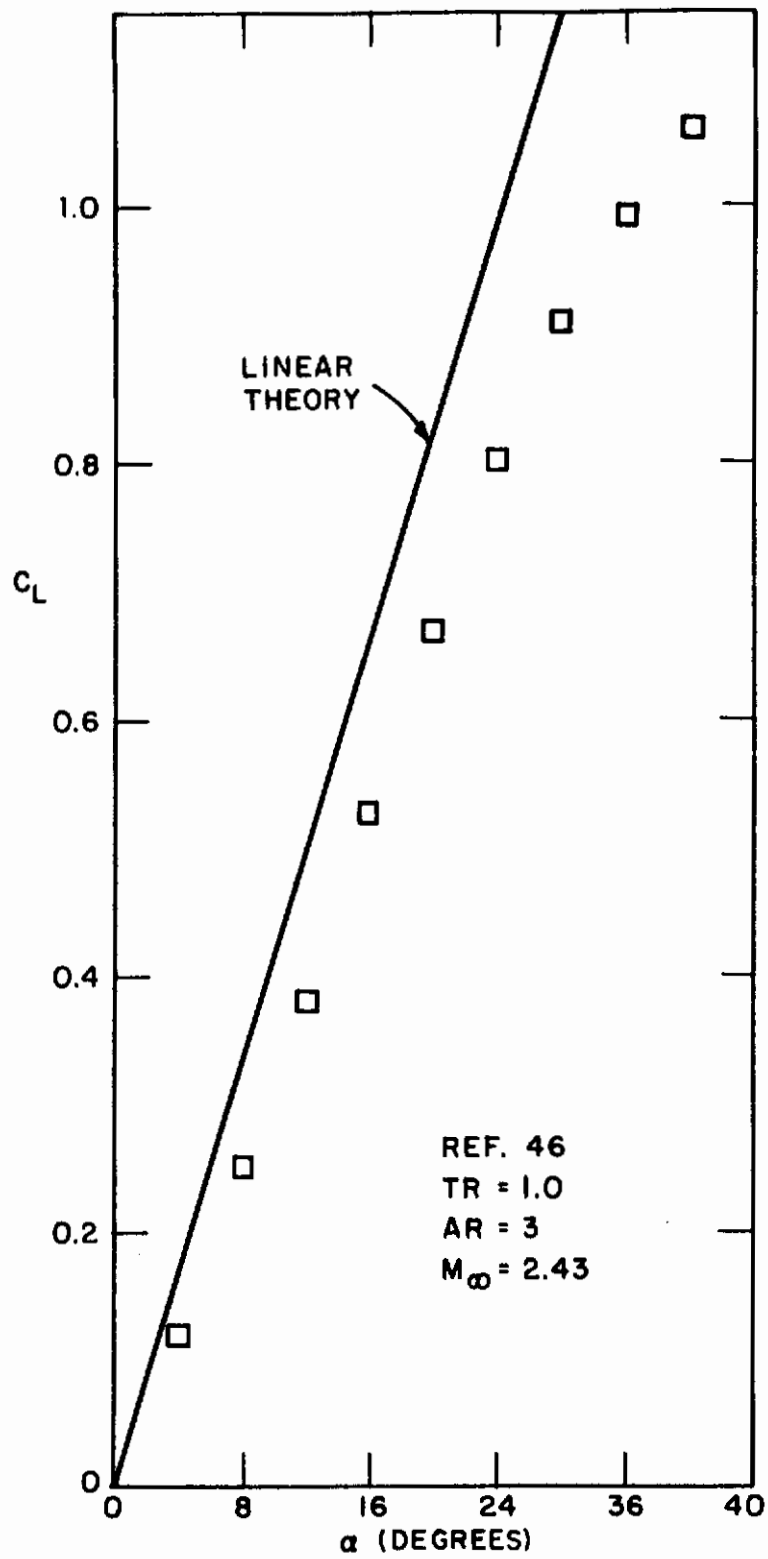

Figure 44. Lift curve for rectangular wing at $M_\infty = 2.43$. Comparison with linear theory

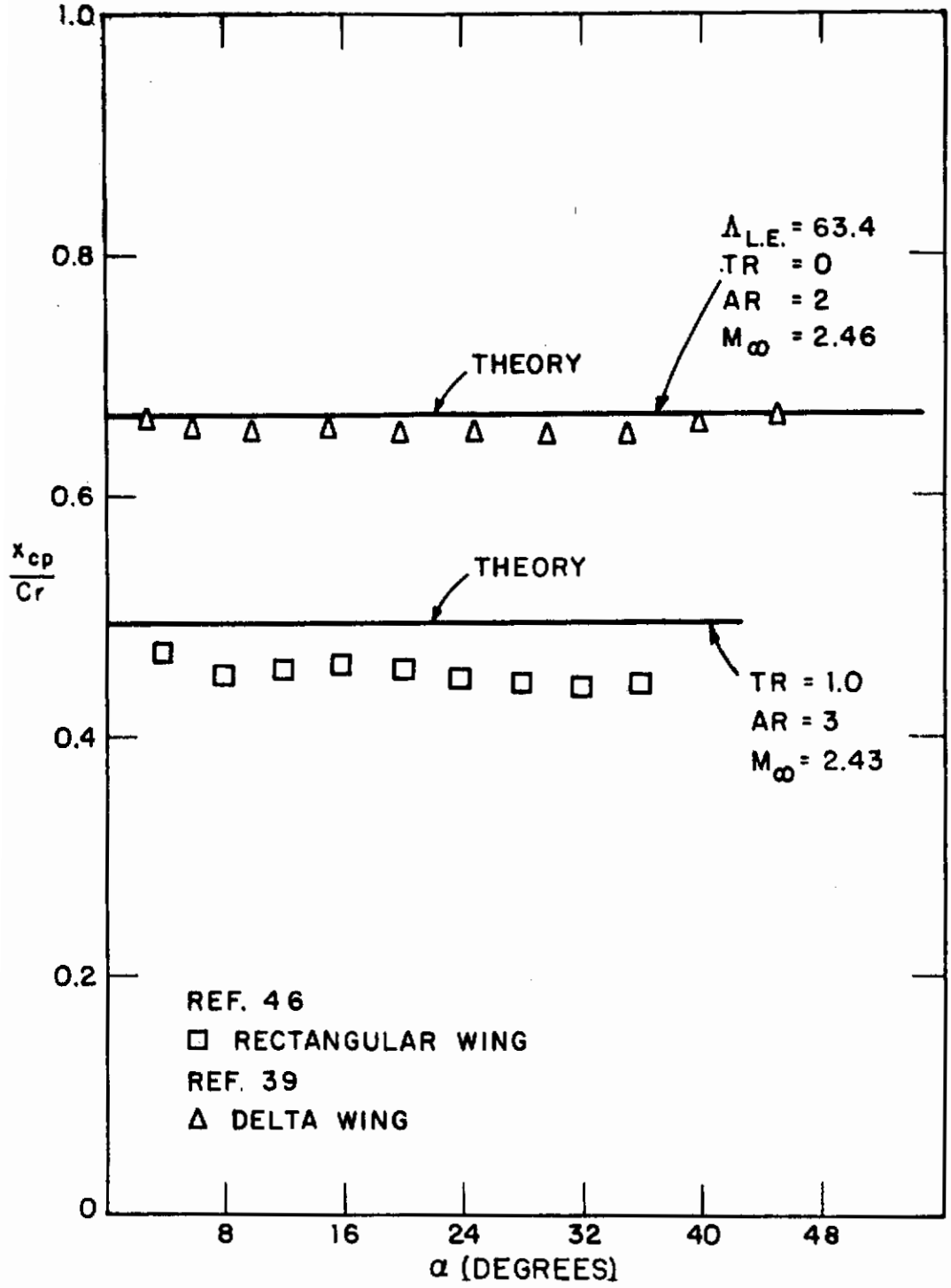

Figure 45. Streamwise centers of pressure for delta and rectangular wings at supersonic speed. Comparison with linear theory

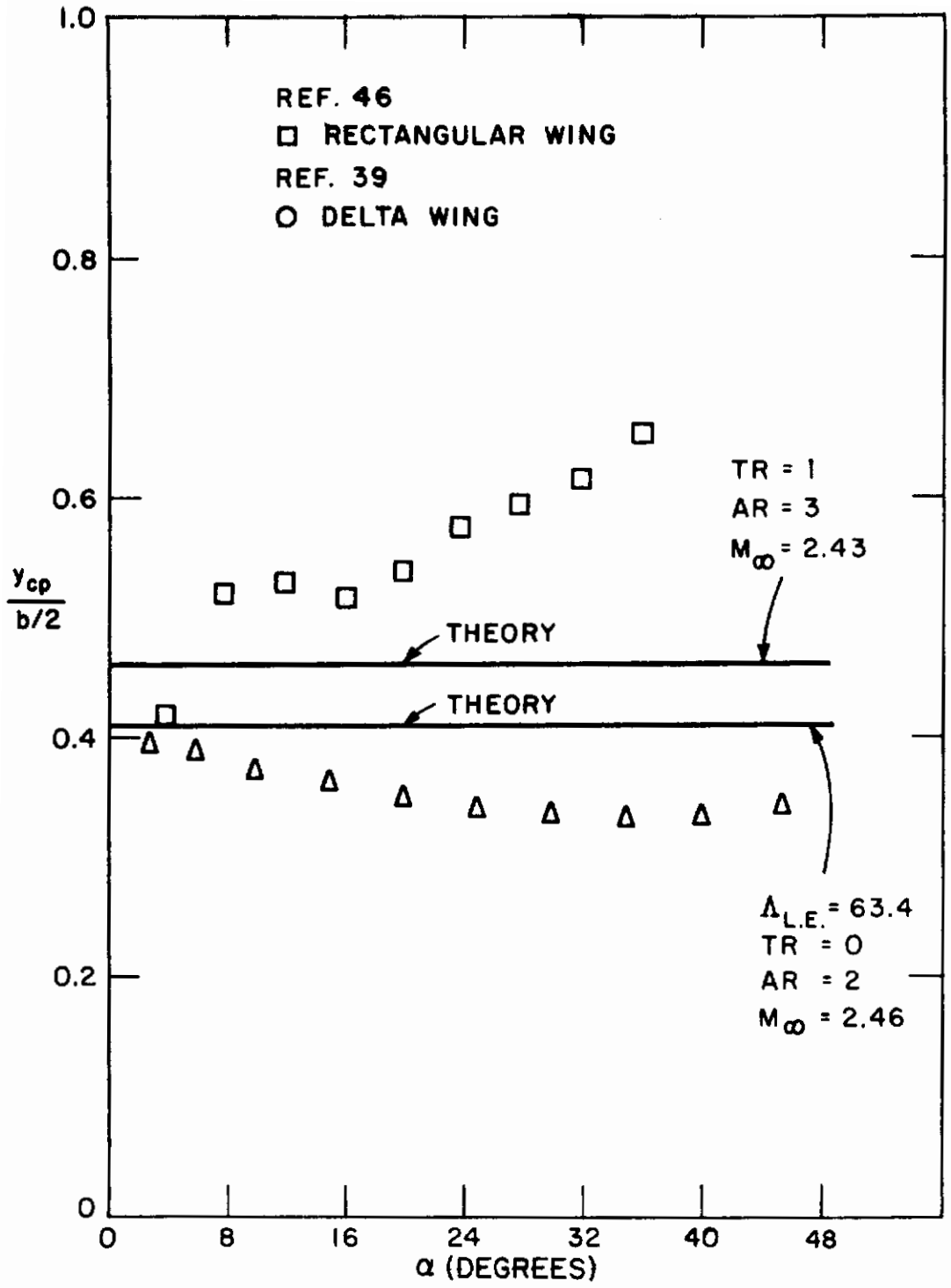

Figure 46. Spanwise centers of pressure for delta and rectangular wings at supersonic speed. Comparison with linear theory

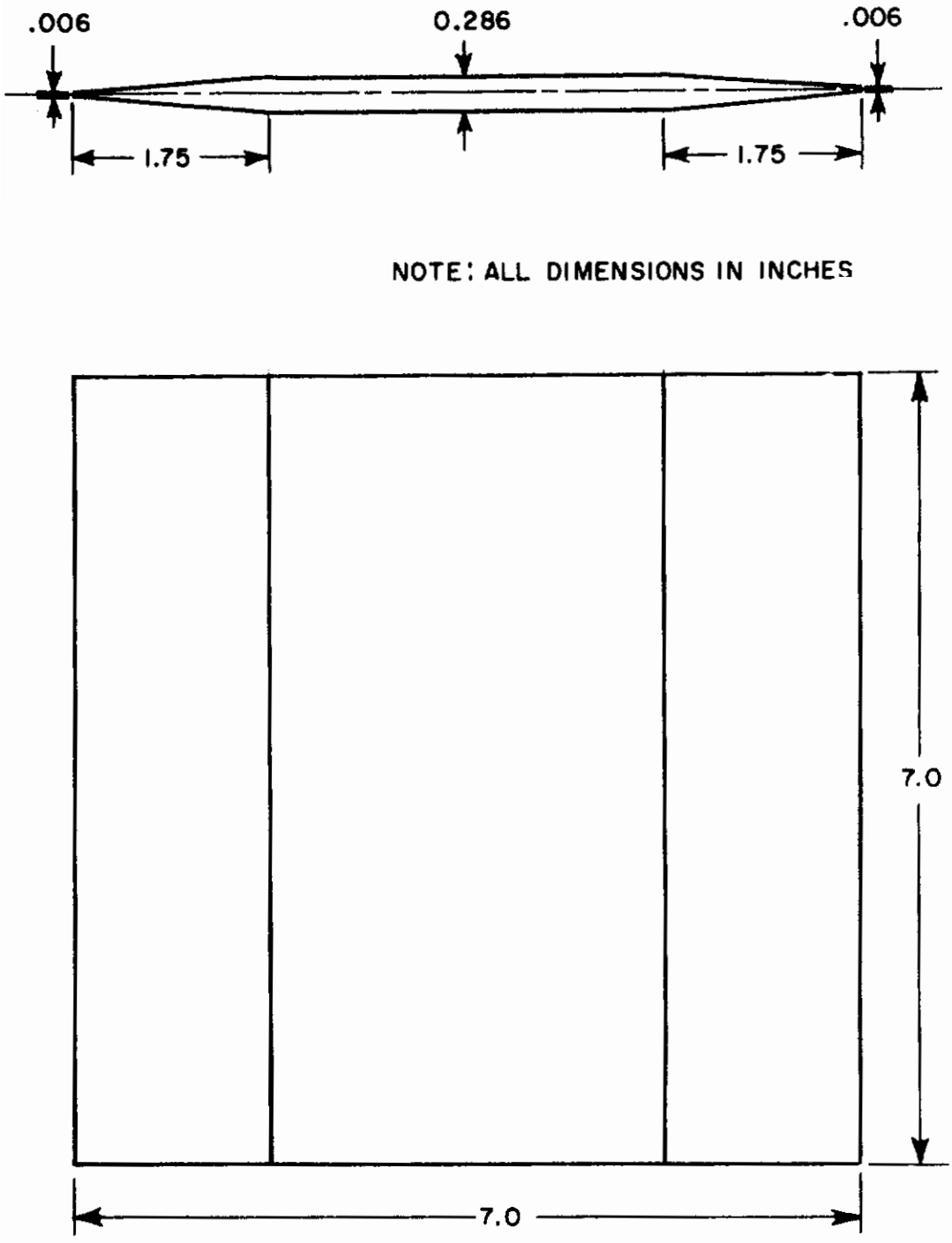

Figure 47. Dimensions of reflection--plane - mounted flat rectangular wing model

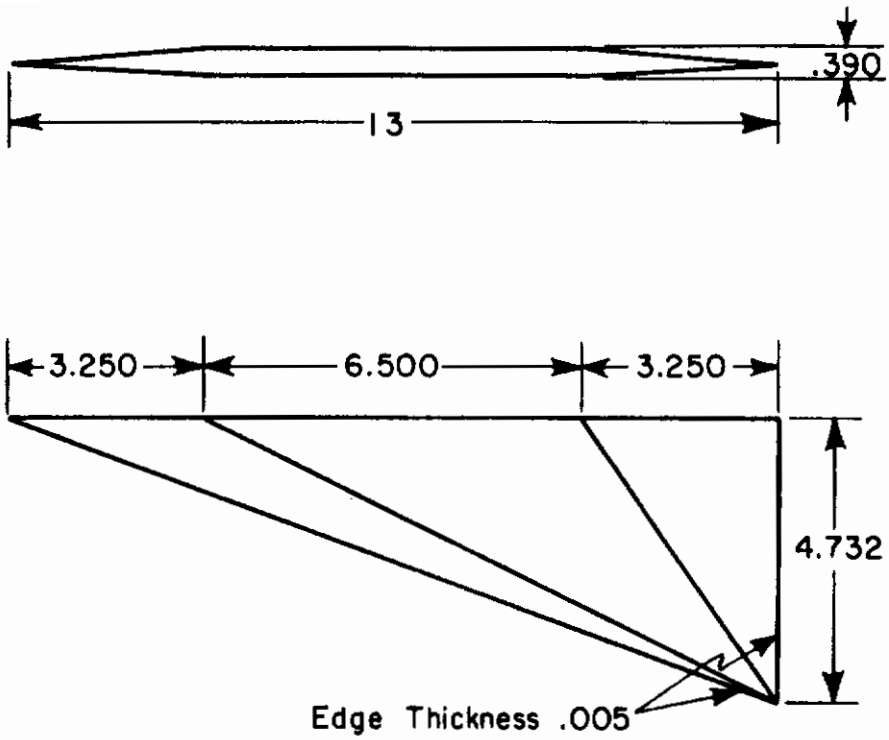

NOTE: ALL DIMENSIONS IN INCHES

Figure 48. Dimensions of reflection-plane-mounted flat triangular wing model

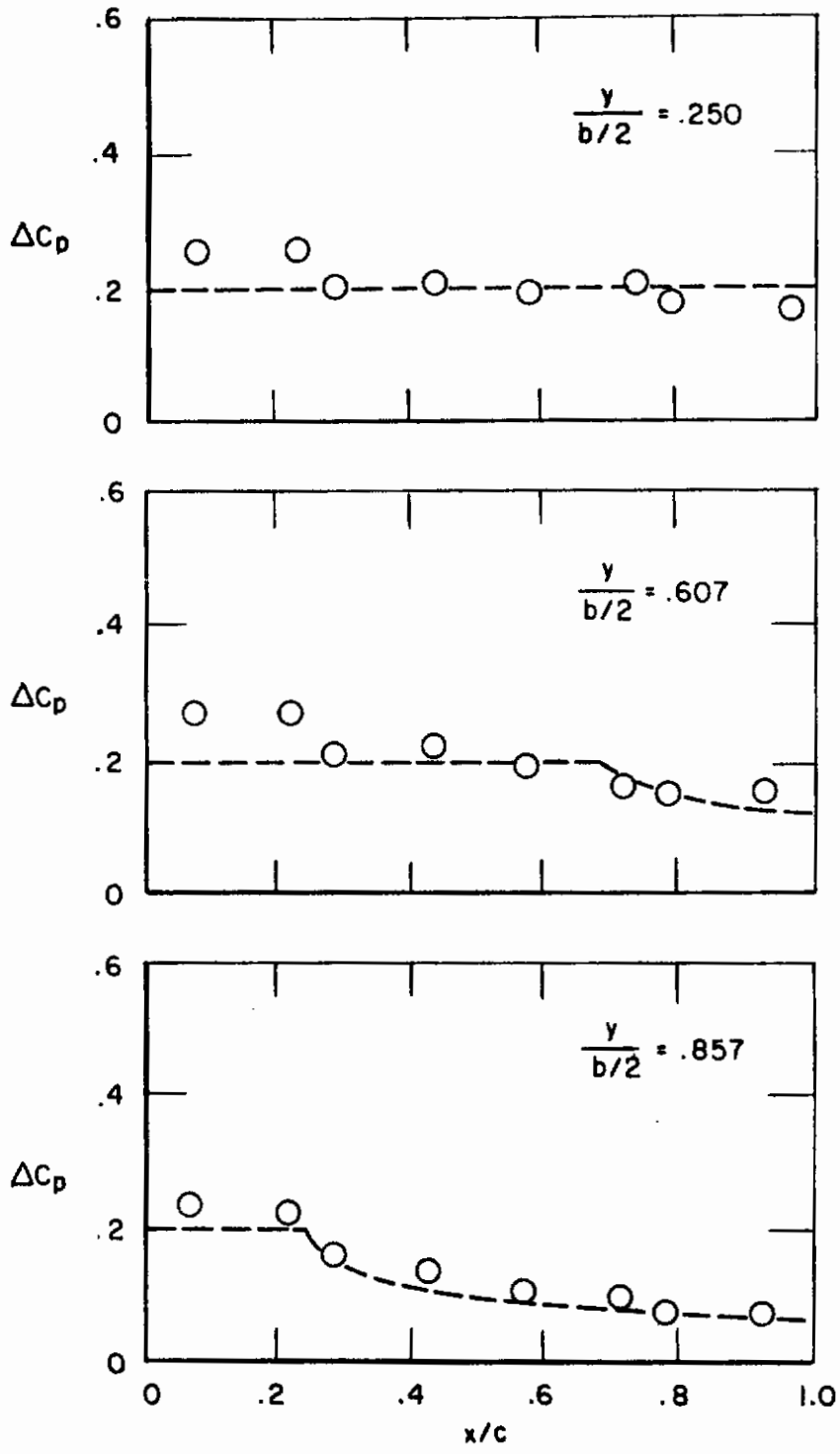

Figure 49. Comparison of theoretical and experimental lift distributions on flat rectangular wing at $M_\infty = 2$, $\alpha = 5°$

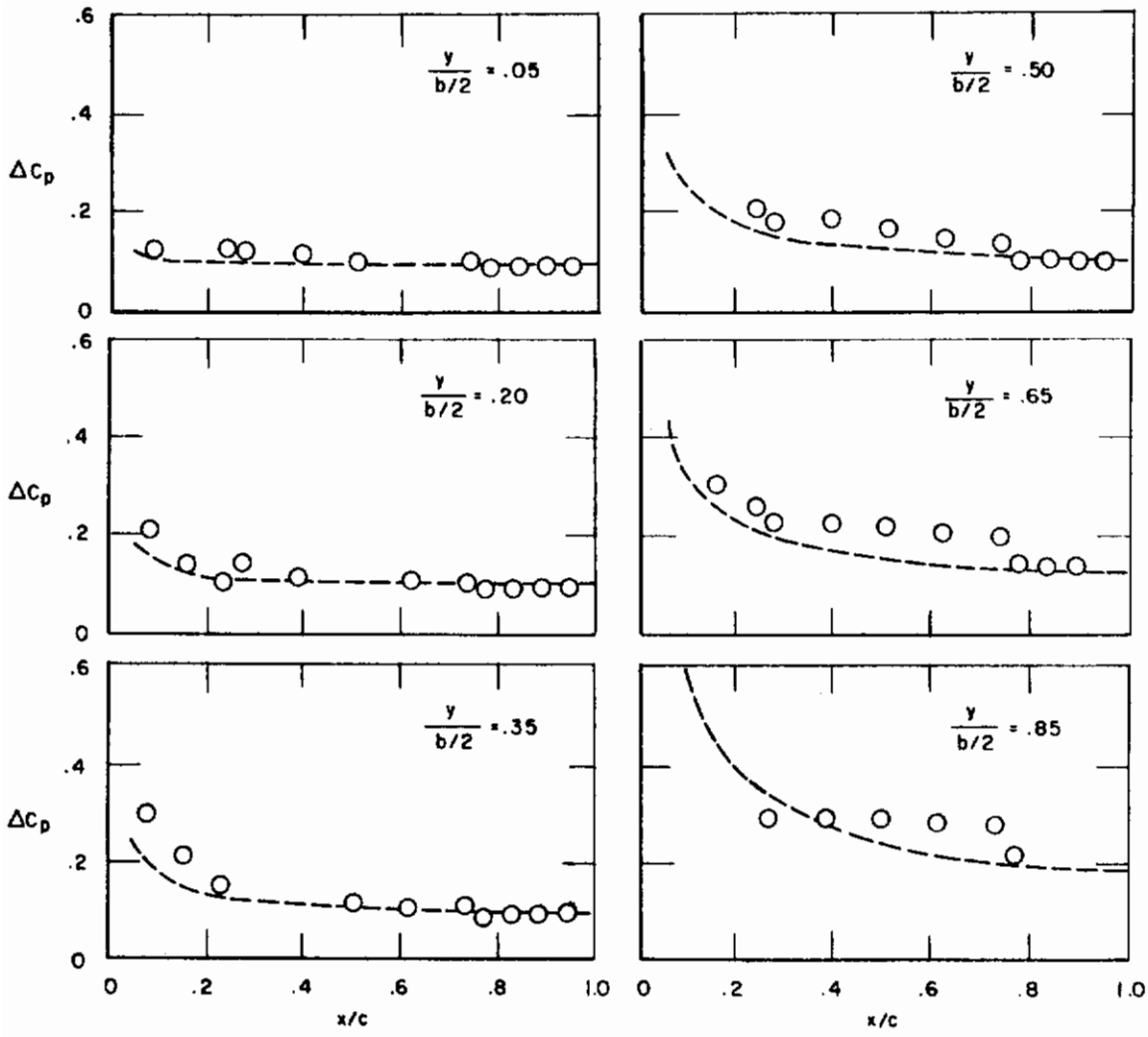

Figure 50. Comparison of theoretical and experimental lift distributions on flat triangular wing at $M_\infty = 2$, $\alpha = 5°$

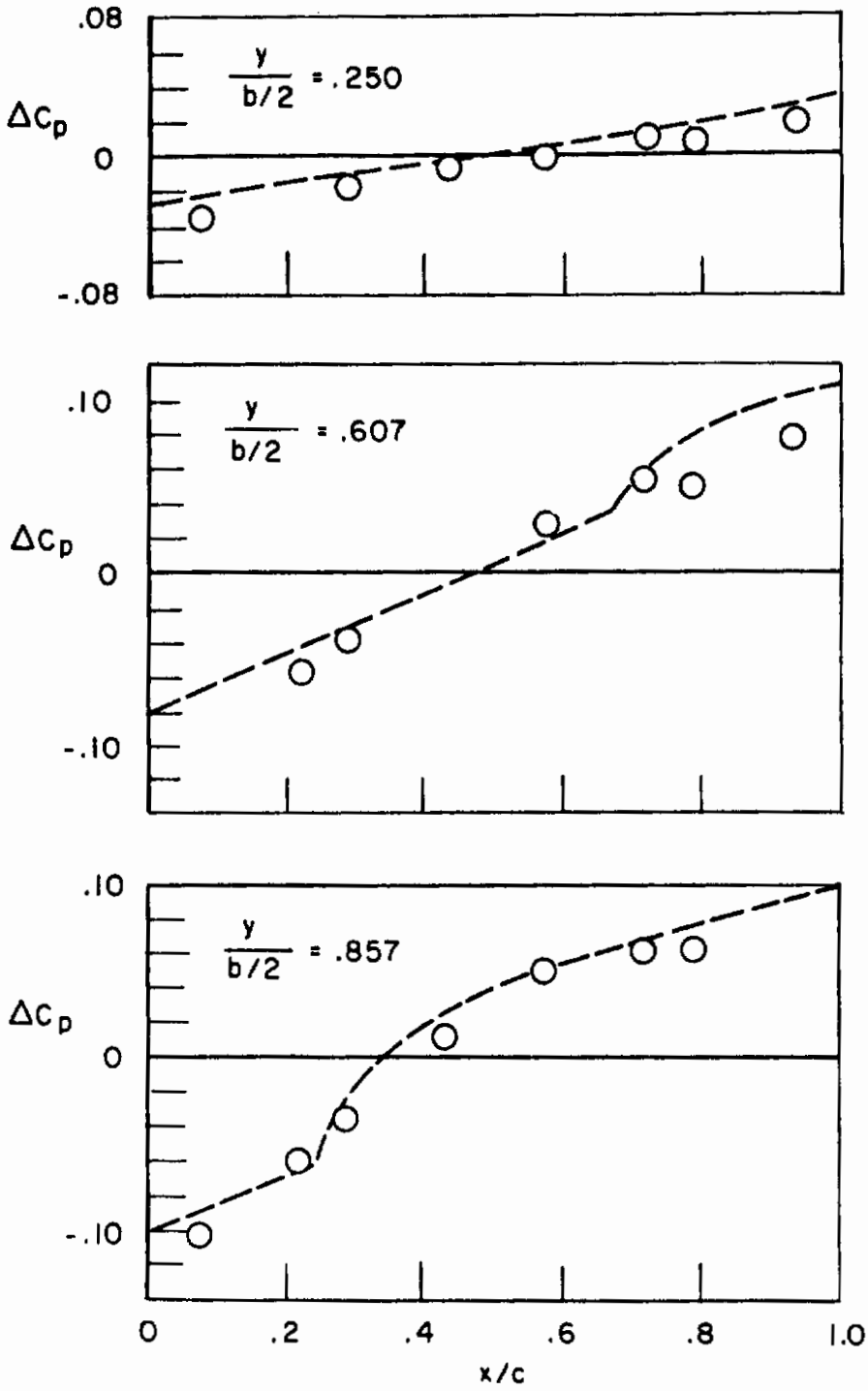

Figure 51. Theoretical and experimental lift distributions on cambered rectangular wing at $M_\infty = 2.0$

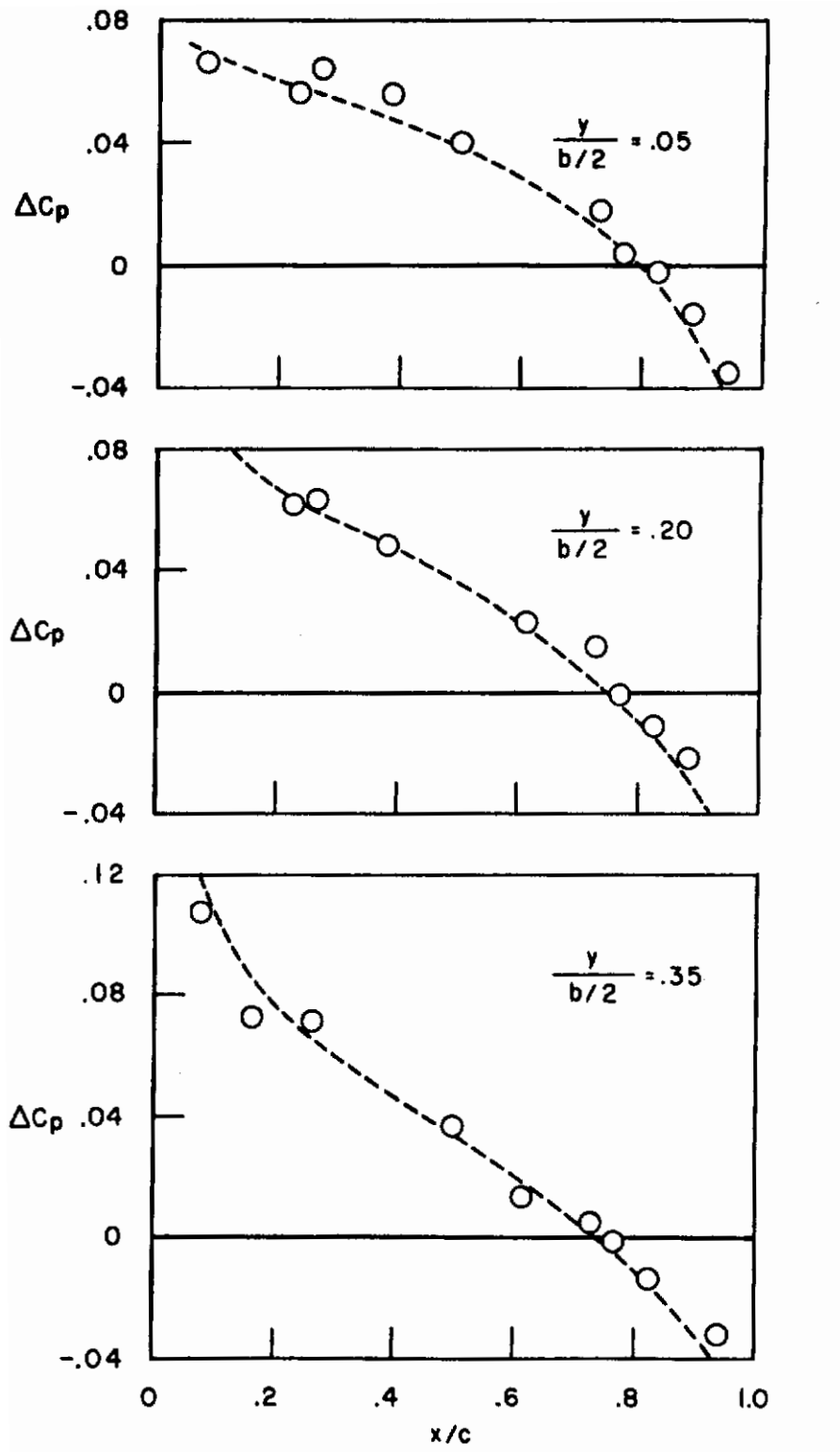

Figure 52. Theoretical and experimental lift distributions on cambered delta wing at $Mach_{\infty} = 2.0$

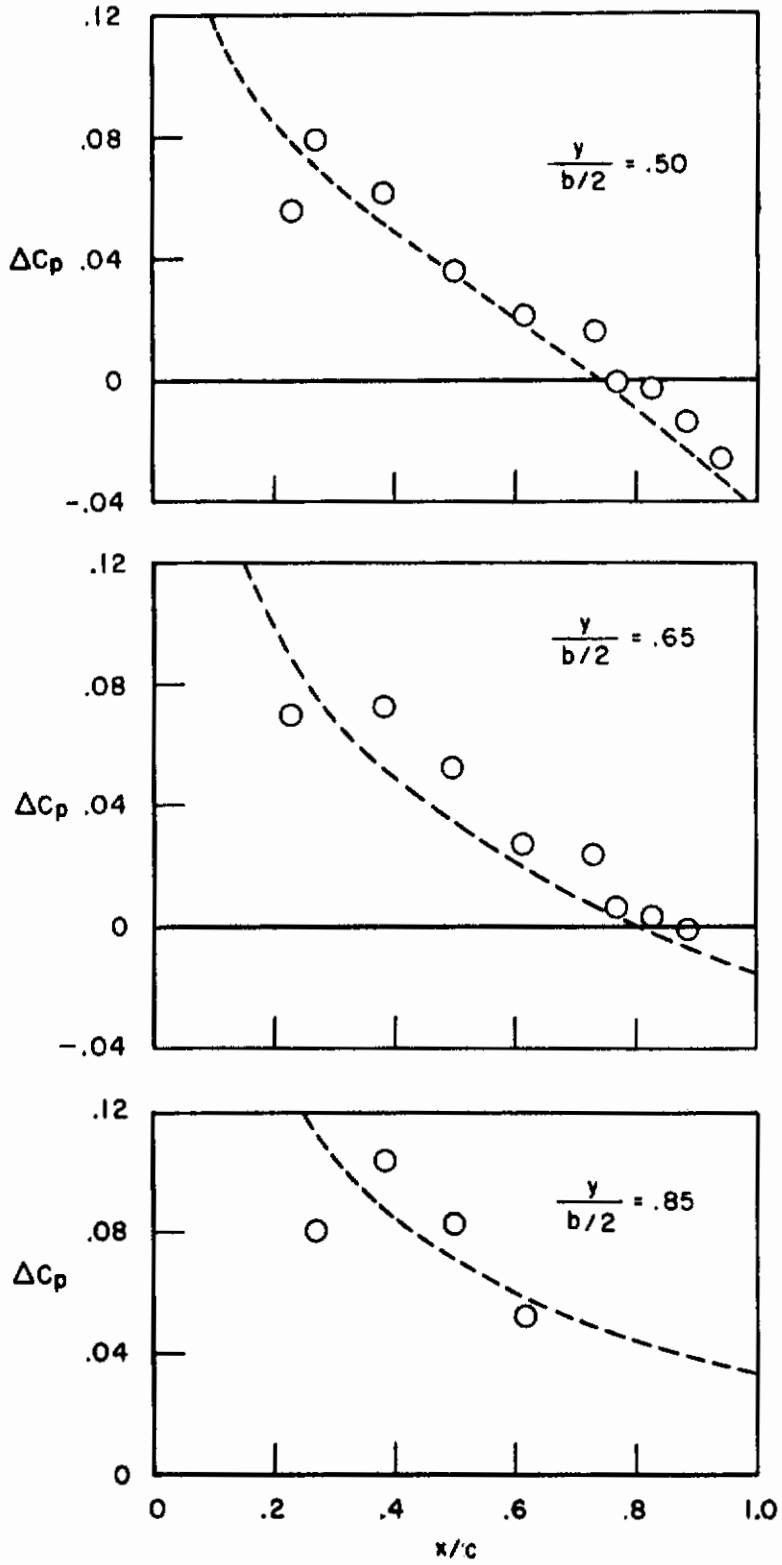

Figure 52 (Continued)

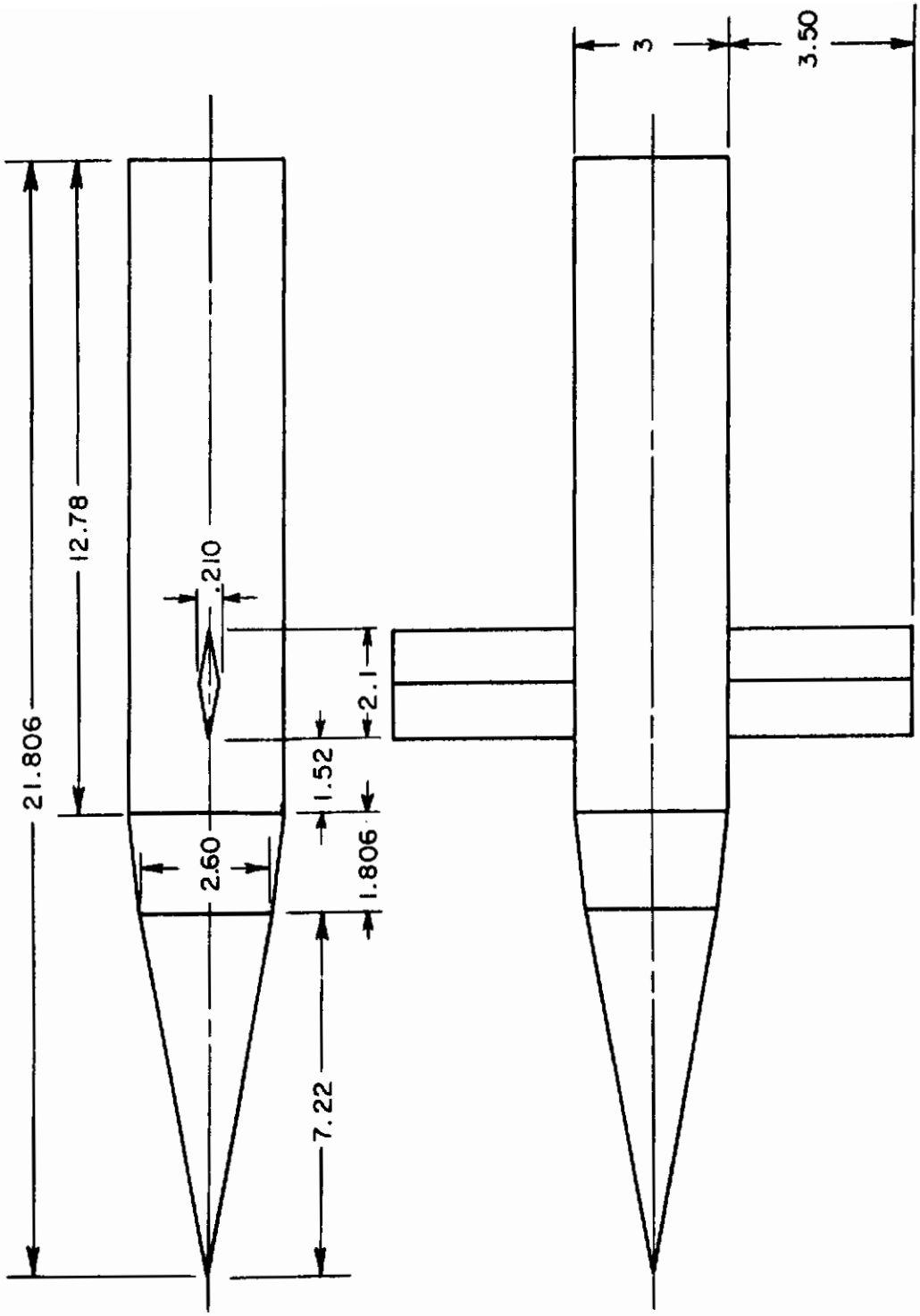

Figure 53. Wing-body pressure model (Ref. 54)

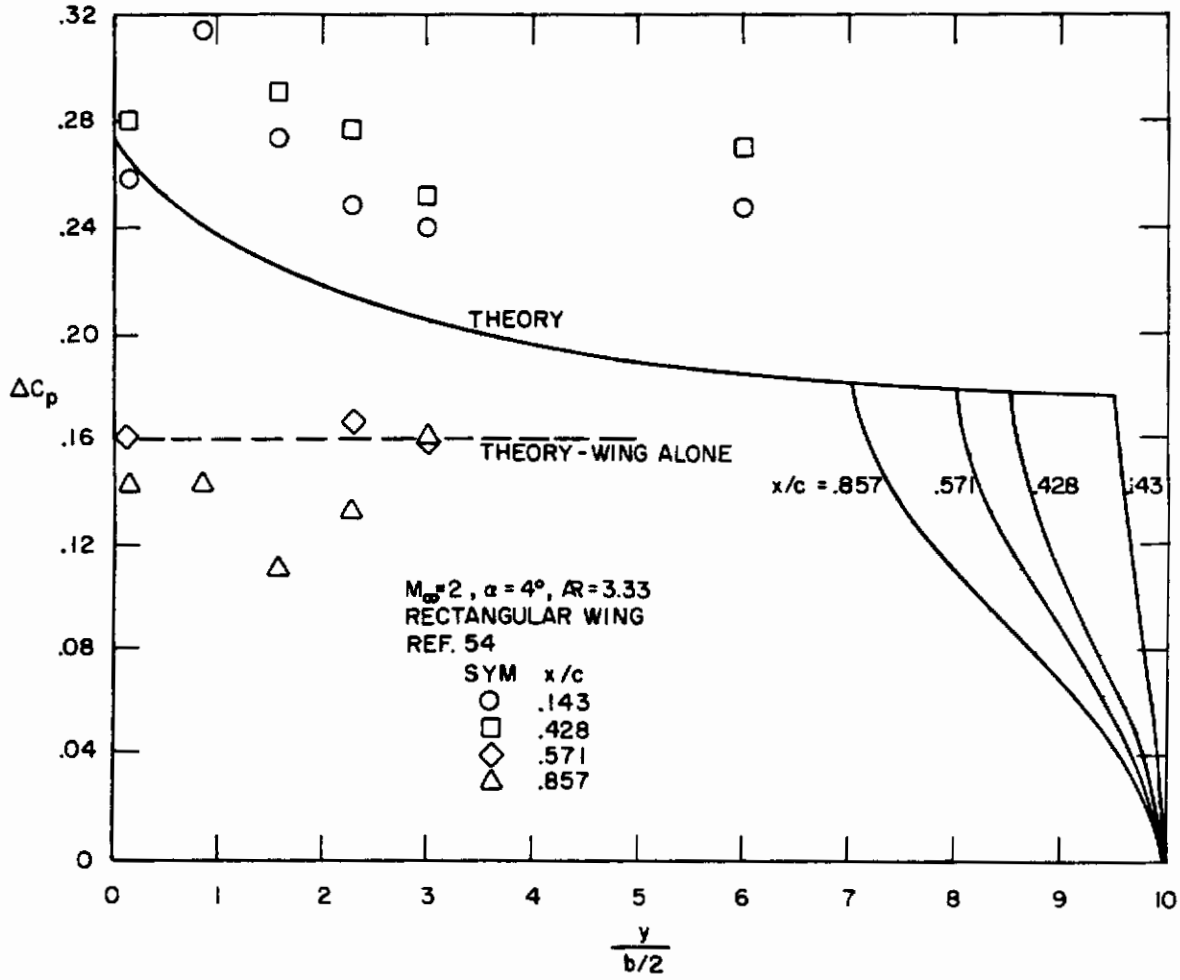

Figure 54. Comparison of theoretical and experimental pressure on rectangular wing in presence of circular body at $\alpha = 4°$, $M_\infty = 2.0$

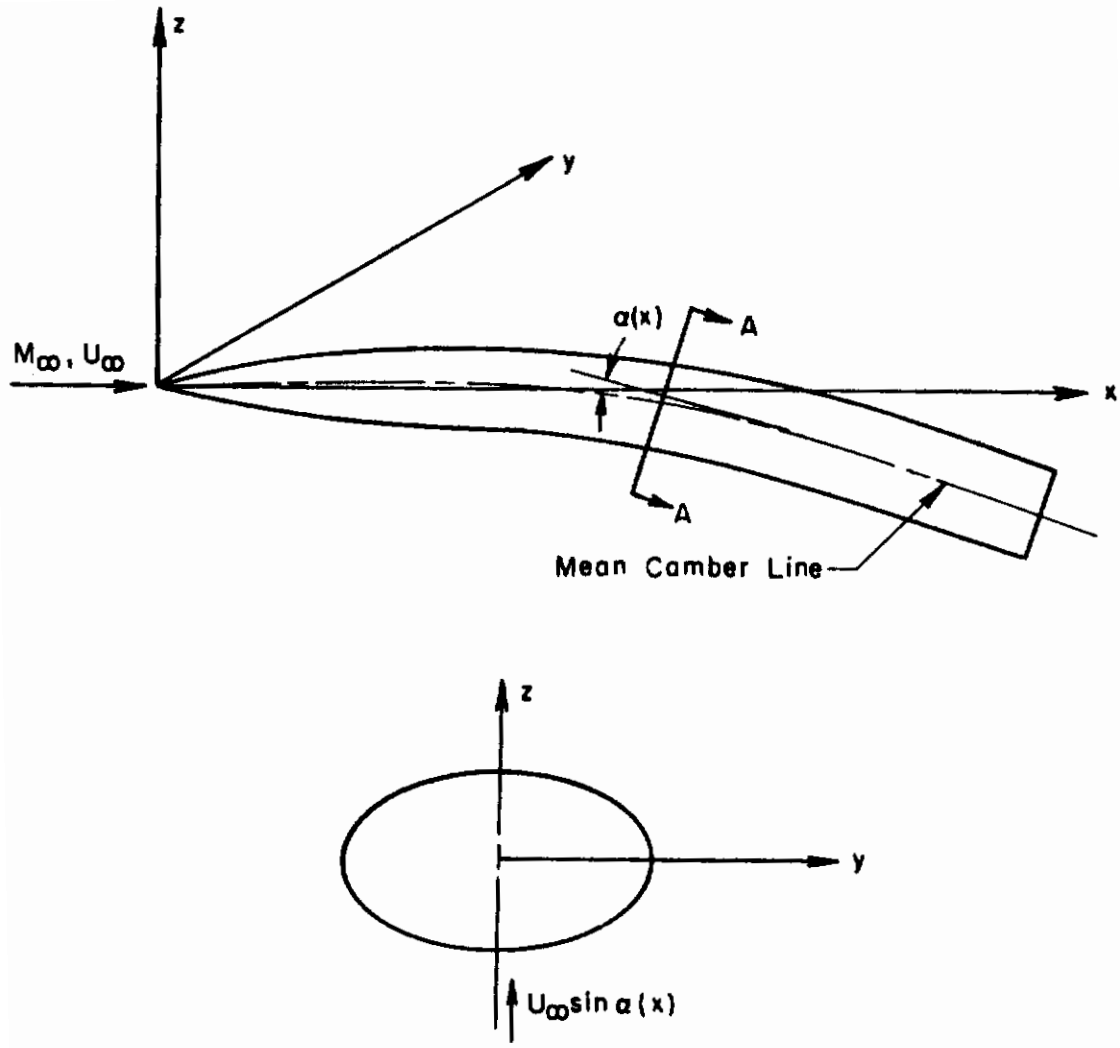

Figure 55. Body geometry

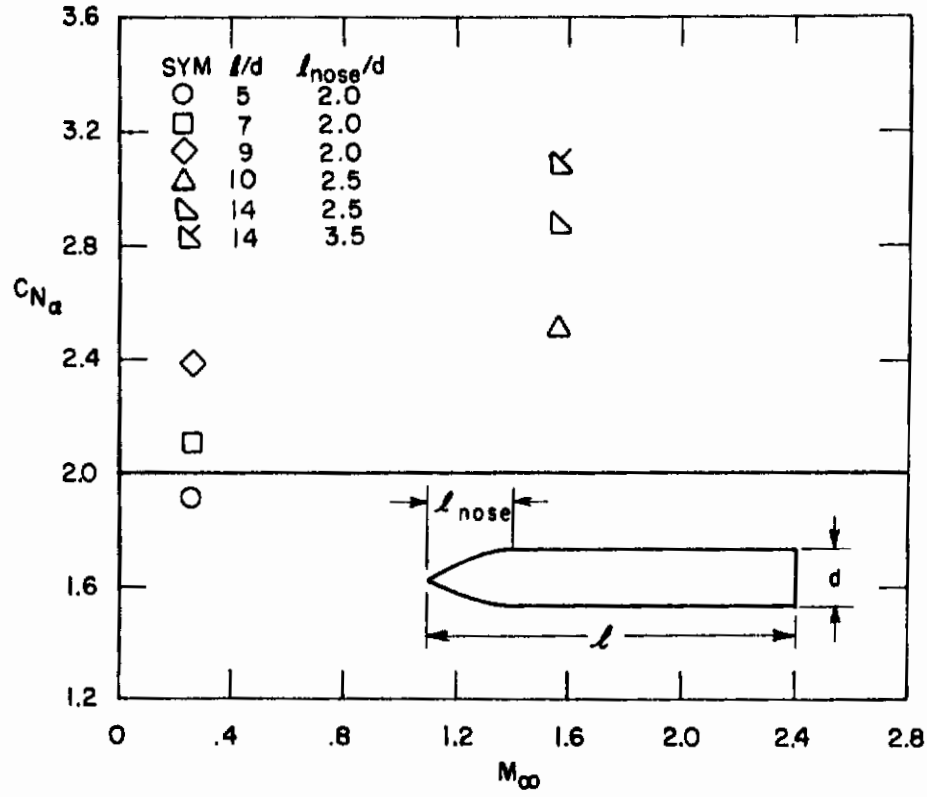

Figure 56. Lift curve slopes of various bodies of revolution. Comparison with slender body theory

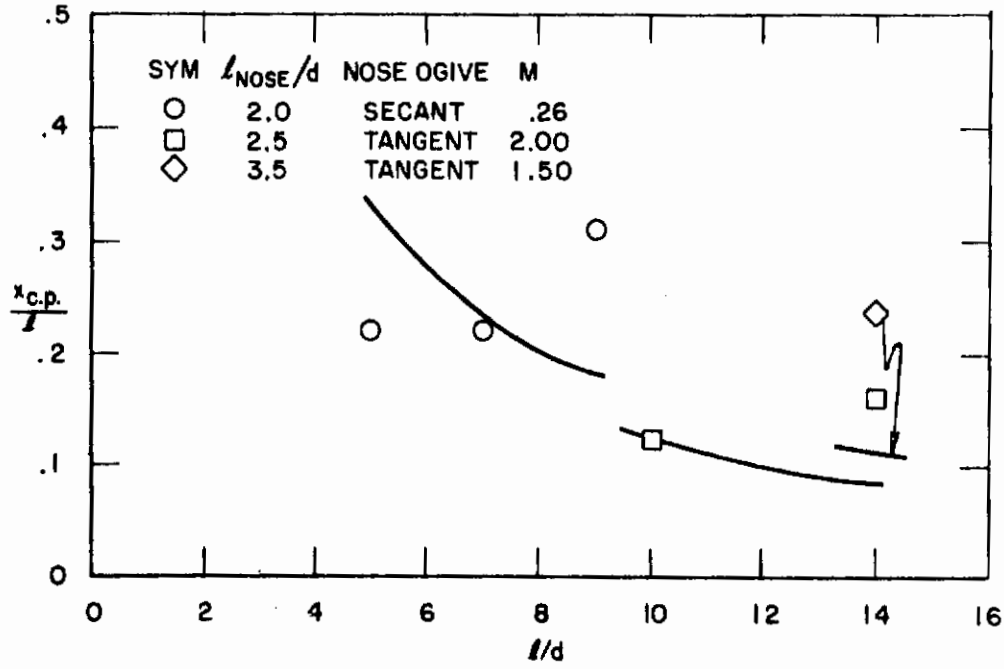

Figure 57. Center of pressure of bodies of revolution. Comparison with slender body theory

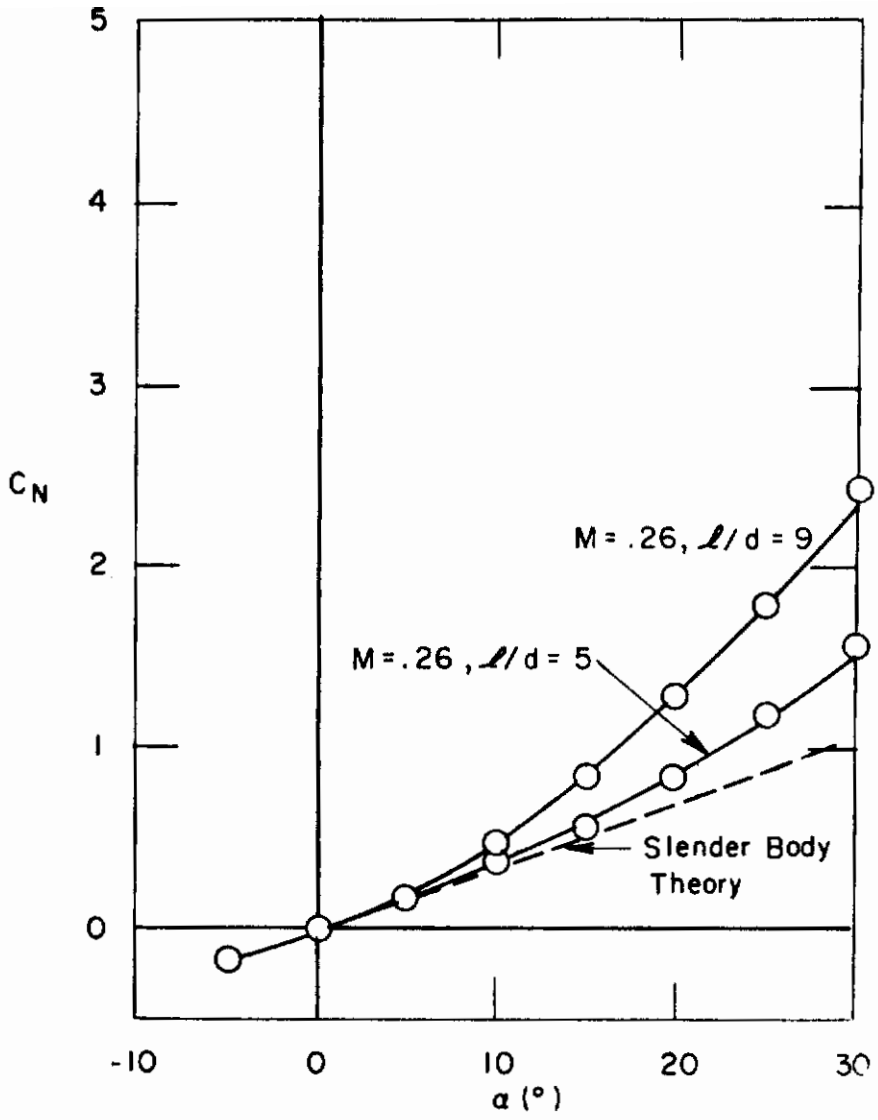

Figure 58. Variation of normal force coefficient with angle of attack for two ogive-cylinder bodies

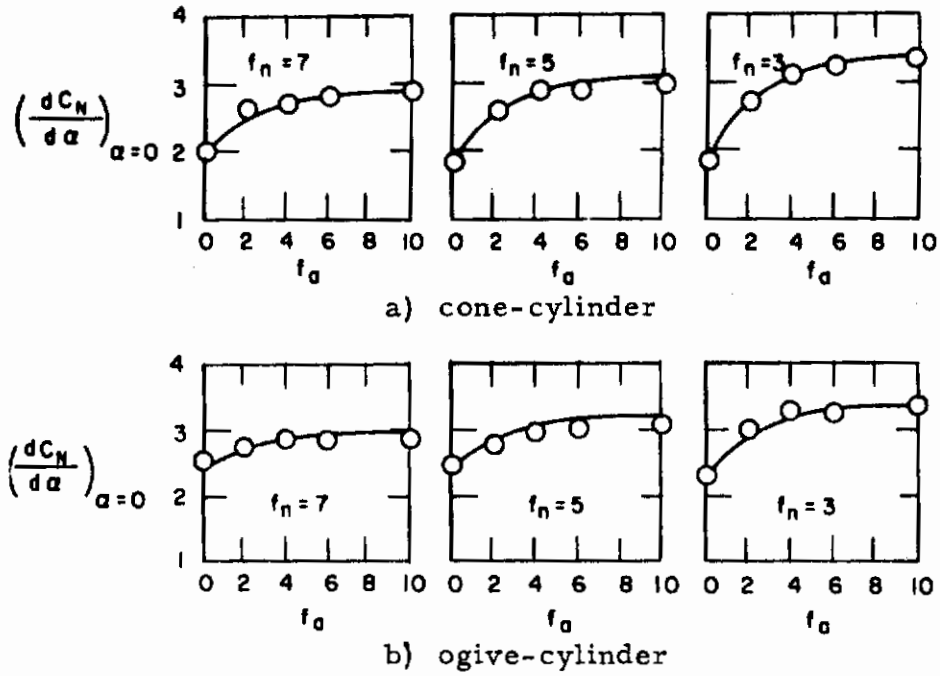

Figure 59. Initial lift curve slopes for cone-cylinder and ogive-cylinder bodies at $M_\infty = 3.0$. Comparison of theory and experiment for various values of nose fineness ratio, f_n, and afterbody fineness ratio, f_a.

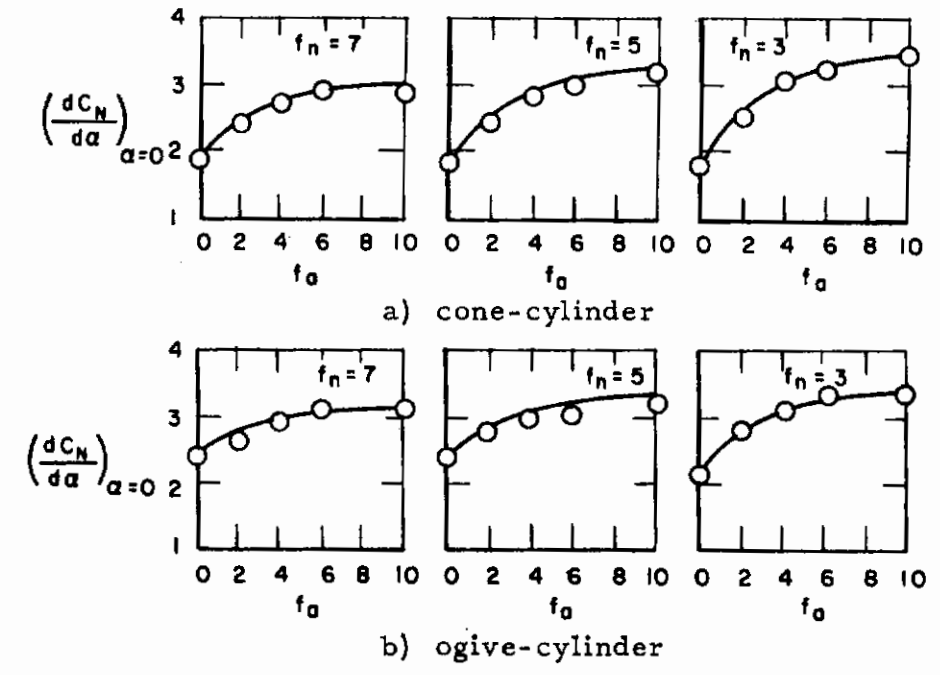

Figure 60. Initial lift curve slopes for cone-cylinder and ogive-cylinder bodies at $M_\infty = 4.24$. Comparison of theory and experiment for various values of nose fineness ratio, f_n, and afterbody fineness ratio, f_a.

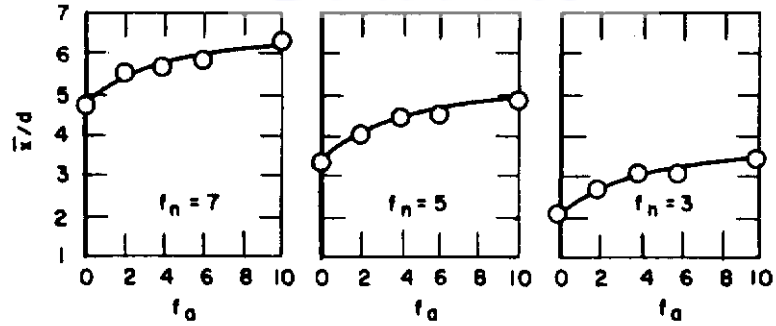

a) cone-cylinder

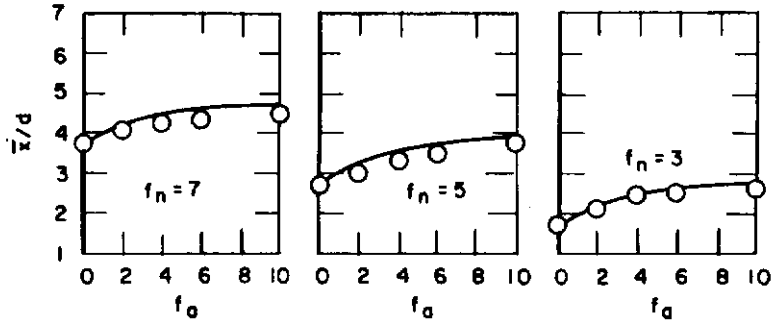

b) ogive-cylinder

Figure 61. Center of pressure at $\alpha = 0$ fore cone-cylinder and ogive-cylinder bodies at $M_\infty = 3.0$. Comparison of theory and experiment for various values of nose fineness ratio, f_n, and afterbody fineness ratio, f_a.

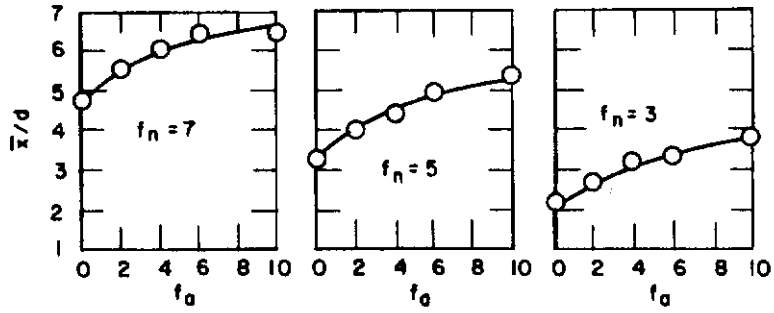

a) cone-cylinder

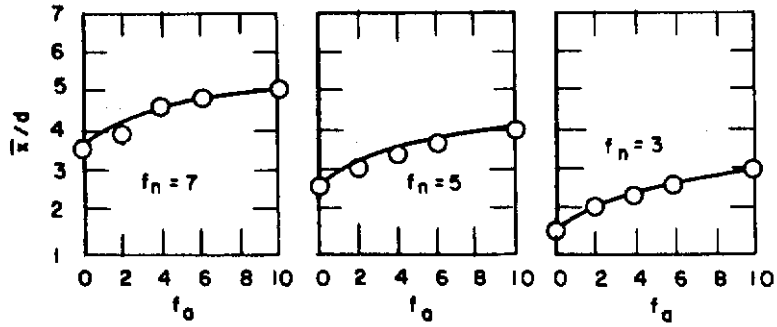

b) ogive-cylinder

Figure 62. Center of pressure at $\alpha = 0$ fore cone-cylinder and ogive-cylinder bodies at $M_\infty = 4.24$. Comparison of theory and experiment for various values of nose fineness ratio, f_n, and afterbody fineness ratio, f_a.

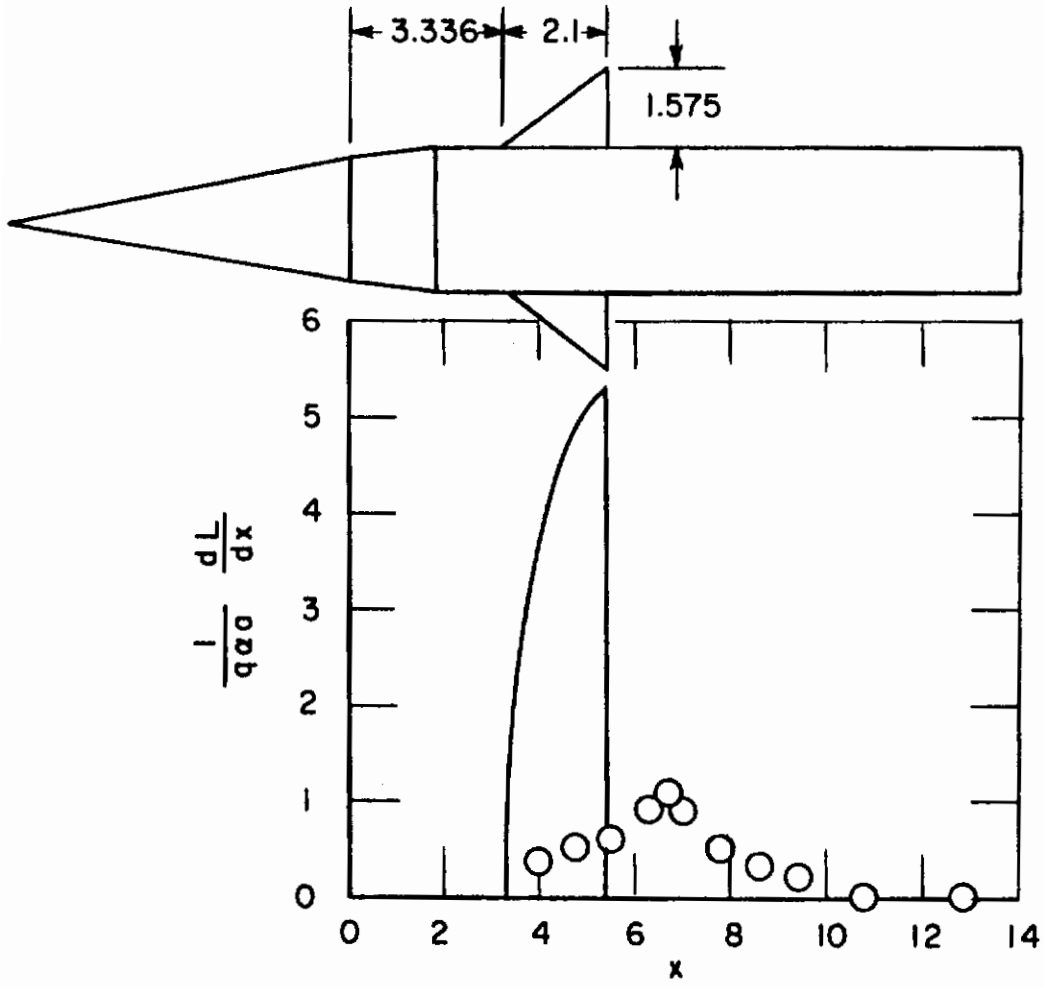

Figure 63. Comparison of theoretical and experimental lift on body due to wing carry-over interference at $M_\infty = 2.0$

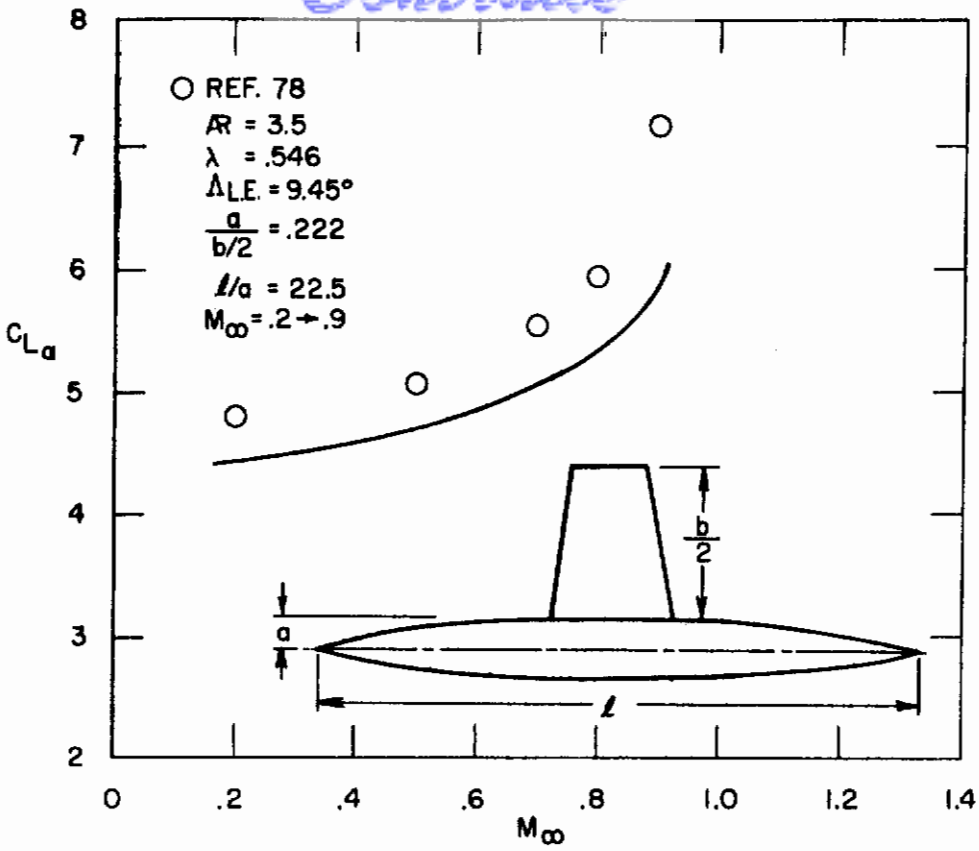

Figure 64. Lift curve slope for wing-body combination at subsonic speeds. Comparison with theory

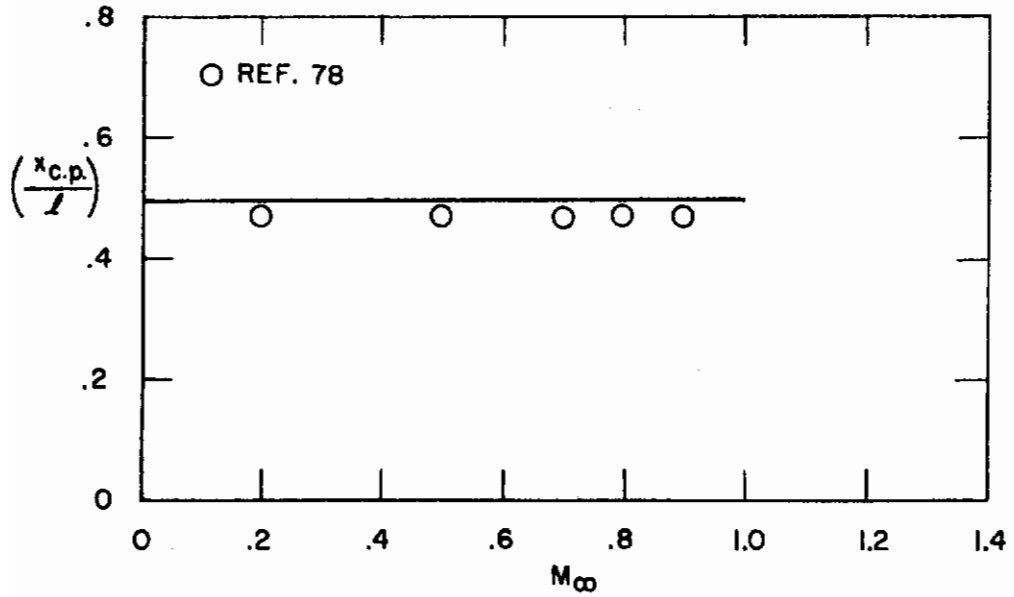

Figure 65. Center of pressure for wing-body combination at subsonic speeds. Comparison with theory

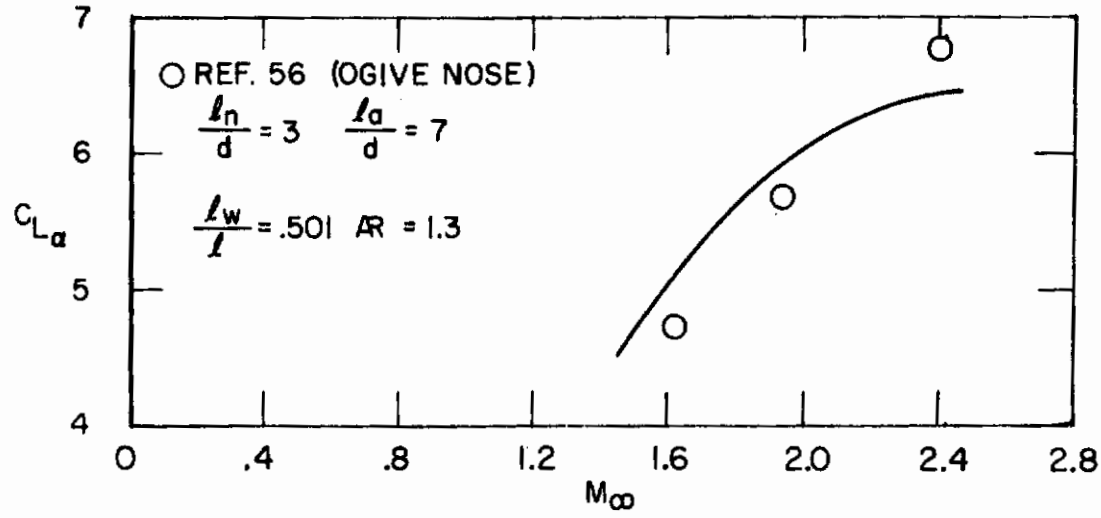

Figure 66. Lift curve slope for wing-body combination at supersonic speeds. Comparison with theory

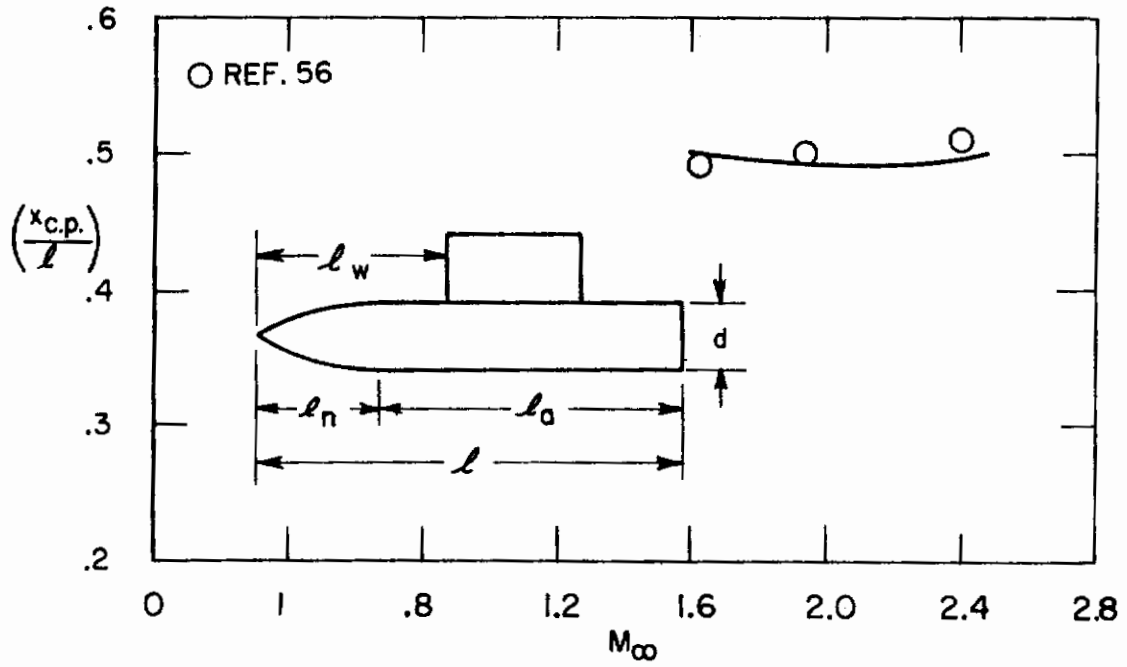

Figure 67. Center of pressure for wing-body combination at supersonic speeds. Comparison with theory

APPENDIX A

(By Christopher J. Borland)

"WEISSINGER'S PROCEDURE" AS PROGRAMMED FOR THE IBM 709/7094 IN FORTRAN II

1. DESCRIPTION OF PROGRAM

a. SUBSONIC LOAD DISTRIBUTIONS

This executive program receives the geometrical parameters (sweep angle, aspect ratio, taper ratio, angle of attack, and spanwise twist distribution) as input data, controls the calculation of the spanwise loading, and prints the total lift coefficient, lift curve slope, root bending moment curve slope, spanwise center of pressure, section lift coefficient, spanwise loading parameter, chordwise center of pressure, and spanwise angle of attack distribution as output data.

b. WEISS

This subroutine calculates the locations of the spanwise stations, and sets up Eq. (IV-52) for solution.

Eq. (IV-52) may be written as

$$\alpha_\nu = \sum_{n=1}^{m+1/2} a_{\nu n} G_n$$

where

$$a_{\nu n} = 2b_{\nu\nu} + \frac{b}{c_\nu}\bar{g}_{\nu\nu} \qquad \text{for} \qquad n = \nu$$

$$-2B_{\nu n} + \frac{b}{c_\nu}\bar{g}_{\nu n} \qquad \text{for} \qquad n \neq \nu$$

or, in matrix notation,

$$[\alpha] = [a]\ [G] \ .$$

c. AMAT

This subroutine generates the elements a_{ij} of the square matrix.

d. B

This FORTRAN Function generates the value of $b_{\nu n}$ for use in AMAT, from Eq. (IV-52).

e. GBAR

This FORTRAN Function generates the value of $\bar{g}_{\nu n}$ for use in AMAT, from Eq. (IV-52).

f. FBAR

This FORTRAN Function generates the value of $\bar{f}_{n\mu}$ for use in GBAR, from Eq. (IV-53).

g. ELSTAR

This FORTRAN Function generates the value of $L^*_{\nu\mu}$ for use in GBAR, where

$L^*_{\nu\mu} = L_{\nu\mu} - L_{\nu\ M+1-\mu}$, given by Eq. (IV-55).

h. MATINV

This subroutine solves the matrix equation set up by WEISS. It is an IBM SHARE routine, No. 664.

i. Library and Machine Requirements

The program may be used with any IBM 709, 7090, or 7094 32K system with a standard FORTRAN II compiler, and a library tape including

SINF, COSF, ATANF, ASINF, ACOSF, SQRTF, and Input/Output routines. The LIST8, LABEL, and SYMBOL TABLE cards shown in the listings are for use with FMS, the FORTRAN Monitor system, and may be replaced by appropriate system control cards.

2. INSTRUCTIONS FOR USE

a. Definition of Input Variables

M	Number of control points on the span.
M1	Number of intervals in the numerical integration.
ALAM	Sweep angle of the quarter-chord line, in degrees.
AR	Aspect Ratio
TR	Taper Ratio
ALPH	Root chord angle of attack, in radians.
ITW	Program input key: = 1 for twisted and/or cambered wing. = 0 for flat wing.
ALPHTW	Section angle of twist in radians.

b. Order of Data Deck

	Columns	Variable
Card 1		
	1 - 5	M
	6 - 10	M1
Card 2		
	1 - 10	ALAM
	11 - 20	AR
	21 - 30	TR
	31 - 40	ALPH
	50	ITW
Card 3, 4, 5, . . etc.		
	1 - 10	ALPHTW

c. Data Values

Both M and M1 must be odd, and they must be different. The values 15 and 25 have been used, respectively, with success. With these values, approximately 1.08 minutes of computation time on the IBM 709 are required to calculate the loading distribution on one wing.

If ITW is given as 1, there must be (M + 1)/2 + 1 cards following Card 2 with the values of the twist angle, ALPHTW, at the (M + 1)/2 + 1 stations on the semi-span, outboard stations first. The stations are located on the semi-span according to a Multhopp distribution,

$$\frac{y_n}{b/2} = \cos\left(\frac{n\pi}{m+1}\right) \quad n = 0, 1, 2 \ldots \frac{m+1}{2}$$

If ITW is given as 0, these cards may be omitted.

The variables M and M1 must be right justified in their fields, and punched without a decimal point. The variables ALAM, AR, TR, ALPH, and ALPHTW must be punched with the decimal point, but need not be right justified. Up to four places after the decimal point are permitted.

If calculations are desired for more than one planform or twist distribution, the data deck may be repeated from Card 2 with the new values.

d. Input and Output Samples

A sample input deck is shown following the listing of the programs. The input values for the three cases tested are as follows:

Case	Λ	AR	TR	α	Twist
1	60°	4	.5	1.0	No
2	30°	1.5	.25	1.0	Yes
3	0°	6	1.0	1.0	No

Note that the twist distribution for Case 2 is given following the geometrical planform parameters.

The output for these cases is also shown. A description of the output follows:

Line 1: Values of AR, TR, Λ

Line 2: Values of $dC_L/d\alpha$, $dC_{my}/d\alpha$, and $\frac{y_{c.p.}}{b/2}$, where C_{my} = root bending moment coefficient.

Line 3-14 Values of $\frac{y}{b/2}$, C_l , $\frac{x_{c.p.}}{c}$, cC_l and α across the semi-span, where C_l is the section lift coefficient, where $x_{c.p.}$ is the section center of pressure, and c is the local chord.

Line 15: Value of C_L

```
*       LIST8
*       LABEL
C            SUBSONIC  LOAD  DISTRIBUTIONS
C           PROGRAM TO CALCULATE LOADING DISTRIBUTIONS ON SUBSONIC
C       WINGS BY WEISSINGER'S METHOD.
C       LIFT CURVE SLOPE IS CALCULATED BY TRAPEZOIDAL INTEGRATION.
C
        DIMENSION THETA(30),TAU(30),BOC(30),TAUBAR(30),ALPHA(30),Y(30),CL
      1 (30),XCP(30),SLOAD(30),CL1(30),ALPHTW(30)
        COMMON TAU,TAUBAR,THETA,AM,AM1,ALAMB,BOC
  100   FORMAT (2I5)
  101   FORMAT (4F10.4,I10)
  102   FORMAT (F10.4)
  201   FORMAT (16H1ASPECT RATIO = ,F10.4,10X,14HTAPER RATIO = ,F5.2,10X,
      1 18H.25 CHORD SWEEP = ,F5.2)
  202   FORMAT (1H0,9HDCL/DA = ,F10.4,5X,10HDCMY/DA = ,F10.4,5X,9HYBAR/B
      1= ,F10.4)
  203   FORMAT (5(F10.4,5X))
  205   FORMAT (1H0,24X,30HSPANWISE LOADING  (WING ALONE)//
      1 7X,3HY/B,11X,2HCL,12X,4HX-CP,7X,10HLOAD COEFF,8X,5HALPHA)
  207   FORMAT (12HOCL-TOTAL = ,F10.4)
   10   READ 100, M,M1
    2   READ 101, ALAM,AR,TR,ALPH,ITW
        IF (AR) 11,10,11
   11   ALAMB=ALAM/57.295779
        LIMIT=((M+1)/2)+1
        IF (ITW) 5,6,5
    5   DO 9 J=1,LIMIT
        READ 102, ALPHTW(J)
    9   ALPHA(J)=ALPH+ALPHTW(J)
        GO TO 7
    6   DO 1 J=1,LIMIT
    1   ALPHA(J)=ALPH
    7   AM=M
        AM1=M1
        CALL WEISS(AR,TR,ALPHA,Y,CL,XCP)
        PRINT 201,AR,TR,ALAM
        LIM=(M+1)/2
        LIMP=LIM+1
        DO 8 I=1,LIMP
    8   CL1(I)=CL(I)*2.*(1.-(Y(I)*(1.-TR)))/(1.+TR)
        SUM=0.
        DO 3 I=1,LIM
        TERM=(Y(I)-Y(I+1))*.5*(CL1(I+1)+CL1(I))
    3   SUM=SUM+TERM
        DCLDA=SUM/ALPH
        CLTOT=SUM
        SUM = 0.
        DO 13 I=1,LIM
        TERM=(Y(I)-Y(I+1))*.5*(CL1(I+1)+CL1(I))*.5*(Y(I)+Y(I+1))
   13   SUM=SUM+TERM
        DCMYDA=SUM/ALPH
        YCP=DCMYDA/DCLDA
        DO 4 I=1,LIMIT
    4   SLOAD(I)=CL(I)*4.*(1.-(Y(I)*(1.-TR)))/((1.+TR)*AR)
        PRINT 202, DCLDA,DCMYDA,YCP
        PRINT 205
        PRINT 203, (Y(I),CL(I),XCP(I),SLOAD(I),ALPHA(I), I=1,LIMIT)
        PRINT 207, CLTOT


        GO TO 2
       END
```

```
*       LIST8
*       LABEL
        SUBROUTINE WEISS (AR,TR,ALPHA,Y,CL,XCP)
        DIMENSION THETA(30),TAU(30),BOC(30),TAUBAR(30),ALPHA(30),Y(30),
      1 CL(30),XCP(30),A(30,30),G(30),ALPHA1(30)
        COMMON TAU,TAUBAR,THETA,AM,AM1,ALAMB,BOC
        M=AM
        PI=3.14159265358979323846
        LIM=(AM+1.)/2.
        DO 6 N=1,M
        EN=N
 6      THETA(N)=(EN*PI)/(AM+1.)
        DO 1 N=1,LIM
        EN=N
        TAU(N)=COSF((EN*PI)/(AM+1.))
        ALPHA1(N)=ALPHA(N)
 1      BOC(N)=(AR*(1.+TR))/(2.*(1.-TAU(N)*(1.-TR)))
        LIM2=(AM1+1.)/2.
        DO 5 N=1,LIM2
        EN=N
 5      TAUBAR(N)=COSF((EN*PI)/(AM1+1.))
        CALL AMAT (A)
        CALL MATINV (A,LIM,ALPHA1,1,DET)
        DO 2 N=1,LIM
        G(N)=ALPHA1(N)
        I=N+1
        CL(I)=2.*G(N)*BOC(N)
        XCP(I)=.25
 2      Y(I)=TAU(N)
        CL(1)=0.
        XCP(1)=.25
        Y(1)=1.0
        RETURN
       END
```

```
*       LIST8
*       LABEL
        SUBROUTINE AMAT (A)
        DIMENSION THETA(30),TAU(30),BOC(30),TAUBAR(30),A(30,30)
        COMMON TAU,TAUBAR,THETA,AM,AM1,ALAMB,BOC
        M=AM
        LIM=(AM+1.)/2.
        DO 1 NU=1,LIM
        DO 7 N=1,LIM
        IF (NU-N) 2,3,2
 2      IF (N-LIM) 4,5,4
 4      ARG2=M+1-N
        ANU=NU
        AN=N
        BIGB=B(ANU,AN)+B(ANU,ARG2)
        GO TO 6
 5      ANU=NU
        AN=N
        BIGB=B(ANU,AN)
        GO TO 6
 3      ANU=NU
        A(NU,N)=2.*B(ANU,ANU)+BOC(NU)*GBAR(ANU,ANU)
        GO TO 7
 6      A(NU,N)=-2.*BIGB+BOC(NU)*GBAR(ANU,AN)
 7      CONTINUE
 1      CONTINUE
        RETURN
       END
```

```
*       LIST8
*       LABEL
        FUNCTION B(ANU,AN)
        DIMENSION THETA(30),TAU(30),BOC(30),TAUBAR(30)
        COMMON TAU,TAUBAR,THETA,AM,AM1,ALAMB,BOC
        NU=ANU
        N=AN
        IF (N-NU) 1,2,1
 2      B=(AM+1.)/(4.*SINF(THETA(NU)))
        RETURN
 1      B=(SINF(THETA(N))/((COSF(THETA(N))-COSF(THETA(NU)))**2))
     1 *(1.-(-1.)**(N-NU))/(2.*(AM+1.))
        RETURN
       END
```

```
*       LIST8
*       LABEL
        FUNCTION GBAR(ANU,AN)
        DIMENSION THETA(30),TAU(30),BOC(30),TAUBAR(30)
        COMMON TAU,TAUBAR,THETA,AM,AM1,ALAMB,BOC
        SUM=0.
        LIM=(AM1-1.)/2.
        LIMP=LIM+1
        DO 1 L=1,LIMP
        LM=L-1
        TERM=FBAR(AN,LM)*ELSTAR(ANU,LM)
        SUM=SUM+TERM
 1      CONTINUE
        GBAR=((-1.)/(2.*(AM1+1.)))*SUM
        RETURN
       END
```

```
*       LIST8
*       LABEL
        FUNCTION FBAR(AN,LM)
        DIMENSION THETA(30),TAU(30),BOC(30),TAUBAR(30)
        COMMON TAU,TAUBAR,THETA,AM,AM1,ALAMB,BOC
        N=AN
        M=AM
        SUM=0.
        DO 1 MU1=1,M,2
        AMU1=MU1
        IF (LM) 2,3,2
 3      TERM=AMU1*SINF(AMU1*THETA(N))
        GO TO 1
 2      ELM=LM
        THETBR=(ELM*3.14159)/(AM1+1.)
        TERM=AMU1*SINF(AMU1*THETA(N))*COSF(AMU1*THETBR)
 1      SUM=SUM+TERM
        F=(2./(AM+1.))*SUM
        IF (LM) 4,5,4
 5      IF (AN-((AM+1.)/2.)) 6,7,6
 7      FBAR=F/2.
        GO TO 8
 6      FBAR=F
        GO TO 8
 4      IF (AN-((AM+1.)/2.))9,10,9
 10     FBAR=F
        GO TO 8
 9      FBAR=2.*F
 8      RETURN
       END
```

```
*       LIST8
*       LABEL
        FUNCTION ELSTAR (ANU,LM)
        DIMENSION THETA(30),TAU(30),BOC(30),TAUBAR(30)
        COMMON TAU,TAUBAR,THETA,AM,AM1,ALAMB,BOC
        TANF(X)=SINF(X)/COSF(X)
        NU=ANU
        IF (LM) 1,2,1
 2      ETAMU=1.
        GO TO 3
 1      ETAMU=TAUBAR(LM)
 3      ETANU=TAU(NU)
        DIF=ETANU-ETAMU
        SUM=ETANU+ETAMU
        BOCN=BOC(NU)
        TERM1=(1./(BOCN*DIF))*(SQRTF(((1.+BOCN*DIF*TANF(ALAMB))**2)+
     1 ((BOCN*DIF)**2))-1.)
        TERM2=(1./(BOCN*SUM))*((SQRTF(((1.+BOCN*DIF*TANF(ALAMB))**2)+
     1  ((BOCN*SUM)**2)))/(1.+2.*BOCN*ETANU*TANF(ALAMB))-1.)
        TERM3=(2.*TANF(ALAMB)*SQRTF(((1.+BOCN*ETANU*TANF(ALAMB))**2)
     1  +((BOCN*ETANU)**2)))/(1.+2.*BOCN*ETANU*TANF(ALAMB))
        ELSTAR=TERM1-TERM2-TERM3
        RETURN
       END
```

```
*       LIST8
*       LABEL
        SUBROUTINE MATINV (A,N,B,M,DETERM)
C
C         SUBROUTINE TO SOLVE THE MATRIX EQUATION AX=B, WHERE A IS
C       AN N X N SQUARE MATRIX, B IS A KNOWN M X N MATRIX, AND X IS
C       AN UNKNOWN M X N MATRIX. UPON RETURN THE INVERSE OF A IS PLACED
C       IN A, AND X IS PLACED IN B. BY SETTING M=0 THE SUBROUTINE MAY
C       BE USED FOR MATRIX INVERSION ALONE.  FOR FURTHER DETAILS SEE
C        IBM SHARE NO. 664.
C
        DIMENSION IPIVOT(30), A(30,30), B(30,1), INDEX(30,2), PIVOT(30)
        EQUIVALENCE (IROW,JROW),(ICOLUM,JCOLUM),(AMAX,T,SWAP)
 10     DETERM=1.0
 15     DO 20 J=1,N
 20     IPIVOT(J)=0
 30     DO 550 I=1,N
 40     AMAX=0.0
 45     DO 105 J=1,N
 50     IF (IPIVOT(J)-1) 60,105,60
 60     DO 100 K=1,N
 70     IF (IPIVOT(K)-1) 80,100,740
 80     IF (ABSF(AMAX)-ABSF(A(J,K)))85,100,100
 85     IROW=J
 90     ICOLUM=K
 95     AMAX=A(J,K)
100     CONTINUE
105     CONTINUE
110     IPIVOT(ICOLUM)=IPIVOT(ICOLUM)+1
130     IF (IROW-ICOLUM) 140,260,140
140     DETERM=-DETERM
150     DO 200 L=1,N
160     SWAP=A(IROW,L)
170     A(IROW,L)=A(ICOLUM,L)
200     A(ICOLUM,L)=SWAP
205     IF (M) 260,260,210
210     DO 250 L=1,M
220     SWAP=B(IROW,L)
230     B(IROW,L)=B(ICOLUM,L)
250     B(ICOLUM,L)=SWAP
260     INDEX(I,1)=IROW
270     INDEX(I,2)=ICOLUM
310     PIVOT(I)=A(ICOLUM,ICOLUM)
320     DETERM=DETERM*PIVOT(I)
330     A(ICOLUM,ICOLUM)=1.0
340     DO 350 L=1,N
350     A(ICOLUM,L)=A(ICOLUM,L)/PIVOT(I)
355     IF (M) 380,380,360
360     DO 370 L=1,M
370     B(ICOLUM,L)=B(ICOLUM,L)/PIVOT(I)
380     DO 550 L1=1,N
390     IF (L1-ICOLUM) 400,550,400
400     T=A(L1,ICOLUM)
420     A(L1,ICOLUM)=0.0
430     DO 450 L=1,N
450     A(L1,L)=A(L1,L)-A(ICOLUM,L)*T
455     IF (M) 550,550,460
460     DO 500 L=1,M
500     B(L1,L)=B(L1,L)-B(ICOLUM,L)*T
```

```
      CONTINUE
      DO 710 I=1,N
      L=N+1-I
      IF (INDEX(L,1)-INDEX(L,2)) 630,710,630
      JROW=INDEX(L,1)
      JCOLUM=INDEX(L,2)
      DO 705 K=1,N
      SWAP=A(K,JROW)
      A(K,JROW)=A(K,JCOLUM)
      A(K,JCOLUM)=SWAP
      CONTINUE
      CONTINUE
      RETURN
      END
```

```
*       DATA
   15   25
60.0        4.0         .50         1.0                  0
30.0        1.5         .25         1.0                  1
.08
.07
.06
.05
.04
.03
.02
.01
.00
0.0         6.0         1.0         1.0                  0
```

ASPECT RATIO = 4.0000 TAPER RATIO = 0.50 .25 CHORD SWEEP = 40.00

CCL/CA = 2.4171 CCMY/CA = 1.1115 YBAR/B = 0.4599

SPANWISE LOADING (WING ALONE)

Y/B	CL	X-CP	LOAD COEFF	ALPHA
1.0000	0.	0.2500	0.	1.0000
0.9808	1.2922	0.2500	0.4390	1.0000
0.9239	2.2787	0.2500	0.8174	1.0000
0.8315	2.7580	0.2500	1.0743	1.0000
0.7071	2.8457	0.2500	1.2281	1.0000
0.5556	2.7498	0.2500	1.3240	1.0000
0.3827	2.5580	0.2500	1.3790	1.0000
0.1951	2.2595	0.2500	1.3594	1.0000
0.	1.8686	0.2500	1.2457	1.0000

CL-TOTAL = 2.4171

ASPECT RATIO = 1.5000 TAPER RATIO = 0.25 .25 CHORD SWEEP = 30.00

CCL/CA = 2.0556 CCMY/CA = 0.8741 YBAR/B = 0.4244

SPANWISE LOADING (WING ALONE)

Y/B	CL	X-CP	LOAD COEFF	ALPHA
1.0000	0.	0.2500	0.	1.0000
0.9808	1.2239	0.2500	0.6961	1.0000
0.9239	2.0810	0.2500	1.3502	1.0000
0.8315	2.4354	0.2500	1.6556	1.0000
0.7071	2.4812	0.2500	2.4861	1.0000
0.5556	2.3492	0.2500	2.5234	1.0000
0.3827	2.1389	0.2500	3.2504	1.0000
0.1951	1.8555	0.2500	3.4528	1.0000
0.	1.6500	0.2500	3.5214	1.0000

CL-TOTAL = 2.0556

ASPECT RATIO = 6.0000 TAPER RATIO = 1.00 .25 CHORD SWEEP = 0.

CCL/CA = 4.1544 CCMY/CA = 1.8224 YBAR/B = 0.4411

SPANWISE LOADING (WING ALONE)

Y/B	CL	X-CP	LOAD COEFF	ALPHA
1.0000	0.	0.2500	0.	1.0000
0.9808	1.2617	0.2500	0.4204	1.0000
0.9239	2.4011	0.2500	0.8004	1.0000
0.8315	3.3280	0.2500	1.1093	1.0000
0.7071	4.0115	0.2500	1.3372	1.0000
0.5556	4.4767	0.2500	1.4921	1.0000
0.3827	4.7674	0.2500	1.5891	1.0000
0.1951	4.9252	0.2500	1.6417	1.0000
0.	4.9756	0.2500	1.6585	1.0000

CL-TOTAL = 4.1544

APPENDIX B

(By Christopher J. Borland)

"LAWRENCE'S METHOD" AS PROGRAMMED FOR THE IBM 709/7094 IN FORTRAN II

1. DESCRIPTION OF PROGRAM

a. TRANSONIC LOAD DISTRIBUTIONS

This executive program receives as input data the geometrical parameters of the wing planform and the Mach no., performs the Prandtl-Glauert transformation, and sets up the calculation for the Lawrence method.

b. LAWRNC

This subroutine performs the calculation of the chordwise load distribution on the transformed wing, performs the inverse transformation, and prints the aspect ratio, lift curve slope, chordwise and spanwise location of the center of pressure, and chordwise load distribution as output data.

c. MATINV

This subroutine, used for solving the set of simultaneous equations (IV - 105), is identical to the subrontine of the same name listed in Appendix A, with the exception that the DIMENSION statement must be changed so that the maximum dimension of the arrays IPIVOT, A, B, INDEX, and PIVOT matches the maximum dimension of the arrays in LAWRNC; in this case, 50. The listing may be found in Appendix A.

d. Library and Machine Requirements

The Library and Machine requirements for this program are identical to those listed in Appendix A.

2. INSTRUCTIONS FOR USE

a. Definition of Input Variables

MBIG	Number of intervals in the trapezoidal integration.
NBIG	Number of stations on the chord.
ALAM1	Leading edge sweep angle in degrees.
ALAM2	Tip sweep angle in degrees (See sketch on Page 236)
AOC	Value of a/c (See sketch on Page 236)
X1OC	Value of x_1/c (See sketch on Page 236)
EM	Mach Number
KEY	Program Input Key:
	= 1 for twisted and/or cambered wing.
	= 0 for flat wing.
FUNC	Values of $f(\theta_n)$ (See Section 2-c.)

b. Order of Data Deck

	Columns	Variable
Card 1		
	1-5	MBIG
	6-10	NBIG
Card 2		
	1-10	ALAM1
	11-20	ALAM2
	21-30	AOC
	31-40	X1OC
	41-50	EM
	60	KEY
Cards 3, 4, 5, etc.		
	1-10	FUNC

c. Data Values

The maximum size of both MBIG and NBIG is 50, but it has not been necessary, for the cases tested, to use values this large. It has been found that the solution is relatively insensitive to changes in MBIG above a value of about 12, and to changes in NBIG above values of about 20. Since MBIG and NBIG must be different, and may not be multiples of each other, values of 13 and 24 have been used, respectively, with success. With these values, approximately 1.54 minutes of computation time on the IBM 709 are required to calculate the complete chordwise load distribution on one wing at one Mach Number.

If KEY is given as 1, there must be NBIG-1 cards following Card 2 with the values of the function $f(\theta_n)$ at the NBIG-1 stations on the wing (excluding the leading edge). If KEY is given as 0, these cards may be omitted.

The function $f(\theta_n)$ is given by

$$f(\theta_n) = \frac{4}{\pi} \frac{1}{(b(\theta_n)/b)^2} \int_{-\frac{b(\theta_n)}{b}}^{\frac{b(\theta_n)}{b}} \frac{1}{2} \alpha\left(\theta_n, \frac{y}{b/2}\right) \sqrt{\left(\frac{b(\theta_n)}{b}\right)^2 - \left(\frac{y}{b/2}\right)^2}\, d\left(\frac{y}{b/2}\right)$$

$$= \frac{1}{\pi} k(\theta_n) \Big/ \left(\frac{b(\theta_n)}{b}\right)^2$$

If there is no spanwise variation in effective angle of attack, i.e. $\alpha(\theta_n, y) = \alpha(\theta_n)$, then

$$f(\theta_n) = \alpha(\theta_n)$$

given in radians. For the case of an uncambered, untwisted wing at unit angle of attack

$$f(\theta_n) = 1$$

Chordwise load distributions for this case are found by letting KEY be zero.

The variables MBIG and NBIG must be right-justified in their fields and punched without the decimal point. The variables ALAM1, ALAM2, AOC, X1OC, EM, and FUNC must be punched with the decimal point, but need not be right justified. Up to two places after the decimal

point are permitted for ALAM1, ALAM2, AOC, X1OC, and EM, and up to four places for FUNC.

If calculations are desired for more than one planform, Mach number, or set of values of $f(\theta_n)$, the data deck may be repeated from Card 2 with the new values.

The following should be noted, with reference to the sketch below. If a rectangular planform is to be solved, Λ_1 must be set equal to zero, Λ_2 to 90.0, and x_1/c to 0. If a triangular wing is to be solved, a/c must be set equal to 0, Λ_1 to the leading edge sweep angle, Λ_2 to 90.0, and x_1/c to 1.0

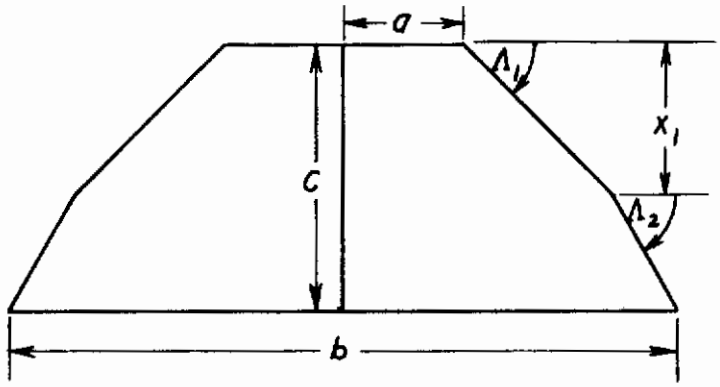

d. Input and Output Samples

A sample input deck is shown following the listing of the program. The input value for the three cases tested are as follows:

Case	Λ	Λ	a/c	x_1/c	M	Key
1	0.0	90.0	4.0	0.0	.85	0
2	45.0	90.0	0.0	1.0	.98	0
3	63.0	90.0	0.0	.6	1.10	0

Note: that as "Key" is 0 in all cases, none of these wings is considered to have a twist or camber distribution.

The output for these cases is also shown. A description of the output follows:

Line 1:	Values of Λ_1 , Λ_2 .
Line 2:	Values of a/c, x_1/c, M
Line 3:	Value of AR
Line 4:	Values of $dC_L/d\alpha$, and x_{cp}/C_{root}
Line 5 – 29:	Values of x/c, $g'(x)$.
Line 30:	Value of $y_{cp}/b/2$

```
*       LIST8
*       LABEL
*       SYMBOL TABLE
C             TRANSONIC LOAD DISTRIBUTIONS
C
C       PROGRAM TO CALCULATE CHORDWISE LOAD DISTRIBUTIONS, CENTER OF
C       PRESSURE, AND LIFT CURVE SLOPE ON TRANSONIC WINGS, USING LAWRENCE'S
C       METHOD WITH THE PRANDTL-GLAUERT CORRECTION.
C
        DIMENSION FUNC(50)
 101    FORMAT (2I5)
 102    FORMAT (5F10.2,I10)
 103    FORMAT (F10.4)
 201    FORMAT (13H1LAMBDA(1) = ,F10.4,5X,12HLAMBDA(2) = ,F10.4,5X//
     1 7H A/C = ,F10.4,5X,7HX1/C = ,F10.4,5X,11HMACH NO. = ,F5.2)
        TANF(X)=SINF(X)/COSF(X)
        PI=3.14159265358
        READ 101, MBIG,NBIG
 1      READ 102, ALAM1,ALAM2,AOC,X1OC,EM,KEY
        PRINT 201,ALAM1,ALAM2,AOC,X1OC,EM
        IF (KEY) 10,10,8
 8      LIM2=NBIG-1
        DO 9 I=1,LIM2
 9      READ 103, FUNC(I)
        GO TO 2
 10     LIM2=NBIG-1
        DO 11 I=1,LIM2
 11     FUNC(I)=1.0
 2      IF (EM-1.0) 3,3,4
 3      BETA=SQRTF(1.-EM*EM)
        GO TO 5
 4      BETA=SQRTF(EM*EM-1.)
 5      AOCT=BETA*AOC*2.
        X1OC=X1OC*2.
        ALAMB1=ALAM1/57.295779
        ALAMT1=ATANF(TANF(ALAMB1)/BETA)*57.295779
        IF (ALAM2-90.0) 6,7,6
 6      ALAMB2=ALAM2/57.295779
        ALAMT2=ATANF(TANF(ALAMB2)/BETA)*57.295779
 7      CALL LAWRNC (MBIG,NBIG,ALAMT1,ALAMT2,AOCT,X1OC,CLALPH,AR,BETA,
     1 FUNC)
        GO TO 1
       END
```

```
*       LIST8
*       LABEL
*       SYMBOL TABLE
        SUBROUTINE LAWRNC (MBIG,NBIG,ALAM1,ALAM2,AOC,X1OC,CLALPH,AR,
     1 BETA,FUNC)
        DIMENSION BETAOC(50), H(50,50), F(50,50), HO(50),FO(50),
     1 BETAOB(50), C(50,50), A(50), B(50), XOC1(50), DGDX(50),FUNC(50)
        TANF(X)=SINF(X)/COSF(X)
        COTF(X)=COSF(X)/SINF(X)
        GARBF(X)=((SQRTF((COSF(X)-COSF(THETA))**2+(BTASBN)**2)-BTASBN)
     1  /(COSF(X)-COSF(THETA)))
 105    FORMAT (20H0LIFT CURVE SLOPE = ,F10.4,10X,21HCENTER OF PRESSURE =
     1 ,F10.4)
 106    FORMAT (16H0ASPECT RATIO = ,F10.4)
 107    FORMAT (1H0,25X,27HCHORDWISE LOAD DISTRIBUTION//1H0,25X,3HX/C,
     1 14X,5HDG/DX)
 108    FORMAT (23X,F8.3,10X,F10.5)
 109    FORMAT (31H0SPANWISE CENTER OF PRESSURE = ,F10.4)
        LIM=MBIG-1
        LIM2=NBIG-1
        ENBIG=NBIG
        EMBIG=MBIG
        PI=3.14159265358
        ALAMB1=ALAM1/57.295779
        ALAMB2=ALAM2/57.295779
        IF (ALAM1) 3,3,2
 2      COB=1.0/(AOC+(X1OC*COTF(ALAMB1))+(2.-X1OC)*COTF(ALAMB2))
        AR=4.*((AOC+X1OC*COTF(ALAMB1)+(2.-X1OC)*COTF(ALAMB2))**2)/(4.*
     1 AOC+((X1OC)**2)*COTF(ALAMB1)+2.*X1OC*COTF(ALAMB1)*(2.-X1OC)
     2 +((2.-X1OC)**2)*COTF(ALAMB2))
        GO TO 4
 3      COB=1.0/(AOC+2.*COTF(ALAMB2))
        AR=4.*((AOC+2.*COTF(ALAMB2))**2)/(4.*AOC+4.*COTF(ALAMB2))
 4      DO 5 N=1,LIM2
        EN = N
        THETA=(EN*PI)/ENBIG
        XOC=COSF(THETA)
        IF (XOC+1.0-X1OC) 6,6,7
 6      BETAOC(N)=AOC+(XOC+1.0)*COTF(ALAMB1)
        BTASBN=BETAOC(N)
        GO TO 8
 7      IF (X1OC) 9,9,10
 9      BETAOC(N)=(XOC+1.0)*COTF(ALAMB2)+AOC
        BTASBN=BETAOC(N)
        GO TO 8
 10     BETAOC(N)=X1OC*COTF(ALAMB1)+(XOC+1.0-X1OC)*COTF(ALAMB2)+AOC
        BTASBN=BETAOC(N)
 8      DO 11 L=1,LIM2
        EL=L
        SUM=0.
        DO 12 M=1,LIM
        EM=M
        TERM=COSF((EM*PI*EL)/EMBIG)*GARBF((EM*PI)/EMBIG)
 12     SUM=SUM+TERM
        H(L,N)=(1./EMBIG)*(((GARBF(0.0)+((-1.)**L)*GARBF(PI))/2.)+SUM)
 11     F(L,N)=(2.*SINF(EL*THETA)/(EL*PI))+(BETAOC(N)*SINF(EL*THETA)
     1  /(SINF(THETA)))+H(L,N)
        SUM=0.
        DO 13 M=1,LIM
```

```
      EM =M
      TERM=GARBF((EM*PI)/EMBIG)
 13   SUM=SUM+TERM
      HO(N)=(1./EMBIG)*(((GARBF(0.0)+GARBF(PI))/2.)+SUM)
      FO(N)=((2.*THETA)/PI)+HO(N)-3.0
      BETAOB(N)=BETAOC(N)*COB
 5    B(N)=((BETAOB(N))**2)*FUNC(N)
      DO 14 I=1,LIM2
      C(I,1)=F(1,I)-FO(I)
 14   C(I,2)=F(2,I)-FO(I)
      DO 23 I=1,LIM2
      DO 15 J=3,LIM2
 15   C(I,J)=F(J,I)-F(J-2,I)
 23   CONTINUE
      CALL MATINV(C,LIM2,B,1,DETERM)
 16   DO 20 I=1,LIM2
20    A(I)=B(I)
      A(NBIG)=0.0
      CLALPH=2.*PI*AR*(A(1)+A(2))
      CLALPH=CLALPH/BETA
      XCP=.50-(.25*((A(1)-A(3))/(A(1)+A(2))))
      AR=AR/BETA
      PRINT 106, AR
      PRINT 105, CLALPH,XCP
      PRINT 107
      DO 21 N=1,LIM2
      EN=N
      THETA=(EN*PI)/ENBIG
      XOC1(N)=COSF(THETA)
      XOC1(N)=XOC1(N)*.5+.5
      SUM=0.
      DO 22 L=2,LIM2
      EL=L
      TERM=A(L)*SINF((EL-1.)*THETA)
 22   SUM=SUM+TERM
      DGDX(N)=A(1)*TANF(THETA/2.)+2.*SUM
      DGDX(N)=DGDX(N)/BETA
 21   PRINT 108, XOC1(N), DGDX(N)
      SUM1=0.
      SUM2=0.
      DO 30. N=2,LIM2
      BETAOC(N)=BETAOC(N)/BETA
      DX=XOC1(N)-XOC1(N-1)
      TERM1=BETAOC(N)*DGDX(N)*DX
      TERM2=DGDX(N)*DX
      SUM1=SUM1+TERM1
30    SUM2=SUM2+TERM2
      SUM1=SUM1+BETAOC(1)*DGDX(1)*XOC1(1)
      SUM2=SUM2+DGDX(1)*XOC1(1)
      YBAR=(SUM1/(SUM2*(PI/2.)))*COB*BETA
      PRINT 109, YBAR
      RETURN
     END
```

```
*       DATA
    13   24
0.0         90.0        4.0         0.0         .85                 0
45.0        90.0        0.0         1.0         .98                 0
63.0        90.0        0.0         .6          1.10                0
```

LAMBDA(1) = 0. LAMBDA(2) = 90.0000

A/C = 4.0000 X1/C = 0. MACH NO. = 0.85

ASPECT RATIO = 8.0000

LIFT CURVE SLOPE = 7.0185 CENTER OF PRESSURE = 0.2318

CHORDWISE LOAD DISTRIBUTION

X/C	DG/DX
0.996	0.01518
0.983	0.03041
0.962	0.04587
0.933	0.06172
0.897	0.07819
0.854	0.09554
0.804	0.11410
0.750	0.13423
0.691	0.15641
0.629	0.18120
0.565	0.20933
0.500	0.24174
0.435	0.27968
0.371	0.32483
0.309	0.37961
0.250	0.44757
0.196	0.53423
0.146	0.64867
0.103	0.80718
0.067	1.04203
0.038	1.42844
0.017	2.19097
0.004	4.45230

SPANWISE CENTER OF PRESSURE = 0.6474

LAMBDA(1) = 45.0000 LAMBDA(2) = 90.0000

A/C = 0. X1/C = 1.0000 MACH NO. = 0.98

ASPECT RATIO = 4.0000

LIFT CURVE SLOPE = 5.2629 CENTER OF PRESSURE = 0.6138

CHORDWISE LOAD DISTRIBUTION

X/C	DG/DX
0.996	0.63369
0.983	1.17971
0.962	1.66653
0.933	2.04579
0.897	2.33333
0.854	2.51070
0.804	2.59903
0.750	2.59333
0.691	2.52098
0.629	2.38194
0.565	2.20602
0.500	1.98922
0.435	1.76475
0.371	1.51492
0.309	1.28651
0.250	1.03725
0.196	0.83472
0.146	0.61995
0.103	0.44818
0.067	0.30768
0.038	0.14161
0.017	0.11834
0.004	-0.14497

SPANWISE CENTER OF PRESSURE = 0.5494

LAMBDA(1) = 63.0000 LAMBDA(2) = 90.0000

A/C = 0. X1/C = 0.6000 MACH NO. = 1.10

ASPECT RATIO = 0.8735

LIFT CURVE SLOPE = 1.3534 CENTER OF PRESSURE = 0.4110

CHORDWISE LOAD DISTRIBUTION

X/C	DG/DX
0.996	-0.00947
0.983	0.02326
0.962	0.02643
0.933	0.04945
0.897	0.05962
0.854	0.09585
0.804	0.12719
0.750	0.22148
0.691	0.33824
0.629	0.80578
0.565	1.60481
0.500	1.91882
0.435	1.86707
0.371	1.70774
0.309	1.48952
0.250	1.23472
0.196	0.99816
0.146	0.75060
0.103	0.54601
0.067	0.36689
0.038	0.18746
0.017	0.13089
0.004	-0.11683

SPANWISE CENTER OF PRESSURE = 0.4184

APPENDIX C

"ETKIN'S PROCEDURE" AS PROGRAMMED FOR THE IBM 709/7094 IN FORTRAN II

1. DESCRIPTIONS OF PROGRAM

a. SUPERSONIC LOAD DISTRIBUTIONS

This executive program receives the Mach number and geometrical parameters (sweep angle, aspect ratio, taper ratio, angle of attack, and spanwise twist distribution) as input data; controls the calculation of spanwise loading; and prints the total lift coefficient, lift curve slope, root bending moment curve slope, spanwise and chordwise location of the center of pressure, section lift coefficient, section center of pressure, spanwise loading parameter, spanwise angle of attack distribution, and complete pressure distribution as output data.

b. EVVARD

This subroutine checks to see that the leading edge is sonic or subsonic, and that the trailing edge is supersonic. If these conditions are fulfilled, the calculation continues. If not, an error message, indicating the actual conditions, is given, and another case is attempted.

c. SUBSLE

This subroutine calculates the pressure distribution over the entire wing by Etkin's procedure, and calculates the section lift coefficient and center of pressure by integration of the pressure distribution.

d. Library and Machine Requirements

Library and machine requirements are identical to those listed in Appendix A.

2. INSTRUCTION FOR USE

a. Definition of Input Variables

M	Number of station on the semi-span, including root and tip.
N	Number of stations on the chord, not including the leading edge.
MG, NG, KPG, KQG	Parameters M, N, P, and Q defined in Etkin's procedure (Ref. 49)
EM	Mach number
ALAM	Leading edge sweep angle in degrees.
AR	Aspect ratio
TR	Taper ratio
ALPH	Root chord angle of attack, in radians.
ITW	Program input key: = 1 for twisted wing = 0 for flat wing
ALPHTW	Section angle of twist in radians.

b. Order of Data Deck

	Columns	Variable
Card 1		
	1-5	M
	6-10	N
	11-15	MG
	16-20	NG
	21-25	KPG
	26-30	KQG
Card 2		
	1-10	EM
	11-20	ALAM
	21-30	AR

Columns	Variable
31-40	TR
41-50	ALPH
60	ITW

Cards 3, 4, 5, etc. (If ITW = 1)

1-10	ALPHTW

c. Data Values

The values of M, N, MG, NG, KPG, and KQG are dependent only on the desired accuracy. Values of 10, 5, 20, 20, 5, and 5 respectively, have been used successfully, with little sensitivity shown in the solution. With these values, approximately 4.65 minutes of computation time on the IBM 709 are required to calculate the complete pressure distribution and spanwise loading on one wing.

If the pressure distribution on a flat wing is to be computed, ITW is given as 0, and only Cards 1 and 2 are required. If, however, an arbitrary spanwise variation in angle of attack is desired, ITW is given as 1, and N cards with the values of ALPHTW, the angle of twist with respect to the root chord at the N stations on the semi-span must follow Cards 1 and 2. The locations of the stations are given by:

$$\frac{y_n}{b/2} = 1 - \left(\frac{n-1}{N-1}\right) \; ; \qquad n = 1, 2, \ldots N$$

It must be noted that the angle of attack is constant between stations, i.e., between, for example, y_1 and y_2, the angle of attack has the value given for y_2. The variables M, N, MG, NG, KPG, KQG, and ITW must be right justified in their fields and punched without the decimal point. The variables EM, ALAM, AR, TR, ALPH, and ALPHTW must be punched with the decimal point, but need not be right justified. Up to four places after the decimal point are permitted.

If calculations are desired for more than one planform, Mach number, or twist distribution, the data deck may be repeated from Card 2 with the new values. Card 1 may not be repeated.

The value of ALPH is most conveniently given as 1.0, although other values may be given if desired.

d. Input and Output Samples

A sample input deck is shown following the listing of the programs. The input values for the cases tested are as follows:

Case	Mach No.	$\Lambda_{L.E.}$	AR	TR	α	Twist
1	1.45	63.42	2	0	3.4°	0
2	1.97	63.42	2	0	15°	0
3	1.45	63.42	2	0	17.4°	0
4	1.97	63.42	2	0	30°	0

The output for these cases is also shown:

Sheet 1:

Line 1: Values of M, AR, TR, $\Lambda_{L.E.}$

Line 2: Statement of leading and trailing edge conditions.

Line 3: Values of $dC_L/d\alpha$, $dCm_y/d\alpha$, $y_{cp}/b/2$, x_{cp}/c_{root}.

Lines 4-9: Values of $y/b/2$, C_ℓ, x_{cp}/C (section center of pressure referred to the local chord) CC_ℓ, α.

Line 10: Values of C_L.

Sheet 2:

Values of $x/b/2$, $y/b/2$, $1/2\ \Delta\ C_p\ (x,y)$.

```
*       LIST8
*       LABEL
*       SYMBOL TABLE
C                 SUPERSONIC  LOAD  DISTRIBUTIONS
C
C           PROGRAM TO CALCULATE  LOAD DISTRIBUTIONS ON SUPERSONIC
C       WINGS WITH SUBSONIC LEADING EDGES, SUPERSONIC TRAILING EDGES,
C       AND AN ARBITRARY SPANWISE DISTRIBUTION OF TWIST.
        DIMENSION ALPHA(25),Y(25),CL(25),XCP(25),SLOAD(25),CL1(25),WOU(25
      1 ),ALPHTW(25),CP(25,25),X(25,25)
        COMMON EM,ALAM,AR,TR,N,ALPHA,Y,CL,XCP,FLAG,DCMDA,M,MG,NG,KPG,KQG
      1 ,CP,X
  100   FORMAT (6I5)
  101   FORMAT (5F10.4,I10)
  102   FORMAT (F10.4)
  201   FORMAT (8H1MACH = ,F10.4,5X,5HAR = ,F10.4,5X,5HTR = ,F10.4,5X,
      1 14HL. E. SWEEP = ,F10.4)
  202   FORMAT (10H0DCL/DA = ,F10.4,5X,10HDCMY/DA = ,F10.4,5X,6HYCP = ,
      1 F10.4,5X,6HXCP = ,F10.4)
  203   FORMAT (5F15.5)
  204   FORMAT (72H0       Y/B             CL              XCP             COEF
     1F         ALPHA     )
  207   FORMAT (12H0CL-TOTAL = ,F10.4)
  301   FORMAT (1H1,25X,21HPRESSURE DISTRIBUTION)
  302   FORMAT (72H0    X/C         Y/B         CP                  X/C       Y/
     1B           CP      /1H0)
  303   FORMAT (2(F7.4,3X,F7.4,3X,E11.5,8X))
   50   READ 100, M,N,MG,NG,KPG,KQG
C       N IS THE NUMBER OF SPANWISE STATIONS
C       M IS THE NUMBER OF CHORDWISE STATIONS
    1   READ 101, EM,ALAM,AR,TR,ALPH,ITW
        IF (AR) 50,50,51
   51   ALAMB=ALAM/57.295779
        IF (ITW) 15,16,15
   15   DO 17 J=1,N
        READ 102, ALPHTW(J)
   17   ALPHA(J)=ALPH+ALPHTW(J)
        GO TO 18
   16   DO 2 J=1,N
    2   ALPHA(J)=ALPH
   18   PRINT 201,EM,AR,TR,ALAM
        FLAG=0.
        CALL EVVARD
        IF (FLAG) 20,20,1
   20   LIM=N-1
        SUM=0.
        DO 8 I=1,N
    8   CL1(I)=CL(I)*2.*(1.-(Y(I)*(1.-TR)))/(1.+TR)
        DO 3 I=1,LIM
        TERM=(Y(I)-Y(I+1))*.5*(CL1(I+1)+CL1(I))
    3   SUM=SUM+TERM
        DCLDA=SUM/ALPH
        CLTOT=SUM
        SUM=0.
        DO 13 I=1,LIM
        TERM=(Y(I)-Y(I+1))*.5*(CL1(I+1)+CL1(I))*.5*(Y(I)+Y(I+1))
   13   SUM=SUM+TERM
        DCMYDA=SUM/ALPH
        YCP=DCMYDA/DCLDA
```

```
      XBAR=DCMDA/DCLDA
      DO 4 I=1,N
4     SLOAD(I)=CL(I)*4.*(1.-(Y(I)*(1.-TR)))/((1.+TR)*AR)
      PRINT 202, DCLDA,DCMYDA,YCP,XBAR
      PRINT 204
      PRINT 203, (Y(I),CL(I),XCP(I),SLOAD(I),ALPHA(I), I=1,N)
      PRINT 207, CLTOT
      PRINT 301
      TOT=N/2
      NUM=TOT
      TOT1=NUM
      IF (TOT1-TOT) 40,40,41
40    NUM=NUM+1
41    PRINT 302
      DO 42 J=1,NUM
      J2=J+NUM
      PRINT 303, (X(I,J),Y(J),CP(I,J),X(I,J2),Y(J2),CP(I,J2), I=1,M)
42    CONTINUE
      GO TO 1
     END
```

```
*     LIST8
*     LABEL
*     SYMBOL TABLE
      SUBROUTINE EVVARD
      DIMENSION ALPHA(25),Y(25),CL(25),XCP(25)
      COMMON EM,ALAM,AR,TR,N,ALPHA,Y,CL,XCP,FLAG ,DCMDA
101   FORMAT (49H2TRAILING EDGE SUBSONIC,  PROGRAM CANNOT CONTINUE)
102   FORMAT (58H2UNSWEPT SUPERSONIC LEADING EDGE,  PROGRAM CANNOT CONT
     1INUE)
103   FORMAT (49H0SUBSONIC LEADING EDGE,  SUPERSONIC TRAILING EDGE)
104   FORMAT (46H0SONIC LEADING EDGE,  SUPERSONIC TRAILING EDGE)
105   FORMAT (50H2LEADING EDGE SUPERSONIC,  PROGRAM CONNOT CONTINUE)
      TANF(X)=SINF(X)/COSF(X)
      BETA=SQRTF((EM**2)-1.)
      ALAMB=ALAM/57.295779
      ALAMTE=ATANF(TANF(ALAMB)-((4.*(1.-TR))/(AR*(1.+TR))))
      IF (ABSF(ALAMTE)-ATANF(BETA)) 1,1,2
2     PRINT 101
      FLAG=1.0
      RETURN
1     IF (ALAMB) 3,3,4
3     PRINT 102
      FLAG=1.0
      RETURN
4     IF (ABSF(BETA/TANF(ALAMB)-1.0)-.0001) 6,6,8
8     IF ((BETA/TANF(ALAMB))-1.0) 5,6,7
5     PRINT 103
      CALL SUBSLE
      RETURN
6     PRINT 104
      CALL SUBSLE
      RETURN
7     PRINT 105
      FLAG=1.0
      RETURN
     END
```

```
*       LIST8
*       LABEL
*       SYMBOL TABLE
        SUBROUTINE SUBSLE
        DIMENSION Y(25),XL(25),C(25),XC(25,25),X(25,25),TK(25,25),
     1 C1(25,25),D(25,25),A(25,25),B(25,25),YS(25,25),DSDX(25,25),
     2 SPQ(25,25),CP1(25,25),CP2(25,25),CP(25,25),CL(25),CCL(25),SLOAD
     3 (25),ALPHA(25),XCP(25)
        DIMENSION DCP(25,25),XARM(25)
        COMMON EM,ALAM,AR,TR,M,ALPHA,Y,CL,XCP,FLAG,DCMDA,N,MG,NG,KPG,KQG
     1 ,CP,X
C       N IS THE NUMBER OF CHORDWISE STATIONS
C       M IS THE NUMBER OF SPANWISE STATIONS
        TANF(X)=SINF(X)/COSF(X)
        ALAMB=ALAM/57.295779
        BETA=SQRTF((EM**2)-1.)
        CAPPA=(1.-(BETA/TANF(ALAMB)))/(1.+(BETA/TANF(ALAMB)))
        AK=1./(BETA*(1./TANF(ALAMB)))
        AM=M
        MM=M-1
        DO 1 J=1,M
        AJ=J
        Y(J)=1.-((AJ-1.)/(AM-1.))
        XL(J)=Y(J)*TANF(ALAMB)
 1      C(J)=4.*(1.-Y(J)*(1.-TR))/(AR*(1.+TR))
        EN=N
        DO 2 J=1,M
        DO 3 I=1,N
        EYE=I
        XC(I,J)=EYE*C(J)/EN
        X(I,J)=XL(J)+XC(I,J)
 3      TK(I,J)=AK*BETA*Y(J)/X(I,J)
 2      CONTINUE
        EMG=MG
        ENG=NG
        PG=KPG
        QG=KQG
        THETA=ATANF(BETA)
        DO 4 J=1,M
        DO 5 I=1,N
        YLE=X(I,J)/TANF(ALAMB)
        A1=YLE-Y(J)
        EMA=A1*SINF(ALAMB)/SINF(ALAMB+THETA)
        IF (EMA*COSF(THETA)+Y(J)-1.0) 30,30,31
 31     EMA=(1.0-Y(J))/COSF(THETA)
 30     A2=YLE+Y(J)
        ENB=A2*SINF(ALAMB)/SINF(ALAMB+THETA)
        IF (ENB*COSF(THETA)-Y(J)-1.0) 32,32,33
 33     ENB=(1.0+Y(J))/COSF(THETA)
 32     A(I,J)=EMA/EMG
        B(I,J)=ENB/ENG
        XPP=X(I,J)-EMA*SINF(THETA)-ENB*SINF(THETA)
        XP=X(I,J)-ENB*SINF(THETA)
        YLEP=XP/TANF(ALAMB)
        YLEPP=XPP/TANF(ALAMB)
        YSTAR=YLEP-EMA*COSF(THETA)
       B1=YLEPP+YSTAR
        B2=YLEPP-YSTAR
        PC=B1*SINF(ALAMB)/SINF(ALAMB+THETA)
```

```
      QD=B2*SINF(ALAMB)/SINF(ALAMB+THETA)
      IF (PC*COSF(THETA)-YSTAR-1.0) 34,34,35
35    PC=(1.0+YSTAR)/COSF(THETA)
34    IF (QD*COSF(THETA)+YSTAR-1.0) 36,36,37
37    QD=(1.0-YSTAR)/COSF(THETA)
36    C1(I,J)=PC/PG
      D(I,J)=QD/QG
5     YS(I,J)=YSTAR
4     CONTINUE
      DO 8 J=1,M
      DO 9 I=1,N
      SUM2=0.
      DO 6 MS=1,MG
      AMS=MS
      SUM1=0.
      DO 7 NS=1,NG
      ANS=NS
      Y1=AMS*A(I,J)*COSF(THETA)-ANS*B(I,J)*COSF(THETA)+Y(J)
      IF (ABSF(Y1)-1.0) 40,40,41
41    ALPH=0.
      GO TO 39
40    DO 10 K=2,M
      IF (Y(K)-ABSF(Y1)) 11,11,10
10    CONTINUE
11    ALPH=ALPHA(K)+((ALPHA(K-1)-ALPHA(K))/(Y(K-1)-Y(K)))*(ABSF(Y1)-Y(K
     1 ))
39    TERM=ALPH*((SQRTF(AMS)-SQRTF(AMS-1.))*(SQRTF(ANS)-SQRTF(ANS-1.)))
     1 /SQRTF(ENG*FMG)
      IF (A(I,J)) 42,42,7
42    TERM=0.
7     SUM1=SUM1+TERM
      TERM=SUM1
6     SUM2=SUM2+TERM
      SMN=SUM2
      SUM2=0.
      DO 12 IP=1,KPG
      P=IP
      SUM1=0.
      DO 13 IQ=1,KQG
      Q=IQ
      Y2=P*C1(I,J)*COSF(THETA)-Q*D(I,J)*COSF(THETA)-YS(I,J)
      DO 14 K=1,M
      IF (Y(K)-ABSF(Y2)) 15,15,14
14    CONTINUE
15    ALPH=ALPHA(K)+((ALPHA(K-1)-ALPHA(K))/(Y(K-1)-Y(K)))*(ABSF(Y1)-Y(K
     1 ))
      TERM=ALPH/SQRTF((1.+((1.-TK(I,J))*CAPPA*P)/((1.+TK(I,J))*PG))*
     1 (1.+((1.-TK(I,J))*CAPPA*Q)/((1.+TK(I,J))*QG)))
13    SUM1=SUM1+TERM
      TERM=SUM1
12    SUM2=SUM2+TERM
      SPQ(I,J)=SUM2/(PG*QG)
9     CONTINUE
      DO 16 I=1,N
      IF (I-1) 17,17,18
17    DSDX(I,J)=(-3.*SPQ(1,J)+4.*SPQ(2,J)-SPQ(3,J))*(1./(2.*XC(N,J)/
     1  FN))
      GO TO 16
18    IF(I-N) 19,20,20
```

```
20      DSDX(I,J)=(SPQ(N-2,J)-4.*SPQ(N-1,J)+3.*SPQ(N,J))*(1./(2.*XC(N,J)/
     1 EN))
        GO TO 16
19      DSDX(I,J)=(-SPQ(I-1,J)+SPQ(I+1,J))*(1./(2.*XC(N,J)/EN))
16      CONTINUE
        DO 21 I=1,N
        SQT=SQRTF(ABSF(1.-(TK(I,J)**2)))
        CP1(I,J)=-(8./(3.14159*BETA*(1.+AK)))*(SMN/SQT)
        CP2(I,J)=(2.*(AK-1.)/(BETA*3.14159*((1.+AK)**3)))*(SPQ(I,J)
     1 /SQT+SQT*X(I,J)*DSDX(I,J))
        CP(I,J)=CP1(I,J)+CP2(I,J)
21      CONTINUE
        DO 22 I=1,N
22      DCP(I,J) = 2.*CP(I,J)
        TERM1=2.*DCP(1,J)*(X(1,J)-XL(J))
        SUM=0.
        DO 23 I=2,N
        TERM=.5*(DCP(I-1,J)+DCP(I,J))*(X(I,J)-X(I-1,J))
23      SUM=SUM+TERM
        SUM=SUM+TERM1
        CL(J)=-SUM/C(J)
        CCL(J)=-SUM
        TERMM1=(2./3.)*DCP(1,J)*((X(1,J)-XL(J))**2)
        SUM2=0.
        DO 24 I=2,N
        TERM=.5*(DCP(I,J)+DCP(I-1,J))*(X(I,J)-X(I-1,J))*(X(I,J)+X(I-1,J)
     1 -2.*XL(J))*.5
24      SUM2=SUM2+TERM
        SUM2=SUM2+TERMM1
        XCP(J)=SUM2/(SUM*C(J))
        XARM(J)=SUM2/SUM+XL(J)
8       CONTINUE
        SUM3=0.
        DO 25 J=1,MM
        TERM=(CCL(J+1)+CCL(J))*.5*(XARM(J+1)+ XARM(J))*.5*(Y(J)-Y(J+1))
25      SUM3=SUM3+TERM
        ALPH=ALPHA(M)
        DCMDA=SUM3/(ALPH*C(M))
100     RETURN
      END
```

```
*       DATA
   10     5    20    20     5     5
1.45        63.42       2.0         0.          .0593                0
1.97        63.42       2.0         0.          .2617                0
1.45        63.42       2.0         0.          .3036                0
1.97        63.42       2.0         0.          .5235                0
```

MACH = 1.4500 AR = 2.0000 TR = 0. L. E. SWEEP = 63.4200

SUBSONIC LEADING EDGE, SUPERSONIC TRAILING EDGE

DCL/DA = 2.5235 DCMY/DA = 1.0258 YCP = 0.4065 XCP = 0.6503

Y/B	CL	XCP	COEFF	ALPHA
1.00000	-0.	0.	0.	0.05930
0.75000	0.25783	0.35141	0.12892	0.05930
0.50000	0.17012	0.37584	0.17012	0.05930
0.25000	0.12869	0.41117	0.19304	0.05930
0.	0.10650	0.45606	0.21300	0.05930

CL-TOTAL = 0.1496

PRESSURE DISTRIBUTION

X/C	Y/B	CP	X/C	Y/B	CP
1.9987	1.0000	0.76875E 01	0.6497	0.2500	0.75545E-01
1.9987	1.0000	0.76875E 01	0.7997	0.2500	0.61896E-01
1.9987	1.0000	0.76875E 01	0.9497	0.2500	0.56855E-01
1.9987	1.0000	0.76875E 01	1.0997	0.2500	0.54292E-01
1.9987	1.0000	0.76875E 01	1.2497	0.2500	0.52776E-01
1.9987	1.0000	0.76875E 01	1.3997	0.2500	0.51793E-01
1.9987	1.0000	0.76875E 01	1.5497	0.2500	0.51116E-01
1.9987	1.0000	0.76875E 01	1.6997	0.2500	0.50627E-01
1.9987	1.0000	0.76875E 01	1.8497	0.2500	0.50261E-01
1.9987	1.0000	0.76875E 01	1.9997	0.2500	0.49979E-01
1.5490	0.7500	0.19132E-00	0.2000	0.	0.48408E-01
1.5990	0.7500	0.13855E-00	0.4000	0.	0.48408E-01
1.6490	0.7500	0.11576E-00	0.6000	0.	0.48408E-01
1.6990	0.7500	0.10250E-00	0.8000	0.	0.48408E-01
1.7490	0.7500	0.93660E-01	1.0000	0.	0.48408E-01
1.7990	0.7500	0.87289E-01	1.2000	0.	0.48408E-01
1.8490	0.7500	0.82450E-01	1.4000	0.	0.48408E-01
1.8990	0.7500	0.78636E-01	1.6000	0.	0.48408E-01
1.9490	0.7500	0.75547E-01	1.8000	0.	0.48408E-01
1.9990	0.7500	0.72990E-01	2.0000	0.	0.48408E-01
1.0993	0.5000	0.11576E-00	0.	0.	0.
1.1993	0.5000	0.87289E-01	0.	0.	0.
1.2993	0.5000	0.75547E-01	0.	0.	0.
1.3993	0.5000	0.69000E-01	0.	0.	0.
1.4993	0.5000	0.64807E-01	0.	0.	0.
1.5993	0.5000	0.61894E-01	0.	0.	0.
1.6993	0.5000	0.59759E-01	0.	0.	0.
1.7993	0.5000	0.58131E-01	0.	0.	0.
1.8993	0.5000	0.56854E-01	0.	0.	0.
1.9993	0.5000	0.55827E-01	0.	0.	0.

MACH = 1.9700 AR = 2.0000 TR = 0. L. E. SWEEP = 63.4200

SUBSONIC LEADING EDGE, SUPERSONIC TRAILING EDGE

DCL/DA = 2.1144 DCMY/DA = 0.8600 YCP = 0.4067 XCP = 0.6504

Y/B	CL	XCP	COEFF	ALPHA
1.00000	-0.	0.	0.	0.26170
0.75000	0.95473	0.35127	0.47737	0.26170
0.50000	0.62939	0.37560	0.62939	0.26170
0.25000	0.47562	0.41094	0.71344	0.26170
0.	0.39313	0.45606	0.78626	0.26170

CL-TOTAL = 0.5533

PRESSURE DISTRIBUTION

X/C	Y/B	CP	X/C	Y/B	CP
1.9987	1.0000	0.97775E 01	0.6497	0.2500	0.27952E-00
1.9987	1.0000	0.97775E 01	0.7997	0.2500	0.22883E-00
1.9987	1.0000	0.97775E 01	0.9497	0.2500	0.21010E-00
1.9987	1.0000	0.97775E 01	1.0997	0.2500	0.20058E-00
1.9987	1.0000	0.97775E 01	1.2497	0.2500	0.19494E-00
1.9987	1.0000	0.97775E 01	1.3997	0.2500	0.19129E-00
1.9987	1.0000	0.97775E 01	1.5497	0.2500	0.18877E-00
1.9987	1.0000	0.97775E 01	1.6997	0.2500	0.18695E-00
1.9987	1.0000	0.97775E 01	1.8497	0.2500	0.18559E-00
1.9987	1.0000	0.97775E 01	1.9997	0.2500	0.18454E-00
1.5490	0.7500	0.70876E 00	0.2000	0.	0.17870E-00
1.5990	0.7500	0.51316E 00	0.4000	0.	0.17870E-00
1.6490	0.7500	0.42866E-00	0.6000	0.	0.17870E-00
1.6990	0.7500	0.37949E-00	0.8000	0.	0.17870E-00
1.7490	0.7500	0.34672E-00	1.0000	0.	0.17870E-00
1.7990	0.7500	0.32309E-00	1.2000	0.	0.17870E-00
1.8490	0.7500	0.30514E-00	1.4000	0.	0.17870E-00
1.8990	0.7500	0.29099E-00	1.6000	0.	0.17870E-00
1.9490	0.7500	0.27952E-00	1.8000	0.	0.17870E-00
1.9990	0.7500	0.27003E-00	2.0000	0.	0.17870E-00
1.0993	0.5000	0.42866E-00	0.	0.	0.
1.1993	0.5000	0.32309E-00	0.	0.	0.
1.2993	0.5000	0.27952E-00	0.	0.	0.
1.3993	0.5000	0.25522E-00	0.	0.	0.
1.4993	0.5000	0.23965E-00	0.	0.	0.
1.5993	0.5000	0.22883E-00	0.	0.	0.
1.6993	0.5000	0.22090E-00	0.	0.	0.
1.7993	0.5000	0.21485E-00	0.	0.	0.
1.8993	0.5000	0.21010E-00	0.	0.	0.
1.9993	0.5000	0.20629E-00	0.	0.	0.

MACH = 1.4500 AR = 2.0000 TR = 0. L. E. SWEEP = 63.4200

SUBSONIC LEADING EDGE, SUPERSONIC TRAILING EDGE

DCL/DA = 2.5235 DCMY/DA = 1.0258 YCP = 0.4065 XCP = 0.6503

Y/B	CL	XCP	COEFF	ALPHA
1.00000	-0.	0.	0.	0.30360
0.75000	1.32004	0.35141	0.66002	0.30360
0.50000	0.87095	0.37584	0.87095	0.30360
0.25000	0.65887	0.41117	0.98831	0.30360
0.	0.54524	0.45606	1.09049	0.30360

CL-TOTAL = 0.7661

PRESSURE DISTRIBUTION

X/C	Y/B	CP	X/C	Y/B	CP
1.9987	1.0000	0.39358E 02	0.6497	0.2500	0.38677E-00
1.9987	1.0000	0.39358E 02	0.7997	0.2500	0.31689E-00
1.9987	1.0000	0.39358E 02	0.9497	0.2500	0.29108E-00
1.9987	1.0000	0.39358E 02	1.0997	0.2500	0.27796E-00
1.9987	1.0000	0.39358E 02	1.2497	0.2500	0.27020E-00
1.9987	1.0000	0.39358E 02	1.3997	0.2500	0.26517E-00
1.9987	1.0000	0.39358E 02	1.5497	0.2500	0.26170E-00
1.9987	1.0000	0.39358E 02	1.6997	0.2500	0.25919E-00
1.9987	1.0000	0.39358E 02	1.8497	0.2500	0.25732E-00
1.9987	1.0000	0.39358E 02	1.9997	0.2500	0.25588E-00
1.5490	0.7500	0.97949E 00	0.2000	0.	0.24784E-00
1.5990	0.7500	0.70933E 00	0.4000	0.	0.24784E-00
1.6490	0.7500	0.59264E 00	0.6000	0.	0.24784E-00
1.6990	0.7500	0.52475E 00	0.8000	0.	0.24784E-00
1.7490	0.7500	0.47951E-00	1.0000	0.	0.24784E-00
1.7990	0.7500	0.44689E-00	1.2000	0.	0.24784E-00
1.8490	0.7500	0.42212E-00	1.4000	0.	0.24784E-00
1.8990	0.7500	0.40260E-00	1.6000	0.	0.24784E-00
1.9490	0.7500	0.38678E-00	1.8000	0.	0.24784E-00
1.9990	0.7500	0.37369E-00	2.0000	0.	0.24784E-00
1.0993	0.5000	0.99263E 00	0.	0.	0.
1.1993	0.5000	0.44690E-00	0.	0.	0.
1.2993	0.5000	0.38678E-00	0.	0.	0.
1.3993	0.5000	0.35326E-00	0.	0.	0.
1.4993	0.5000	0.33179E-00	0.	0.	0.
1.5993	0.5000	0.31688E-00	0.	0.	0.
1.6993	0.5000	0.30595E-00	0.	0.	0.
1.7993	0.5000	0.29761E-00	0.	0.	0.
1.8993	0.5000	0.29107E-00	0.	0.	0.
1.9993	0.5000	0.28582E-00	0.	0.	0.

MACH = 1.9700 AR = 2.0000 TR = 0. L. E. SWEEP = 63.4200

SUBSONIC LEADING EDGE, SUPERSONIC TRAILING EDGE

DCL/DA = 2.1144 DCMY/DA = 0.8600 YCP = 0.4067 XCP = 0.6503

Y/B	CL	XCP	COEFF	ALPHA
1.00000	-0.	0.	0.	0.52350
0.75000	1.90983	0.35127	0.95492	0.52350
0.50000	1.25902	0.37560	1.25902	0.52350
0.25000	0.95143	0.41094	1.42714	0.52350
0.	0.78641	0.45606	1.57283	0.52350

CL-TOTAL = 1.1069

PRESSURE DISTRIBUTION

X/C	Y/B	CP	X/C	Y/B	CP
1.9987	1.0000	0.19559E 02	0.6497	0.2500	0.55915E 00
1.9987	1.0000	0.19559E 02	0.7997	0.2500	0.45775E-00
1.9987	1.0000	0.19559E 02	0.9497	0.2500	0.42029E-00
1.9987	1.0000	0.19559E 02	1.0997	0.2500	0.40123E-00
1.9987	1.0000	0.19559E 02	1.2497	0.2500	0.38996E-00
1.9987	1.0000	0.19559E 02	1.3997	0.2500	0.38265E-00
1.9987	1.0000	0.19559E 02	1.5497	0.2500	0.37761E-00
1.9987	1.0000	0.19559E 02	1.6997	0.2500	0.37397E-00
1.9987	1.0000	0.19559E 02	1.8497	0.2500	0.37125E-00
1.9987	1.0000	0.19559E 02	1.9997	0.2500	0.36916E-00
1.5490	0.7500	0.14178E 01	0.2000	0.	0.35746E-00
1.5990	0.7500	0.10265E 01	0.4000	0.	0.35746E-00
1.6490	0.7500	0.85748E 00	0.6000	0.	0.35746E-00
1.6990	0.7500	0.75913E 00	0.8000	0.	0.35746E-00
1.7490	0.7500	0.69358E 00	1.0000	0.	0.35746E-00
1.7990	0.7500	0.64630E 00	1.2000	0.	0.35746E-00
1.8490	0.7500	0.61039E 00	1.4000	0.	0.35746E-00
1.8990	0.7500	0.58208E 00	1.6000	0.	0.35746E-00
1.9490	0.7500	0.55915E 00	1.8000	0.	0.35746E-00
1.9990	0.7500	0.54017E 00	2.0000	0.	0.35746E-00
1.0993	0.5000	0.95748E 00	0.	0.	0.
1.1993	0.5000	0.64630E 00	0.	0.	0.
1.2993	0.5000	0.55915E 00	0.	0.	0.
1.3993	0.5000	0.51054E 00	0.	0.	0.
1.4993	0.5000	0.47939E-00	0.	0.	0.
1.5993	0.5000	0.45775E-00	0.	0.	0.
1.6993	0.5000	0.44188E-00	0.	0.	0.
1.7993	0.5000	0.42978E-00	0.	0.	0.
1.8993	0.5000	0.42029E-00	0.	0.	0.
1.9993	0.5000	0.41266E-00	0.	0.	0.

APPENDIX D

(By Christopher J. Borland)

"METHOD OF GREY AND SCHENK" AS PROGRAMMED FOR THE IBM 709/7094 IN FORTRAN II

1. DESCRIPTIONS OF PROGRAMS

a. SUBSONIC LOAD DISTRIBUTIONS AND INTERFERENCE

This executive program is basically the same as that described in Appendix A, but modified to receive the geometrical parameters of the body as well as those of the wing, to control the interference calculations, and to print out the spanwise loading, lift curve slope, etc., with and without the effect of the body included.

b. EFBDWG

This subroutine computes an effective angle of attack distribution over the wing due to the presence of the body, when used with the subsonic load distribution and interference program.

c. Additional Subroutines

The following subroutines, described in Appendix A, are also required for subsonic interference calculation: WEISS, AMAT, B, GBAR, FBAR, ELSTAR, and MATINV. Listings are given for convenience. The Library and Machine requirements are the same as those listed in Appendix A.

d. SUPERSONIC LOAD DISTRIBUTION AND INTERFERENCE

This executive program is similar to that of Appendix C, but modified in the manner given in Section 1a of this Appendix.

e. SPEFBW

This subroutine is identical to EFBDWG, but modified for use with the supersonic distribution and interference program.

f. Additional Subrontines

The subroutines EVVARD and SUBSLE, described in Appendix C, are also required for the supersonic interference calculation. Listings are given for convenience.

g. Library and Machine Requirement

Library and Machine requirements are identical to those given in Appendix A.

2. INSTRUCTIONS FOR USE

a. Definitions of Input Variables

All of the definitions of Appendix A, Section 2-a, and Appendix C, Section 2-a, hold, with the following additions:

Subsonic

A	Body Radius / Semi-span of wing panel.
WTHET	Wing attachment angle, θ defined in the following sketch, in degrees.

Supersonic

A	Same as Subsonic
THETA	Same as WTHET

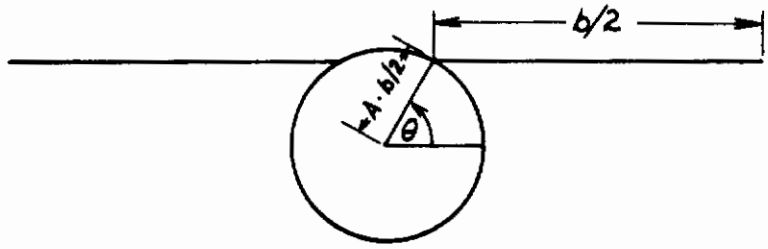

b. Order of the Data Deck

Subsonic

The order of the data deck is the same as that of Appendix A, with the following exception:

	Column	Variable
Card 2		
	1-10	ALAM
	11-20	AR
	21-30	TR
	31-40	ALPH
	41-50	A
	51-60	WTHET
	70	ITW

Supersonic

The order of the data deck is the same as that of Appendix C, with the following exception:

	Column	Variable
Card 2		
	1-10	EM
	11-20	ALAM
	21-30	AR
	31-40	TR
	41-50	ALPH
	51-60	A
	61-70	THETA
	80	ITW

c. Data Values

Again, the remarks of Appendices A and C apply with the following additions:

A, WTHET, and THETA must be punched with the decimal point, but need not be justified in their fields.

A may vary from 0.0 to ∞ and WTHET and THETA may vary from -90.0 to 90.0.

d. Input and Output Samples

Subsonic

A sample input deck is shown following the listing of the programs. The input values are as follows:

Case	Λ	AR	TR	α	A	θ	Twist
1	4.77	3.48	.546	1.0	.218	0.0	No
2	4.37	3.43	.546	1.0	.222	0.0	No
3	5.45	3.02	.546	1.0	.251	0.0	No

The output for these cases is also shown. The description given in Appendix A, Section 2d, may be followed, except that now the values of ALPHA show the sum of the geometrical angle of attack and the effective angle of attack due to the presence of the body.

Supersonic

A sample input deck is shown following a listing of the programs. The input values are as follows:

Case	Mach No.	$\Lambda_{L.E.}$	AR	TR	α	A	θ	Twist
1	1.08	45.0	4.0	0.0	1.0	.50	0.0	No
2	1.25	45.0	4.0	0.0	1.0	.25	45.0	No

The output for these cases is shown, and is similar to that described in Appendix C, except that output values are given with and without the effect of the body. It will be noticed that a spurious pressure is predicted at the tip of the delta wing due to the presence of the singularity at the leading edge.

```
*       LISTB
*       LABEL
C               SUBSONIC LOAD DISTRIBUTION AND INTERFERENCE
C           PROGRAM TO CALCULATE LOADING DISTRIBUTIONS ON SUBSONIC
C       WINGS BY WEISSINGER'S METHOD, INCLUDING THE EFFECT OF A BODY
C       OF INFINITE LENGTH, BY THE METHOD OF GREY AND SCHENK.
C       LIFT CURVE SLOPE IS CALCULATED BY TRAPEZOIDAL INTEGRATION.
C
        DIMENSION THETA(30),TAU(30),BOC(30),TAUBAR(30),ALPHA(30),Y(30),CL
     1 (30),XCP(30),SLOAD(30),CL1(30),ALPHTW(30),WOU(30)
        COMMON TAU,TAUBAR,THETA,AM,AM1,ALAMB,BOC
  100   FORMAT (2I5)
  101   FORMAT (6F10.4,I10)
  102   FORMAT (F10.4)
  201   FORMAT (16H1ASPECT RATIO = ,F10.4,10X,14HTAPER RATIO = ,F5.2,10X,
     1 18H.25 CHORD SWEEP = ,F5.2)
  202   FORMAT (1H0,9HDCL/DA = ,F10.4,5X,10HDCMY/DA = ,F10.4,5X,9HYBAR/B
     1= ,F10.4)
  203   FORMAT (5(F10.4,5X))
  204   FORMAT (1H0,24X,29HSPANWISE LOADING  (WING-BODY)//
     1 7X,3HY/B,11X,2HCL,12X,4HX-CP,7X,10HLOAD COEFF,8X,5HALPHA)
  205   FORMAT (1H0,24X,30HSPANWISE LOADING  (WING ALONE)//
     1 7X,3HY/B,11X,2HCL,12X,4HX-CP,7X,10HLOAD COEFF,8X,5HALPHA)
  206   FORMAT (1H0, 4HA = , F5.2,5X,8HTHETA = ,F10.4)
  207   FORMAT (12H0CL-TOTAL = ,F10.4)
   10     AD 100, M,M1
    2     AD 101, ALAM,AR,TR,ALPH,A,WTHET,ITW
        IF (AR) 11,10,11
   11   ALAMB=ALAM/57.295779
        WTHET=WTHET/57.295779
        LIMIT=((M+1)/2)+1
        IF (ITW) 15,16,15
   15   DO 17 J=1,LIMIT
        READ 102, ALPHTW(J)
   17   ALPHA(J)=ALPH+ALPHTW(J)
        GO TO 18
   16   DO 1 J=1,LIMIT
    1   ALPHA(J)=ALPH
   18   AM=M
        AM1=M1
        CALL WEISS(AR,TR,ALPHA,Y,CL,XCP)
        PRINT 201,AR,TR,ALAM
        PRINT 206, A, WTHET
        LIM=(M+1)/2
        LIMP=LIM+1
        DO 8 I=1,LIMP
    8   CL1(I)=CL(I)*2.*(1.-(Y(I)*(1.-TR)))/(1.+TR)
        SUM=0.
        DO 3 I=1,LIM
        TERM=(Y(I)-Y(I+1))*.5*(CL1(I+1)+CL1(I))
    3   SUM=SUM+TERM
        DCLDA=SUM/ALPH
        CLTOT=SUM
        SUM = 0.
        DO 13 I=1,LIM
        TERM=(Y(I)-Y(I+1))*.5*(CL1(I+1)+CL1(I))*.5*(Y(I)+Y(I+1))
   13   SUM=SUM+TERM
        DCMYDA=SUM/ALPH
        YCP=DCMYDA/DCLDA
```

```
      DO 4 I=1,LIMIT
4     SLOAD(I)=CL(I)*4.*(1.-(Y(I)*(1.-TR)))/((1.+TR)*AR)
      PRINT 202, DCLDA,DCMYDA,YCP
      PRINT 205
      PRINT 203, (Y(I),CL(I),XCP(I),SLOAD(I),ALPHA(I), I=1,LIMIT)
      PRINT 207, CLTOT
      IF (A) 2,2,5
5     N=LIMIT
      CALL EFBDWG(ALPH,AR,TR,A,WTHET,N,Y,CL,XCP,WOU)
      DO 12 I=1,N
12    ALPHA(I)=ALPHA(I)-WOU(I)
      CALL WEISS(AR,TR,ALPHA,Y,CL,XCP)
      DO 9 I=1,LIMP
9     CL1(I)=CL(I)*2.*(1.-(Y(I)*(1.-TR)))/(1.+TR)
      SUM=0.
      DO 6 I=1,LIM
      TERM=(Y(I)-Y(I+1))*.5*(CL1(I+1)+CL1(I))
6     SUM=SUM+TERM
      DCLDA=SUM/ALPH
      CLTOT=SUM
      SUM = 0.
      DO 14 I=1,LIM
      TERM=(Y(I)-Y(I+1))*.5*(CL1(I+1)+CL1(I))*.5*(Y(I)+Y(I+1))
14    SUM=SUM+TERM
      DCMYDA=SUM/ALPH
      YCP=DCMYDA/DCLDA
      DO 7 I=1,LIMIT
7     SLOAD(I)=CL(I)*4.*(1.-(Y(I)*(1.-TR)))/((1.+TR)*AR)
      PRINT 202, DCLDA,DCMYDA,YCP
      PRINT 204
      PRINT 203, (Y(I),CL(I),XCP(I),SLOAD(I),ALPHA(I), I=1,LIMIT)
      PRINT 207, CLTOT
      GO TO 2
     END
```

```
*       LIST8
*       LABEL
        SUBROUTINE AMAT (A)
        DIMENSION THETA(30),TAU(30),BOC(30),TAUBAR(30),A(30,30)
        COMMON TAU,TAUBAR,THETA,AM,AM1,ALAMB,BOC
        M=AM
        LIM=(AM+1.)/2.
        DO 1 NU=1,LIM
        DO 7 N=1,LIM
        IF (NU-N) 2,3,2
 2      IF (N-LIM) 4,5,4
 4      ARG2=M+1-N
        ANU=NU
        AN=N
        BIGB=B(ANU,AN)+B(ANU,ARG2)
        GO TO 6
 5      ANU=NU
        AN=N
        BIGB=B(ANU,AN)
        GO TO 6
 3      ANU=NU
        A(NU,N)=2.*B(ANU,ANU)+BOC(NU)*GBAR(ANU,ANU)
        GO TO 7
 6      A(NU,N)=-2.*BIGB+BOC(NU)*GBAR(ANU,AN)
 7      CONTINUE
 1      CONTINUE
        RETURN
       END
```

```
*       LIST8
*       LABEL
        SUBROUTINE WEISS (AR,TR,ALPHA,Y,CL,XCP)
        DIMENSION THETA(30),TAU(30),BOC(30),TAUBAR(30),ALPHA(30),Y(30),
     1 CL(30),XCP(30),A(30,30),G(30),ALPHA1(30)
        COMMON TAU,TAUBAR,THETA,AM,AM1,ALAMB,BOC
        M=AM
        PI=3.14159265358979323846
        LIM=(AM+1.)/2.
        DO 6 N=1,M
        EN=N
 6      THETA(N)=(EN*PI)/(AM+1.)
        DO 1 N=1,LIM
        EN=N
        TAU(N)=COSF((EN*PI)/(AM+1.))
        ALPHA1(N)=ALPHA(N)
 1      BOC(N)=(AR*(1.+TR))/(2.*(1.-TAU(N)*(1.-TR)))
        LIM2=(AM1+1.)/2.
        DO 5 N=1,LIM2
        EN=N
 5      TAUBAR(N)=COSF((EN*PI)/(AM1+1.))
        CALL AMAT (A)
        CALL MATINV (A,LIM,ALPHA1,1,DET)
        DO 2 N=1,LIM
        G(N)=ALPHA1(N)
        I=N+1
        CL(I)=2.*G(N)*BOC(N)
        XCP(I)=.25
 2      Y(I)=TAU(N)
        CL(1)=0.
        XCP(1)=.25
        Y(1)=1.0
        RETURN
       END
```

```
*       LIST8
*       LABEL
        FUNCTION B(ANU,AN)
        DIMENSION THETA(30),TAU(30),BOC(30),TAUBAR(30)
        COMMON TAU,TAUBAR,THETA,AM,AM1,ALAMB,BOC
        NU=ANU
        N=AN
        IF (N-NU) 1,2,1
 2      B=(AM+1.)/(4.*SINF(THETA(NU)))
        RETURN
 1      B=(SINF(THETA(N))/((COSF(THETA(N))-COSF(THETA(NU)))**2))
     1 *(1.-(-1.)**(N-NU))/(2.*(AM+1.))
        RETURN
       END
```

```
*       LIST8
*       LABEL
        FUNCTION GBAR(ANU,AN)
        DIMENSION THETA(30),TAU(30),BOC(30),TAUBAR(30)
      . COMMON TAU,TAUBAR,THETA,AM,AM1,ALAMB,BOC
        SUM=0.
        LIM=(AM1-1.)/2.
        LIMP=LIM+1
        DO 1 L=1,LIMP
        LM=L-1
        TERM=FBAR(AN,LM)*ELSTAR(ANU,LM)
        SUM=SUM+TERM
 1      CONTINUE
        GBAR=((-1.)/(2.*(AM1+1.)))*SUM
        RETURN
       END
```

```
*       LIST8
*       LABEL
        FUNCTION FBAR(AN,LM)
        DIMENSION THETA(30),TAU(30),BOC(30),TAUBAR(30)
        COMMON TAU,TAUBAR,THETA,AM,AM1,ALAMB,BOC
        N=AN
        M=AM
        SUM=0.
        DO 1 MU1=1,M,2
        AMU1=MU1
        IF (LM) 2,3,2
 3      TERM=AMU1*SINF(AMU1*THETA(N))
        GO TO 1
 2      ELM=LM
        THETBR=(ELM*3.14159)/(AM1+1.)
        TERM=AMU1*SINF(AMU1*THETA(N))*COSF(AMU1*THETBR)
 1      SUM=SUM+TERM
        F=(2./(AM+1.))*SUM
        IF (LM) 4,5,4
 5      IF (AN-((AM+1.)/2.)) 6,7,6
 7      FBAR=F/2.
        GO TO 8
 6      FBAR=F
        GO TO 8
 4      IF (AN-((AM+1.)/2.))9,10,9
 10     FBAR=F
        GO TO 8
 9      FBAR=2.*F
 8      RETURN
       END
```

```
*       LIST8
*       LABEL
        FUNCTION ELSTAR (ANU,LM)
        DIMENSION THETA(30),TAU(30),BOC(30),TAUBAR(30)
        COMMON TAU,TAUBAR,THETA,AM,AM1,ALAMB,BOC
        TANF(X)=SINF(X)/COSF(X)
        NU=ANU
        IF (LM) 1,2,1
 2      ETAMU=1.
        GO TO 3
 1      ETAMU=TAUBAR(LM)
 3      ETANU=TAU(NU)
        DIF=ETANU-ETAMU
        SUM=ETANU+ETAMU
        BOCN=BOC(NU)
        TERM1=(1./(BOCN*DIF))*(SQRTF(((1.+BOCN*DIF*TANF(ALAMB))**2)+
     1 ((BOCN*DIF)**2))-1.)
        TERM2=(1./(BOCN*SUM))*((SQRTF(((1.+BOCN*DIF*TANF(ALAMB))**2)+
     1  ((BOCN*SUM)**2)))/(1.+2.*BOCN*ETANU*TANF(ALAMB))-1.)
        TERM3=(2.*TANF(ALAMB)*SQRTF(((1.+BOCN*ETANU*TANF(ALAMB))**2)
     1  +((BOCN*ETANU)**2)))/(1.+2.*BOCN*ETANU*TANF(ALAMB))
        ELSTAR=TERM1-TERM2-TERM3
        RETURN
       END
```

```
*       LIST8
*       LABEL
        SUBROUTINE MATINV (A,N,B,M,DETERM)
C
C         SUBROUTINE TO SOLVE THE MATRIX EQUATION AX=B, WHERE A IS
C       AN N X N SQUARE MATRIX, B IS A KNOWN M X N MATRIX, AND X IS
C       AN UNKNOWN M X N MATRIX. UPON RETURN THE INVERSE OF A IS PLACED
C       IN A, AND X IS PLACED IN B. BY SETTING M=0 THE SUBROUTINE MAY
C       BE USED FOR MATRIX INVERSION ALONE.  FOR FURTHER DETAILS SEE
C        IBM SHARE NO. 664.
C
        DIMENSION IPIVOT(30), A(30,30), B(30,1), INDEX(30,2), PIVOT(30)
        EQUIVALENCE (IROW,JROW),(ICOLUM,JCOLUM),(AMAX,T,SWAP)
 10     DETERM=1.0
 15     DO 20 J=1,N
 20     IPIVOT(J)=0
 30     DO 550 I=1,N
 40     AMAX=0.0
 45     DO 105 J=1,N
 50     IF (IPIVOT(J)-1) 60,105,60
 60     DO 100 K=1,N
 70     IF (IPIVOT(K)-1) 80,100,740
 80     IF (ABSF(AMAX)-ABSF(A(J,K)))85,100,100
 85     IROW=J
 90     ICOLUM=K
 95     AMAX=A(J,K)
 100    CONTINUE
 105    CONTINUE
 110    IPIVOT(ICOLUM)=IPIVOT(ICOLUM)+1
 130    IF (IROW-ICOLUM) 140,260,140
 140    DETERM=-DETERM
 150    DO 200 L=1,N
 160    SWAP=A(IROW,L)
 170    A(IROW,L)=A(ICOLUM,L)
 200    A(ICOLUM,L)=SWAP
 205    IF (M) 260,260,210
 210    DO 250 L=1,M
 220    SWAP=B(IROW,L)
 230    B(IROW,L)=B(ICOLUM,L)
 250    B(ICOLUM,L)=SWAP
 260    INDEX(I,1)=IROW
 270    INDEX(I,2)=ICOLUM
 310    PIVOT(I)=A(ICOLUM,ICOLUM)
 320    DETERM=DETERM*PIVOT(I)
 330    A(ICOLUM,ICOLUM)=1.0
 340    DO 350 L=1,N
 350    A(ICOLUM,L)=A(ICOLUM,L)/PIVOT(I)
 355    IF (M) 380,380,360
 360    DO 370 L=1,M
 370    B(ICOLUM,L)=B(ICOLUM,L)/PIVOT(I)
 380    DO 550 L1=1,N
 390    IF (L1-ICOLUM) 400,550,400
 400    T=A(L1,ICOLUM)
 420    A(L1,ICOLUM)=0.0
 430    DO 450 L=1,N
 450    A(L1,L)=A(L1,L)-A(ICOLUM,L)*T
 455    IF (M) 550,550,460
 460    DO 500 L=1,M
 500    B(L1,L)=B(L1,L)-B(ICOLUM,L)*T
```

```
550    CONTINUE
600    DO 710 I=1,N
610    L=N+1-I
620    IF (INDEX(L,1)-INDEX(L,2)) 630,710,630
630    JROW=INDEX(L,1)
640    JCOLUM=INDEX(L,2)
650    DO 705 K=1,N
660    SWAP=A(K,JROW)
670    A(K,JROW)=A(K,JCOLUM)
700    A(K,JCOLUM)=SWAP
705    CONTINUE
710    CONTINUE
740    RETURN
       END
```

```
*       LIST8
*       LABEL
        SUBROUTINE EFBDWG (ALPH,AR,TR,A,THETA,N,Y,CL,XCP,WOU)
        DIMENSION Y(30),CL(30),XCP(30),WOU(30),DLBRDY(30),R(30),BLAM(30),
     1 RI(30),H(30),ALP(30),DEL(30),GAM(30),XO(30),YO(30),ZO(30),YV(30),
     2  ZV(30),YB(30),ZB(30),XPM(30,30),YPM(30,30),ZPM(30,30),ABIG(30,30
     3 ),BBIG(30,30),F(30,30),XC(30),WA(30,30),WAB(30,30),WB(30,30),
     4 WAP(30,30),WBP(30,30),WABP(30,30),PHI(30),RBIG(30),WF(30),
     5 EPS(30,30),CAPPA(30,30),APM(30,30),BPM(30,30),FPM(30,30),DELT(30)
     6 ,TAU(30),TAUBAR(30),DUM(30),BOC(30),C(30)
        COMMON TAU,TAUBAR,DUM,AM,AM1,ALAMB,BOC,APM,BPM,FPM,CAPPA,
     1  EPS,WAP,WBP,WABP,WAB,WB
        TANF(X)=SINF(X)/COSF(X)
        ALAML=ATANF(TANF(ALAMB)+((1.-TR)/(AR*(1.+TR))))
        PI=3.14159265358979323846
        CR=4./(AR*(1.+TR))
        DO 14 I=1,N
14      C(I)=4.*(1.-Y(I)*(1.-TR))/(AR*(1.+TR))
        NM=N-1
        NM2=N-2
        DO 1 I=1,N
        R(I)=SQRTF(((Y(I)+A*COSF(THETA))**2)+((A*SINF(THETA))**2))
        BLAM(I)=ATANF((A*SINF(THETA))/(Y(I)+A*COSF(THETA)))
1       RI(I)=(A*A)/R(I)
        DO 2 I=1,NM
        DLBRDY(I)=.5*(CL(I+1)*C(I+1)+CL(I)*C(I))
        H(I)=.5*SQRTF(((RI(I))**2)+((RI(I+1))**2)-(2.*RI(I)*RI(I+1)*
     1 COSF(BLAM(I+1)-BLAM(I))))
        ARG    =      ((((2.*H(I))**2)+((RI(I+1))**2)-((RI(I))**2))/
     1  (4.*H(I)*RI(I+1)))
        IF (ABSF(ARG)-1.0) 16,16,17
17      ARG=1.0
16      ALP(I)=ACOSF(ARG)
        DEL(I)=ALP(I)+(BLAM(I+1)-BLAM(I))
2       GAM(I)=DEL(I)+BLAM(I)
        DO 3 I=1,NM
        XO(I)=Y(I)*TANF(ALAML)+XCP(I)*C(I)
        YO(I)=((RI(I)*COSF(BLAM(I)))+(RI(I+1)*COSF(BLAM(I+1))))/2.
3       ZO(I)=((RI(I)*SINF(BLAM(I)))+(RI(I+1)*SINF(BLAM(I+1))))/2.
        DO 15 I=1,N
        YV(I)=RI(I)*COSF(BLAM(I))
15      ZV(I)=RI(I)*SINF(BLAM(I))
        DO 4 I=1,NM
        DO 5 J=1,N
        YB(J)=Y(J)+A*COSF(THETA)
        YPM(I,J)=Y(J)+A*COSF(THETA)-YO(I)
        ZB(J)=A*SINF(THETA)
        ZPM(I,J)=A*SINF(THETA)-ZO(I)
        ABIG(I,J)=SQRTF(((ZB(J)-ZV(I+1))**2)+((YB(J)-YV(I+1))**2))
        BBIG(I,J)=SQRTF(((ZB(J)-ZV(I))**2)+((YB(J)-YV(I))**2))
        F(I,J)=YPM(I,J)*SINF(GAM(I))-ZPM(I,J)*COSF(GAM(I))
        XC(J)=Y(J)*TANF(ALAML)+XCP(J)*C(J)+C(J)/2.
        XPM(I,J)=XC(J)-XO(I)
        EPS(I,J)=ACOSF((A*SINF(THETA)-ZV(I+1))/ABIG(I,J))
        CAPPA(I,J)=ACOSF((A*SINF(THETA)-ZV(I))/BBIG(I,J))
        APM(I,J)=SQRTF(((2.*RI(I+1)*COSF(BLAM(I+1)))**2)+((ABIG(I,J))**2)
     1 +(4.*RI(I+1)*ABIG(I,J)*COSF(BLAM(I+1))*SINF(EPS(I,J))))
        BPM(I,J)=SQRTF(((2.*RI(I)*COSF(BLAM(I)))**2)+((BBIG(I,J))**2)+
     1 (4.*RI(I)*BBIG(I,J)*COSF(BLAM(I))*SINF(CAPPA(I,J))))
```

```
      DELT(I)=2.*(RI(I+1)*COSF(BLAM(I+1))-H(I)*COSF(GAM(I)))
5     FPM(I,J)=(YPM(I,J)+DELT(I))*SINF(GAM(I))+ZPM(I,J)*COSF(GAM(I))
4     CONTINUE
      DO 6 I=1,NM2
      DO 7 J=1,N
      WA(I,J)=- (DLBRDY(I)/2.) *(1./(4.*PI*(ABIG(I,J)**2)))*(1.+(XPM(I,
     1  J)/SQRTF((XPM(I,J)**2)+(ABIG(I,J)**2))))*(YPM(I,J)-
     2  H(I)*COSF(GAM(I)))
7     WAP(I,J)=  (DLBRDY(I)/2.) *(1./(4.*PI*(APM (I,J)**2)))*(1.+(XPM(I,
     1  J)/SQRTF((XPM(I,J)**2)+(APM (I,J)**2))))*(YPM(I,J)-
     2 H(I)*COSF(GAM(I))+2.*RI(I+1)*COSF(BLAM(I+1)))
6     CONTINUE
      DO 8 J=1,N
      WAP (NM,J)=0.
8     WA (NM,J)=0.
      DO 9 I=1,NM
      DO 10 J=1,N
      WB(I,J)=  (DLBRDY(I)/2.) *(1./(4.*PI*(BBIG(I,J)**2)))*(1.+(XPM(I,
     1  J)/SQRTF((XPM(I,J)**2)+(BBIG(I,J)**2))))(YPM(I,J)+H(I)*COSF(GAM
     2 (I)))
      WBP(I,J)=- (DLBRDY(I)/2.) *(1./(4.*PI*(BPM (I,J)**2)))*(1.+(XPM(I,
     1  J)/SQRTF((XPM(I,J)**2)+(BPM (I,J)**2))))(YPM(I,J)+H(I)*COSF(GAM
     2 (I)))+2.*RI(I)*COSF(BLAM(I)))
      WAB(I,J)= (DLBRDY(I)/2.) *(1./(4.*PI))*(XPM(I,J)/((F(I,J)**2)
     1  +(XPM(I,J)**2)))*(SQRTF(((BBIG(I,J)**2)-(F  (I,J)**2))/((BBIG(I,
     2J)**2)+(XPM(I,J)**2)))-SQRTF(ABSF(((ABIG(I,J)**2)-(F(I,J)**2))/
     3  ((ABIG(I,J)**2)+(XPM(I,J)**2)))))
10    WABP(I,J)= (DLBRDY(I)/2.) *(1./(4.*PI))*(XPM(I,J)/((FPM(I,J)**2)
     1 +(XPM(I,J)**2)))*(SQRTF(ABSF(((BPM(I,J)**2)-(FPM(I,J)**2))/((BPM(
     2 I,J)**2)+(XPM(I,J)**2))))-SQRTF(ABSF(((APM(I,J)**2)-(FPM(I,J)**2)
     3 )/((APM(I,J)**2)+(XPM(I,J)**2)))))
9     CONTINUE
      DO 11 J=1,N
      PHI(J)=ATANF((ZB(J))/(YB(J)))
      RBIG(J)=SQRTF((YB(J)**2)+(ZB(J)**2))
11    WF(J)=-(ALPH*(A**2)*COSF(2.*PHI(J)))/(RBIG(J)**2)
      DO 12 J=1,N
      SUM=0.
      DO 13 I=1,NM
      TERM=WA(I,J)+WB(I,J)+WAB(I,J)+WAP(I,J)+WBP(I,J)+WABP(I,J)
13    SUM=SUM+TERM
      WOU(J)=SUM+WF(J)
12    CONTINUE
      RETURN
     END
```

```
*       DATA
    15    25
4.77        3.48        .546        1.0        .218        0.0                0
4.87        3.43        .546        1.0        .222        0.0                0
5.45        3.02        .546        1.0        .251        0.0                0
```

ASPECT RATIO = 3.4800 TAPER RATIO = 0.55 .25 CHORD SWEEP = 4.77

A = 0.22 THETA = 0.

DCL/DA = 3.4088 DCMY/DA = 1.4516 YBAR/B = 0.4258

SPANWISE LOADING (WING ALONE)

Y/B	CL	X-CP	LOAD COEFF	ALPHA
1.0000	0.	0.2500	0.	1.0000
0.9808	1.2394	0.2500	0.5112	1.0000
0.9239	2.2963	0.2500	0.9912	1.0000
0.8315	3.0616	0.2500	1.4170	1.0000
0.7071	3.5238	0.2500	1.7788	1.0000
0.5556	3.7327	0.2500	2.0752	1.0000
0.3827	3.7497	0.2500	2.3035	1.0000
0.1951	3.6228	0.2500	2.4549	1.0000
0.	3.3802	0.2500	2.5131	1.0000

CL-TOTAL = 3.4088

DCL/DA = 3.5722 DCMY/DA = 1.5125 YBAR/B = 0.4234

SPANWISE LOADING (WING-BODY)

Y/B	CL	X-CP	LOAD COEFF	ALPHA
1.0000	0.	0.2500	0.	1.0205
0.9808	1.2779	0.2500	0.5270	1.0211
0.9239	2.3697	0.2500	1.0228	1.0228
0.8315	3.1655	0.2500	1.4651	1.0261
0.7071	3.6540	0.2500	1.8445	1.0317
0.5556	3.8879	0.2500	2.1615	1.0412
0.3827	3.9290	0.2500	2.4136	1.0588
0.1951	3.8281	0.2500	2.5940	1.1085
0.	3.6029	0.2500	2.6787	1.4464

CL-TOTAL = 3.5722

ASPECT RATIO = 3.4300 TAPER RATIO = 0.55 .25 CHORD SWEEP = 4.87

A = 0.22 THETA = 0.

DCL/DA = 3.3839 DCMY/DA = 1.4408 YBAR/B = 0.4258

SPANWISE LOADING (WING ALONE)

Y/B	CL	X-CP	LOAD COEFF	ALPHA
1.0000	0.	0.2500	0.	1.0000
0.9808	1.2289	0.2500	0.5142	1.0000
0.9239	2.2775	0.2500	0.9974	1.0000
0.8315	3.0379	0.2500	1.4265	1.0000
0.7071	3.4978	0.2500	1.7914	1.0000
0.5556	3.7060	0.2500	2.0904	1.0000
0.3827	3.7229	0.2500	2.3204	1.0000
0.1951	3.5967	0.2500	2.4728	1.0000
0.	3.3555	0.2500	2.5311	1.0000

CL-TOTAL = 3.3839

DCL/DA = 3.5493 DCMY/DA = 1.5026 YBAR/B = 0.4233

SPANWISE LOADING (WING-BODY)

Y/B	CL	X-CP	LOAD COEFF	ALPHA
1.0000	0.	0.2500	0.	1.0211
0.9808	1.2679	0.2500	0.5306	1.0216
0.9239	2.3521	0.2500	1.0300	1.0234
0.8315	3.1434	0.2500	1.4761	1.0268
0.7071	3.6300	0.2500	1.8592	1.0325
0.5556	3.8634	0.2500	2.1792	1.0421
0.3827	3.9046	0.2500	2.4336	1.0599
0.1951	3.8042	0.2500	2.6154	1.1104
0.	3.5803	0.2500	2.7007	1.4443

CL-TOTAL = 3.5493

ASPECT RATIO = 3.0200 TAPER RATIO = 0.55 .25 CHORD SWEEP = 5.45

A = 0.25 THETA = 0.

DCL/DA = 3.1632 DCMY/DA = 1.3454 YBAR/B = 0.4253

SPANWISE LOADING (WING ALONE)

Y/B	CL	X-CP	LOAD COEFF	ALPHA
1.0000	0.	0.2500	0.	1.0000
0.9808	1.1367	0.2500	0.5402	1.0000
0.9239	2.1123	0.2500	1.0506	1.0000
0.8315	2.8277	0.2500	1.5081	1.0000
0.7071	3.2662	0.2500	1.9000	1.0000
0.5556	3.4675	0.2500	2.2214	1.0000
0.3827	3.4855	0.2500	2.4673	1.0000
0.1951	3.3660	0.2500	2.6283	1.0000
0.	3.1387	0.2500	2.6890	1.0000

CL-TOTAL = 3.1632

DCL/DA = 3.3372 DCMY/DA = 1.4110 YBAR/B = 0.4228

SPANWISE LOADING (WING-BODY)

Y/B	CL	X-CP	LOAD COEFF	ALPHA
1.0000	0.	0.2500	0.	1.0248
0.9808	1.1788	0.2500	0.5602	1.0254
0.9239	2.1928	0.2500	1.0907	1.0273
0.8315	2.9414	0.2500	1.5687	1.0310
0.7071	3.4083	0.2500	1.9826	1.0372
0.5556	3.6354	0.2500	2.3290	1.0475
0.3827	3.6770	0.2500	2.6029	1.0668
0.1951	3.5820	0.2500	2.7970	1.1223
0.	3.3704	0.2500	2.8875	1.4294

CL-TOTAL = 3.3372

```
*       LIST8
*       LABEL
*       SYMBOL TABLE
C         SUPERSONIC LOAD DISTRIBUTION AND INTERFERENCE
C
C            PROGRAM TO CALCULATE  LOAD DISTRIBUTIONS ON SUPERSONIC
C       WINGS WITH SUBSONIC LEADING EDGES, SUPERSONIC TRAILING EDGES,
C       AND AN ARBITRARY SPANWISE DISTRIBUTION OF TWIST.  THE EFFECT OF
C       AN INFINITELY LONG BODY IS CALCULATED BY THE METHOD OF GREY AND
C       SCHENK.
        DIMENSION ALPHA(25),Y(25),CL(25),XCP(25),SLOAD(25),CL1(25),WOU(25
     1 ),ALPHTW(25),CP(25,25),X(25,25)
        COMMON EM,ALAM,AR,TR,N,ALPHA,Y,CL,XCP,FLAG,DCMDA,M,MG,NG,KPG,KQG
     1 ,CP,X
  100   FORMAT (6I5)
  101   FORMAT (7F10.4,I10)
  102   FORMAT (F10.4)
  201   FORMAT (8H1MACH = ,F10.4,5X,5HAR = ,F10.4,5X,5HTR = ,F10.4,5X,
     1 14HL. E. SWEEP = ,F10.4)
  202   FORMAT (10H0DCL/DA = ,F10.4,5X,10HDCMY/DA = ,F10.4,5X,6HYCP = ,
     1 F10.4,5X,6HXCP = ,F10.4)
  203   FORMAT (5F15.5)
  204   FORMAT (72H0       Y/B             CL                XCP             COEF
     1F         ALPHA     )
  206   FORMAT (5H0A = ,F10.4,5X,8HTHETA = ,F10.4)
  207   FORMAT (12H0CL-TOTAL = ,F10.4)
  301   FORMAT (1H2,25X,21HPRESSURE DISTRIBUTION)
  302   FORMAT (72H0   X/C         Y/B         CP                  X/C       Y/
     1B           CP      /1H0)
  303   FORMAT (2(F7.4,3X,F7.4,3X,E11.5,8X))
  401   FORMAT (1H0////11H0WING ALONE)
  402   FORMAT (22H1WING-BODY COMBINATION)
   50   READ 100, M,N,MG,NG,KPG,KQG
C       N IS THE NUMBER OF SPANWISE STATIONS
C       M IS THE NUMBER OF CHORDWISE STATIONS
    1   READ 101, EM,ALAM,AR,TR,ALPH,A,THETA,ITW
        IF (AR) 50,50,51
   51   ALAMB=ALAM/57.295779
        THETA=THETA/57.295779
        IF (ITW) 15,16,15
   15   DO 17 J=1,N
        READ 102, ALPHTW(J)
   17   ALPHA(J)=ALPH+ALPHTW(J)
        GO TO 18
   16   DO 2 J=1,N
    2   ALPHA(J)=ALPH
   18   PRINT 201,EM,AR,TR,ALAM
        PRINT 206,A,THETA
        FLAG=0.
        CALL EVVARD
        IF (FLAG) 20,20,1
   20   LIM=N-1
        SUM=0.
        DO 8 I=1,N
    8   CL1(I)=CL(I)*2.*(1.-(Y(I)*(1.-TR)))/(1.+TR)
        DO 3 I=1,LIM
        TERM=(Y(I)-Y(I+1))*.5*(CL1(I+1)+CL1(I))
    3   SUM=SUM+TERM
        DCLDA=SUM/ALPH
```

```
      CLTOT=SUM
      SUM=0.
      DO 13 I=1,LIM
      TERM=(Y(I)-Y(I+1))*.5*(CL1(I+1)+CL1(I))*.5*(Y(I)+Y(I+1))
 13   SUM=SUM+TERM
      DCMYDA=SUM/ALPH
      YCP=DCMYDA/DCLDA
      XBAR=DCMDA/DCLDA
      DO 4 I=1,N
 4    SLOAD(I)=CL(I)*4.*(1.-(Y(I)*(1.-TR)))/((1.+TR)*AR)
      PRINT 401
      PRINT 202, DCLDA,DCMYDA,YCP,XBAR
      PRINT 204
      PRINT 203, (Y(I),CL(I),XCP(I),SLOAD(I),ALPHA(I), I=1,N)
      PRINT 207, CLTOT
      PRINT 301
      TOT=N/2
      NUM=TOT
      TOT1=NUM
      IF (TOT1-TOT) 40,41,41
 40   NUM=NUM+1
 41   PRINT 302
      DO 42 J=1,NUM
      J2=J+NUM
      PRINT 303, (X(I,J),Y(J),CP(I,J),X(I,J2),Y(J2),CP(I,J2), I=1,M)
 42   CONTINUE
      IF (A) 1,1,5
 5    CALL SPEFBW (ALPH,A,THETA,WOU)
      DO 12 I=1,N
 12   ALPHA(I)=ALPHA(I)-WOU(I)
      CALL EVVARD
      SUM=0.
      DO 11 I=1,N
 11   CL1(I)=CL(I)*2.*(1.-(Y(I)*(1.-TR)))/(1.+TR)
      DO 6 I=1,LIM
      TERM=(Y(I)-Y(I+1))*.5*(CL1(I+1)+CL1(I))
 6    SUM=SUM+TERM
      DCLDA=SUM/ALPH
      CLTOT=SUM
      SUM=0.
      DO 14 I=1,LIM
      TERM=(Y(I)-Y(I+1))*.5*(CL1(I+1)+CL1(I))*.5*(Y(I)+Y(I+1))
 14   SUM=SUM+TERM
      DCMYDA=SUM/ALPH
      YCP=DCMYDA/DCLDA
      XBAR=DCMDA/DCLDA
      DO 7 I=1,N
 7    SLOAD(I)=CL(I)*4.*(1.-(Y(I)*(1.-TR)))/((1.+TR)*AR)
      PRINT 402
      PRINT 202, DCLDA,DCMYDA,YCP,XBAR
      PRINT 204
      PRINT 203, (Y(I),CL(I),XCP(I),SLOAD(I),ALPHA(I), I=1,N)
      PRINT 207, CLTOT
      PRINT 301
      PRINT 302
      DO 44 J=1,NUM
      J2=J+NUM
      PRINT 303, (X(I,J),Y(J),CP(I,J),X(I,J2),Y(J2),CP(I,J2), I=1,M)



      GO TO 1
      END
```

```
*       LIST8
*       LABEL
*       SYMBOL TABLE
        SUBROUTINE EVVARD
        DIMENSION ALPHA(25),Y(25),CL(25),XCP(25)
        COMMON EM,ALAM,AR,TR,N,ALPHA,Y,CL,XCP,FLAG ,DCMDA
 101    FORMAT (49H2TRAILING EDGE SUBSONIC,  PROGRAM CANNOT CONTINUE)
 102    FORMAT (58H2UNSWEPT SUPERSONIC LEADING EDGE,  PROGRAM CANNOT CONT
     1INUE)
 103    FORMAT (49H0SUBSONIC LEADING EDGE,  SUPERSONIC TRAILING EDGE)
 104    FORMAT (46H0SONIC LEADING EDGE,  SUPERSONIC TRAILING EDGE)
 105    FORMAT (50H2LEADING EDGE SUPERSONIC,  PROGRAM CONNOT CONTINUE)
        TANF(X)=SINF(X)/COSF(X)
        BETA=SQRTF((EM**2)-1.)
        ALAMB=ALAM/57.295779
        ALAMTE=ATANF(TANF(ALAMB)-((4.*(1.-TR))/(AR*(1.+TR))))
        IF (ABSF(ALAMTE)-ATANF(BETA)) 1,1,2
 2      PRINT 101
        FLAG=1.0
        RETURN
 1      IF (ALAMB) 3,3,4
 3      PRINT 102
        FLAG=1.0
        RETURN
 4      IF (ABSF(BETA/TANF(ALAMB)-1.0)-.0001) 6,6,8
 8      IF ((BETA/TANF(ALAMB))-1.0) 5,6,7
 5      PRINT 103
        CALL SUBSLE
        RETURN
 6      PRINT 104
        CALL SUBSLE
        RETURN
 7      PRINT 105
        FLAG=1.0
        RETURN
       END
```

```
*       LIST8
*       LABEL
*       SYMBOL TABLE
        SUBROUTINE SUBSLE
        DIMENSION Y(25),XL(25),C(25),XC(25,25),X(25,25),TK(25,25),
      1 C1(25,25),D(25,25),A(25,25),B(25,25),YS(25,25),DSDX(25,25),
      2 SPQ(25,25),CP1(25,25),CP2(25,25),CP(25,25),CL(25),CCL(25),SLOAD
      3 (25),ALPHA(25),XCP(25)
        DIMENSION DCP(25,25),XARM(25)
        COMMON EM,ALAM,AR,TR,M,ALPHA,Y,CL,XCP,FLAG,DCMDA,N,MG,NG,KPG,KQG
      1 ,CP,X
C       N IS THE NUMBER OF CHORDWISE STATIONS
C       M IS THE NUMBER OF SPANWISE STATIONS
        TANF(X)=SINF(X)/COSF(X)
        ALAMB=ALAM/57.295779
        BETA=SQRTF((EM**2)-1.)
        CAPPA=(1.-(BETA/TANF(ALAMB)))/(1.+(BETA/TANF(ALAMB)))
        AK=1./(BETA*(1./TANF(ALAMB)))
        AM=M
        MM=M-1
        DO 1 J=1,M
        AJ=J
        Y(J)=1.-((AJ-1.)/(AM-1.))
        XL(J)=Y(J)*TANF(ALAMB)
 1      C(J)=4.*(1.-Y(J)*(1.-TR))/(AR*(1.+TR))
        EN=N
        DO 2 J=1,M
        DO 3 I=1,N
        EYE=I
        XC(I,J)=EYE*C(J)/EN
        X(I,J)=XL(J)+XC(I,J)
 3      TK(I,J)=AK*BETA*Y(J)/X(I,J)
 2      CONTINUE
        EMG=MG
        ENG=NG
        PG=KPG
        QG=KQG
        THETA=ATANF(BETA)
        DO 4 J=1,M
        DO 5 I=1,N
        YLE=X(I,J)/TANF(ALAMB)
        A1=YLE-Y(J)
        EMA=A1*SINF(ALAMB)/SINF(ALAMB+THETA)
        IF (EMA*COSF(THETA)+Y(J)-1.0) 30,30,31
 31     EMA=(1.0-Y(J))/COSF(THETA)
 30     A2=YLE+Y(J)
        ENB=A2*SINF(ALAMB)/SINF(ALAMB+THETA)
        IF (ENB*COSF(THETA)-Y(J)-1.0) 32,32,33
 33     ENB=(1.0+Y(J))/COSF(THETA)
 32     A(I,J)=EMA/EMG
        B(I,J)=ENB/ENG
        XPP=X(I,J)-EMA*SINF(THETA)-ENB*SINF(THETA)
        XP=X(I,J)-ENB*SINF(THETA)
        YLEP=XP/TANF(ALAMB)
        YLEPP=XPP/TANF(ALAMB)
        YSTAR=YLEP-EMA*COSF(THETA)
       B1=YLEPP+YSTAR
        B2=YLEPP-YSTAR
        PC=B1*SINF(ALAMB)/SINF(ALAMB+THETA)
```

```
      QD=B2*SINF(ALAMB)/SINF(ALAMB+THETA)
      IF (PC*COSF(THETA)-YSTAR-1.0) 34,34,35
35    PC=(1.0+YSTAR)/COSF(THETA)
34    IF (QD*COSF(THETA)+YSTAR-1.0) 36,36,37
37    QD=(1.0-YSTAR)/COSF(THETA)
36    C1(I,J)=PC/PG
      D(I,J)=QD/QG
5     YS(I,J)=YSTAR
4     CONTINUE
      DO 8 J=1,M
      DO 9 I=1,N
      SUM2=0.
      DO 6 MS=1,MG
      AMS=MS
      SUM1=0.
      DO 7 NS=1,NG
      ANS=NS
      Y1=AMS*A(I,J)*COSF(THETA)-ANS*B(I,J)*COSF(THETA)+Y(J)
      IF (ABSF(Y1)-1.0) 40,40,41
41    ALPH=0.
      GO TO 39
40    DO 10 K=2,M
      IF (Y(K)-ABSF(Y1)) 11,11,10
10    CONTINUE
11    ALPH=ALPHA(K)+((ALPHA(K-1)-ALPHA(K))/(Y(K-1)-Y(K)))*(ABSF(Y1)-Y(K
     1 ))
39    TERM=ALPH*((SQRTF(AMS)-SQRTF(AMS-1.))*(SQRTF(ANS)-SQRTF(ANS-1.)))
     1 /SQRTF(ENG*EMG)
      IF (A(I,J)) 42,42,7
42    TERM=0.
7     SUM1=SUM1+TERM
      TERM=SUM1
6     SUM2=SUM2+TERM
      SMN=SUM2
      SUM2=0.
      DO 12 IP=1,KPG
      P=IP
      SUM1=0.
      DO 13 IQ=1,KQG
      Q=IQ
      Y2=P*C1(I,J)*COSF(THETA)-Q*D(I,J)*COSF(THETA)-YS(I,J)
      DO 14 K=1,M
      IF (Y(K)-ABSF(Y2)) 15,15,14
14    CONTINUE
15    ALPH=ALPHA(K)+((ALPHA(K-1)-ALPHA(K))/(Y(K-1)-Y(K)))*(ABSF(Y1)-Y(K
     1 ))
      TERM=ALPH/SQRTF((1.+((1.-TK(I,J))*CAPPA*P)/((1.+TK(I,J))*PG))*
     1 (1.+((1.-TK(I,J))*CAPPA*Q)/((1.+TK(I,J))*QG)))
13    SUM1=SUM1+TERM
      TERM=SUM1
12    SUM2=SUM2+TERM
      SPQ(I,J)=SUM2/(PG*QG)
9     CONTINUE
      DO 16 I=1,N
      IF (I-1) 17,17,18
17    DSDX(I,J)=(-3.*SPQ(1,J)+4.*SPQ(2,J)-SPQ(3,J))*(1./(2.*XC(N,J)/
     1  EN))
      GO TO 16
18    IF(I-N) 19,20,20
```

```
20      DSDX(I,J)=(SPQ(N-2,J)-4.*SPQ(N-1,J)+3.*SPQ(N,J))*(1./(2.*XC(N,J)/
     1 EN))
        GO TO 16
19      DSDX(I,J)=(-SPQ(I-1,J)+SPQ(I+1,J))*(1./(2.*XC(N,J)/EN))
16      CONTINUE
        DO 21 I=1,N
        SQT=SQRTF(ABSF(1.-(TK(I,J)**2)))
        CP1(I,J)=-(8./(3.14159*BETA*(1.+AK)))*(SMN/SQT)
        CP2(I,J)=(2.*(AK-1.)/(BETA*3.14159*((1.+AK)**3)))*(SPQ(I,J)
     1 /SQT+SQT*X(I,J)*DSDX(I,J))
        CP(I,J)=CP1(I,J)+CP2(I,J)
21      CONTINUE
        DO 22 I=1,N
22      DCP(I,J) = 2.*CP(I,J)
        TERM1=2.*DCP(1,J)*(X(1,J)-XL(J))
        SUM=0.
        DO 23 I=2,N
        TERM=.5*(DCP(I-1,J)+DCP(I,J))*(X(I,J)-X(I-1,J))
23      SUM=SUM+TERM
        SUM=SUM+TERM1
        CL(J)=-SUM/C(J)
        CCL(J)=-SUM
        TERMM1=(2./3.)*DCP(1,J)*((X(1,J)-XL(J))**2)
        SUM2=0.
        DO 24 I=2,N
        TERM=.5*(DCP(I,J)+DCP(I-1,J))*(X(I,J)-X(I-1,J))*(X(I,J)+X(I-1,J)
     1 -2.*XL(J))*.5
24      SUM2=SUM2+TERM
        SUM2=SUM2+TERMM1
        XCP(J)=SUM2/(SUM*C(J))
        XARM(J)=SUM2/SUM+XL(J)
8       CONTINUE
        SUM3=0.
        DO 25 J=1,MM
        TERM=(CCL(J+1)+CCL(J))*.5*(XARM(J+1)+ XARM(J))*.5*(Y(J)-Y(J+1))
25      SUM3=SUM3+TERM
        ALPH=ALPHA(M)
        DCMDA=SUM3/(ALPH*C(M))
100     RETURN
      END
```

```
*       LIST8
*       LABEL
        SUBROUTINE SPEFBW (ALPH,A,THETA,WOU)
        DIMENSION Y(25),CL(25),XCP(25),WOU(25),DLBRDY(25),R(25),BLAM(25),
     1 RI(25),H(25),ALP(25),DEL(25),GAM(25),XO(25),YO(25),ZO(25),YV(25),
     2  ZV(25),YB(25),ZB(25),XPM(25,25),YPM(25,25),ZPM(25,25),ABIG(25,25
     3 ),BBIG(25,25),F(25,25),XC(25),WA(25,25),WAB(25,25),WB(25,25),
     4 WAP(25,25),WBP(25,25),WABP(25,25),PHI(25),RBIG(25),WF(25),
     5 EPS(25,25),CAPPA(25,25),APM(25,25),BPM(25,25),FPM(25,25),DELT(25)
     6 ,C(25),ALPHA(25),CP(25,25),X(25,25)
        COMMON EM,ALAM,AR,TR,N,ALPHA,Y,CL,XCP,FLAG,DCMDA,M,MG,NG,KPG,KQG,
     1 CP,X,APM,BPM,FPM,CAPPA,EPS,WAP,WBP,WABP,WAB,WB
        TANF(X)=SINF(X)/COSF(X)
        ALAMB=ALAM/57.295779
        ALAML=ALAMB
        PI=3.14159265358979323846
        CR=4./(AR*(1.+TR))
        DO 14 I=1,N
 14     C(I)=4.*(1.-Y(I)*(1.-TR))/(AR*(1.+TR))
        NM=N-1
        NM2=N-2
        DO 1 I=1,N
        R(I)=SQRTF(((Y(I)+A*COSF(THETA))**2)+((A*SINF(THETA))**2))
        BLAM(I)=ATANF((A*SINF(THETA))/(Y(I)+A*COSF(THETA)))
 1      RI(I)=(A*A)/R(I)
        DO 2 I=1,NM
        DLBRDY(I)=.5*(CL(I+1)*C(I+1)+CL(I)*C(I))
        H(I)=.5*SQRTF(((RI(I))**2)+((RI(I+1))**2)-(2.*RI(I)*RI(I+1)*
     1 COSF(BLAM(I+1)-BLAM(I))))
        ARG    =      ((((2.*H(I))**2)+((RI(I+1))**2)-((RI(I))**2))/
     1  (4.*H(I)*RI(I+1)))
        IF (ABSF(ARG)-1.0) 16,16,17
 17     ARG=1.0
 16     ALP(I)=ACOSF(ARG)
        DEL(I)=ALP(I)+(BLAM(I+1)-BLAM(I))
 2      GAM(I)=DEL(I)+BLAM(I)
        DO 3 I=1,NM
        XO(I)=Y(I)*TANF(ALAML)+XCP(I)*C(I)
        YO(I)=((RI(I)*COSF(BLAM(I)))+(RI(I+1)*COSF(BLAM(I+1))))/2.
 3      ZO(I)=((RI(I)*SINF(BLAM(I)))+(RI(I+1)*SINF(BLAM(I+1))))/2.
        DO 15 I=1,N
        YV(I)=RI(I)*COSF(BLAM(I))
 15     ZV(I)=RI(I)*SINF(BLAM(I))
        DO 4 I=1,NM
        DO 5 J=1,N
        YB(J)=Y(J)+A*COSF(THETA)
        YPM(I,J)=Y(J)+A*COSF(THETA)-YO(I)
        ZB(J)=A*SINF(THETA)
        ZPM(I,J)=A*SINF(THETA)-ZO(I)
        ABIG(I,J)=SQRTF(((ZB(J)-ZV(I+1))**2)+((YB(J)-YV(I+1))**2))
        BBIG(I,J)=SQRTF(((ZB(J)-ZV(I))**2)+((YB(J)-YV(I))**2))
        F(I,J)=YPM(I,J)*SINF(GAM(I))-ZPM(I,J)*COSF(GAM(I))
        XC(J)=Y(J)*TANF(ALAML)+XCP(J)*C(J)+C(J)/2.
        XPM(I,J)=XC(J)-XO(I)
        EPS(I,J)=ACOSF((A*SINF(THETA)-ZV(I+1))/ABIG(I,J))
        CAPPA(I,J)=ACOSF((A*SINF(THETA)-ZV(I))/BBIG(I,J))
        APM(I,J)=SQRTF(((2.*RI(I+1)*COSF(BLAM(I+1)))**2)+((ABIG(I,J))**2)
     1 +(4.*RI(I+1)*ABIG(I,J)*COSF(BLAM(I+1))*SINF(EPS(I,J))))
        BPM(I,J)=SQRTF(((2.*RI(I)*COSF(BLAM(I)))**2)+((BBIG(I,J))**2)+
```

```
     1 (4.*RI(I)*BBIG(I,J)*COSF(BLAM(I))*SINF(CAPPA(I,J))))
       DELT(I)=2.*(RI(I+1)*COSF(BLAM(I+1))-H(I)*COSF(GAM(I)))
5      FPM(I,J)=(YPM(I,J)+DELT(I))*SINF(GAM(I))+ZPM(I,J)*COSF(GAM(I))
4      CONTINUE
       DO 6 I=1,NM2
       DO 7 J=1,N
       WA(I,J)=- (DLBRDY(I)/2.) *(1./(4.*PI*(ABIG(I,J)**2)))*(1.+(XPM(I,
     1  J)/SQRTF((XPM(I,J)**2)+(ABIG(I,J)**2))))*(YPM(I,J)-
     2  H(I)*COSF(GAM(I)))
7      WAP(I,J)=  (DLBRDY(I)/2.) *(1./(4.*PI*(APM (I,J)**2)))*(1.+(XPM(I,
     1  J)/SQRTF((XPM(I,J)**2)+(APM (I,J)**2))))*(YPM(I,J)-
     2 H(I)*COSF(GAM(I)))+2.*RI(I+1)*COSF(BLAM(I+1)))
6      CONTINUE
       DO 8 J=1,N
       WAP (NM,J)=0.
8      WA (NM,J)=0.
       DO 9 I=1,NM
       DO 10 J=1,N
       WB(I,J)=  (DLBRDY(I)/2.) *(1./(4.*PI*(BBIG(I,J)**2)))*(1.+(XPM(I,
     1  J)/SQRTF((XPM(I,J)**2)+(BBIG(I,J)**2))))(YPM(I,J)+H(I)*COSF(GAM
     2 (I)))
       WBP(I,J)=- (DLBRDY(I)/2.) *(1./(4.*PI*(BPM (I,J)**2)))*(1.+(XPM(I,
     1  J)/SQRTF((XPM(I,J)**2)+(BPM (I,J)**2))))(YPM(I,J)+H(I)*COSF(GAM
     2 (I))+2.*RI(I)*COSF(BLAM(I)))
       WAB(I,J)= (DLBRDY(I)/2.) *(1./(4.*PI))*(XPM(I,J)/((F(I,J)**2)
     1  +(XPM(I,J)**2)))*(SQRTF(((BBIG(I,J)**2)-(F  (I,J)**2))/((BBIG(I,
     2J)**2)+(XPM(I,J)**2)))-SQRTF(ABSF(((ABIG(I,J)**2)-(F(I,J)**2))/
     3  ((ABIG(I,J)**2)+(XPM(I,J)**2)))))
10     WABP(I,J)= (DLBRDY(I)/2.) *(1./(4.*PI))*(XPM(I,J)/((FPM(I,J)**2)
     1 +(XPM(I,J)**2)))*(SQRTF(ABSF(((BPM(I,J)**2)-(FPM(I,J)**2))/((BPM(
     2 I,J)**2)+(XPM(I,J)**2))))-SQRTF(ABSF(((APM(I,J)**2)-(FPM(I,J)**2)
     3 )/((APM(I,J)**2)+(XPM(I,J)**2)))))
9      CONTINUE
       DO 11 J=1,N
       PHI(J)=ATANF((ZB(J))/(YB(J)))
       RBIG(J)=SQRTF((YB(J)**2)+(ZB(J)**2))
11     WF(J)=-(ALPH*(A**2)*COSF(2.*PHI(J)))/(RBIG(J)**2)
       DO 12 J=1,N
       SUM=0.
       DO 13 I=1,NM
       TERM=WA(I,J)+WB(I,J)+WAB(I,J)+WAP(I,J)+WBP(I,J)+WABP(I,J)
13     SUM=SUM+TERM
       WOU(J)=SUM+WF(J)
12     CONTINUE
       RETURN
       END
```

```
*       DATA
   10     5    20     20     5     5
1.08       45.0        4.0         0.0         1.0         .50         0.0                  0
1.25       45.0        4.0         0.0         1.0         .25         45.0                 0
```

MACH = 1.0800 AR = 4.0000 TR = 0. L. E. SWEEP = 45.0000

A = 0.5000 THETA = 0.

SUBSONIC LEADING EDGE, SUPERSONIC TRAILING EDGE

WING ALONE

DCL/DA = 5.4507 DCMY/DA = 2.2152 YCP = 0.4064 XCP = 0.3253

Y/B	CL	XCP	COEFF	ALPHA
1.00000	-0.	0.	0.	1.00000
0.75000	9.38585	0.35148	2.34646	1.00000
0.50000	6.19515	0.37595	3.09757	1.00000
0.25000	4.68874	0.41127	3.51655	1.00000
0.	3.88165	0.45606	3.88165	1.00000

CL-TOTAL = 5.4507

PRESSURE DISTRIBUTION

X/C	Y/B	CP	X/C	Y/B	CP
1.0000	1.0000	0.31914E 03	0.5500	0.5000	0.42137E 01
1.0000	1.0000	0.31914E 03	0.6000	0.5000	0.31782E 01
1.0000	1.0000	0.31914E 03	0.6500	0.5000	0.27512E 01
1.0000	1.0000	0.31914E 03	0.7000	0.5000	0.25131E 01
1.0000	1.0000	0.31914E 03	0.7500	0.5000	0.23607E 01
1.0000	1.0000	0.31914E 03	0.8000	0.5000	0.22548E 01
1.0000	1.0000	0.31914E 03	0.8500	0.5000	0.21771E 01
1.0000	1.0000	0.31914E 03	0.9000	0.5000	0.21179E 01
1.0000	1.0000	0.31914E 03	0.9500	0.5000	0.20715E 01
1.0000	1.0000	0.31914E 03	1.0000	0.5000	0.20342E 01
0.7750	0.7500	0.69629E 01	0.3250	0.2500	0.27510E 01
0.8000	0.7500	0.50429E 01	0.4000	0.2500	0.22548E 01
0.8250	0.7500	0.42137E 01	0.4750	0.2500	0.20716E 01
0.8500	0.7500	0.37313E 01	0.5500	0.2500	0.19784E 01
0.8750	0.7500	0.34099E 01	0.6250	0.2500	0.19233E 01
0.9000	0.7500	0.31782E 01	0.7000	0.2500	0.18875E 01
0.9250	0.7500	0.30022E 01	0.7750	0.2500	0.18629E 01
0.9500	0.7500	0.28635E 01	0.8500	0.2500	0.18451E 01
0.9750	0.7500	0.27512E 01	0.9250	0.2500	0.18318E 01
1.0000	0.7500	0.26582E 01	1.0000	0.2500	0.18215E 01

SUBSONIC LEADING EDGE, SUPERSONIC TRAILING EDGE

WING-BODY COMBINATION

CCL/DA = 5.9147 DCMY/DA = 2.4029 YCP = 0.4063 XCP = 0.3067

Y/B	CL	XCP	COEFF	ALPHA
1.00000	-0.	0.	0.	1.05606
0.75000	10.15721	0.35149	2.53930	1.07311
0.50000	6.73256	0.37595	3.36628	1.09271
0.25000	5.09558	0.41125	3.82169	1.09698
0.	4.20440	0.45606	4.20440	1.06060

CL-TOTAL = 5.9147

PRESSURE DISTRIBUTION

X/C	Y/B	CP	X/C	Y/B	CP
1.0000	1.0000	0.35624E 03	0.5500	0.5000	0.45792E 01
1.0000	1.0000	0.35624E 03	0.6000	0.5000	0.34539E 01
1.0000	1.0000	0.35624E 03	0.6500	0.5000	0.29899E 01
1.0000	1.0000	0.35624E 03	0.7000	0.5000	0.27311E 01
1.0000	1.0000	0.35624E 03	0.7500	0.5000	0.25655E 01
1.0000	1.0000	0.35624E 03	0.8000	0.5000	0.24504E 01
1.0000	1.0000	0.35624E 03	0.8500	0.5000	0.23660E 01
1.0000	1.0000	0.35624E 03	0.9000	0.5000	0.23016E 01
1.0000	1.0000	0.35624E 03	0.9500	0.5000	0.22511E 01
1.0000	1.0000	0.35624E 03	1.0000	0.5000	0.22108E 01
0.7750	0.7500	0.75347E 01	0.3250	0.2500	0.29899E 01
0.8000	0.7500	0.54571E 01	0.4000	0.2500	0.24506E 01
0.8250	0.7500	0.45598E 01	0.4750	0.2500	0.22514E 01
0.8500	0.7500	0.40381E 01	0.5500	0.2500	0.21501E 01
0.8750	0.7500	0.36906E 01	0.6250	0.2500	0.20902E 01
0.9000	0.7500	0.34396E 01	0.7000	0.2500	0.20513E 01
0.9250	0.7500	0.32490E 01	0.7750	0.2500	0.20246E 01
0.9500	0.7500	0.30992E 01	0.8500	0.2500	0.20052E 01
0.9750	0.7500	0.29777E 01	0.9250	0.2500	0.19905E 01
1.0000	0.7500	0.28765E 01	1.0000	0.2500	0.19787E 01

MACH = 1.2500 AR = 4.0000 TR = 0. L. E. SWEEP = 45.0000

A = 0.2500 THETA = 0.7854

SUBSONIC LEADING EDGE, SUPERSONIC TRAILING EDGE

WING ALONE

DCL/DA = 4.4413 DCMY/DA = 1.8063 YCP = 0.4067 XCP = 0.3253

Y/B	CL	XCP	COEFF	ALPHA
1.00000	-0.	0.	0.	1.00000
0.75000	7.66191	0.35129	1.91548	1.00000
0.50000	5.05148	0.37563	2.52574	1.00000
0.25000	3.81783	0.41096	2.86337	1.00000
0.	3.15611	0.45606	3.15611	1.00000

CL-TOTAL = 4.4413

PRESSURE DISTRIBUTION

X/C	Y/B	CP	X/C	Y/B	CP
1.0000	1.0000	0.	0.5500	0.5000	0.34400E 01
1.0000	1.0000	0.	0.6000	0.5000	0.25930E 01
1.0000	1.0000	0.	0.6500	0.5000	0.22434E 01
1.0000	1.0000	0.	0.7000	0.5000	0.20484E 01
1.0000	1.0000	0.	0.7500	0.5000	0.19235E 01
1.0000	1.0000	0.	0.8000	0.5000	0.18368E 01
1.0000	1.0000	0.	0.8500	0.5000	0.17731E 01
1.0000	1.0000	0.	0.9000	0.5000	0.17246E 01
1.0000	1.0000	0.	0.9500	0.5000	0.16865E 01
1.0000	1.0000	0.	1.0000	0.5000	0.16559E 01
0.7750	0.7500	0.56876E 01	0.3250	0.2500	0.22434E 01
0.8000	0.7500	0.41181E 01	0.4000	0.2500	0.18368E 01
0.8250	0.7500	0.34400E 01	0.4750	0.2500	0.16865E 01
0.8500	0.7500	0.30455E 01	0.5500	0.2500	0.16101E 01
0.8750	0.7500	0.27826E 01	0.6250	0.2500	0.15649E 01
0.9000	0.7500	0.25930E 01	0.7000	0.2500	0.15356E 01
0.9250	0.7500	0.24489E 01	0.7750	0.2500	0.15154E 01
0.9500	0.7500	0.23354E 01	0.8500	0.2500	0.15008E 01
0.9750	0.7500	0.22434E 01	0.9250	0.2500	0.14899E 01
1.0000	0.7500	0.21673E 01	1.0000	0.2500	0.14815E 01

SUBSONIC LEADING EDGE, SUPERSONIC TRAILING EDGE

WING-BODY COMBINATION

DCL/DA = 4.3698 DCMY/DA = 1.7901 YCP = 0.4097 XCP = 0.3674

Y/B	CL	XCP	COEFF	ALPHA
1.00000	-0.	0.	0.	1.01733
0.75000	7.66165	0.35129	1.91541	1.02225
0.50000	5.01568	0.37562	2.50784	1.02421
0.25000	3.73503	0.41096	2.80127	1.00165
0.	3.02996	0.45606	3.02996	0.88760

CL-TOTAL = 4.3698

PRESSURE DISTRIBUTION

X/C	Y/B	CP	X/C	Y/B	CP
1.0000	1.0000	0.	0.5500	0.5000	0.34157E 01
1.0000	1.0000	0.	0.6000	0.5000	0.25746E 01
1.0000	1.0000	0.	0.6500	0.5000	0.22275E 01
1.0000	1.0000	0.	0.7000	0.5000	0.20339E 01
1.0000	1.0000	0.	0.7500	0.5000	0.19099E 01
1.0000	1.0000	0.	0.8000	0.5000	0.18237E 01
1.0000	1.0000	0.	0.8500	0.5000	0.17605E 01
1.0000	1.0000	0.	0.9000	0.5000	0.17123E 01
1.0000	1.0000	0.	0.9500	0.5000	0.16745E 01
1.0000	1.0000	0.	1.0000	0.5000	0.16441E 01
0.7750	0.7500	0.56874E 01	0.3250	0.2500	0.21948E 01
0.8000	0.7500	0.41180E 01	0.4000	0.2500	0.17969E 01
0.8250	0.7500	0.34399E 01	0.4750	0.2500	0.16499E 01
0.8500	0.7500	0.30454E 01	0.5500	0.2500	0.15752E 01
0.8750	0.7500	0.27825E 01	0.6250	0.2500	0.15309E 01
0.9000	0.7500	0.25929E 01	0.7000	0.2500	0.15023E 01
0.9250	0.7500	0.24488E 01	0.7750	0.2500	0.14825E 01
0.9500	0.7500	0.23353E 01	0.8500	0.2500	0.14682E 01
0.9750	0.7500	0.22433E 01	0.9250	0.2500	0.14575E 01
1.0000	0.7500	0.21672E 01	1.0000	0.2500	0.14493E 01

Contrails

Security Classification

DOCUMENT CONTROL DATA - R&D

(Security classification of title, body of abstract and indexing annotation must be entered when the overall report is classified)

1. ORIGINATING ACTIVITY (Corporate author) Massachusetts Institute of Technology 560 Memorial Drive Cambridge 39, Massachusetts	2a. REPORT SECURITY CLASSIFICATION Unclassified 2b. GROUP

3. REPORT TITLE

AN EVALUATION OF PROCEDURES FOR CALCULATING AERODYNAMIC LOADS

4. DESCRIPTIVE NOTES (Type of report and inclusive dates)

Final Report; March-December 1964

5. AUTHOR(S) (Last name, first name, initial)

Schindel, Leon H.

6. REPORT DATE	7a. TOTAL NO. OF PAGES	7b. NO. OF REFS
May 1965	287 + 22	112

8a. CONTRACT OR GRANT NO. AF33(615)-1199 b. PROJECT NO. 1367 c. 136715 d.	9a. ORIGINATOR'S REPORT NUMBER(S) TR 103 9b. OTHER REPORT NO(S) (Any other numbers that may be assigned this report) AFFDL-TR-65-18

10. AVAILABILITY/LIMITATION NOTICES

Qualified requesters may obtain copies of this report from DDC.
DDC release to OTS (CFSTI) is not authorized.

11. SUPPLEMENTARY NOTES	12. SPONSORING MILITARY ACTIVITY
	AFFDL (FDTR) Wright-Patterson AFB, Ohio

13. ABSTRACT

Existing theories are examined with the object of selecting the best methods for computing aerodynamic lift distributions for use in structural design. Subsonic, transonic and supersonic Mach numbers are included. Configurations consist of wing-body combinations such as might be employed for airplane-type vehicles. The present investigation is limited to the linear range of angle of attack.

The simplest theories which give accuracy consistent with structural design practice are reduced to computational procedure; the accuracy of a theory having been established by comparison with existing experimental data. In cases where no adequate theory is available or experimental data is lacking, further research is recommended. Future extensions to nonlinear regimes, more general configurations, and higher Mach numbers are also described.

DD FORM 1 JAN 64 1473

Security Classification

Security Classification

14. KEY WORDS	LINK A		LINK B		LINK C	
	ROLE	WT	ROLE	WT	ROLE	WT

INSTRUCTIONS

1. **ORIGINATING ACTIVITY:** Enter the name and address of the contractor, subcontractor, grantee, Department of Defense activity or other organization *(corporate author)* issuing the report.

2a. **REPORT SECURITY CLASSIFICATION:** Enter the overall security classification of the report. Indicate whether "Restricted Data" is included. Marking is to be in accordance with appropriate security regulations.

2b. **GROUP:** Automatic downgrading is specified in DoD Directive 5200.10 and Armed Forces Industrial Manual. Enter the group number. Also, when applicable, show that optional markings have been used for Group 3 and Group 4 as authorized.

3. **REPORT TITLE:** Enter the complete report title in all capital letters. Titles in all cases should be unclassified. If a meaningful title cannot be selected without classification, show title classification in all capitals in parenthesis immediately following the title.

4. **DESCRIPTIVE NOTES:** If appropriate, enter the type of report, e.g., interim, progress, summary, annual, or final. Give the inclusive dates when a specific reporting period is covered.

5. **AUTHOR(S):** Enter the name(s) of author(s) as shown on or in the report. Enter last name, first name, middle initial. If military, show rank and branch of service. The name of the principal author is an absolute minimum requirement.

6. **REPORT DATE:** Enter the date of the report as day, month, year; or month, year. If more than one date appears on the report, use date of publication.

7a. **TOTAL NUMBER OF PAGES:** The total page count should follow normal pagination procedures, i.e., enter the number of pages containing information.

7b. **NUMBER OF REFERENCES:** Enter the total number of references cited in the report.

8a. **CONTRACT OR GRANT NUMBER:** If appropriate, enter the applicable number of the contract or grant under which the report was written.

8b, 8c, & 8d. **PROJECT NUMBER:** Enter the appropriate military department identification, such as project number, subproject number, system numbers, task number, etc.

9a. **ORIGINATOR'S REPORT NUMBER(S):** Enter the official report number by which the document will be identified and controlled by the originating activity. This number must be unique to this report.

9b. **OTHER REPORT NUMBER(S):** If the report has been assigned any other report numbers *(either by the originator or by the sponsor)*, also enter this number(s).

10. **AVAILABILITY/LIMITATION NOTICES:** Enter any limitations on further dissemination of the report, other than those imposed by security classification, using standard statements such as:

(1) "Qualified requesters may obtain copies of this report from DDC."

(2) "Foreign announcement and dissemination of this report by DDC is not authorized."

(3) "U. S. Government agencies may obtain copies of this report directly from DDC. Other qualified DDC users shall request through _____."

(4) "U. S. military agencies may obtain copies of this report directly from DDC. Other qualified users shall request through _____."

(5) "All distribution of this report is controlled. Qualified DDC users shall request through _____."

If the report has been furnished to the Office of Technical Services, Department of Commerce, for sale to the public, indicate this fact and enter the price, if known.

11. **SUPPLEMENTARY NOTES:** Use for additional explanatory notes.

12. **SPONSORING MILITARY ACTIVITY:** Enter the name of the departmental project office or laboratory sponsoring *(paying for)* the research and development. Include address.

13. **ABSTRACT:** Enter an abstract giving a brief and factual summary of the document indicative of the report, even though it may also appear elsewhere in the body of the technical report. If additional space is required, a continuation sheet shall be attached.

It is highly desirable that the abstract of classified reports be unclassified. Each paragraph of the abstract shall end with an indication of the military security classification of the information in the paragraph, represented as *(TS)*, *(S)*, *(C)*, or *(U)*.

There is no limitation on the length of the abstract. However, the suggested length is from 150 to 225 words.

14. **KEY WORDS:** Key words are technically meaningful terms or short phrases that characterize a report and may be used as index entries for cataloging the report. Key words must be selected so that no security classification is required. Identifiers, such as equipment model designation, trade name, military project code name, geographic location, may be used as key words but will be followed by an indication of technical context. The assignment of links, rules, and weights is optional.

Security Classification